Boundary Element Analysis for Convection-Diffusion-Reaction Problems Combining Dual Reciprocity and Radial Integration Methods

By

SALAM ADEL AL-BAYATI

A Thesis Submitted

in Partial Fulfilment of the Requirements for the Degree of

DOCTOR OF PHILOSOPHY

Department of Mathematics

College of Engineering, Design and Physical Sciences

BRUNEL UNIVERSITY LONDON

August 2018

Dedication

I dedicate this thesis to:

- ♡ **The loving memory of my father;**
- ♡ **My beloved Mum, for her prayers and wishes;**
- ♡ **My wife for her patience and steadfast support;**
- ♡ **My Brother and Sisters, for their wishes and help.**
- ♡ **My son, Ali.**

Declaration

I declare that this thesis is my own work and is submitted for the first time to the Post-Graduate Research Office. The study was originated, composed and reviewed by myself and my supervisor in the Department of Mechanical Engineering, College of Engineering, Design and Physical Sciences, Brunel University London UK. All the information derived from other works has been properly referenced and acknowledged.

Salam Adel Ahmed

August 2018

Acknowledgements

First, I would like to express my sincere gratitude to my supervisor Professor L.C. Wrobel for his ongoing support of my PhD study, for his patience, inspiration, and immense knowledge. His supervision helped me throughout the research period and the writing up of this thesis. His noble advices and his role in my life will be a valuable asset for me and I am thinking that I am extremely lucky to have him as PhD supervisor.

I would also like to thank my sponsor, the Iraqi Ministry of Higher Education and Scientific Research, as represented by the Iraqi Cultural Attaché in London, for giving me this opportunity to complete my study and I am also grateful for their unstinting support and care.

Additionally, I am grateful to my brothers in law Sajad, Bassam, Ammar and my fiend Laith for the limitless backing they gave.

In addition, I am thankful to staff of Mathematics department, at Brunel University for their advices and support over 4 years for fruitful-collaborations and insightful-discussions.

I want to pay special thanks to my wife for her endless support and patience in the completion of this degree. She was the person who bears all the direct and indirect tension of my PhD. I also want to acknowledge her for her unconditional love all the time.

Numerous thanks to my family: my parents and my brother and sisters for supporting me spiritually throughout writing this thesis and my life in general.

Finally, I would like to acknowledge the greatness of my friend Dr. Jurij Iljaž for his valuable comments and suggestions.

Abstract

In this research project, the Boundary Element Method (BEM) is developed and formulated for the solution of two-dimensional convection-diffusion-reaction problems. A combined approach with the dual reciprocity boundary element method (DRBEM) has been applied to solve steady-state problems with variable velocity and transient problems with constant and variable velocity fields. Further, the radial integration boundary element method (RIBEM) is utilised to handle non-homogeneous problems with variable source term. For all cases, a boundary-only formulation is produced.

Initially, the steady-state case with constant velocity is considered, by employing constant boundary elements and a fundamental solution of the adjoint equation. This fundamental solution leads to a singular integral equation. The conservation laws, usually applied to avoid this integration, do not hold when a chemical reaction is taking place. Then, the integrals are successfully computed using Telles' technique. The application of the BEM for this particular equation is discussed in detail in this work.

Next, the steady-state problem for variable velocity fields is presented and investigated. The velocity field is divided into an average value plus a perturbation. The perturbation is taken to the right-hand-side of the equation generating a non-homogeneous term. This non-homogeneous equation is treated by utilising the DRM approach resulting in a boundary-only equation. Then, an integral equation formulation for the transient problem with constant velocity is derived, based on the DRM approach utilising the fundamental solution of the steady-state case. Therefore, the convective terms will be encompassed by the fundamental solution and lie within the boundary integral after application of Greens's second identity, leaving on the right-hand-side of the equation a domain integral involving the time-derivative

only. The proposed DRM method needs the time-derivative to be expanded as a series of functions that will allow the domain integral to be moved to the boundary. The expansion required by the DRM uses functions which take into account the geometry and physics of the problem, if velocity-dependent terms are used.

After that, a novel DRBEM model for transient convection-diffusion-reaction problems with variable velocity field is investigated and validated. The fundamental solution for the corresponding steady-state problem is adopted in this formulation. The variable velocity is decomposed into an average which is included into the fundamental solution of the corresponding equation with constant coefficients, and a perturbation which is treated using the DRM approximation. The mathematical formulation permits the numerical solution to be represented in terms of boundary-only integrals.

Finally, a new formulation for non-homogeneous convection-diffusion-reaction problems with variable source term is achieved using RIBEM. The RIM is adopted to convert the domain integrals into boundary-only integrals. The proposed technique shows very good solution behaviour and accuracy in all cases studied.

The convergence of the methods has been examined by implementing different error norm indicators and increasing the number of boundary elements in all cases.

Numerical test cases are presented throughout this research work. Their results are sufficiently encouraging to recommend the use of the techniques developed for solution of general convection-diffusion-reaction problems. All the simulated solutions for several examples showed very good agreement with available analytical solutions, with no numerical problems of oscillation and damping of sharp fronts.

List of Publications

- S. A. AL-Bayati and L. C. Wrobel, A Novel Dual Reciprocity Boundary Element Formulation for Two-Dimensional Transient Convection-Diffusion-Reaction Problems with Variable Velocity, Engineering Analysis with Boundary Elements, Vol.(94), 60-68 (2018).

- S. A. AL-Bayati and L. C. Wrobel, The Dual Reciprocity Boundary Element Formulation for Convection-Diffusion-Reaction Problems with Variable Velocity Field Using Different Radial Basis Functions, International Journal of Mechanical Sciences, Vol.(145), 367–377 (2018).

- S. A. AL-Bayati and L. C. Wrobel, Radial Integration Boundary Element Method for Non-Homogeneous Convection-Diffusion-Reaction with Variable Velocity, accepted for publication on Engineering Analysis with Boundary Elements.

- S. A. AL-Bayati and L. C. Wrobel, DRBEM Formulations for Convection-Diffusion-Reaction Problems with Variable Velocity, Eleventh UK Conference on Boundary Integral Methods (UKBIM 11), Nottingham Trent University Press, pp. 5-14 (2017).

- S. A. AL-Bayati and L. C. Wrobel, Transient Convection-Diffusion-Reaction Problems with Variable Velocity Field using DRBEM with Different Radial Basis Functions, 15th International Conference on Integral Methods in Science and Engineering (IMSE 15), Brighton University Press, (2018).

- S. A. AL-Bayati and L.C. Wrobel, Numerical Modelling of Convective-Diffusive-Reactive Problems in Thermo-Fluids, Poster Conference at Brunel University, 2018.

Table of contents

List of figures

List of tables

List of Abbreviations

BEM	Boundary Element Method
DRM	Dual Reciprocity Method
DRBEM	Dual Reciprocity Boundary Element Method
FEM	Finite Element Method
FDM	Finite Difference Method
BIE	Boundary Integral Equation
2D	Two-Dimensional Space
3D	Three-Dimensional Space
TPS	Thin-Plate Spline Radial Basis Function
MQ	Multiquadric Radial Basis Function
Pé	Péclet Number
RIM	Radial Integration Method
RIBEM	Radial Integration Boundary Element Method
BDIEM	Boundary-Domain Integral Equation Method
RBF	Radial Basis Function

List of abbreviations

DBEM Domain Boundary Element Method

SBEM Singular Boundary Element Method

PDE Partial Differential Equation

RMS Root Mean Square Error Norm

List of Notations

$erfc$	Complementary error function
ϕ	Concentration profile
D	Diffusivity
A, B	Auxiliar matrices
H, G	Integrand kernels
∇	Gradient
∇^2	Laplacian operator
v_x	Velocity component along x-axis
v_y	Velocity component along y-axis
k	Reaction coefficient
K_0	Modified Bessel function of second kind and zero order
K_1	Modified Bessel function of second kind and first order
$v\left(v_x, v_y\right)$	Velocity vector
$n\left(n_x, n_y\right)$	Outward normal unit vector
ξ	Source point
χ	Field point

Ω	Problem domain
L^{∞}	Error norm
τ	Time parameter
t	Time
ξ_g	Gauss coordinate
w_g	Associate weight
$\mathscr{L}$	Convection-diffusion-reaction operator
Γ	Boundary of the problem
N	Number of boundary elements
J	Jacobian
v_n	Normal velocity
$\mathscr{L}^*$	Adjoint operator to the convection-diffusion-reaction equation
r	Euclidean distance between source and field point
θ	Parameter which positions the value of ϕ and q between time levels.
r, θ	Polar coordinates
$rd\theta$	Differential arc
κ	Kronecker delta function
$\delta(\xi,\chi)$	Dirac delta function
$C(\xi)$	Free influence coefficient
Φ^*	Fundamental solution
μ	Constant for the fundamental solution of the convection-diffusion-reaction equation
$\mathbf{q}$	Normal flux (Derivative of concentration with respect to n)
.	Scalar product

Chapter 1

Introduction

1.1 Introduction

It is widely known that practical engineering problems may not be solved exactly utilising analytical means, most often because of the presence of irregular geometries, complex boundary conditions, or non-linearity in either material properties or the governing equation itself. Solutions are most often sought by using numerical techniques, for example, the finite element method (FEM), the finite difference method (FDM) and the boundary element method (BEM), which have reached a high level of development that have made them substantial tools for modern scientists, researchers and engineers.

The FEM is routinely used as a generalised analysis tool in design and industry [1]. This method involves the approximation of the variables over small parts of the domain, called finite elements, in terms of polynomial interpolation functions. The FEM is based upon variational principles, which can handle almost any linear, nonlinear or time-dependent PDE on domains with a curved boundary [2]. The FEM is one of the most general and powerful methods for solving PDEs. The FEM [3–5] has been widely implemented in various areas, due to its capability to handle any type of geometry and material inhomogeneity without any need to alter the formulation or computer code. Therefore, it provides geometrical fidelity and unrestricted material treatment. Furthermore, the application of the FEM normally generates symmetric and sparse matrix systems which can be stored with low memory requirements.

The FDM approximates the derivatives in the differential equation which govern each problem using some type of truncated Taylor expansion. The FDM usually demands the geometry of the problem to be sufficiently simple, such as rectangular or curvilinear. It should be stressed that the FEM and the BEM have the ability to handle problem domains with complex geometries, whilst relying on a rigorous problem reformulation that is free of the approximations present in FDM formulations [6].

The BEM requires discretisation of the boundary only, thus reducing the quantity of data necessary to run a program [7]. The BEM is considered as the best alternative technique for the FEM for a wide range of disciplines in engineering [2].

In the literature, numerous approaches using BEM have been proposed in order to solve different PDE problems. This method has become a powerful technique for the numerical solution of boundary-value problems (BVPs), because of its ability (at least for problems with constant coefficients) of reducing a BVP for a linear PDE defined in a domain to an integral equation defined on the boundary, leading to a simplified discretisation process with boundary elements only. On the other hand, the coefficients in the mathematical model of a physical problem typically correspond to the material parameters of the problem [8, 9, 1, 10]. The Green‘s functions, or fundamental solutions, are usually difficult to integrate as they contain singularities at the source point. For simple element geometries, analytical integration can sometimes be employed. For more general elements, it is possible to architecture purely numerical techniques that adapt to the singularity [11].

One approximation technique which has been growing popularity amongst scientist and engineers is called mesh free or ‘meshless method’. The mesh free method does not require an element mesh for the purposes of interpolation of the solution variables [12, 13], and has been widely accepted as a useful tool in engineering and mathematics.

A recent numerical computational method for solving PDEs is the method of fundamental solutions (MFS) [14, 15]. The MFS is a meshless method which has been proposed and developed as an approximation approach in [14, 16, 17]. One of the crucial advantages of the MFS is that it avoids the numerical integration of the singular fundamental solution, while the BEM needs special treatment to handle singular integrals.

It should be mentioned that other different boundary-type techniques have been proposed. One of these methods is the boundary node method (BNM), which can be considered as a method that combines the BEM with the moving least squares (MLS) technique [18–21]. The least squares method (MLS) is also a meshfree approximation that does not need any meshing of the interior domain.

1.2 Research Motivation

The motivation behind this work is to develop new BEM formulations for two-dimensional steady-state and transient convection-diffusion-reaction problems with constant and variable velocity. The BEM is implemented in this work and combined with the radial integration method (RIM) and the dual reciprocity method (DRM) to handle these complicated problems.

1.3 Research Aims and Objectives

A BEM formulation for the solution of the PDE governing the two-dimensional convection-diffusion-reaction equation will be presented, developed theoretically and implemented numerically. We will proceed by presenting the work for both two-dimensional steady-state and transient convection-diffusion-reaction problems with constant and variable velocity. The corresponding non-homogeneous problem with constant and variable source term is also formulated and solved successfully. A graphical demonstration of the number of published materials on the BEM for convection-diffusion-reaction problems from 2008 to 2018 is shown at the top of Fig. 1.1, while the bottom left of the figure represents the number of published papers according to the subject area and finally, the bottom right part shows the percentage of each number of published materials according to documents type, i.e. conferences and journal papers. The source of these figures is Scopus®, the comprehensive search engine provided by Elsevier B.V. There are very few papers published on the BEM

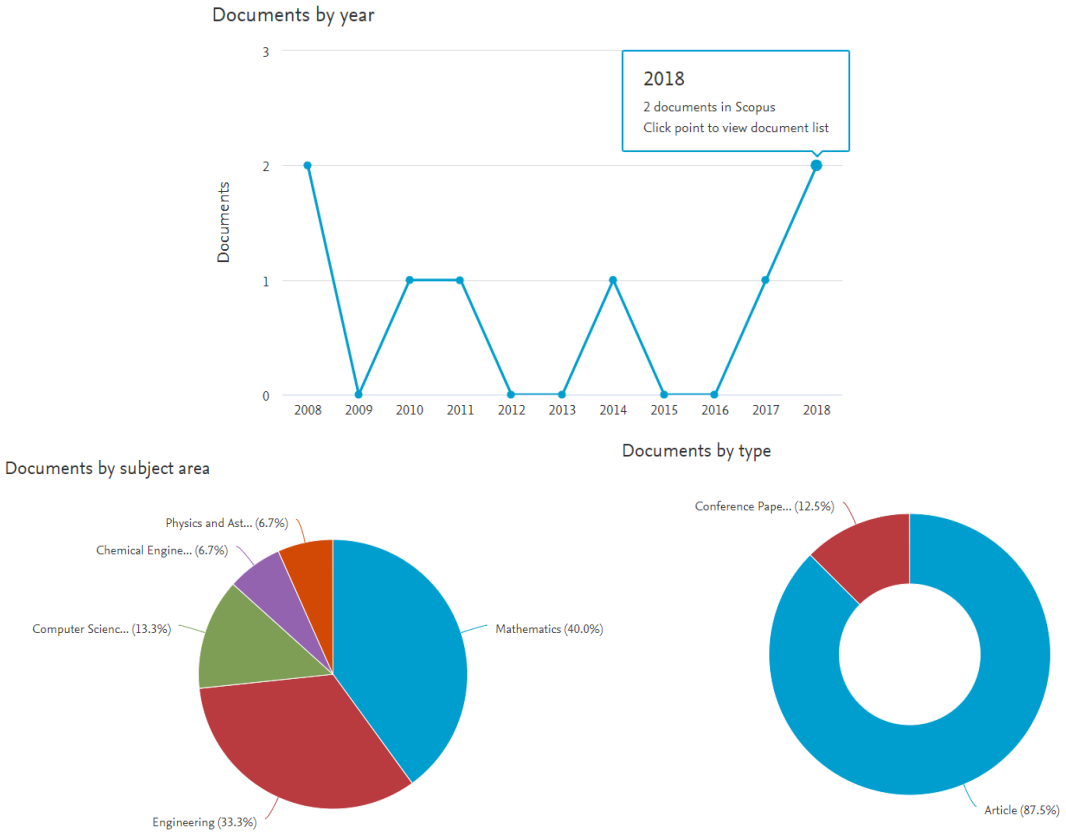

Figure 1.1: Number of published paper in last ten years for different subject area and types on BEM for convection-diffusion-reaction problems, from 2008-2018 according to Scopus®

for convection-diffusion-reaction problems, which indicates that there is a need to introduce an effective solution to deal with these kind of problems using BEM.

1.3.1 Research Aims

This thesis aims to develop innovative numerical formulations for 2D steady-state and transient convection-diffusion-reaction problems with constant and variable velocity using the boundary element method (BEM), combined with two different approaches which are the dual reciprocity method (DRM) and the radial integration method (RIM). The study also aims to provide good insight into the proposed techniques used for the convection-diffusion-reaction models. Through the development of novel numerical methods, the effects of boundary conditions, internal points, velocity field, reaction coefficient and concentration

profile should be quantified and their relative effect in the proposed model assessed. Although this study is concerned with the convection-diffusion-reaction problem in isotropic media, the numerical methods are developed with general applicability to steady-state and transient transport problems in fluid flow and heat transfer. All numerical methods in this study are coded and programmed by the author using the Matlab® package for both regular desktop PC architectures and laptop.

1.3.2 Research Challenges and Objectives

The proposed schemes are shown to produce very good results amongst the different aspects, trends and challenges that are concurrent with BEM, such as developing the formulation, convergence, efficiency and implementation for convection-diffusion-reaction problems. The main objective of this work is to develop suitable and powerful approximation methods for different numerical models, for instance, steady-state, transient and non-homogeneous problems. The formulations are applicable and convenient to fit the 2D convection-diffusion-reaction problems with constant and variable velocity fields, and constant and variable source terms at different values of the non-dimensional Péclet number.

Some difficulties and challenges are demonstrated in this thesis:

- How does the BEM formulate and solve the two-dimensional steady-state convection-diffusion-reaction problems numerically with constant velocity field? How does it handle the singularity included in the formulation? Is it possible to avoid the oscillations and damping occurring in other numerical techniques such as FDM and FEM?

- How can the previous formulations of the 2D steady-state convection-diffusion-reaction problem be extended to treat variable velocity fields? Furthermore, how does the DRM with different RBFs can improve the numerical outcomes in terms of boundary-only solution?

- The derivation and formulation of the 2D transient convection-diffusion-reaction problem with constant velocity field is considered as a difficult challenge. How can we approximate the time-derivative term of the corresponding equation?

- Can the new formulation for this type of problems be extended to variable velocity fields with good accuracy and convergence? How could the DRM with different radial basis functions handle the transformation from domain integral to boundary-only integration without losing the advantage of reducing the dimension by one?

- How can the 2D non-homogeneous convection-diffusion-reaction problem with constant and variable source-free terms be formulated?

- How does the error caused by the discretisation in the mathematical modelling of the 2D steady-state and the transient convection-diffusion-reaction problem with constant velocity field be minimised in these formulations? Do such formulations show good accuracy and convergence for the entire range of numerical simulations?

To deal with the above challenges effectively, the following objectives are briefly presented:

- The present study presents a model for the numerical simulation of 2D steady-state convective-diffusive-reactive problems. The BEM is employed with the fundamental solution for the convection-diffusion-reaction equation with constant coefficients. Besides, the significant advantage and robustness of the BEM permitted us to implement it for this kind of problems, and the accuracy and efficiency of the technique is evaluated with good agreement between numerical results and the corresponding analytical solutions. Test examples were solved with low, moderate and high values of the Péclet number up to 10^3 for assessing the accuracy of the numerical results.
  It should be stressed that, when the velocity field is significant compared to the diffusivity (i.e., high Péclet numbers), the DRM approximation in the present form fails to properly reproduce the perturbation terms and the accuracy of the solution degrades. In these situations, one must resort to domain discretisation.

  This work has adopted an efficient numerical integration scheme suitable for weakly singular integrals which appear in boundary element formulations for convection-diffusion-reaction problems with low and high Péclet numbers. The weakly singular integral was evaluated by using Gauss quadrature with a cubic transformation developed by Telles [22], the Jacobian of which cancels the singularity.

- Next, mathematical modelling of the two-dimensional steady-state convection-diffusion-reaction problem with variable velocity field is developed.

  The DRM is adopted to handle the variable velocity field of the convective terms using an approach that expands the concentration as a series.

  Thin-plate splines (TPS-RBF), multiquadric radial basis function (MQ-RBF) and cubic radial basis function (Cubic-RBF) have been implemented for all test cases.

- A novel formulation of the DRBEM for the 2D transient convection-diffusion-reaction problem with variable velocity field was developed and implemented.

  The boundary transformation for domain integrals consisting of unknown functions is accomplished with the use of RBFs.

- A novel formulation for the 2D non-homogeneous convection-diffusion-reaction problem with constant and variable source terms is developed by employing the RIM. Implementation and validation of the new RIBEM formulation for low and moderate values of the Péclet number is described for isotropic inhomogeneous media.

1.4 Thesis Structure and Original Contributions

After this introductory chapter, the thesis is structured as follows. In each chapter, a detailed literature review pertaining specifically to the content of the chapter is given. At the end of each chapter a brief summary is also presented. References for each chapter are included in a single bibliography at the end of the thesis. This chapter details some discussions on the background and rationale of the research, objectives of research, scope of the study and chapter organization.

- In **Chapter 2**, a comprehensive literature survey and theoretical background for the BEM are documented.

- A mathematical formulation for the solution of 2D steady-state convection-diffusion-reaction models with constant velocity is developed in **Chapter 3**. The method is

validated on several transport problems using constant elements, for steady-state convection-diffusion problems with reactive term in an isotropic medium. The singularity which appears in the formulation has been treated utilising Telles' technique. Different problems are solved with various boundary condition types such as Dirichlet, Neumann, mixed and Robin boundary conditions.

- **Chapter 4** describes the development of the DRBEM for 2D steady-state convection-diffusion-reaction problems with variable velocity fields. The DRBEM plays a crucial role to transform the resulting domain integral into corresponding boundary integrals using different radial basis functions (RBFs). Three RBFs, thin-plate spline (TPS), multiquadric (MQ) and cubic radial basis functions (Cubic) are derived and applied in all the following chapters.

  The DRBEM is implemented for 2D transient convection-diffusion-reaction problems with constant velocity in **Chapter 5**. Different problems are solved with various domains and boundary conditions types such as Dirichlet, Neumann, mixed and time-dependent boundary conditions at different initial concentrations in an isotropic medium. These models and the numerical methods allow the transient convection-diffusion-reaction equation to be explored for the first time in the context of various flows. To ease the computational cost imposed by the transient solution, an FDM time-marching scheme is utilised to handle the first-order time derivative.

- In **Chapter 6**, novel DRBEM formulations are developed and applied to the 2D transient convection-diffusion-reaction problems with variable velocity. The velocity field is treated by decomposition into average (constant) part, which is included into the fundamental solution of the corresponding equation with constant coefficients, and a perturbation (variable) part which is treated using a dual reciprocity approximation.

  The effects of the DRBEM and using low and high numbers of boundary elements and internal points on the transient solutions are explored at the early and late time levels of this type of problem. Through the development of a novel numerical formulation, the effects of increasing and decreasing the time step Δt are also examined. This chapter

concludes with different time scale simulation results of 2D convection-diffusion-reaction problem using DRBEM.

- **Chapter 7** is concerned with the development and application of the RIM to formulate 2D convection-diffusion-reaction problems with constant and variable source terms. This chapter represents the first attempt to solve this type of transport problems using RIBEM.
- Finally, the thesis is concluded and the findings discussed in **Chapter 8**, alongside the recommendations for future work.

Chapter 2

Background and Literature Review

2.1 Introduction

The origins of the boundary integral equation method, better known as the boundary element method (BEM), are found in Green's paper in 1882. Fredholm in 1903 made a rigorous study of integral equations which formed the basis of the numerical procedures developed later. The treatise by Kellogg (1929) presents much of the underlying material and ideas are also discussed by Muskhelishvili (1953) and Mikhlin (1957) [23, 24].

In 2005, a good historical account of the development of the BEM with short biographies of the major contributors has been given by [25]. One can view BEM as the numerical implementation of boundary integral equations based on Green's formula, in which the piecewise element concept of the FEM is utilised [26]. Even more broadly, BEM was used as a generic term for a variety of numerical methods that use a boundary or boundary-like discretisation [27]. The most substantial feature of the BEM is that it requires only the discretisation of the boundary rather than the domain, which makes the discretisation steps much easier.

In the modern day, the method has gained quite considerable popularity and is being incorporated into fast computer algorithms useful to the practicing analyst [28]. In contrast, some researchers and pioneers believed that the BEM occupies a less prominent role in engineering than its features and capability deserve due to the complexity of the mathematical background

[29]. More introductory discussions on this subject can be found in [30].

This chapter starts with the background for the BEM and gives a full explanation of the proposed method in section 2.2. Section 2.3 shows a research overview for the different types of domain approximation techniques. Then, section 2.4 presents a comprehensive study of the BEM. Next, section 2.5 highlights the DRM technique, while section 2.6 highlights the RIM approximation used in this work. Section 2.7 illustrates the BEM researches for the steady-state convection-diffusion-reaction problems. After that, the research on BEM for transient convection-diffusion-reaction problems with constant and variable velocity fields are presented, with extensive research study in section 2.8. Furthermore, section 2.9 describes a research study of BEM for non-homogeneous convection-diffusion-reaction problems with variable and constant source term. Finally, section 2.10 gives a brief summary of this chapter.

2.2 Background

Transport of pollutants in surface water and ground-water is a complex physical phenomenon, especially if an effort is made to cover all aspects of the transport processes involved. The convection-diffusion equation is one of the most basic governing equations describing macroscopic phenomena in classical physics, which is useful in various fields of science and engineering [31]. However, it is still difficult to numerically solve the convection-diffusion equation when the convective term is dominant.

The relative influence between the convective diffusion components is described by a non-dimensional number named Péclet number, Pé $= |v|L/D$, where v is the velocity, D the diffusivity and L a reference length.

Many physical processes in engineering can be modelled using the convection-diffusion equation, for instance, the transport and dispersion of pollutants in ground and surface water, diffusion in semiconductor devices, traveling magnetic fields and magnetohydrodynamics, etc. In the heat transfer field, the problems of crystal growth, laser-assisted surface hardening, metal cutting, casting and forming, etc, are engineering applications. A substantial number of numerical models for the convection-diffusion equation has been presented in the

literature. Most of these engineering models utlise either the FDM or FEM of solution, and give emphasis on algorithms to suppress the well-known phenomenon of 'artificial diffusion' intrinsic to these techniques [32].

With respect to the importance of hydrodynamic dispersion process studies, in water quality management and pollution control, particularly in aquifers, dispersion has been referred to as a hydraulic mixing process by which the waste concentrations are attenuated while the waste pollutants are being transported downstream. The concentration profile behaviour with space and time is described by a PDE of parabolic type known as advection-diffusion equation. This equation is equally important in soil physics, bio-physics, petroleum engineering and chemical engineering for describing similar processes.

This study is concerned with the development of accurate and efficient techniques for solving linear PDEs such as the steady-state convection-diffusion-reaction problems in 2D domains. The methodology is investigated in the context of a BEM approach which involves singular kernels. It is well established that boundary-value problems with known Green's functions admit integral formulations which lead to very effective numerical schemes. The advantages of these BEM algorithms are classified as follows:

(i) there is no need of domain discretisation, only boundary mesh generation is required.

(ii) the singularities in the kernels, when properly handled, lead to a discretised well-conditioned system of algebraic equations.

One must bear in mind that applications of the BEM to steady-state and transient convection-diffusion have shown that the BEM appears to be relatively free from numerical problems such as oscillations and damping. However, since the BEM formulation requires the evaluation of singular integrals, oscillations may develop at high values of the Péclet number if this integration is not properly carried out.

In 1988, Tanaka *et al.* [33] attempted to establish a relationship between the Pé number and the size of elements in the discretisation, while Enokizono and Nagata [34] showed that, if standard Gauss integration is used for high Pé number, the required number of integration points may be of the order of thousands, that will affect the computational efficiency of the method. More recently, Zagar *et al.* [35] developed an efficient numerical integration scheme

and presented results for values of Pé up to 10^6.

Banerjee and Shi [36] developed a different integration scheme (partly analytical) and presented results for Pé up to 10^4 although they stated that at Pé $= 10^4$, quadratic boundary elements were required in order to obtain accurate solutions.

Zakerdoost and Ghassemi [37] presented a formulation of the BEM in which the DRM was employed for solving the 2D steady-state convection-diffusion-radiation problem. The considerable advantage and the efficiency of the DRBEM allowed them to apply it for this transport-type problems with variable velocity coefficient. Good accuracy and efficiency for this proposed approach were achieved and the agreement between numerical results and the analytical solutions was very good.

Rap *et al*. [38] were concerned with the approximation solution of convection-diffusion problems with variable coefficients associated with an inverse source. They implemented the DRBEM combined with an iterative Sequential Quadratic Programming (SQP) approach to identify the locations and strengths of several point sources. As the number of sources needs to be estimated a *priori*, there are three possible test cases, namely correct, over and under estimation of this number. These three situations are numerically studied and an investigation of the stability of the proposed numerical technique is performed by adding random noise into the exact input data.

Cholewa *et al* [39] described a 2D diffusion-convection boundary problem which models a continuous casting process of a pure substance (e.g. copper). They used the BEM in both liquid and solid subdomains separated by a phase change front. The location of the phase change front is unknown and has to be updated during the iteration process utilising a front tracking algorithm. The solution procedure involves the total derivative of the temperature and relevant sensitivity coefficients to find a correct position of the phase change front. In order to considerably reduce the number of degrees of freedom in the front tracking algorithm, the position and shape of the phase change front is interpolated by a small number of Bezier segments. Numerical examples show the main features of the developed algorithms.

2.3 Domain Integral Approximation

Over the past decades, several techniques have been proposed in the literature to deal with domain integrals. Some of difficulties that have to be faced, when numerically modelling convection-diffusion-reaction problems, are related to the different characteristics of the processes involved. The conventional techniques used to treat diffusion problems cannot simply be extended to convection-diffusion-reaction problems, if flows at moderate and high Péclet number are considered. This situation was already recognised by finite difference practitioners in the early 1950s, when successful applications of the method to diffusion-dominated problems, like heat conduction or tidal motion, could not be reached for solving problems involving non-symmetrical operators. The standard central difference approximation leads to oscillatory solutions. The problems were mitigated but not completely overcome by the use of upwind differencing.

An extensive bibliography on this subject can be found in [40]. Some authors reason that the non-symmetry of the convection operator does not allow it to be encompassed by the variational theory which forms the basis of success in the symmetric case [41].

Christie *et al*. [42] seem to be the first to demonstrate how finite element analogues of unwinding differencing could be applied to convection-diffusion modelling. Different trial and test functions are utilised, i.e. a Petrov-Galerkin weighted residual FEM. Following that, Huyakorn [43] and Heinrich *et al* [44] developed methods for 2D problems. Heinrich and Zienkiewicz [45] extended the upwind approach to quadratic elements. Christie and Mitchell [46] described the construction of higher order methods and several other papers were published extending the ideas in a variety of directions.

In several chapters in Gallagher *et al*. [47], Hughes [48] and Anderson [49], a good survey of the early development in this area can be found. Several approaches have contributed to the solution of the problem. In the majority of them the presence of spurious oscillations is reported for significantly convection-dominated flows, characterised by a high Péclet number. Donea [50] seems to have improved the stability properties, phase accuracy and reduced numerical damping of Petrov-Galerkin scheme through the use of the Taylor-Galerkin technique for convective-type transport problem. In this scheme, a forward-time Taylor series

expansion is used including time derivative of second and third order, and also the spatial derivatives derived from the original convection equation. This process yields a generalised equation discretised in time only, where the spatial variable is continuous. The problem is later discretised in space by using conventional Bubnov-Galerkin FEMs.

The Taylor-Galerkin technique is third-order accurate in time. It has all the advantages of the Petrov-Galerkin methods whilst allowing straightforward generalisations for higher dimensions [51, 52]. On the other hand, Carey and Jiang [53] utilised least-squares finite elements for the first-order hyperbolic systems. They showed that the semi-discretised equation of the least-squares method is very similar to the one of the Taylor-Galerkin scheme.

Then, Park and Liggett [54] proposed the Taylor-least squares method as a direct generalisation of the Taylor-Galerkin and least-square FEMs. Higher-order spatial derivatives in this formulation necessitate higher-degree polynomials, and Hermite cubic shape functions are employed to this end. The authors claim that the technique is free of numerical crosswind diffusion and offers straightforward generalisation to higher dimensions.

Yu and Heinrich [55] presented, for the transient case, an extension of the Petrov-Galerkin method developed for the steady-state convection-diffusion case in one dimension. This was accomplished by means of time-space elements. Two parameters were introduced in the weighting function which can be precisely calculated locally on each element to optimise accuracy. Later, the authors extended the technique for multidimensional, convection-diffusion equations.

Westerink and Shea [56] examined the influence of using, for the test function, polynomials two degrees higher than the ones used for the trial functions. It is advocated that it yields dramatically improved solutions which seem to get better as the Courant number increases to 1.

Li [57] utilised the approach of characteristics combined with the method of least-squares to handle the advection equation by the FEM. Fourier series analysis is implemented to show stability and accuracy even when linear basis functions are employed. However, it was found that better results are obtained when C^1 continuous Hermitian cubic basis functions are used. Although it appears that a tighter control of the mesh size and time-step, possibly in conjunc-

tion with upwinding or other techniques, may be effective in enforcing stability and reducing spurious oscillations [44, 58], it seems that some controversy still exists [59] concerning whether or not the oscillation-removing techniques are not giving away vital information about the modelling [60].

These facts reported in the early stages of Finite Element applications stimulated researchers of BEMs to develop algorithms for the solution of this tenacious problem that became itself a challenge in the field of numerical modelling.

2.4 Boundary Element Method

Over the past 40 years, numerous papers have been published on the BEM [30]. The underlying principle of the BEM can be defined as a combination of both the classical integral equation technique and a numerical interpolation technique [61].

The BEM is a suitable method for solving PDEs, for which it only demands a discretisation of the boundary of the domain [62]. The approximate solution of boundary value problems for PDEs became possible since 1960 [25], because of the invention of the computer and the development of the first high level programming language.

The BEM at all times needs a fundamental solution to the original differential equation to avoid obtaining domain integrals in the formulation of the BIE, which is considered as one of the disadvantages of the method. These methods have appeared under different names such as panel methods, surface singularity methods, boundary integral equation methods. By 1970, efforts were being made to make the BEM more applicable. At the beginning of 1973, Jaswon worked on boundary elements in the field of elasticity [63]. Researches into boundary elements have been sharply increased between 1980 and 1990. Several textbooks were written during this period [9, 1, 23, 30].

The BEM is now firmly established as a significant numerical method and it offers an excellent platform for learning and teaching a computational method for solving problems in physical and engineering science.

Until the beginning of the eighties, the BEM was mostly known as Boundary Integral Equa-

tion Method (BIEM) [64]. There is no doubt that the FEM is much more widely used than the BEM and that the computational development of the BEM is more recent. There is a large quantity of finite element legacy codes in industry and this itself is a disincentive to move to new techniques. It is not so clear, however, if the FEM precedes the BEM.

In engineering practice, the BEM is useful for very large domains where a FEM approximation would have too many elements to be practical [65]. Probably the major disadvantage of the BEM is that the solution of the system of equations is expensive for large problems. However, with the recent development of 'test' solvers, e.g. multipole [66] and wavelet [67], such difficulties are less significant. In general, the two techniques complement one another. The FEM offers a more general approach to solving field problems whereas the BEM is somewhat specialist, e.g. it performs exceptionally well in areas such as acoustics and fracture mechanics.

Presently, the BEM is a very active field of study especially within the engineering community, and it is experiencing very rapid development in research and applications worldwide. The following are some points of view about the features and the capability of BEM from researchers. One of the most interesting features of the BEM compared with FEM is the much smaller system of equations and the considerable reduction of the data required to run a program. Moreover, the numerical accuracy of the method is generally greater than that of FEM [28]. The BEM has emerged as a powerful alternative to FEM, particularly in cases where better accuracy is required due to difficulties such as stress concentration or where the domain extends to infinity [68]. The BEM is a well established numerical technique by now, as an accurate and powerful numerical technique in continuum mechanics [69].

Domain decomposition ideas have been applied to a wide variety of problems. We could not hope to include all these techniques in this work. For an extensive survey of recent advances, we refer to the proceedings of the annual domain decomposition meetings (see http://www.ddm.org).

Domain decomposition algorithms are divided into two classes, those that use overlapping domains, which are referred to as Schwarz methods, and those that use non-overlapping domains, which we refer to as substructuring. The subdomain BEM technique was developed

with the target of reducing memory and computer time requirements of BEM computations. The subdomain technique has been applied in different areas in engineering and mathematics, for instance, heat transfer, linear elasticity, heat conduction, fluid flow, etc, [70–72].

The boundary-domain integral equations methods (BDIEs) are called segregated BDIEs when the unknown boundary functions are considered as formally unrelated to the unknown functions inside the domain while for the united BDIEs, the unknown boundary functions are related to the unknown functions inside the domain. The analysis of segregated and direct united BDIEs were discussed in [73, 74]. More details about the BDIEs existence, uniqueness, regularity and the asymptotic behaviour of the solution can be found in [75]. On the other hands, BDIEs lose the advantage of the dimensionality reduced by one, such as for BIEs, because they do not only have the boundary integrals but domain integrals concurrently. For the numerical solution of the BDIEs, discretisation is needed not only for the boundary but also for the domain itself. This leads the discretised BDIEs to systems of equations of the same size as obtained from FEM but in contrast to the FEM, the system of linear algebric equations will be non-symmetric and fully populated. It should be remarked that the parametrix (Levi function) represents a replacement for the fundamental solution, which means that if it is singular then it needs more extensive computations in comparison with FEM (see [76, 77]).

The second kind of methodology is to avoid the discretisation of the domain and transforming the domain integrals into equivalent boundary integrals. The frequently utilised transformation technique is the dual reciprocity method (DRM) developed by Nardini [78]. In this method, the transformation is carried out by using particular solutions, which is not easy to apply for complex problems [8, 79, 80].

This technique approximates part of the integrand using radial basis functions (RBF) to approximate the unknown variables which enable the transformation of the domain integrals that includes unknown variables to the boundary. For the more details of RBF, see [8, 81–83].

A new powerful transformation technique, called radial integration method (RIM), has been developed by Gao [84, 85] and applied to many problems in physics, engineering and mathematics. It is simple to implement and it can transform any domain integrals into equivalent

boundary integrals after removing the singularity which appears in the formulation.
Takhteyev and Brebbia [86] suggested an analytical method to transform the domain integrals over cells to the cell boundary. The integrals over the cell boundary can be calculated analytically which makes this approach efficient and accurate. However, this method still needs domain discretisation. Brebbia (1978), Power and Wrobel (1995), Wrobel (2002), Aliabadi (2002), Schanz *et al.* (2007), Ang (2007), Zalewski (2008) and Katsikadelis (2016) developed different applications of the boundary element formulations for many kinds of PDEs for elliptic, parabolic and hyperbolic equations in [87, 9, 1, 24, 88–90].
A brief comment on the popularly used methods described above is made as follows:

- Dual reciprocity method (DRM). This technique can handle general problems, but it demands particular solutions. It may be very difficult to obtain the particular solutions for some complicated three-dimensional (3D) problems. In addition, even for known body force problems, this method still requires an approximation function. Therefore, the computational results are not as accurate as other methods.

- Multiple reciprocity method (MRM). As an extension of the idea of DRM, Nowak and Brebbia developed a powerful technique called the multiple reciprocity method (MRM) to solve Poisson and Helmholtz equations [91]. Afterwards, this method was extended to solve the Navier equations of elasticity by Neves and Brebbia [92] and to solve elastoplasticity problems by Ochiai and Kobayashi [93]. This approach is very robust, but it may be hard to compute the primitives in the recurrence formula governed by the Laplace operator. Moreover, this technique requires defining a constant contained in the displacement fundamental solutions. Different values of this constant may produce different findings. The technique is comprised of a repeated implementation of the reciprocity theorem utilising a sequence of higher order fundamental solutions to transform the domain integrals to the boundary. As a result, the method can lead in the limit to the exact boundary only formulation of the domain integrals. The resulting recurrence formula, while increasing the order of the fundamental solution, reduces the order of the polynomial representing the body forces [92].

- The Galerkin Vector Technique. This method provides accurate findings, but it should be stressed that it can be implemented just for linear and constant body forces [10, 23, 92].

- Analytical integration method. This method analytically transfers the domain integrals to the boundary, thus, it can save remarkable computational time when compared with other methods. When the internal points are close to the boundary, accurate results can still be obtained. The drawback of this technique is that only straight-line elements can be utilised. For curved line elements or surface elements, it may be quite difficult to derive analytical expressions. Furthermore, for the cases of complicated regions or body forces, this approach demands dividing the field into subdomains and approximating the body forces by polynomials in each subdomain. Therefore, this method is an approximation method and not convenient to code for different cases in a unified way.

- The Fourier Expansion Technique. The Fourier expansion method is not straightforward to implement in most cases as the evaluation of the coefficients can be computationally cumbersome, therefore, the technique has been employed with some success to relatively simple cases [94, 95].

- Loading Boundary Technique. This technique was developed by Azevedo and Brebbia [84, 85] for potential problems and consists of replacing the integral corresponding to any sources acting on an internal region into equivalent sources distributed on the boundary of that region by using particular solutions [96].

- Radial Integration Method (RIM). In this approach, a domain integral is transformed into an equivalent boundary integral by use of straight-path integrals emanating from the source point. In general, these straight-path integrals are carried out numerically. However, the development of the RIM still requires an in-depth mathematical scrutiny. A somewhat similar technique can be found in [84] wherein the straight-path integral or radial integral is computed exactly owing to the simple form of the RBFs used to expand the source term.

2.5 Dual Reciprocity Method (DRM)

Over the past decades, many different techniques have been proposed in the literature to deal with domain integrals without discretising the computational domain into volume elements or internal cells. The DRM was proposed by Nardini and Brebbia [97]. This method, which approximates the body force effect by a series of prescribed basis functions, transforms the domain integrals to the boundary employing particular solutions derived from the differential operator of the problem.

The merits of this approach are that it needs neither to evaluate any volume integral nor to perform eigenvalue searches. As such, it opened a wide range of applications for the BEM, including the extension of the described technique to many types of engineering, physics and mathematical problems. To date, the DRM is the most popular approach used to transform domain integrals into boundary-only integrals. Further, the accuracy and efficiency of the DRM approach depend largely on the distribution and location of the RBFs used to handle the source term.

2.6 Radial Integration Method (RIM)

An efficient approach for evaluating two- and three-dimensional domain integrals named the RIM was presented by Gao [85]. This approach is based on pure mathematical treatments and can transform any domain integral into an equivalent boundary integral by use of straight-path integrals emanating from the source point. The RIBEM has been successfully implemented to linear thermoelasticity, elastic inclusion problems, creep damage mechanics problems, transient heat conduction problems and viscous flow problems [98–102]. Although the RIM is very robust and flexible in transforming domain integrals into equivalent boundary integrals, the evaluation of the radial integrals numerically is very time-consuming, especially for large 3D problems [103].

The RIBEM was implemented and developed for 2D and 3D dynamic coupled thermoelastic problems [99]. The BDIEs for the dynamic thermoelastic equations are mathematically derived utilising the weighted residual method. The elastostatic and steady-state heat con-

duction fundamental solutions are employed in deriving the integral equations for dynamic coupled thermoelastic problems and this approach yields domain integrals appearing in the resulting integral equations. They discretised the problem surface and transformed it into a system of time-dependent linear algebraic equations, which is handled by the standard Newmark time-integration method. Numerical findings for various tests are given to represent the efficiency and the accuracy of this numerical formulation.

Yao *et al.* [100], developed a RIBEM with a step-by-step integration method for solving non-Fourier heat conduction problems. Firstly, the system of second-order ordinary differential equations is obtained by using the RIBEM to discretise the space domain. Then, they implemented the Newmark method and the central difference method to solve the system of ordinary linear differential equations with respect to time. They tested several numerical examples with laser heat sources to demonstrate the performance of the proposed method.

Yang *et al.* [101] described a new approach using analytical expressions in the RIBEM for solving three types of representative variable coefficient heat conduction problems. This approach can improve the computational efficiency considerably and can overcome the time-consuming deficiency of RIBEM in computing radial integrals. The fourth-order spline RBF was employed to approximate the unknowns appearing in the domain integrals arising from the varying heat conductivity. The RIM is used to transform the domain integrals to the boundary, which results in a pure boundary discretisation algorithm.

Yu *et al.* [102] proposed a new BEM approach for solving one-phase solidification and freezing problems based on the RIM. The Green's function for the Laplace equation is adopted in deriving basic integral equations for time-dependent problems with constant heat conductivities and, as a result, a domain integral is involved in the derived integral equations. Based on the FDM, an implicit time marching solution scheme is developed for solving the time-dependent system of equations. Front-tracking method is used to simulate the motion of the phase boundary. To accomplish this purpose, an iterative implicit solution algorithm was developed by employing the RIBEM. They validated the proposed method by two typical examples to show the results in comparison with semi-analytical solutions.

Recently, Hai *et al.* [104] have implemented the RIBEM to solve steady convection-

conduction problem with spatially variable velocity and thermal conductivity. The temperature boundary integral equation is derived by employing the fundamental solution for the potential problem, which results in the appearance of domain integrals including the unknown temperature. They used RIM and approximated the normalized temperature with the use of a compactly supported fourth-order spline radial basis function combined with polynomials in global coordinates to transform the domain integrals to the boundary, avoiding the evaluating of domain integrals.

2.7 BEM For Steady-State Convection-Diffusion -Reaction Problems

The study of mass and energy in solids and fluids is of fundamental importance in a great number of fields in science and technology. The numerical solution of convection-diffusion-reaction problems is a real challenging task for all numerical techniques due to the nature of the governing equation, which contains a non-dissipative (convective) component and a dissipative (diffusive) component. According to the value of the Péclet number, the equation is elliptic or parabolic (for diffusion-dominated processes, low Pé) or hyperbolic (for convection-dominated processes, high Pé). Generally, standard numerical methods can easily solve the former but not the latter.

Ikeuchi and Onishi [31] seem to be the first to develop a formulation for convection-diffusion considering the BEM. Ikeuchi *et al*. [105] formulated a BEM approach for steady-state convective diffusion equation with Dirichlet boundary conditions. A simple example is considered in 3D using constant elements. Some results were presented for a global Péclet number of 80 and a local one of 16.

Fundamental solutions for convection-diffusion problems are only available for cases with constant velocity or very simple velocity variations. Because of that, boundary element researchers have in the past not been able to confine their discretisation procedures only to the boundary of the studied domains for general convection-diffusion problems involving variable velocity fields. The author decided to investigate this problem in depth trying to find

alternative solutions which could result in a boundary-only technique.

Brebbia and Sǩerget [106] developed a BEM formulation to solve steady-state and transient convection-diffusion problems applying the fundamental solution to the associated diffusion problem and discretising the domain with cells to consider the convective effects which were simulated as equivalent source distributions.

Ikeuchi [106] applied the steady formulation for orthotropic materials using constant boundary elements. Okamoto [107] included a first-order chemical reaction in the convection-diffusion process and solved the steady case using constant boundary elements. As a chemical reaction was taken into account, the usual conservation laws used for the evaluation of the diagonal terms, avoiding singular integrals, can no longer be applied. He calculated the diagonal terms using Gaussian quadrature with as much as 20 integration points.

Taigbenu and Liggett [108] applied an integral method to solve the advection-diffusion equation for the transport of pollutants in porous media. The fundamental solution used was the one for Laplace's equation. This procedure produced boundary integrals corresponding to those terms while the remaining, convective terms were integrated over the solution domain, weighted by this fundamental solution. The domain was then discretised into triangular cells, and internal unknowns included in the solution process.

Okamoto [109] improved the accuracy of the evaluation of the singular integrals in his previous work [107], by applying a splitting technique to the Gaussian quadrature. As constant elements were being used (with the node at the centre of the element), the singular integration for the diagonal terms was carried out in two parts: From the centre to the right and from the centre to the left extreme of the element, avoiding the singularity at the central node. Through this technique, the number of integration points is reduced when compared to the conventional scheme of integration over the whole element, for the same level of accuracy.

Wrobel and DeFigueiredo [110] proposed a boundary element formulation for steady-state convection-diffusion problems with variable velocity fields using linear elements. In this formulation, the fundamental solution of the corresponding equation is used. The formulation allows the numerical solution to be represented in terms of boundary values only. Numerical applications have shown that the formulation produces satisfactory results for problems

where the velocity field is small (i.e. diffusion-dominated problems).

Grigor'ev [111] described a new BEM technique for solving equations of the convection-diffusion type. The whole domain is divided into K subdomains, in which the convective velocity is expressed in the form of a constant and a variable velocity sum. For the resulting differential operators, the known fundamental solution of the convection-diffusion equation is used. The employment of such fundamental solutions in a steady-state case allows to obtain a boundary integral equation, involving the variables only on the border of the subdomain if the variable convective velocity contribution is not taken into consideration. Employing this method to unsteady problems leads to the appearance of an integral over the subdomain, including that known from the previous time step variables. Written for every subdomain the BEM in 2D or 3D cases may be discretised similarly as it is customary in the BEM technique. Then, the formation of the global matrix takes place and it turns out to be of block band structure. In general cases, both the discretised and global equations system for each subdomain BIE are non-linear. The employment of the Newton-Raphson method for solving non-linear system of equations is obviously less efficient than the employment of a simple iterative procedure, described in [111].

Tanaka *et al*. [112] used mixed boundary elements in steady convection-diffusion problems with a velocity profile in 3D. In this mixed boundary element scheme, potentials are interpolated linearly and their normal derivatives are assumed constant over the elements. In their work, they treated the convection-diffusion equation as a Poisson equation with an additional non-linear inhomogenous term involving the convective term. Consequently, as the fundamental solution used was the one for the adjoint harmonic field, cells had to be used for the resulting domain integral of the remaining terms. The scheme considered, although producing good results, uses cells in the domain and therefore a boundary-only formulation was not achieved. Later on, the scheme was extended to transient analysis [33].

Enokizono and Nagata [34] developed a numerical analysis for 2D convection-diffusion at high Péclet number. In their work, two investigations were carried out to analyse the source of numerical error when the Péclet number was high. The first verified the influence of the approximation on the boundary; it was demonstrated that this influence was small on the

numerical error. The second analysis looked at the influence of the numerical integration error; it was shown that the accuracy of the singular integrations on the boundary elements was very important.

Aral and Tang [113] transformed the equation using the convection-diffusion fundamental solution for the harmonic field and treated the domain integral involving the remaining terms by using a variant of the DRBEM [114, 8]. The integrand of the resulting domain integral is treated according to a scheme called secondary reduction [113] - an expansion of the convective plus time-dependent and reaction terms as a series of functions of position defined at certain arbitrary points and weighted with certain coefficients, function of time. The domain is then discretised into triangular cells and the integration performed numerically over each cell. Some examples were presented for a maximum Péclet number of 20 and compared with standard FDM results, showing good agreement.

Partridge and Brebbia [115] solved the convection-diffusion equation for simple particular cases with constant velocities in steady-state using the DRBEM. This technique expands the convective terms as a series of harmonic functions, allowing a second application of Green's secondary identity (then dual reciprocity) to take the resulting domain integral to the boundary. This approach succeeds in obtaining a boundary-only formulation although using the fundamental solution for the Laplace equation in this case.

Wrobel and DeFigueiredo [116] proposed a boundary element formulation for steady-state convection-diffusion problems with variable velocity fields. In this formulation, the velocity field is decomposed into an average, which is included into the fundamental solution of the corresponding equation with constant coefficients, and a perturbation which is treated using a DRM approximation. The formulation allows the numerical solution to be represented in terms of boundary values only, and produces accurate results for diffusion-dominated problems with low velocity values.

Gupta *et al.* [117] made a numerical analysis of BEM for steady-state conduction-convection problems with variable velocity field. The spatially varying velocity field is split into constant and variable terms. This gives rise to an accurate representation of the advection characteristics of the problem. They implemented the steady-state fundamental solution based on the

constant part of the convective velocity. Further to the boundary integrals for the constant velocity case, variable velocity needs a domain integral in the BEM formulation. Two different approaches, iterative and non-iterative, were utilised to handle the BEM equation including the domain integral term. The effect of the decomposition level between the constant and variable velocity parts was also investigated. The simulated results obtained from the proposed formulation are first validated versus analytical findings. Some test examples are investigated and a detailed parametric study is conducted to understand the effects of the decomposition level and mesh refinement.

Rap *et al*. [118] developed a mathematical formulation for inverse analysis using the DRBEM combined with the Tikhonov regularisation method, and also with the Truncated Singular Value Decomposition technique (TSVD), to handle the Cauchy problem associated with the steady-state convection-diffusion problem with variable coefficients. The simulated findings gained from the test cases investigated prove that the Tikhonov regularisation method is quite suitable for the smooth geometries considered, for example, circular and annular geometries, whereas for the non-smooth rectangular shape-domain the TSVD technique provides accurate and stable solution behaviour. Their choice for the regularisation and the truncation level is based on the L-curve criterion.

Qiu *et al*. [119] presented an assessment of three alternative BEM schemes for the solution of convection-diffusion problems with variable velocity fields. The two DRM approaches provided satisfactory results when the velocity field is slow (i.e. for diffusion-dominated problems) but may develop oscillations when speeds are high. It appears that the main problem arises in the approximation of the partial derivatives rather than in the function itself; therefore, they used an alternative DRM formulation to avoid the need to approximate partial derivatives. They also implemented a cell formulation which produced very good results even for rapid velocity fields. The formulation, when implemented with the fundamental solution of the convection-diffusion equation with constant velocity, is convergent and does not produce oscillations. The same authors [120] have solved convection-diffusion problems at high Péclet numbers. A new approach to deal with singular integrations is described which allows BEM formulations to be employed and derivatives calculated for problems

with very high Péclet numbers. The authors in [120] were motivated from a problem in electrochemistry to simulate mass and charge transfer in electrochemical cells.The mathematical model includes the combined effects of diffusion, convection and migration for ions concentrations and electric potential, and is described by a coupled system of non-linear equations. The BEM model rewrites these equations as linear convection-diffusion equations with non-linear forcing terms, and solves them iteratively. The iterative process requires the evaluation of the variables and their first derivatives, both along the boundaries and in the domain. Although velocities are normally low (of the order 10^{-2} (m/s)), diffusivities may be of order 10^{-11} $\left(m^2/s\right)$ which, for the typical geometrical dimensions involved, give Péclet numbers of the order 10^6. It should be noticed that a new approach to deal with singular integrations is described which allows BEM formulations to be employed and derivatives calculated for problems with high Péclet numbers. The work starts by isolating the singular integration problem and proceeds to describe the measures taken and a scheme to optimize the integration [120].

Ikeuchi and Sakakihara [105] developed the BEM to solve the steady convective-diffusion equation. A transformation into a self-adjoint or symmetric operator is utilised under a certain assumption, and a boundary integral equation is derived from Green's second identity. For the discretisation of the boundary integral equation, constant or linear boundary elements are employed. Moreover, they employed a simple model problem as numerical experiment, and a comparison with the FEM is given. They show that the BEM solution is stable with respect to large Péclet numbers and has second-order accuracy.

Gregory *et al.* [121] described the BEM to solve the steady-state convection-diffusion problem with constant velocity in a 2D region with a free interface. These problems arise in a number of important heat transfer applications including melting or solidification, for example, food processing, composite production and bulk crystal growth in Bridgman furnaces. The BEM is particularly well-suited to free-surface problems in which the position and shape of the solid-liquid interface are of primary importance. The results are demonstrated for a case study problem representing solidification in a 2D rectangular configuration.

Ravnik and Škerget [122] have derived a boundary-domain integral formulation for steady-

state convection-diffusion problem with variable coefficient. The equation does not contain the gradient of the unknown function, which is the essential advantage of the formulation. This numerical formulation enabled the solution of the convection-diffusion problem with variable velocity field by a single solution of a system of linear algebraic equations. Two discretisation techniques were used to show the validity of the formulation. The classical approach, in which the integrals are computed and their values saved in fully populated matrices, and a subdomain technique, where a domain decomposition method is employed, which gives sparse matrices of integrals. Both methods were found to provide similar performance and accuracy. The memory requirements are smaller in the case of the domain decomposition.

Singh and Tanaka [123] showed an alternative BEM formulation based on an exponential variable transformation for the steady-state convection-diffusion problems. By using this transformation, the convection-diffusion problem converts into a modified Helmholtz equation. A standard BEM formulation is utilised to derive the integral equation for the resulting modified Helmholtz equation. Further, they used three different strategies for the solution of this boundary integral equation. These techniques are: (a) the solution of the modified Helmholtz equation followed by transformation at post-processing stage, (b) inverse transformation before BEM discretisation, and (c) inverse transformation after the BEM discretisation to achieve the discretised equations for the convection-diffusion problem. It is found that strategy (a) is the most accurate and efficient choice for diffusion-dominated situations. Strategy (c) is as accurate as (a), but is of little practical use owing to its computational inefficiency. Furthermore, strategy (b), which is like the BEM formulation using the fundamental solution of the adjoint of the convection-diffusion equation, is the most accurate and efficient approach for convection-dominated problems.

2.8 BEM for Transient Convection-Diffusion-Reaction Problems

In the literature, different numerical approaches are suggested to handle such parabolic PDEs utilising the BEM. These approaches might be classified into two groups: the first is a method which employs the fundamental solution for the convection-diffusion operator, while the second group uses the fundamental solution of Laplace's equation for the diffusive term [124].

Mustafa *et al.* [124] presented a formulation to handle the transient convective-diffusion equation, demonstrating the characteristics and the advantages of the secondary reduction boundary element method (SR-BEM) to reduce the standard BEM formulation to a boundary-only form. For these kind of problems it is shown that the first scheme yields a boundary-only procedure, whereas the second approach necessitates domain-type solutions, thus eliminating the basic advantage of the BEM. In their work, they show that when the first approach is used, the boundary element solution of steady-state convective-diffusion problems yields very accurate results even for high Péclet numbers. When transient problems are studied, if one uses the FDM to numerically integrate the temporal term, then both approaches described above necessitate domain-type solutions which are not desired. They mentioned that, although other procedures exist for boundary-only formulation of time-dependent problems, such as the use of time-dependent fundamental solution and Laplace transform procedures, they are not considered efficient when compared to FDM. Therefore, among the techniques, the FDM solution of the resulting matrix equations is preferred in most cases if computational efficiency is the primary concern. However, this technique necessitates the inclusion of all boundary and interior nodes into the computation process. To overcome this deficiency without sacrificing accuracy and efficiency, a secondary reduction process (SR-BEM) was proposed for the solution of diffusion-dominant parabolic PDEs.

Honma *et al.* [125] presented a formulation named the Regular BEM (R-BEM) to analyse the time-dependent convective-diffusion equation. They dealt with a two-dimensional model as a simple example in order to study stability and accuracy of transient regular boundary

element (R-BE) solutions. They found that R-BEM solutions are unconditionally stable even for the condition that the Courant number $C = v\Delta t/L, C > 1$ and the diffusion number $D_n = D\Delta t/\left(\Delta x^2\right), D_n > 0.5$.

Ikeuchi and Onishi [31] proved mathematically that for transient convection-diffusion problems, boundary element solutions are stable for large diffusion number and Courant number. Their approach was not boundary-only and the domain was discretised into triangular cells to take into account the initial conditions and internal source distribution.

Wrobel and DeFigueiredo [110] presented a boundary element formulation for transient convection-diffusion problems with constant velocity by employing the fundamental solution of the corresponding steady-state equation with constant coefficients and a DRM approximation. The formulation allows the mathematical problem to be described in terms of boundary values only. Numerical results show that the BEM does not present oscillations or damping of the wave front as appear in other numerical techniques.

Chandra *et al.* [126] also developed a BEM formulation for the solution of transient conduction-convection problems. A time-dependent fundamental solution for moving heat source problems is utilised for this purpose. This reduces the governing parabolic PDE to a boundary-only form and obviates the need for any internal discretisation. Such a formulation is also expected to be stable at high Péclet numbers. Numerical examples were included to establish the validity of the approach and to demonstrate the salient features of the BEM.

Cunha *et al.* [127] have developed a BEM formulation for transient convection-diffusion problems. They used the domain boundary element method (DBEM) formulation, even with the counter part of the domain discretisation. Following this reasoning, the solution of problems with variable velocity field appears as a natural development for the BEM formulations, as well as problems with variable reaction term and problems with variable diffusion coefficient. The search for adequate fundamental solutions turns time domain formulations more difficult to cope with, but the elegance of the formulation and the accuracy of the results it produces, justifies facing this challenge. In fact, the key part of their work falls on the development of a time domain BEM formulation. The numerical results were compared with the analytical solution, when available, and with the results from the FEM.

Lim *et al.* [128] introduced a BEM formulation for 2D transient conduction-convection problems. This formulation is based on the time-dependent fundamental solution of the transient conduction-convection operator. Thus, the governing parabolic PDE is reduced to a boundary-only form that does not require any domain discretisation. This makes the proposed algorithm stable and avoids any false diffusion. The boundary-only formulation also requires a small amount of core memory. The 2D BEM is applied to solve a 1D problem whose analytical solution is possible by separation of variables. A standard successive-over-relaxation (SOR) FDM is also applied to the same problem. All of these results are compared to each other. The asymptotic solution for large Pé, where the method of separation of variables fails, is also obtained and compared to BEM and SOR results. They also found that the BEM provides a more accurate solution than SOR for the same mesh size.

Fajie *et al.* [129] derived the time-dependent fundamental solution of transient convection-diffusion problems and documented the first attempt to apply the singular boundary method (SBM) with this time-dependent fundamental solution. The SBM is a semi-analytical meshless method, in which the fundamental solution of the governing equation is employed as the interpolation basis function. The SBM methodology is considered to be mathematically simple and computationally efficient, since it directly simulates transient problems without using a FDM scheme and the DRM. Consequently, compared with the standard steady-state fundamental solution scheme, the present strategy is truly semi-analytical and boundary-only. It is stressed that the proposed SBM scheme has a matrix-free explicit formulation, which means the method requires much less memory and is computationally more stable because it does not need to solve any algebraic equations. Numerical results of 2D and 3D examples involving both regular and irregular domains were examined in detail in their work. The findings indicate that this approach has high accuracy for diffusive and convection-dominant problems, and is convergent with respect to an increasing number of source points. This technique can be considered as an alternative for solution of the time-dependent convection-diffusion problem [130].

DeSilva *et al.* [131] developed a BEM formulation for the transient conduction-convection problem with spatially varying convective velocity field. The general velocity field is decom-

posed into a constant part and a variable part. A transient fundamental solution based on the constant part of the convective velocity is used here. This facilitates accurate representation of the advection characteristics of the problem. The effect of the spatial variation of the convective velocity field is incorporated through a domain integral and an iterative technique is pursued. Comparisons between the analytical solution and the BEM results established the validity of the proposed approach. It is observed that mesh refinement plays an important role when the high Pé number flows give rise to traveling waves with sharp gradient. It is found that BEM is effective at high values of Péclet numbers and can provide accurate results for situations dominated by convection.

Ravnik and Škerget [132] have derived an integral formulation of transient time-dependent convection-diffusion problem with sources and variable velocity field and variable diffusion coefficient. Their formulation does not include the gradient of the unknown function. The formulation was based on the steady-state fundamental solution of the corresponding equation. The problem remains linear and after discretisation it is solved by a single solution of a linear system of equations. They also proposed two different discretisation schemes for 2D and 3D problems. Both are based on the use of the BEM combined with domain integration. The first technique utilised the BDIEM method, which requires the computation of domain integrals and yields a fully populated linear algebraic system of equations. The second approach is derived and implemented as a domain decomposition technique, handling each element as a subdomain and using the BDIEM technique for each subdomain.

Pan *et al.* [133] presented a BEM for the solution of convection-diffusion problems involving phase change and nonlinear boundaries. With this method, the field variables of interest for convection-diffusion problems with constant speed can be formulated along the boundaries only, thereby maintaining the advantage of the traditional BEM. The boundary nonlinearities, such as those caused by nonlinear heat transfer coefficient or radiation to the environment, were handled by a Newton-based method, with the initial guess provided by a few successive substitutions. The internal free boundary was solved by an additional iteration procedure involving an initial guess of the interface for the temperature solution and then subsequent updating of the free boundary shape until convergence is achieved.

Bozkaya and Tezer-Sezgin [134] implemented BEM to solve 2D convection-diffusion-type equations employing the time-dependent fundamental solution of the corresponding problem. The solution of magnetohydrodynamic (MHD) duct flow problems with arbitrary wall conductivity was included in this work. The boundary and time integrals in the BEM formulation are computed numerically assuming constant variations of the unknowns on both the boundary elements and the time intervals. Then, the solution is advanced to the steady-state iteratively. Thus, it is possible to use quite large time increments and stability problems are not encountered. They also examined the time-domain BEM solution procedure on some convection-diffusion problems and the MHD duct flow problem with insulated walls to establish the validity of the approach. The numerical results for these sample problems compare very well to analytical results.

Singh and Tanaka [135] showed an application of the DRBEM to transient convection-diffusion problems. Cubic and augmented TPS RBFs were employed in the DRBEM approximation. Linear multistep methods were employed for the time integration. Numerical findings are shown for the standard case studied of convection-diffusion of a sharp front. Use of TPS yields the most accurate results. However, damping appeared with one step backward difference scheme, whilst higher order methods produce perceptible numerical dispersion for convection-dominated problems.

Andrés and Popov [136] presented a BEM formulation to solve the time-dependent 1D advection-diffusion equation. The 1D solution is part of a 3D numerical scheme for solving advection-diffusion problems in fractured porous media. The full 3D scheme includes a 3D solution for the porous matrix, which is coupled with a 2D solution for fractures and a 1D solution for fracture intersections. As the hydraulic conductivity of the fracture, intersections is usually higher than the hydraulic conductivity of the fractures and by at least one order of magnitude higher than the hydraulic conductivity of the porous matrix, the fastest flow and solute transport occurs in the fracture intersections. Therefore, it is important to have an accurate and stable 1D solution of the transient advection-diffusion problems. This article presents two different 1D BEM formulations for solution of the advection-diffusion problems. The particular advantage of these formulations is that they provide one of the

most straightforward and simplest ways to couple multiple intersecting 2D BEM problems discretised with linear discontinuous elements. Both formulations are tested and compared for accuracy, stability, and consistency.

Romero and Benitez [137] studied a numerical simulation for the 2D convection-diffusion model. A study has been made of the different techniques followed in order to apply an integral equation of the gradient, by means of the BEM, to the convection-diffusion equation. In the analytical setting, the approach of solving both boundary equations for the potential and the gradient of the potential simultaneously is worth mentioning. In this analysis different problems governed by simplified versions of the convection-diffusion problem, with known analytical solution and growing levels of complexity, are formulated in order to validate the gradient equation put forward in this research.

Pettres and De Lacerda [138] show a formulation of the BEM for the study of heat diffusion and advective effects in isotropic and homogeneous media. The proposed formulation utilised a time-independent fundamental solution carried out from the 2D Laplace equation. The first-order time derivative term that appears in the integral equation formulation is handled by a backward FDM. Homogeneous subregions are considered in the analysis of a specific model simulating a non-uniform flow passing by a circular obstacle under internal heat generation. The backward difference scheme is used to approximate the first-order time derivative in the formulations. The numerical findings for the advection-diffusion problem are also obtained from a model containing a circular obstacle with a heat generation source. The source was symmetrically placed in the restricted domain forcing a non-uniform velocity field distribution, which was represented by an approximated analytical velocity field based on an infinite domain. The result of this problem displayed the heat dissipation and transport around the circular obstacle toward the flow direction, representing the coherent advective effect on the diffusive process. For the same problem, it is noticed that the temperature solution in the advective domain close to the source represented good differences depending on the location, for using a set of domain diffusive coefficients and field velocity. Small differences are observed within the heat source close to its boundary. In spite of the need for domain discretisation, the findings demonstrated in the context confirm the efficiency of the

proposed DBEM for computation of time-dependent advective-diffusion problems with heat sources.

Fendoğlu *et al* [139] presented a numerical analysis of the transient convection-diffusion-reaction equation in which the governing equation is transformed into a modified Helmholtz equation by a exponential type transformation and employing the fundamental solution of the modified Helmholtz equation. In the time-discretisation of the problem, two different techniques, namely DBEM and DRBEM, are employed. A fully implicit backward FDM time integration is used to handle the time derivative part. The techniques are different in treating the domain integrals in the formulation, i.e. the domain integral of the DBEM is kept and calculated by quadrature whilst the domain integral is reduced to an equivalent boundary-only integral for the DRBEM approximation implementing RBFs. The numerical calculations are performed for different values of diffusivity for the transient convection-diffusion-reaction problem and the results showed that the DBEM displays more accurate results for only small values of diffusion coefficient compared to the DRBEM.

2.9 BEM for Non-Homogeneous Convection-Diffusion-Reaction Problems with Variable Source Term

Samec and Škerget [140] show a numerical solution of the diffusion-convection equation with source terms based on a BEM formulation using the fundamental solution of the convection-diffusion equation with constant coefficients. Great attention has been dedicated to the numerical solubility of the diffusion-convection transport equation for high Pé number and source term values, when the convection or generation term becomes dominant compared with the diffusion one. The numerical efficiency of the developed numerical implementation is tested against analytical and numerical results for typical test cases of diffusion-convection transport problems with source terms.

2.10 Summary

In this chapter, a comprehensive review of the BEM for convection-diffusion-reaction models has been carried out to discuss the implementation and the mathematical formulations for different engineering and mathematical applications. This comprehensive review gives a full background of the BEM combined with DRM and RIM for several types of convection-diffusion-reaction problems that have been implemented for a wide range of applications.

Chapter 3

BEM Modelling for Steady-State Convection-Diffusion-Reaction Problems with Constant Velocity Fields

3.1 Introduction

The convection transport of mass and heat plays an important role in a great number of technological processes such as continuous casting, cooling in general, single crystal growth, laser-assisted surface hardening, dispersion of pollutants in both air and water, flow in chemical reactors, etc. [141]. In order to conveniently control those processes, it is of great importance to be able to predict with reasonable accuracy the distribution of the field variable such as temperature and concentration. This control will enable the manufacturer to reach the desired specification of the products or in some cases to simulate the possible effects (reactors and pollution) that could result from the processes. The importance of these processes has generated increasing research interest towards the understanding and control of the involved phenomena.

In order to simulate fluid flow, heat transfer, and other related physical phenomena, it is necessary to describe the associated physics in mathematical terms. Nearly all the physical phenomena of interest to us in this work are governed by principles of conservation and are

expressed in terms of PDEs expressing these principles. In the present chapter we will derive and model a typical convection-diffusion-reaction equation and examine its mathematical properties.

The general formulation of the problem in fluids involves the solution of the Navier-Stokes equation coupled with the energy equation [142]. Analytical solutions are only available for very simple problems and in general simplifications are necessary for solving engineering problems [40]. One of most useful practical cases involves convection in the solution of problems such as when the workpiece is a solid that moves at a constant velocity and this can be described by the convection-diffusion equation [143]. The same equation can be used to represent the transport and dispersion of pollutants in a fluid [144] or in porous medium [108], [145]. In a more general case a chemical reaction could also take place, and the equation would have one additional term, i.e. the decay term [107].

In dealing with the problem of numerically solving the convection-diffusion equation, several techniques have been applied such as Finite Differences, Finite Elements and Boundary Elements. Comprehensive studies and extensive lists of works using Finite Differences and Finite Elements can be found in references [40], [48], [49], [146] and [57], while for Boundary Elements, the papers [31], [105], [107], [108], [112], [106], [109] and [147], refer to the majority of works done on the subject. The motivation to work on Boundary Elements resides in the fact that when applying the first two mentioned approaches, several numerical problems such as oscillations and smoothing of wave fronts have been reported. A large number of authors have solved the problem for a low local Péclet number to achieve accurate results. A large Péclet number identifies a highly convection-dominated process, producing undesired oscillations and damping of numerical solutions.

While the use of finite differences and finite elements generally presents oscillations and smoothing for large Péclet number, the boundary element technique seems to be relatively free from inherent numerical problems. The only special requirement is the existence of a fundamental solution for the governing equation. Fortunately for the cases covered in this chapter, i.e. steady-state homogeneous convection-diffusion equation with constant velocity components, the fundamental solution of the corresponding problem is available in the

literature [141]. The increasing interest on applying boundary elements to solve engineering problems in general has its fulcrum on its potential to reduce the problem dimensionality [23] which at the same time cuts down a great amount of data preparation. The application of the BEM seems to overcome the damping problem associated with spatial discretisation, but the integration of the fundamental solution involves problems with singularities ([106], [109]).

In this chapter the steady convection-diffusion equation with constant velocity coefficients is solved, including first-order chemical reactions. The results obtained seem to encourage the use of the BEM in convective problems of greater complexity. In the present thesis, the BEM is developed to solve such problems. Constant elements were used throughout the numerical examples of this work and the weakly singular integral was evaluated by using Gaussian quadrature with a cubic transformation developed by Telles [22].

The In this chapter, remarks on Péclet number are given in section 3.2, followed by the representation of the steady-state convection-diffusion-reaction equation as shown in section 3.3. In section 3.4 the formulation of the boundary integral equation is presented. The the fundamental solution of the corresponding problem and its normal derivative are shown in Section 3.5 and 3.6, respectively. Section 3.7 demonstrates the space-discretisation of the BEM. Handling the singularity appeared in the BEM formulation is discussed comprehensively in section 3.8. In section 3.9 error indicator is discussed briefly. Numerical experiments and discussions are presented to show the accuracy and the performance of the BEM method. Finally, at the end of this chapter a brief conclusions is also presented.

3.2 Remarks on Péclet Number

This number is a dimensionless number relevant in the study of transport phenomena in fluid flows. It is named after the French physicist Jean Claude Eugène Péclet [148]. The Péclet number mentioned so far is the so-called global Péclet number defined as:

$$\text{Pé} = \frac{|v|L}{D}$$

where $|v|$, D and L are the magnitude of velocity, diffusivity and characteristic length of the problem, respectively. However, when numerically solving practical problems, what is really taken into account is the so-called pore Péclet number, cell Péclet number or simply local number, that one will referred to as Pé_c and is defined as:

$$\text{Pé}_c = \frac{|v|\,\Delta\Gamma}{D}$$

where $\Delta\Gamma$ denotes the boundary element size and therefore, is closely related to the mesh (discretisation) of the problem. It has to be emphasized that the numerical problems mentioned in the literature for the standard FDM and FEM generally appear for a local Péclet number, defined as above, larger than 2.

3.3 The Steady-State Convection-Diffusion-Reaction Problem

The general form of the steady-state convection-diffusion-reaction equation can be expressed as follows:

$$-D\nabla^2\phi\,(x,y) + v_x\frac{\partial\phi\,(x,y)}{\partial x} + v_y\frac{\partial\phi\,(x,y)}{\partial y} + v_z\frac{\partial\phi\,(x,y)}{\partial z} = f\,(x,y,z,\phi) \tag{3.1}$$

with boundary conditions that can be of Dirichlet (essential), Neumann (natural), and Robin type, and where $\phi\,(x,y)$ is a potential (temperature or concentration), x, y, z are spatial coordinates, v_x, v_y, v_z velocity components according to the three Cartesian directions, D is the diffusivity or dispersion coefficient and ∇^2 is the Laplacian operator defined as:

$$\nabla^2 = \frac{\partial^2}{\partial x^2} + \frac{\partial^2}{\partial y^2} + \frac{\partial^2}{\partial z^2}. \tag{3.2}$$

If one is dealing with a reactive medium in which a first-order chemical reaction is taking place, a new term appears in the equation to account for the growth or decay of the observed reactant (for more details see Fig. 3.1). In this case, the non-homogeneous term $f = -k\phi$

and Eq.(3.1) becomes:

$$-D\nabla^2\phi\,(x,y)+v_x\frac{\partial\phi\,(x,y)}{\partial x}+v_y\frac{\partial\phi\,(x,y)}{\partial y}+v_z\frac{\partial\phi\,(x,y)}{\partial z}+k\phi\,(x,y)=0. \tag{3.3}$$

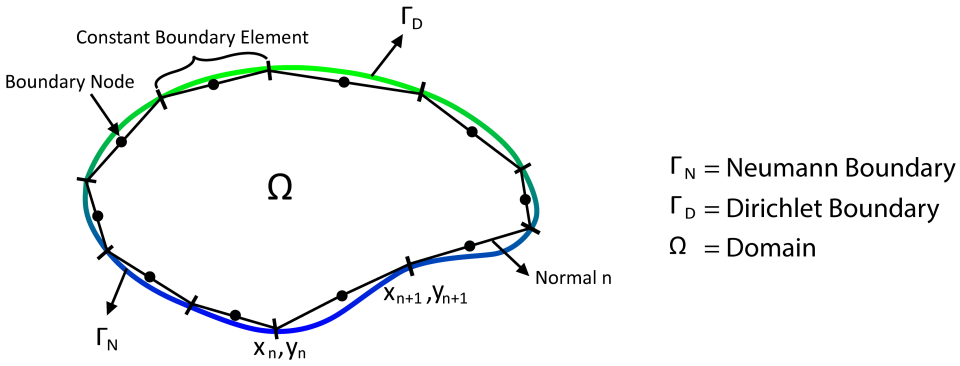

Figure 3.1: Definition of domain, boundary, and constant elements

3.4 Formulation of the Boundary Integral Equation

The main interest when trying to find a boundary integral formulation is to be able to express the governing equation in terms of values on the boundary only. The simplest procedure is to apply a weighted residual approach using an arbitrary weighting function [10] to the operator.

$$\mathscr{L}\,[\phi]=-D\nabla^2\phi+v.\nabla\phi+k\phi \tag{3.4}$$

Using Φ^* as an arbitrary weighting function, one can write the weighted residual statement as

$$\int_\Omega \mathscr{L}\,[\phi]\,\Phi^* d\Omega=0. \tag{3.5}$$

The next step is to integrate the above expression by parts twice. For the sake of clarity let us do it in a step-by-step procedure. First it is convenient to write down the above equation in the open form of the operator, i.e.

$$\int_{\Omega}\left(-D\frac{\partial^2\phi}{\partial x^2}-D\frac{\partial^2\phi}{\partial y^2}-D\frac{\partial^2\phi}{\partial z^2}+v_x\frac{\partial\phi}{\partial x}+v_y\frac{\partial\phi}{\partial y}+v_z\frac{\partial\phi}{\partial z}+k\phi\right)\Phi^* d\Omega=0. \tag{3.6}$$

The integration can then be carried out in a term-by-term procedure. Integrating the first term one has to remember the rule of derivation of a product

$$\frac{\partial}{\partial x}\left(\Phi^*\frac{\partial\phi}{\partial x}\right)=\Phi^*\frac{\partial^2\phi}{\partial x^2}+\frac{\partial\phi}{\partial x}\frac{\partial\Phi^*}{\partial x} \tag{3.7}$$

and consequently

$$\Phi^*\frac{\partial^2\phi}{\partial x^2}=\frac{\partial}{\partial x}\left(\Phi^*\frac{\partial\phi}{\partial x}\right)-\frac{\partial\phi}{\partial x}\frac{\partial\Phi^*}{\partial x}. \tag{3.8}$$

If the same is applied to the second term on the right hand side of the above equation one has

$$-\frac{\partial\phi}{\partial x}\frac{\partial\Phi^*}{\partial x}=\phi\frac{\partial^2\Phi^*}{\partial x^2}-\frac{\partial}{\partial x}\left(\phi\frac{\partial\Phi^*}{\partial x}\right) \tag{3.9}$$

which substituted in Eq.(3.8) results in

$$\Phi^*\frac{\partial^2\phi}{\partial x^2}=\frac{\partial}{\partial x}\left(\Phi^*\frac{\partial\phi}{\partial x}\right)-\frac{\partial}{\partial x}\left(\phi\frac{\partial\Phi^*}{\partial x}\right)+\phi\frac{\partial^2\Phi^*}{\partial x^2}. \tag{3.10}$$

Applying this result under the integration sign for the first term in Eq.(3.6) one can write:

$$\int_{\Omega}-D\left[\frac{\partial^2\phi}{\partial x^2}\Phi^*\right]d\Omega=\int_{\Omega}D\left[-\frac{\partial}{\partial x}\left(\Phi^*\frac{\partial\phi}{\partial x}\right)+\frac{\partial}{\partial x}\left(\phi\frac{\partial\Phi^*}{\partial x}\right)-\phi\frac{\partial^2\Phi^*}{\partial x^2}\right]d\Omega \tag{3.11}$$

On dealing with the term in v_x in Eq.(3.6) it is necessary to apply the same rule for derivation of product, i.e.

$$\frac{\partial}{\partial x}(\phi\,\Phi^*)=\Phi^*\frac{\partial\phi}{\partial x}+\phi\frac{\partial\Phi^*}{\partial x} \tag{3.12}$$

that can be recast as

$$\Phi^* \frac{\partial \phi}{\partial x} = \frac{\partial}{\partial x}(\phi \Phi^*) - \phi \frac{\partial \Phi^*}{\partial x} \tag{3.13}$$

Then, replacing this value under the integral sign for the term in v_x it comes that

$$\int_\Omega v_x \Phi^* \frac{\partial \phi}{\partial x} d\Omega = \int_\Omega v_x \left[\frac{\partial}{\partial x}(\phi \Phi^*) - \phi \frac{\partial \Phi^*}{\partial x} \right] d\Omega. \tag{3.14}$$

Adding this expression to Eq.(3.11) it can be written that

$$\int_\Omega \left(-D\Phi^* \frac{\partial^2 \phi}{\partial x^2} + v_x \Phi^* \frac{\partial \phi}{\partial x} \right) d\Omega$$

$$= \int_\Omega \left\{ D \left[-\frac{\partial}{\partial x}\left(\Phi^* \frac{\partial \phi}{\partial x} \right) + \frac{\partial}{\partial x}\left(\phi \frac{\partial \Phi^*}{\partial x} \right) - \phi \frac{\partial^2 \Phi^*}{\partial x^2} \right] + v_x \frac{\partial}{\partial x}(\phi\, \Phi^*) - v_x \phi \frac{\partial \Phi^*}{\partial x} \right\} d\Omega. \tag{3.15}$$

The term can be rearranged to produce

$$\int_\Omega \left(-D\Phi^* \frac{\partial^2 \phi}{\partial x^2} + v_x \Phi^* \frac{\partial \phi}{\partial x} \right) d\Omega = \int_\Omega \left(-D\phi \frac{\partial^2 \Phi^*}{\partial x^2} - v_x \phi \frac{\partial \Phi^*}{\partial x} \right) d\Omega$$

$$+ \int_\Omega \left\{ D \left[-\frac{\partial}{\partial x}\left(\Phi^* \frac{\partial \phi}{\partial x} \right) + \frac{\partial}{\partial x}\left(\phi \frac{\partial \Phi^*}{\partial x} \right) \right] + v_x \frac{\partial}{\partial x}(\phi\, \Phi^*) \right\} d\Omega. \tag{3.16}$$

Assume that v_x is a component of a constant velocity v, one can integrate the term of the second integral on the right-hand-side of the above equation using the divergence theorem [149] and applying it independently to any particular component of the vector under consideration. Then

$$\int_\Omega -D \frac{\partial}{\partial x}\left(\Phi^* \frac{\partial \phi}{\partial x} \right) d\Omega = -D \int_\Gamma \Phi^* \frac{\partial \phi}{\partial x} n_x d\Gamma. \tag{3.17}$$

and finally

$$\int_{\Omega} v_x \frac{\partial}{\partial x}(\phi\Phi^*)\, d\Omega = \int_{\Gamma} v_x (\Phi^*\phi)\, n_x d\Gamma. \tag{3.18}$$

The substitution of the above two equations into Eq.(3.16) leads to

$$\int_{\Omega} \left(-D\Phi^* \frac{\partial^2\phi}{\partial x^2} + v_x \Phi^* \frac{\partial\phi}{\partial x} \right) d\Omega = \int_{\Omega} \left(-D\phi \frac{\partial^2\Phi^*}{\partial x^2} - v_x \phi \frac{\partial\Phi^*}{\partial x} \right) d\Omega$$

$$+D\int_{\Gamma} \left(-\Phi^* \frac{\partial\phi}{\partial x} + \phi \frac{\partial\Phi^*}{\partial x} \right) n_x d\Gamma + \int_{\Gamma} v_x (\Phi^*\phi)\, n_x d\Gamma \tag{3.19}$$

It is convenient to notice that this procedure was carried out for the term x of Eq.(3.6) and consequently one can proceed analogously for the terms in y and z directions. For the terms in y:

$$\int_{\Omega} \left(-D\Phi^* \frac{\partial^2\phi}{\partial y^2} + v_y \Phi^* \frac{\partial\phi}{\partial y} \right) d\Omega = \int_{\Omega} \left(-D\phi \frac{\partial^2\Phi^*}{\partial y^2} - v_y \phi \frac{\partial\Phi^*}{\partial y} \right) d\Omega$$

$$+D\int_{\Gamma} \left(-\Phi^* \frac{\partial\phi}{\partial y} + \phi \frac{\partial\Phi^*}{\partial y} \right) n_y d\Gamma + \int_{\Gamma} v_y (\Phi^*\phi)\, n_y d\Gamma. \tag{3.20}$$

For the terms in z:

$$\int_{\Omega} \left(-D\Phi^* \frac{\partial^2\phi}{\partial z^2} + v_z \Phi^* \frac{\partial\phi}{\partial z} \right) d\Omega = \int_{\Omega} \left(-D\phi \frac{\partial^2\Phi^*}{\partial z^2} - v_z \phi \frac{\partial\Phi^*}{\partial z} \right) d\Omega$$

$$+D\int_{\Gamma} \left(-\Phi^* \frac{\partial\phi}{\partial z} + \phi \frac{\partial\Phi^*}{\partial z} \right) n_z d\Gamma + \int_{\Gamma} v_z (\Phi^*\phi)\, n_z d\Gamma. \tag{3.21}$$

Then, Eq.(3.5) may be written as

$$\int_\Omega \mathscr{L}[\phi]\,\Phi^* d\Omega = \int_\Omega \left(-D\,\phi\frac{\partial^2\Phi^*}{\partial x^2} - D\,\phi\frac{\partial^2\Phi^*}{\partial y^2} - D\,\phi\frac{\partial^2\Phi^*}{\partial z^2}\right) d\Omega$$

$$+\int_\Omega \left(-v_x\,\phi\frac{\partial\Phi^*}{\partial x} - v_y\,\phi\frac{\partial\Phi^*}{\partial y} - v_z\,\phi\frac{\partial\Phi^*}{\partial z} + k\phi\Phi^*\right) d\Omega + D\int_\Gamma \left(-\Phi^*\frac{\partial\phi}{\partial x} + \phi\frac{\partial\Phi^*}{\partial x}\right) n_x\,d\Gamma$$

$$+D\int_\Gamma \left(-\Phi^*\frac{\partial\phi}{\partial y} + \phi\frac{\partial\Phi^*}{\partial y}\right) n_y\,d\Gamma + D\int_\Gamma \left(-\Phi^*\frac{\partial\phi}{\partial z} + \phi\frac{\partial\Phi^*}{\partial z}\right) n_z\,d\Gamma$$

$$+\int_\Gamma v_x\,(\Phi^*\phi)\,n_x\,d\Gamma + D\int_\Gamma v_y\,(\Phi^*\phi)\,n_y\,d\Gamma + D\int_\Gamma v_z\,(\Phi^*\phi)\,n_z\,d\Gamma. \tag{3.22}$$

In this expression it is recognised the Laplacian operator and scalar products. After collecting the terms in a suitable manner, the equation becomes:

$$\int_\Omega \mathscr{L}[\phi]\,\Phi^* d\Omega = \int_\Omega \left(-\phi D\nabla^2\Phi^* - (v.\nabla\Phi^*)\,\phi + k\Phi^*\phi\right) d\Omega$$

$$-D\int_\Gamma \Phi^*\nabla\phi.n d\Gamma + D\int_\Gamma \phi\nabla\Phi^*.n\,d\Gamma + \int_\Gamma (\phi\Phi^*)\,v.n\,d\Gamma, \tag{3.23}$$

where n is the unit outward normal vector.

The integration of the domain integral on the right-hand-side of the equation reveals the presence of a mathematical entity that usually arises from this process of integration by parts and is related to the weighting function Φ^*. This mathematical entity $\mathscr{L}^*$ is called the formal adjoint to the operator $\mathscr{L}$ and, when operating on Φ^*, can be defined as

$$\mathscr{L}^*[\Phi^*] = -D\nabla^2\Phi^* - v.\nabla\Phi^* + k\Phi^*. \tag{3.24}$$

In the light of this new definition, Eq.(3.23) can be written:

$$\int_{\Omega} \mathscr{L}[\phi]\,\Phi^{*}\,d\Omega = \int_{\Omega} \mathscr{L}^{*}[\Phi^{*}]\,\phi\,d\Omega - D\int_{\Gamma} \Phi^{*}\nabla\phi.n\,d\Gamma$$

$$+D\int_{\Gamma} \phi\nabla\Phi^{*}.n\,d\Gamma + \int_{\Gamma} (\phi\Phi^{*})\,v.n\,d\Gamma \tag{3.25}$$

Once the left-hand-side is equal to zero, the process of integration by parts led us finally to

$$\int_{\Omega} \mathscr{L}^{*}[\Phi^{*}]\,\phi\,d\Omega + D\int_{\Gamma} (-\Phi^{*}\nabla\phi.n + \phi\nabla\Phi^{*}.n)\,d\Gamma + \int_{\Gamma} (\phi\Phi^{*})\,v.n\,d\Gamma = 0 \tag{3.26}$$

or, in an alternative form

$$\int_{\Omega} \mathscr{L}^{*}[\Phi^{*}]\,\phi\,d\Omega + \int_{\Gamma} \Phi^{*}\left[-D\nabla\phi.n + \phi\,(v.n)\right]d\Gamma + D\int_{\Gamma} \phi\nabla\Phi^{*}.n\,d\Gamma = 0. \tag{3.27}$$

It is important to keep in mind these two alternative forms of the final equation, as one can be more suitable than the other according to the problem under consideration.

Taking a closer look at these equations, it is understood that one has been left with an expression involving domain as well as boundary integrals. There is also one domain integral to be taken into account. It should be noted that, after the integration by parts, its integrand involves the adjoint operating on the weighting function that is, in principle, arbitrary, and therefore the most suitable one can be chosen. If the weighting function is chosen in such a way that

$$\mathscr{L}^{*}[\Phi^{*}] = -D\nabla^{2}\Phi^{*} - v.\nabla\Phi^{*} + k\Phi^{*} = \delta(\xi, x) \tag{3.28}$$

in which ξ is a fixed (source) point, x a moving (field) point, and $\delta(\xi, x)$ is the Dirac delta function; which has the following property:

$$\delta(\xi, x) = \begin{cases} \infty \text{ for } \xi = x, \\ 0 \text{ for } \xi \neq x, \end{cases} \tag{3.29}$$

then the function $\Phi^*(\xi, x)$ called the fundamental solution of Eq.(3.28).
The choice of the non-homogeneous term in Eq.(3.28) to be the Dirac delta function resides in the fact that it has very important properties i.e.

$$\int_{-\infty}^{\infty} \delta(x)\, dx = 1 \tag{3.30}$$

and

$$\int_{\Omega} \phi(x)\, \delta(\xi, x)\, d\Omega = \phi(\xi). \tag{3.31}$$

Taking into account this last property it is possible to write that

$$\int_{\Omega} \mathscr{L}^*[\Phi^*]\, \phi d\Omega = \phi(\xi). \tag{3.32}$$

Applying this result to either of the alternative forms above, i.e. Eqs.(3.26) or (3.27), say the first one, it becomes

$$\phi(\xi) + D\int_{\Gamma} (-\Phi^* \nabla\phi.n + \phi \nabla \Phi^*.\mathrm{n})\, d\Gamma + \int_{\Gamma} (\phi\, \Phi^*)\, v.n\, d\Gamma = 0. \tag{3.33}$$

This equation relates the values of the variable ϕ at a fixed point ξ in the domain with values on the boundary. This, in spite of being a very important achievement, is not yet the one we are looking for, because the problem is still not boundary-only dependent. Expression (3.27)

can be written in a more compact form as

$$\int_{\Omega} \mathscr{L}^* [\Phi^*] \, \phi \, d\Omega + D \int_{\Gamma} \phi \frac{\partial \Phi^*}{\partial n} d\Gamma + \int_{\Gamma} \phi \, \Phi^* v_n d\Gamma - D \int_{\Gamma} \Phi^* \frac{\partial \phi}{\partial n} d\Gamma = 0, \tag{3.34}$$

where $v_n = \mathbf{v}.\mathbf{n}$. As one is trying to find an expression relating values on the boundary only, one has to see what will happen if the interior point ξ is taken to the boundary. The usual procedure is to enclose the point ξ by a sphere and then move it to the boundary. After a limiting process that is going to be shown in Appendix A, the equation becomes

$$C(\xi) \, \phi(\xi) + D \int_{\Gamma} \phi \frac{\partial \Phi^*}{\partial n} d\Gamma + \int_{\Gamma} \left(-D \frac{\partial \phi}{\partial n} + v_n \phi \right) \Phi^* \, d\Gamma = 0. \tag{3.35}$$

That is, the equation is now valid for the whole domain plus the boundary, i.e. the closure of Ω, and the constant $C(\xi)$ will be shown to depend on the shape of the boundary at the point ξ, being equal to 1 at interior points where Eq.(3.35) reduces to Eq.(3.33).
Eq.(3.35) can also be written as

$$C(\xi) \, \phi(\xi) + \int_{\Gamma} \left(D \frac{\partial \Phi^*}{\partial n} + v_n \Phi^* \right) \phi \, d\Gamma - D \int_{\Gamma} \Phi^* \frac{\partial \phi}{\partial n} d\Gamma = 0. \tag{3.36}$$

The limiting process and the evaluation of the constant $C(\xi)$ for values of ξ on the boundary will be carried out in Appendix A. The next section will introduce the expression of the fundamental solution.

3.5 The Fundamental Solution

In the search for a fundamental solution of Eq.(3.3), one way to find analytical solutions, used in the past by [143], is to transform the equation studied into an equation for which the fundamental solution is already known. The idea was also used by [107] for non-homogeneous cases such as the ones that are being solved.

For the sake of clarity let us rewrite Eq.(3.28) in the form:

$$-\nabla^2\Phi^* - \frac{v_x}{D}\frac{\partial\Phi^*}{\partial x} - \frac{v_y}{D}\frac{\partial\Phi^*}{\partial y} - \frac{v_z}{D}\frac{\partial\Phi^*}{\partial z} + \frac{k}{D}\Phi^* = \frac{1}{D}\delta(\xi,x). \tag{3.37}$$

The equation into which one wishes to transform the above is the non-homogeneous modified Helmholtz equation:

$$-\nabla^2 W + \mu^2 W = \frac{1}{D}e^A\delta(\xi,x); \tag{3.38}$$

3.5.1 The Transformation

Let us assume that the following transformation can be carried out

$$\phi^* = \frac{1}{D}e^{-A(x,y,z)}W \tag{3.39}$$

and, for simplicity, let us also define

$$A_x = \frac{\partial}{\partial x}[A(x,y,z)];\ A_y = \frac{\partial}{\partial y}[A(x,y,z)];\quad \text{and}\quad A_z = \frac{\partial}{\partial z}[A(x,y,z)]. \tag{3.40}$$

Consequently,

$$A_{xx} = \frac{\partial^2}{\partial x^2}[A(x,y,z)]; A_{yy} = \frac{\partial^2}{\partial y^2}[A(x,y,z)];\quad \text{and}\quad A_{zz} = \frac{\partial^2}{\partial z^2}[A(x,y,z)]. \tag{3.41}$$

Then, differentiating Eq.(3.39) with respect to x:

$$\frac{\partial\Phi^*}{\partial x} = \frac{1}{D}e^{-A}\left[\frac{\partial W}{\partial x} - WA_x\right]. \tag{3.42}$$

Also

$$\frac{\partial^2\Phi^*}{\partial x^2} = \frac{1}{D}e^{-A}\left[\frac{\partial^2 W}{\partial x^2} - 2\frac{\partial W}{\partial x}A_x - W\left(A_{xx} - A^2{}_x\right)\right] \tag{3.43}$$

Finding the partial derivative in relation to y, one has:

$$\frac{\partial \Phi^*}{\partial y} = \frac{1}{D} e^{-A} \left[\frac{\partial W}{\partial y} - W A_y \right] \tag{3.44}$$

and also

$$\frac{\partial^2 \Phi^*}{\partial y^2} = \frac{1}{D} e^{-A} \left[\frac{\partial^2 W}{\partial y^2} - 2 \frac{\partial W}{\partial y} A_y - W \left(A_{yy} - A^2{}_y \right) \right]. \tag{3.45}$$

Proceeding analogously in relation to z it will produce

$$\frac{\partial \Phi^*}{\partial z} = \frac{1}{D} e^{-A} \left[\frac{\partial W}{\partial z} - W A_z \right] \tag{3.46}$$

also

$$\frac{\partial^2 \Phi^*}{\partial z^2} = \frac{1}{D} e^{-A} \left[\frac{\partial^2 W}{\partial z^2} - 2 \frac{\partial W}{\partial z} A_z - W \left(A_{zz} - A_z^2 \right) \right]. \tag{3.47}$$

Substituting Eqs.(3.39), and (3.42) to (3.47) into Eq.(3.37) one has, after dropping the $1/D$ factor on both sides of the equation, that

$$e^{-A} \{ -\nabla W + \left(2A_x - \frac{v_x}{D} \right) \frac{\partial W}{\partial x} + \left(2A_y - \frac{v_y}{D} \right) \frac{\partial W}{\partial y} + \left(2A_z - \frac{v_z}{D} \right) \frac{\partial W}{\partial z}$$

$$+ \left[A_{xx} - A_x^2 + A_{yy} - A_y^2 + A_{zz} - A_z^2 + \frac{v_x}{D} A_x + \frac{v_y}{D} A_y + \frac{v_z}{D} A_z + \frac{k}{D} \right] W \} = \delta(\xi, x). \tag{3.48}$$

In order to transform this equation into a Helmholtz-like equation one has to make:

$$2A_x - \frac{v_x}{D} = 0, \; 2A_y - \frac{v_y}{D} = 0, \; 2A_z - \frac{v_z}{D} = 0 \tag{3.49}$$

and also

$$A_{xx} - A_x^2 + A_{yy} - A_y^2 + A_{zz} - A_z^2 + \frac{v_x}{D} A_x + \frac{v_y}{D} A_y + \frac{v_z}{D} A_z + \frac{k}{D} = \mu^2. \tag{3.50}$$

From Eq.(3.49) one can write that:

$$A = \frac{1}{D}\int v_x dx + g(y,z),\ A = \frac{1}{D}\int v_y dy + p(x,z),\ A = \frac{1}{D}\int v_z dz + q(y,x) \tag{3.51}$$

Once the value of A has to be equal in the above expressions:

$$A = \frac{1}{2D}\left(\int v_x dx + \int v_y dy + \int v_z dz\right) = \frac{1}{2D}\left(v_x x + v_y y + v_z z\right) = \frac{v.\mathbf{r}}{2D}, \tag{3.52}$$

which makes $A_{xx} = A_{yy} = A_{zz} = 0$. Now one has to see if, in the light of this result, it is possible to find a constant μ^2 coming out from Eq.(3.50), which can be written as,

$$A_x^2 - A_y^2 - A_z^2 + \frac{v_x}{D}A_x + \frac{v_y}{D}A_y + \frac{v_z}{D}A_z + \frac{k}{D} = \mu^2. \tag{3.53}$$

As it is already known from Eq.(3.49),

$$A_x = \frac{v_x}{2D},\ A_y = \frac{v_y}{2D},\ A_z = \frac{v_z}{2D}. \tag{3.54}$$

One can write that the value of μ^2 is:

$$\mu^2 = \left(\frac{|v|}{2D}\right)^2 + \frac{k}{D}. \tag{3.55}$$

Then Eq.(3.28) would transform to

$$e^{-A}\left[-\nabla^2 W + \mu^2 W\right] = \delta(\xi, x). \tag{3.56}$$

Now, the fundamental solution of the modified Helmholtz equation:

$$-\nabla^2 U + \mu^2 U = 0 \tag{3.57}$$

is a function $W(\xi, x)$ that satisfies:

$$-\nabla^2 W + \mu^2 W = \delta(\xi, x) \tag{3.58}$$

which consequently also satisfies Eq.(3.56), and in 3D is given by

$$W_{3D} = W(\xi, x) = \frac{1}{4\pi |\mathbf{r}|} \mathrm{e}^{-|\mu||\mathbf{r}|} \tag{3.59}$$

where

$$|\mathbf{r}| = \left[\sum_{i=1}^{3} (x_i - \xi_i)^2 \right]^{\frac{1}{2}} \tag{3.60}$$

which is known as Yulkawa's potential [109]. Finally, it can be written as

$$\Phi^*(\xi, x) = \frac{1}{4\pi D |\mathbf{r}|} e^{-\frac{v.\mathbf{r}}{2D}} e^{-|\mu||\mathbf{r}|}. \tag{3.61}$$

3.5.2 Search for the Fundamental Solution in 2D

The 2D fundamental solution for the modified Helmholtz equation can be obtained by integration of the 3D solution, i.e.

$$W_{2D} = \int_{-\infty}^{\infty} W_{3D}\, dz. \tag{3.62}$$

Calling temporarily $|\mathbf{r}|$ in 3D as $|\mathbf{r}_3|$ and $|\mathbf{r}|$ in 2D as $|\mathbf{r}_2|$ one can write:

$$|\mathbf{r}_3| = \left| \left[\mathbf{r}_2^2 + (z - z_i)^2 \right]^{\frac{1}{2}} \right| \tag{3.63}$$

and then if additionally one defines a parameter t so that:

$$(z - z_i) = |\mathbf{r}| \sinh(t) \tag{3.64}$$

Consequently,

$$d\left(z-z_i\right)=dz=|\mathbf{r}|\cosh\left(t\right)\,dt \tag{3.65}$$

It is possible to write that

$$|\mathbf{r}_3|=\left|\left[\mathbf{r}_2^2\left(1+\sinh^2\left(t\right)\right)\right]^{\frac{1}{2}}\right|=|\mathbf{r}_2|\cosh\left(t\right) \tag{3.66}$$

which substituted into Eq.(3.62) and taking into consideration Eq.(3.59) will produce

$$W_{2D}=\int_{-\infty}^{\infty}\frac{1}{4\pi\,|\mathbf{r}_2|\cosh\left(t\right)}e^{-|\mu||\mathbf{r}_2|\cosh(t)}\,|r_2|\cosh\left(t\right)dt \tag{3.67}$$

Consequently,

$$W_{2D}=\frac{1}{4\pi}\int_{-\infty}^{\infty}e^{-|\mu||\mathbf{r}_2|\cosh(t)}\,dt \tag{3.68}$$

We can split the integral into two, resulting in:

$$W_{2D}=\frac{1}{4\pi}\left[\int_{-\infty}^{0}e^{-|\mu||\mathbf{r}_2|\cosh(t)}\,dt+\int_{0}^{\infty}e^{-|\mu||\mathbf{r}_2|\cosh(t)}\,dt\right]. \tag{3.69}$$

For the second integral in the above equation there is standard entry in an integration table, whereas for first one a transformation is needed. The integration takes the form:

$$\int_{-\infty}^{0}e^{-|\mu||\mathbf{r}_2|\cosh(t)}\,dt=-\int_{\infty}^{0}e^{-|\mu||\mathbf{r}_2|\cosh(\eta)}\,d\eta=\int_{0}^{\infty}e^{-|\mu||\mathbf{r}_2|\cosh(\eta)}\,d\eta \tag{3.70}$$

Then, the 2D solution can be written in an integral form as a sum of two equal terms:

$$W_{2D}=\frac{2}{4\pi}\int_{0}^{\infty}e^{-|\mu||\mathbf{r}_2|\cosh(t)}\,dt \tag{3.71}$$

which, according to [150], gives as a result:

$$W_{2D} = \frac{1}{2\pi} K_0 \left(|\mu| \, |\mathbf{r}_2| \right), \tag{3.72}$$

where K_0 stands for the modified Bessel function of second kind and order zero. Taking into account this result, and also Eq.(3.39) and (3.52), it can be written as:

$$\Phi^* \left(\xi, x \right) = \frac{1}{2\pi D} e^{-\frac{v.\mathbf{r}}{2D}} K_0 \left(|\mu| \, |\mathbf{r}| \right). \tag{3.73}$$

When applying the fundamental solution to the boundary integral equation one has to bear in mind that the function K_0 has a logarithmic singularity at the point $x = 0$. This will be analysed in a later section.

3.6 The Normal Derivative of the Fundamental Solution

By going back to Eq.(3.33), one can see that it relates the value of ϕ at an interior point to values on the boundary. The question now is how can it be made to work for any point, either inside the domain or on the boundary. This can be achieved by applying Eq.(3.34) to an interior point and then taking this point to the boundary by means of a limiting process to obtain a more general equation. The process can be done in either 2D or 3D, but for the sake of simplicity, one will here perform it for the 2D case. Before undertaking any limiting procedure on Eq.(3.34), one needs first to obtain the expression for the normal derivative of the fundamental solution, which will be needed later on.

The normal derivative of the fundamental solution can be written as

$$\frac{\partial \Phi^*}{\partial n} = \frac{\partial}{\partial n} \left[\frac{1}{2\pi D} e^{\frac{-v.\mathbf{r}}{2D}} K_0 \left(|\mu| \, |\mathbf{r}| \right) \right]. \tag{3.74}$$

Applying the rule for the derivative of a product

$$\frac{\partial \Phi^*}{\partial n} = \frac{1}{2\pi D} e^{\frac{-v.\mathbf{r}}{2D}} \frac{\partial}{\partial n} \left[K_0 \left(|\mu| \, |\mathbf{r}| \right) \right] + \frac{1}{2\pi D} K_0 \left(|\mu| \, |\mathbf{r}| \right) \frac{\partial}{\partial n} \left(e^{\frac{-v.\mathbf{r}}{2D}} \right). \tag{3.75}$$

After some arrangement one has

$$\frac{\partial \Phi^*}{\partial n} = \frac{1}{2\pi D} e^{\frac{-v.\mathbf{r}}{2D}} \left[-|\mu| K_1(|\mu||r|) + K_0(|\mu||r|) \frac{\partial}{\partial n}\left(-\frac{v.r}{2D}\right)\right], \tag{3.76}$$

where $K_1(|\mu||\mathbf{r}|)$ is the modified Bessel function of second kind and order one. As it is known that

$$\frac{\partial}{\partial n}(-v.\mathbf{r}) = -(v_x n_x + v_y n_y) = -v_n \tag{3.77}$$

then the final equation for the normal derivative of the fundamental solution will be

$$\frac{\partial \Phi^*}{\partial n} = \frac{1}{2\pi D} e^{\frac{-v.\mathbf{r}}{2D}} \left[-|\mu| K_1(|\mu||\mathbf{r}|) \frac{\partial r}{\partial n} - \frac{v_n}{2D} K_0(|\mu||\mathbf{r}|)\right]. \tag{3.78}$$

3.7 Space-Discretisation of the Boundary Element Method

For the discretisation of the steady-state convective-diffusive-reactive model, combined application of BEM and DRM are implemented. Therefore, the spatial discretisation is made by utilising DRBEM. In the light of Eqs.(3.73) and (3.78), the term between parenthesis in the first integral in Eq.(3.36) can be written as:

$$D\frac{\partial \Phi^*}{\partial n} + v_n \Phi^* = D\frac{1}{2\pi D} e^{\frac{-v.\mathbf{r}}{2D}} \left[-|\mu| K_1(|\mu||\mathbf{r}|) \frac{\partial \mathbf{r}}{\partial n} - \frac{v_n}{2D} K_0(|\mu||\mathbf{r}|)\right] + \frac{v_n}{2\pi D} e^{\frac{-v.\mathbf{r}}{2D}} K_0(|\mu||\mathbf{r}|) \tag{3.79}$$

or, alternatively, as:

$$D\frac{\partial \Phi^*}{\partial n} + v_n \Phi^* = \frac{1}{2\pi D} e^{\frac{-v.\mathbf{r}}{2D}} \left[-D|\mu| K_1(|\mu||\mathbf{r}|) \frac{\partial \mathbf{r}}{\partial n} - \frac{v_n}{2D} K_0(|\mu||\mathbf{r}|) + v_n K_0(|\mu||\mathbf{r}|)\right] \tag{3.80}$$

Taking the final form:

$$D\frac{\partial \Phi^*}{\partial n} + v_n \Phi^* = \frac{1}{2\pi D} e^{\frac{-v.\mathbf{r}}{2D}} \left[-D|\mu| K_1(|\mu||\mathbf{r}|) \frac{\partial \mathbf{r}}{\partial n} + \frac{v_n}{2D} K_0(|\mu||\mathbf{r}|) \right] \tag{3.81}$$

Then after replacing this result into Eq.(3.36), it becomes:

$$C(\xi)\phi(\xi) = \frac{1}{2\pi D} \int_\Gamma D e^{\frac{-v.\mathbf{r}}{2D}} K_0(|\mu||\mathbf{r}|) \frac{\partial \phi}{\partial n} d\Gamma$$

$$-\frac{1}{2\pi D} \int_\Gamma e^{\frac{-v.\mathbf{r}}{2D}} \left[-D|\mu| K_1(|\mu||\mathbf{r}|) \frac{\partial \mathbf{r}}{\partial n} + \frac{v_n}{2} K_0(|\mu||\mathbf{r}|) \right] \phi d\Gamma \tag{3.82}$$

It is very important to point out that Φ^* is a function of ξ and x, respectively the source and field points, and also that $\frac{\partial \Phi^*}{\partial n}$ is calculated at the field point x. As a consequence, it can be said that the quantities $\frac{\partial \phi}{\partial n}$ and $\frac{\partial \mathbf{r}}{\partial n}$ are also evaluated at the field point x. To be mathematically more accurate and also for clarity, one can write Eq.(3.82) as

$$C(\xi)\phi(\xi) = \frac{1}{2\pi D} \int_\Gamma D e^{\frac{-v.\mathbf{r}}{2D}} K_0(|\mu||\mathbf{r}|) \frac{\partial \phi}{\partial n}(x) d\Gamma(x)$$

$$-\frac{1}{2\pi D} \int_\Gamma e^{\frac{-v.\mathbf{r}}{2D}} \left[-D|\mu| K_1(|\mu||\mathbf{r}|) \frac{\partial \mathbf{r}(\xi,x)}{\partial n(x)} + \frac{v_n}{2} K_0(|\mu||\mathbf{r}|) \right] \phi(x) d\Gamma(x) \tag{3.83}$$

After reaching this point, it is easily seen that one ended up with an integral equation that relates the value of the function ϕ at the fixed point ξ on the boundary to the values of ϕ and its normal derivative $\frac{\partial \phi}{\partial n}$ at all boundary points. In order to solve the problem one has to discretise the integrals. This is achieved by dividing the boundary into segments (for the sake of simplicity, let us consider a 2D domain as in the Fig. 3.2 in such a way that the whole boundary Γ now will be a union of segments Γ_j, i.e. $\Gamma = \cup\Gamma_j$ and the integral on the boundary will be represented by the sum of the integrals over the elements.

If one uses N elements, Eq.(3.83) will be discretised as

$$C(\xi)\,\phi(\xi) = \frac{1}{2\pi D}\sum_{j=1}^{N}\int_{\Gamma_j} D\,e^{\frac{-v.\mathbf{r}}{2D}} K_0(|\mu|\,|\mathbf{r}|)\,\frac{\partial\phi(x)}{\partial n}d\Gamma(x)$$

$$-\frac{1}{2\pi D}\sum_{j=1}^{N}\int_{\Gamma_j} e^{\frac{-v.\mathbf{r}}{2D}}\left[-D\,|\mu|\,K_1(|\mu|\,|\mathbf{r}|)\,\frac{\partial\mathbf{r}(\xi,x)}{\partial n(x)} + \frac{v_n}{2}K_0(|\mu|\,|\mathbf{r}|)\right]\phi(x)\,d\Gamma(x). \tag{3.84}$$

For easy handling, let us define two auxiliary integrand kernels H and G as follows:

$$G(\xi,x) = \frac{1}{2\pi D}\mathrm{e}^{\frac{-v.\mathbf{r}}{2D}} K_0(|\mu|\,|\mathbf{r}|), \tag{3.85}$$

$$H(\xi,x) = \frac{1}{2\pi D}e^{\frac{-v.\mathbf{r}}{2D}}\left[-D\,|\mu|\,K_1(|\mu|\,|\mathbf{r}|)\,\frac{\partial\mathbf{r}(\xi,x)}{\partial n(x)} + \frac{v_n}{2}K_0(|\mu|\,|\mathbf{r}|)\right]. \tag{3.86}$$

The above equations show that, for any source point ξ, one has to sum up all the contributions of the integrations over each and every element including the one which contains the source point.

The integrations over each element j require values of $\phi(x)$ and $\frac{\partial\phi(x)}{\partial n}$ (with x taking values in Γ_j) that are still unknown. To overcome this problem several different assumptions can be made. In this work constant functions ϕ and $\frac{\partial\phi}{\partial n}$ are assumed between two nodal points of the elements.

Then Eq.(3.84) can be recast as

$$C(\xi)\,\phi(\xi) = \sum_{j=1}^{N}\int_{\Gamma_j} G(\xi,x)\,\frac{\partial\phi}{\partial n}(x)\,d\Gamma(x) - \sum_{j=1}^{N}\int_{\Gamma_j} H(\xi,x)\,\phi(x)\,d\Gamma(x) \tag{3.87}$$

Substituting these approximations into Eq.(3.87) and writing in a simplified notation for a point i

$$C_i\,\phi_i = \sum_{j=1}^{N}\int_{\Gamma_j} G(\xi,x)\left(\frac{\partial\phi}{\partial n}\right)d\Gamma(x) - \sum_{j=1}^{N}\int_{\Gamma_j} H(\xi,x)\,\phi\,d\Gamma(x). \tag{3.88}$$

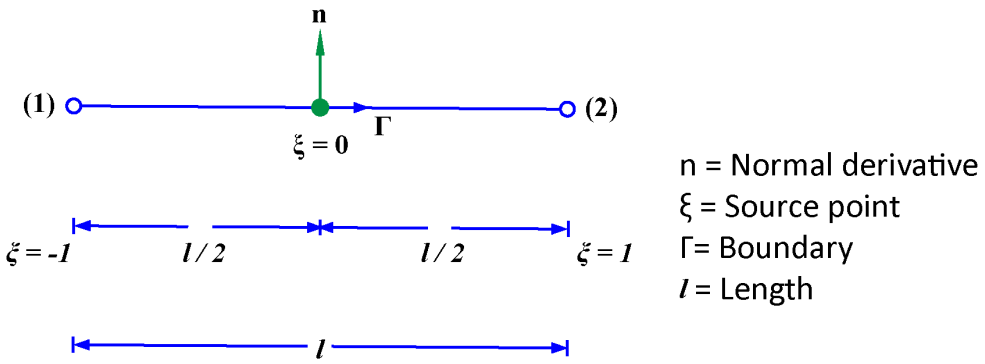

Figure 3.2: Local Coordinate System

Now if one defines

$$g_{ij} = \int_{\Gamma_j} G\, d\Gamma(x), \quad h_{ij} = \int_{\Gamma_j} H\, d\Gamma(x) \tag{3.89}$$

then Eq.(3.88) can be rewritten as:

$$C_i \phi_i = \sum_{j=1}^{N} \left[g_{ij} \left(\frac{\partial \phi}{\partial n} \right)_j - h_{ij} \phi_j \right], \quad i = 1, ..., N. \tag{3.90}$$

Having stated that, Eq.(3.90) can be rewritten as:

$$C_i \phi_i = \sum_{j=1}^{N} G_{ij} \left(\frac{\partial \phi}{\partial n} \right)_j - \sum_{j=1}^{N} \hat{H}_{ij} \phi_j, \tag{3.91}$$

where $G_{ij} = g_{ij}$ and $\hat{H}_{ij} = h_{ij}$.

Alternatively, it can be written that:

$$C_{ij} \phi_i + \sum_{j=1}^{N} \hat{H}_{ij} \phi_j = \sum_{j=1}^{N} G_{ij} q_j, \; i = 1, ..., N, \tag{3.92}$$

where $C_{ij} = C_i\,\delta_{ij}$, $\quad \delta_{ij} = 1$ if $i = j$, and 0 if $i \neq j$, and

$$q_j = \left(\frac{\partial \phi}{\partial n}\right)_j. \tag{3.93}$$

The above equation Eq.(3.92) involves N values of ϕ and N values of q, half of which are prescribed as boundary conditions of the problem. In order to calculate the remaining unknowns, it is necessary to generate N equations. This is achieved using a collocation technique where the equation is assumed to be valid at all boundary nodes. This generates an $N \times N$ system of equations of the form:

$$\mathbf{C}\phi + \hat{\mathbf{H}}\phi = \mathbf{G}q. \tag{3.94}$$

3.8 Singular Integrals

One of the problems encountered in BEM computations is the evaluation of the integrals which occur when the source point is in the target element; in this case, the kernel of the integral equation becomes infinite when the integration variable and collocation point coincide, then the integral becomes singular.

When the source point is not in the target element, then the integrals are regular. Such integrals are commonly evaluated using Gauss quadrature. Eq.(3.95) shows the numerical method for a function with a single independent variable:

$$\int_{-1}^{+1} f(\xi)\,d\xi \approx \sum_{g=1}^{N} w_g\, f(\xi_g), \tag{3.95}$$

where g is the total number of Gauss quadrature points, ξ_g is the Gauss coordinate and w_g is the associated weight. The coordinates, which are roots of Legendre polynomials, and the weights may be found in [151].

For potential problems with constant or linear elements, when the source point is in the target element, the singular integrals may be performed analytically [63]. For quadratic elements with straight edges, analytical values have been given by [152]. However, for isoparametric

quadratic elements, no such analytical values are available and an approximate method is required.

However, in general we must use a fully numerical approach and there are three commonly used ways of dealing with singular integrals, which are the logarithmic Gauss quadrature approach, subtraction of singularity technique and Telles' self-adaptive scheme.

3.8.1 Telles Self-Adaptive Technique

This numerical approach uses a transformation in such a way that the Jacobian is zero at the singular point, thus removing the singularity [22]. Conventional Gauss quadrature may then be used. The effect of the transformation is to bunch the Gauss points towards the singularity. The singular integrals are written in the form

$$I = \int_{-1}^{+1} f(\xi)\, d\xi \tag{3.96}$$

and we seek a transformation $\xi \to \eta$ which maps $[-1,1] \to [-1,1]$ via a cubic polynomial

$$\xi = a\eta^3 + b\eta^2 + c\eta + d. \tag{3.97}$$

Suppose that the integral has a singularity at $\bar{\xi}$ and that $\bar{\eta}$ is the corresponding value of η, then we choose a, b, c and d so that

$$\left(\frac{d^2\xi}{d\eta^2}\right)_{\bar{\eta}} = 0,\ \left(\frac{d\xi}{d\eta}\right)_{\bar{\eta}} = 0,\ \xi(1) = 1,\ \xi(-1) = -1 \tag{3.98}$$

The values of a, b, c and d given by Telles [22], are

$$a = \frac{1}{Q},\ b = -\frac{3\bar{\eta}}{Q},\ c = \frac{3\bar{\eta}^2}{Q},\ d = -b. \tag{3.99}$$

where $Q = 1 + 3\bar{\eta}^2$. With these values, a solution of Eq.(3.97) yields:

$$\bar{\eta} = \left[\bar{\xi}\left(\bar{\xi}^2 - 1\right) + \left|\bar{\xi}^2 - 1\right|\right]^{\frac{1}{3}} + \left[\bar{\xi}\left(\bar{\xi}^2 - 1\right) - \left|\bar{\xi}^2 - 1\right|\right]^{\frac{1}{3}} + \bar{\xi} \tag{3.100}$$

and the value of the integral in Eq.(3.96) becomes

$$I = \int_{-1}^{1} f\left(\frac{(\eta-\bar{\eta})^3 + \bar{\eta}\left(\bar{\eta}^2+3\right)}{1+3\bar{\eta}^2}\right)\frac{3(\eta-\bar{\eta})^2}{1+3\bar{\eta}^2}d\eta. \tag{3.101}$$

The integrand in expression (3.96) is well-behaved in the neighborhood of $\eta \to \bar{\eta}$ and may be integrated using standard Gauss quadrature. As mentioned earlier, the effect of the transformation is to distribute the Gauss points so that they are bunched towards the singularity. In Fig. 3.3 we show a geometrical transformation of a four-point quadrature rule in the case when $\bar{\eta} = 1$, and the parameters in Eq.(3.97) take the following values:

$$a = \frac{1}{4},\ -c = -d = -\frac{3}{4},\ \xi = \frac{1}{4}\left[(\eta-1)^3+4\right],$$

$$I = \frac{3}{4}\int_{-1}^{+1} f\left(\frac{1}{4}\left[(\eta-1)^3+4\right]\right)(\eta-1)^3\, d\eta.$$

Telles' scheme is self-adaptive in that the effect of concentrating the quadrature points towards $\bar{\eta}$ is less marked as the singular point moves outside the domain of integration, i.e. as $|\bar{\eta}| > 1$. In fact $|\bar{\eta}| \to \infty$ we have, from Eq.(3.101),

$$I \to \int_{-1}^{+1} f(\eta)\, d\eta$$

and the integral degenerates to the standard form as in Eq.(3.96). Hence the Telles transformation could be used as a general numerical quadrature rule which deals automatically with regular, near singular and singular integrals.

3.8.2 Handling the Singularities of BEM Formulation

It is clear that the values of the diagonal terms of matrices H and G have singularities that need special treatment in their evaluation.

The G_{ii} terms have singularities of the logarithmic type, for they depend on the kernel integrand $G(\xi, x)$, a function of the Bessel function K_0 according to Eq.(3.85).

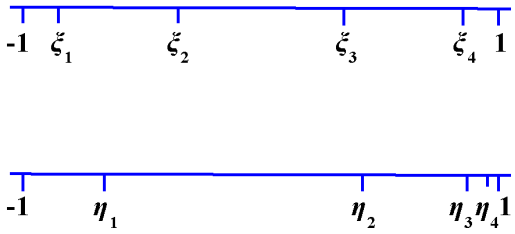

Figure 3.3: Transformation of the quadrature points for a four-point Gauss rule in the case $\bar{\eta} = 1$

The H_{ii} terms have singularities of both logarithmic and Cauchy Principal value $1/r$ types, for the normal derivative is expressed as

$$\frac{1}{2\pi D} e^{\frac{-v.\mathbf{r}}{2D}} \left[-|\mu| K_1(|\mu||\mathbf{r}|) \frac{\partial \mathbf{r}}{\partial n} - \frac{v_n}{2D} K_0(|\mu||\mathbf{r}|) \right]. \tag{3.102}$$

For the constant elements used here, the first expression between brackets vanishes because for the constant element case $\frac{\partial \mathbf{r}}{\partial n} = 0$; then, the only the singularity left is logarithmic.
In order to evaluate these terms, Telles' transformation [22] scheme was used with 10 integration points. The other non-singular terms were evaluated using normal Gaussian quadrature.
The constants C_i in Eq.(3.92) play an important role and introduce an additional difficulty in case of chemical reaction. These constant terms usually need not be directly evaluated, because they can be embodied in the diagonal terms of the matrix H, defined as

$$H = \hat{H} + C \tag{3.103}$$

Then the diagonal terms

$$H_{ii} = \hat{H}_{ii} + C_i \tag{3.104}$$

are calculated applying conditions of uniform concentration distribution or mass conservation of an arbitrary species. To satisfy the conditions just mentioned, the matrix H has to be singular and its diagonal coefficients can be evaluated as the sum of non-diagonal terms in the form:

$$H_{ii} = -\sum_{j=1}^{N} H_{ij}, \ (i \neq j) \tag{3.105}$$

However, when chemical reaction occurs, conservation laws cannot be applied to the reactant species even if a uniform concentration is applied on the whole boundary Γ. In this case, the constants C_i have to be evaluated using expression (A.32).

It is convenient to have the constants embodied in the matrix H, for the sake of consequent application of the boundary conditions. Expression (3.94) then takes the form

$$\mathbf{H}\phi = \mathbf{G}q. \tag{3.106}$$

As for every nodal point either ϕ or $\frac{\partial \phi}{\partial n}$ is prescribed there is an interchange of the corresponding columns between matrices H and G in order to obtain the final system of equations.

3.9 Error Indicator

The accuracy of numerical solutions is usually improved by mesh refinement, as in FDM and the FEM. In this chapter, the solution convergence and accuracy will be presented by root mean square error. Our aim here is to study the convergence behaviour to show accuracy and the efficiency of the proposed method for which results are reported.

In order to estimate the simulation error throughout the numerical experiments, the root mean square norm is utilised as shown below. It is based on the difference between the simulation results ϕ_{numer} and the analytical solution ϕ_{exact} as

$$\text{RMS} = \sqrt{\frac{1}{N}\sum_{i=1}^{N} |\phi_{i,numer} - \phi_{i,exact}|^2}. \tag{3.107}$$

3.10 Numerical Experiments and Discussions

In this section, we begin by introducing some problems solved by the BEM with constant elements using Matlab 2016a Version 9. Numerical examples are presented for problems with different geometries, for which exact solutions are available. Comparison between the solutions is demonstrated through graphs showing the plot of the solution in a two-dimensional space, as well as the error of each problem. Typically, 10 integration points are used to show the numerical behaviour and the convergence for the solution of the PDEs. To show the performance of the boundary element scheme, five numerical benchmark applications were studied.

3.10.1 Steady-State Convection-Diffusion-Reaction Problem over Square Region With Mixed (Neumann-Dirichlet) Boundary Conditions (Moving Long Bar)

The algorithm was initially tested with the problem of a moving bar with constant velocity v_x, $v_y = 0$ and specified concentration at the edges, i.e. $\phi = 300$ at $x = 0$ and $\phi = 0$ at $x = L$. Other values adopted are $D = 1\left(m^2/s\right)$ and $k = 0\,(1/s)$ for this case study, where D and k represent the diffusivity and the reaction coefficient, respectively. Consider the domain Ω is homogeneous and isotropic. The two dimensional steady-state convection-diffusion-reaction problem with constant velocity field is subject to the boundary conditions: Neumann boundary: conditions along the horizontal faces $y = 0$ and $y = 1$: $q = \frac{\partial \phi}{\partial n} = 0$, and Dirichlet boundary conditions along the vertical faces $x = 0$ and $x = L$ (Fig. 3.4).
The analytical solution for this problem is:

$$\phi\,(x,y) = 300\exp\left(\frac{v_x x}{2}\right)\frac{\sinh\left[\left(\frac{v_x}{2}\right)(L-x)\right]}{\sinh\left[\left(\frac{v_x}{2}\right)L\right]}, \tag{3.108}$$

where $v_x\,(m/s)$ is the velocity along the x-axis and L represents the length of the bar. The problem has been modelled as a square shaped-body having a height of $1\,m$ and length $L = 1\,m$. The discretisation employed 30 constant boundary elements on each side of the

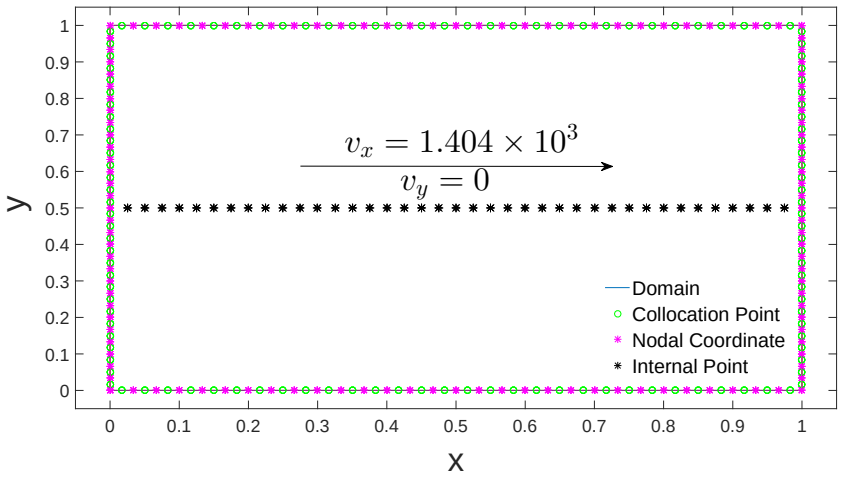

Figure 3.4: Geometry and discretisation for 2D convection-diffusion-reaction model moving long bar with uni-directional velocity v_x and side length $1m$

domain, making up a total of 120 constant elements, with 39 internal nodes which are only used in this case to plot the results along the middle of the channel. The schematic diagram of the problem is shown in Fig. 3.4.

Positive Velocity

Figure 3.5 shows the simulated and analytical solutions at the bottom side of the channel $y = 0$ with very good agreement in this case. Next, results are plotted along the centre of the computational domain, i.e. at internal nodes as presented in Fig. 3.6. The analytical solution is followed in a very accurate manner even for high Pé. Table 3.1 shows a comparison between the simulation and the analytical solutions for different positions along the lower side of the domain. The results for the numerical and the analytical solutions are in excellent agreement. Table 3.2 shows the RMS error norm for different velocities and mesh sizes. It can be noticed that the errors decrease with mesh refinement. The relative error in the RMS norm is of the order 10^{-3} for Pé $= 1$ and 10^{-2} for all other values of Pé.

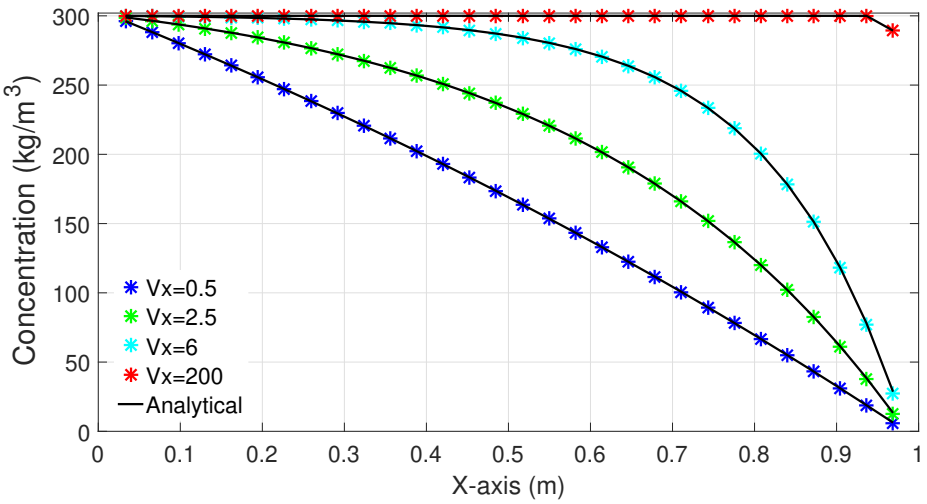

Figure 3.5: Variation of concentration profile ϕ along the bottom horizontal face $y = 0$ with different velocities v_x: comparison between the analytical (solid line) and numerical (star points) solutions

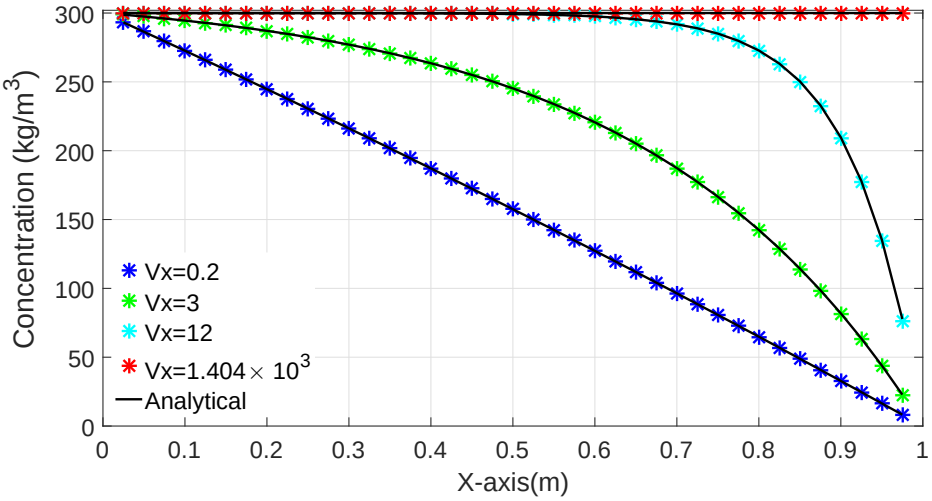

Figure 3.6: Variation of concentration profile ϕ along the middle line $y = 0.5$ with different velocities v_x: comparison between the analytical (solid line) and numerical (star points) solutions

Negative Velocity

In this case, the velocity acts in the negative direction. The results at internal points are plotted in Fig. 3.7 for several velocities values $v_x = -0.2, -3, -12$ and -1.404×10^3 against the analytical solution. The results show very good agreement between numerical and analytical

Table 3.1: BEM results of ϕ for convection-diffusion-reaction problem at Pé $= 1$

x	BEM	Analytical
0.1	278.456	278.395
0.3	234.971	234.956
0.5	181.883	181.900
0.6	151.082	151.117
0.7	117.037	117.097
0.8	79.399	79.498
0.9	37.753	37.946

Table 3.2: RMS norm of BEM for convection-diffusion-reaction problem with different spatial meshes

RMS error norm for ϕ, Problem 1				
Mesh size	Pé $= 1$	Pé $= 5$	Pé $= 10$	Pé $= 15$
60	2.1×10^{-1}	4.4×10^{-1}	6.2×10^{-1}	6.8×10^{-1}
72	1.6×10^{-1}	3.6×10^{-1}	5.3×10^{-1}	6.0×10^{-1}
100	1.0×10^{-1}	2.4×10^{-1}	3.8×10^{-1}	4.6×10^{-1}
200	4.1×10^{-2}	1.3×10^{-1}	1.7×10^{-1}	2.2×10^{-1}
400	1.5×10^{-2}	4.0×10^{-2}	7.2×10^{-2}	9.9×10^{-2}
800	5.5×10^{-3}	1.5×10^{-2}	2.8×10^{-2}	4.0×10^{-2}

solutions along the line $y = 0.5$.

Besides the excellent behaviour of these findings it is also convenient to point out that, unlike results obtained using standard FDM or FEM, the BEM results agreed with the analytical solution all over the front even for high values of the Péclet number (Pé $= 1.404 \times 10^3$ in the present case). Figure 3.8 also shows very good agreement between the numerical

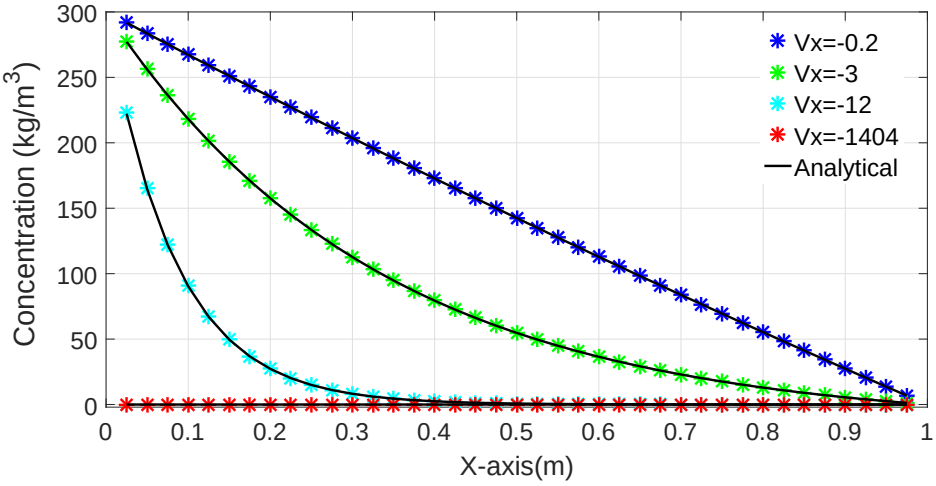

Figure 3.7: Variation of concentration profile ϕ along the middle line $y = 0.5$ with different negative velocities v_x: comparison between the analytical (solid line) and numerical (star points) solutions

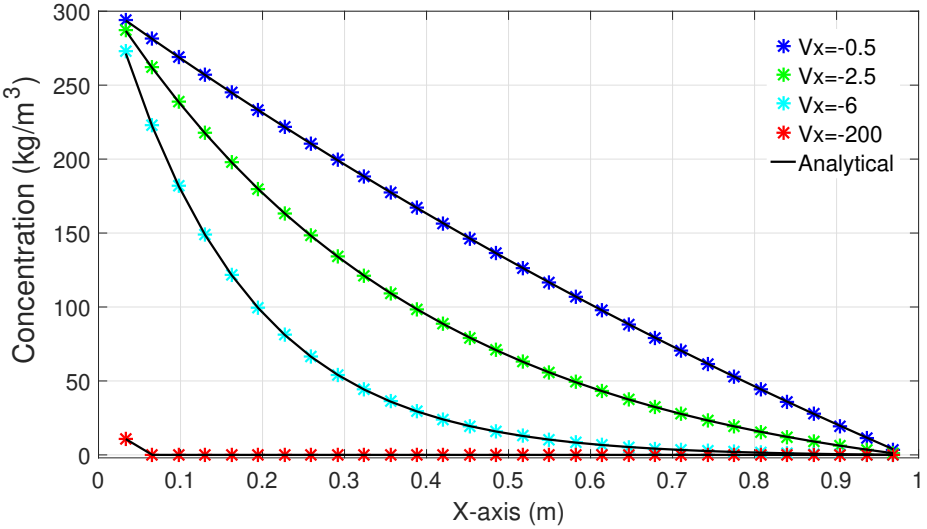

Figure 3.8: Variation of concentration profile ϕ along the bottom face $y = 0$ with different negative velocities v_x: comparison between the analytical (solid line) and numerical (star points) solutions

and analytical solutions along the face $y = 0$ for different negative velocities values $v_x = -0.5, -2.5, -6, -200$.

3.10.2 Steady-State Convection-Diffusion-Reaction Problem over a Square Plate with Dirichlet Boundary Conditions (The Chemical Reaction System)

In this example, the concentration distribution in a plate with a square geometry was studied. The discretisation employed 120 constant elements, 30 on each face and 39 internal nodes distributed along the middle of the computational domain. A unit value was assumed for the diffusion coefficient $D\left(m^2/s\right)$. The domain $\Omega = [1m \times 1m]$ was considered to be homogeneous and the medium is isotropic. The Dirichlet boundary conditions corresponding to the problem are defined as:

$$\begin{aligned} \phi = 0; \quad &\text{along the bottom horizontal face,} \quad 0 \leq x \leq 1. \\ \phi = 0; \quad &\text{along the top horizontal face,} \quad 0 \leq x \leq 1. \\ \phi = 0; \quad &\text{along the right vertical face,} \quad 0 \leq y \leq 1. \\ \phi = \sin(\pi y); \quad &\text{along the left vertical face,} \quad 0 \leq y \leq 1. \end{aligned} \tag{3.109}$$

The analytical solution is of the form:

$$\phi(x,y) = \frac{e^{m_1(L-x)} - e^{m_2(L-x)}}{e^{m_1 L} - e^{m_2 L}} \sin\left(\frac{\pi y}{\ell}\right), \tag{3.110}$$

where

$$m_1 = \frac{1}{2}\left[-v_x + \sqrt{v_x^2 + \left(\frac{\pi^2}{L^2} + k\right)}\right], \; m_2 = \frac{1}{2}\left[-v_x - \sqrt{v_x^2 + \left(\frac{\pi^2}{L^2} + k\right)}\right] \tag{3.111}$$

with $L = 1$ and $\ell = 1$ the dimensions in the x and y-directions, respectively. It can be seen in Fig. 3.9 that the results of the concentration profile ϕ compare very well with the analytical solution along the internal points utilising various positive values of the velocity field $v_x = 0.2$, 3, 12 and 234 with reaction coefficient $k = 0$, with the BEM showing again no oscillation or damping of the wave front in this case. Next, Fig. 3.10 shows that the results of the concentration profile ϕ agree very well with the analytical solution along the internal

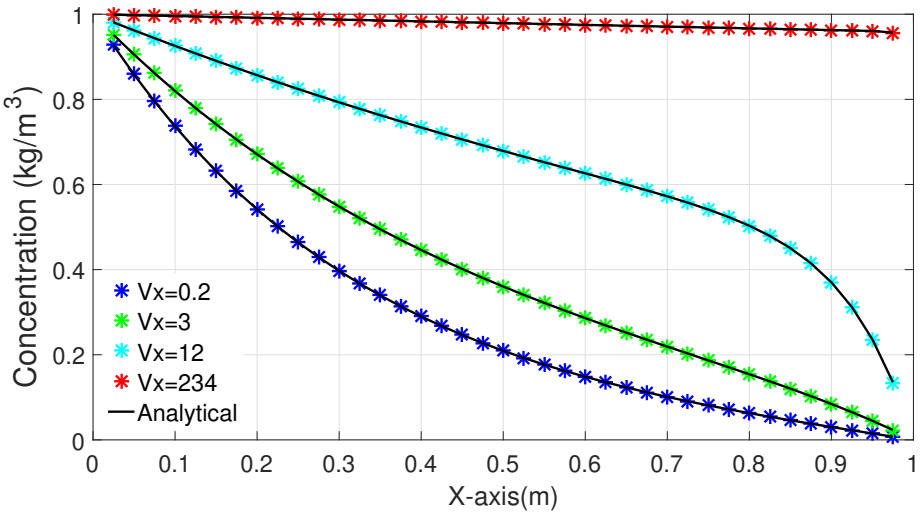

Figure 3.9: Variation of concentration profile ϕ along the middle of the channel with $k = 0$ and different velocities v_x: comparison between the analytical (solid line) and numerical (star points) solutions

points when the velocity $v_x\,(m/s)$ is in the negative direction with $v_x = -0.2, -2, -6$ and -100. The results for the concentration profile ϕ along the middle of the computational

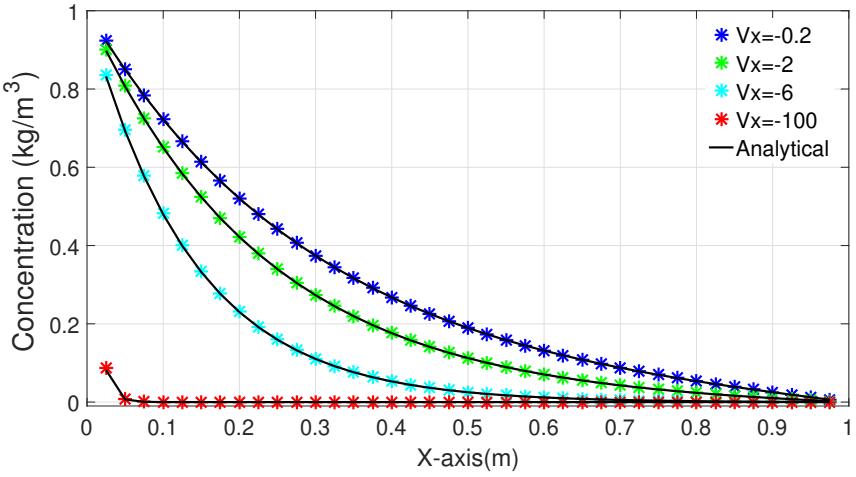

Figure 3.10: Variation of concentration profile ϕ along the middle of the channel with $k = 0$ and different velocities v_x: comparison between the analytical (solid line) and numerical (star points) solutions

domain $y = \frac{1}{2}$ with $v_x = 30$ is shown in Fig. 3.11 for different values of the reaction coefficient $k\,(1/s)$. Figure 3.12 shows that the results of the concentration profile ϕ compares well with

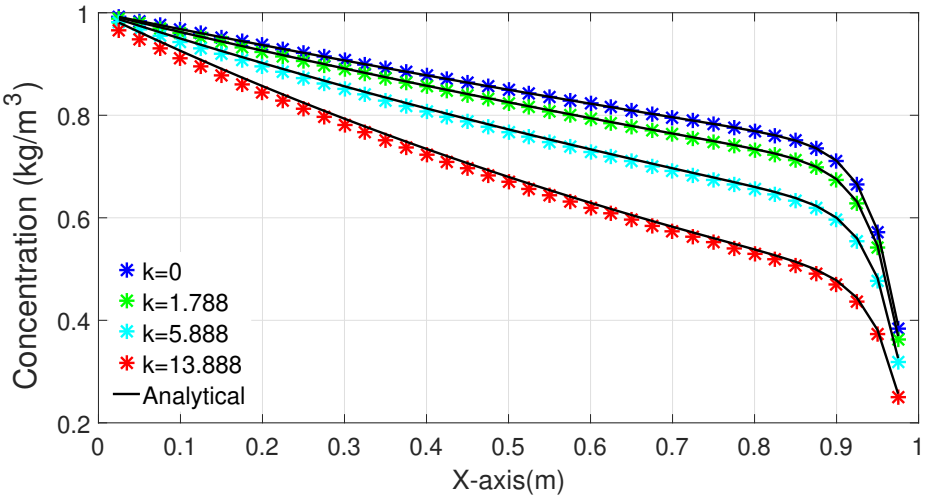

Figure 3.11: Variation of concentration profile ϕ along the middle of the channel with $v_x = 30$ and different values of reaction coefficient k: comparison between the analytical (solid line) and numerical (star points) solutions

the analytical solution for different values of the reaction coefficient $k = 0, 1.788, 5.888$ and 13.888 along the internal points utilising $v_x = 100$, for which the global Péclet number is Pé $= 100$. These specific reaction values are empirically chosen and examined for this numerical experiment to show the solution behaviour for different reaction values. Table

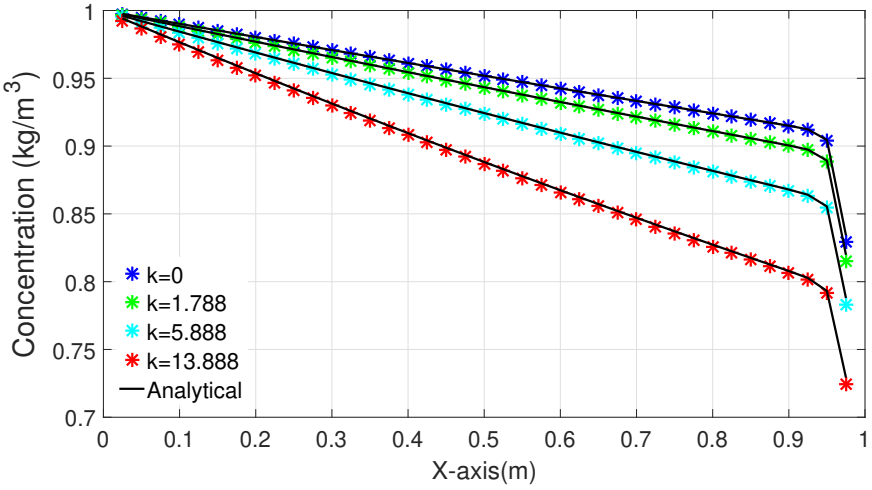

Figure 3.12: Variation of concentration profile ϕ along the middle of the channel with $v_x = 100$ and different reactions k values: comparison between the analytical (solid line) and numerical (star points) solutions

Table 3.3: BEM results of q for convection-diffusion-reaction problem at Pé $= 10$

x	BEM	Analytical
0.33	-2.9456	-2.9991
0.1	-2.8066	-2.8190
0.3	-2.3329	-2.3406
0.5	-1.9322	-1.9382
0.7	-1.5544	-1.5588
0.9	-0.8417	-0.8419

3.3 shows a comparison between the simulation and the analytical solutions for the heat flux $q(x) = -\frac{\partial \phi(x,y)}{\partial y(x,0)}$ at different positions of x along the bottom face of the channel with $k = 2.777$. The results show an excellent agreement between the numerical and the analytical solutions in this case.

The absolute error in the RMS norm at various Péclet numbers with reaction coefficient $k = 0.2777$ is displayed in Table 3.4. Table 3.4 shows the RMS error norm of q for different

Table 3.4: RMS norm of BEM for convection-diffusion-reaction problem with different spatial meshes

RMS error norm for q, Problem 2				
Mesh size	Pé $= 10$	Pé $= 50$	Pé $= 100$	Pé $= 120$
40	1.0×10^{-1}	3.5×10^{-1}	7.7×10^{-1}	9.7×10^{-1}
60	7.5×10^{-2}	1.9×10^{-1}	4.3×10^{-1}	5.8×10^{-1}
72	6.5×10^{-2}	1.5×10^{-1}	3.3×10^{-1}	4.5×10^{-1}
120	4.6×10^{-2}	8.6×10^{-2}	1.6×10^{-1}	2.3×10^{-1}
200	3.5×10^{-2}	5.1×10^{-2}	9.3×10^{-2}	1.2×10^{-1}
400	2.5×10^{-2}	2.8×10^{-2}	4.5×10^{-2}	6.0×10^{-2}

velocities and mesh sizes. It can be noticed that the errors decrease with mesh refinement. The absolute error in the RMS norm for the fluxes q is of the order 10^{-2} for all values of Pé.

3.10.3 Steady-State Convection-Diffusion-Reaction Problem over Rectangular Domain with Mixed (Neumann-Dirichlet) Boundary Conditions (The Chemical Reaction System)

In this case, the diffusivity coefficient and the reference length are assigned a unit value; thus, the Péclet number is always equal to the velocity v_x. This is a convection-diffusion-reaction problem with prescribed values of ϕ at $x = 0$ and at $x = 1$. The velocity along the x-axis is given by $v_x = v$, $v_y = 0$. The domain Ω is considered to be homogeneous and the medium is isotropic.

The boundary conditions are: Neumann boundary conditions $q = 0$ along the faces $y = 0$ and $y = 0.5$, while Dirichlet boundary conditions ϕ are applied along vertical faces. For the right vertical face $x = 1$, $\phi = 2$ and for the left vertical side $x = 0$, $\phi = 1$. The analytical solution takes the form:

$$\phi(x,y) = 2 - \frac{1 - e^{v(x-1)}}{1 - e^{-v}}. \tag{3.112}$$

The problem is discretised with 140 elements equally distributed using 10 constant elements for each vertical side and 60 for the top and the bottom horizontal sides of the rectangular domain. The interior points are imposed to be 39 along the middle side of the cross-section i.e. $y = 0.25$.

Positive Velocity

In this case study, the simulated and the analytical solutions are given in Fig. 3.13. The solution presents very good agreement along the horizontal line $y = 0.25\,(1/s)$ with several positive velocity values $v_x = 0.2, 1, 6\,(m/s)$ and 200 and reaction coefficient $k = 0\,(1/s)$. Figure 3.14 illustrates the comparison of the concentration and the analytical profiles along the bottom face of the domain $y = 0$ for various values of the velocity along the x-axis. The results indicate the applicability and accuracy of the BEM for the proposed model. Table

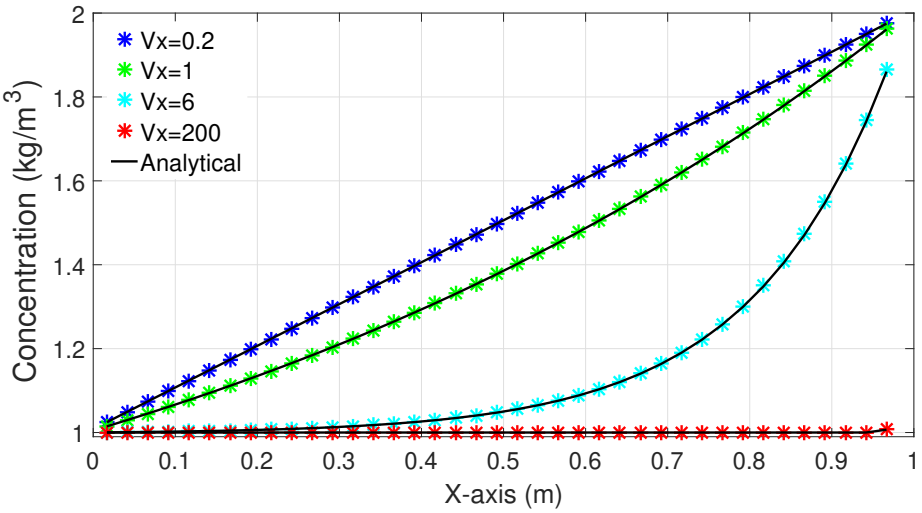

Figure 3.13: Variation of concentration profile ϕ along the middle of the channel $y = 0.25$ with different values of velocities v_x: comparison between the analytical (solid line) and numerical (star points) solutions

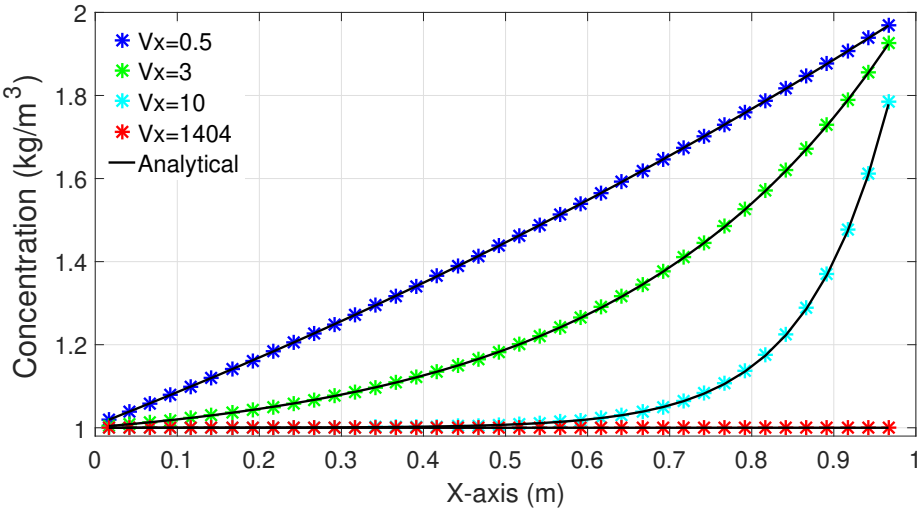

Figure 3.14: Variation of concentration profile ϕ along the bottom face of the channel $y = 0$ with different positive profiles of velocities v_x: comparison between the analytical (solid line) and numerical (star points) solutions

3.5 shows a comparison between the simulation and the analytical solutions for different positions along the middle of the domain, i.e. $y = 0.25$. The results for the numerical and the analytical solutions are in excellent agreement. Now, to measures the relative error in RMS norm for different mesh sizes and Péclet numbers as displayed in Table 3.4. Table 3.6

Table 3.5: BEM results of ϕ for convection-diffusion-reaction problem at Pé $= 10$

x	BEM	Analytical
0.1	1.0001	1.0001
0.25	1.0006	1.0006
0.35	1.0016	1.0016
0.55	1.0120	1.0120
0.65	1.0328	1.0328
0.85	1.2425	1.2425
0.95	1.6596	1.6592

Table 3.6: RMS norm of BEM for convection-diffusion-reaction problem with different spatial meshes

RMS error norm for ϕ, Problem 3				
Mesh size	Pé $= 10$	Pé $= 20$	Pé $= 30$	Pé $= 40$
44	4.0×10^{-3}	4.1×10^{-3}	3.2×10^{-3}	2.2×10^{-3}
60	1.9×10^{-3}	2.3×10^{-3}	2.2×10^{-3}	1.9×10^{-3}
72	3.9×10^{-4}	4.0×10^{-4}	3.1×10^{-4}	2.1×10^{-4}
130	1.8×10^{-4}	2.3×10^{-4}	2.3×10^{-4}	2.0×10^{-4}
200	1.0×10^{-4}	1.5×10^{-4}	1.7×10^{-4}	1.7×10^{-4}
400	1.8×10^{-5}	1.8×10^{-5}	1.6×10^{-5}	1.6×10^{-5}

shows the RMS error norm for different velocities and mesh sizes. It can be noticed that the errors decrease with mesh refinement. The relative error in the RMS norm is just 10^{-5} for all values of Pé.

Negative Velocity

Here negative velocity values are imposed with the flow going in the opposite direction. The results are plotted at the internal nodes along the middle of the domain for a set of values $v_x = -0.2, -1, -6, -200\,(m/s)$ with $k = 0\,(1/s)$. The maximum Péclet number in this case is Pé $= 200$. A comparison of the concentration and the analytical solution profiles along

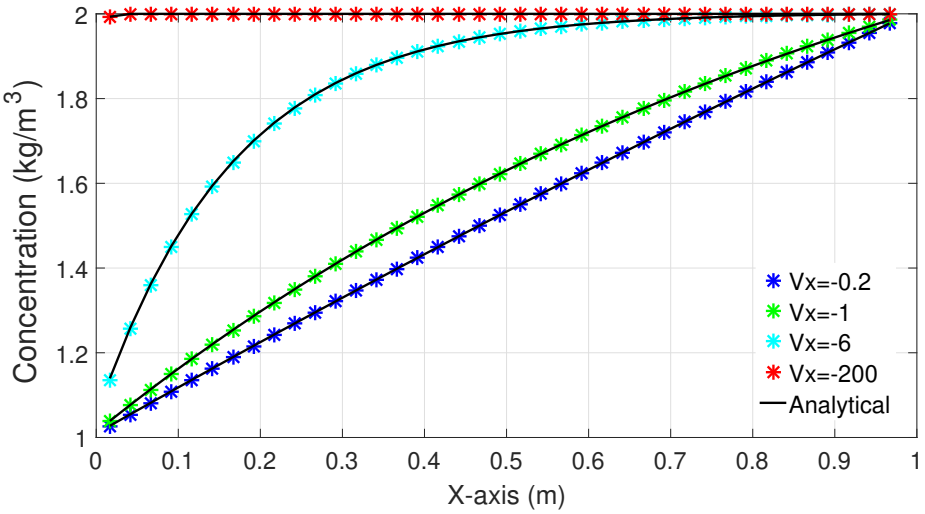

Figure 3.15: Variation of concentration profile ϕ along the middle of the channel $y = 0.25$ with different negative values of velocity v_x: comparison between the analytical (solid line) and numerical (star points) solutions

the bottom face of the domain $y = 0$ for different values of the velocity along the negative direction of the x-axis is shown in Fig. 3.16. The maximum Péclet number in this test case is equal to 7.25×10^2. The results match perfectly the analytical solution in this test case.

3.10.4 Steady-State Convection-Diffusion-Reaction Problem over a Rectangular Region and Robin Boundary Conditions

In this test case, the velocity field is considered to be constant along the longitudinal direction. A sketch of the geometrical model used in this example is depicted in Fig. 3.17. The problem was modelled as a rectangular channel of cross-section $\Omega = [6m \times 4m]$. The boundary

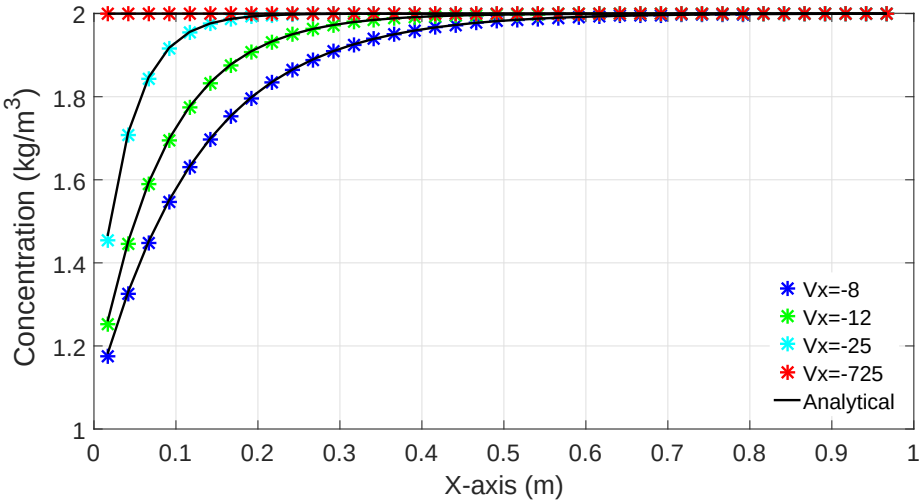

Figure 3.16: Variation of concentration profile ϕ along the bottom face of the channel $y = 0$ with different negative velocity profiles v_x: comparison between the analytical (solid line) and numerical (star points) solutions

conditions corresponding to the problem above are defined as:

$$\begin{aligned}
\phi(x,0) &= 0, \quad \text{along the bottom horizontal face} \quad y = 0;\ 0 \le x \le 6,\\
\phi(x,4) &= 0, \quad \text{along the top horizontal face} \quad y = 1;\ 0 \le x \le 6,\\
\phi(0,y) &= 0, \quad \text{along the left vertical face} \quad x = 0;\ 0 \le y \le 4,\\
\frac{\partial \phi}{\partial x}(6,y) - \frac{v_x}{2}\phi(6,y) &= 100\,\mathrm{e}^{(3v_x)}, \quad \text{along the right vertical face} \quad x = 0;\ 0 \le y \le 4.
\end{aligned}$$

The analytical solution for this transport problem is given by:

$$\phi(x,y) = \frac{400}{\pi}\exp\left(\frac{v_x x}{2}\right)\sum_{n\in\mathscr{O}}\frac{1}{n\beta_n}\frac{\sinh(\beta_n x)}{\sinh(6\beta_n)}\sin\left(\frac{n\pi(y+4)}{8}\right), \tag{3.113}$$

where $\mathscr{O}$ is the set of positive odd integers and $\beta_n^2 = \left(\frac{v_x}{2}\right)^2 + \frac{n^2\pi^2}{8^2}$. This rectangular model is discretised with 440 elements, with 100 constant elements for each vertical side and 120 for each horizontal one.

The first case was analysed for a velocity field $v_x = 0.05\,(m/s)$ along the x-axis and reaction value $k = 0\,(1/s)$, with the results plotted along the horizontal line $y = 2$, as shown in Fig.

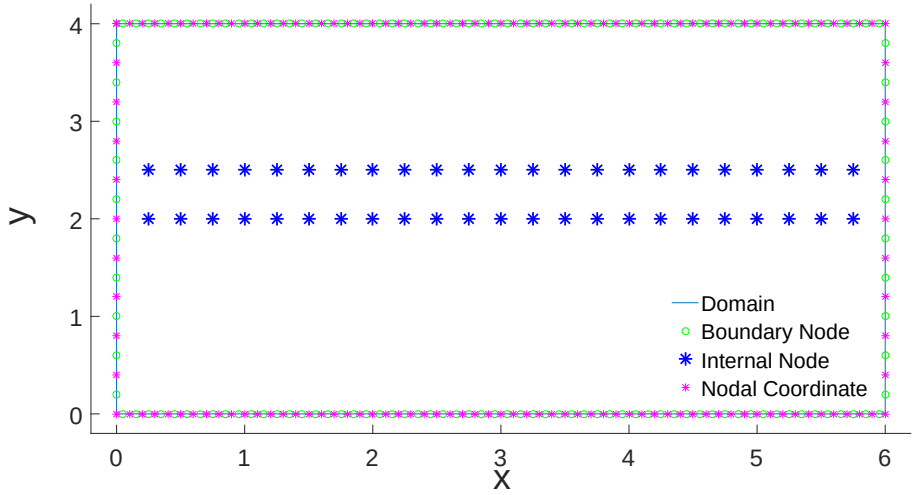

Figure 3.17: BEM discretisation and geometrical properties of rectangular channel for convection-diffusion-reaction model

3.18. Figure 3.19 displays the results along the horizontal line $y = 2.5$ versus the analytical

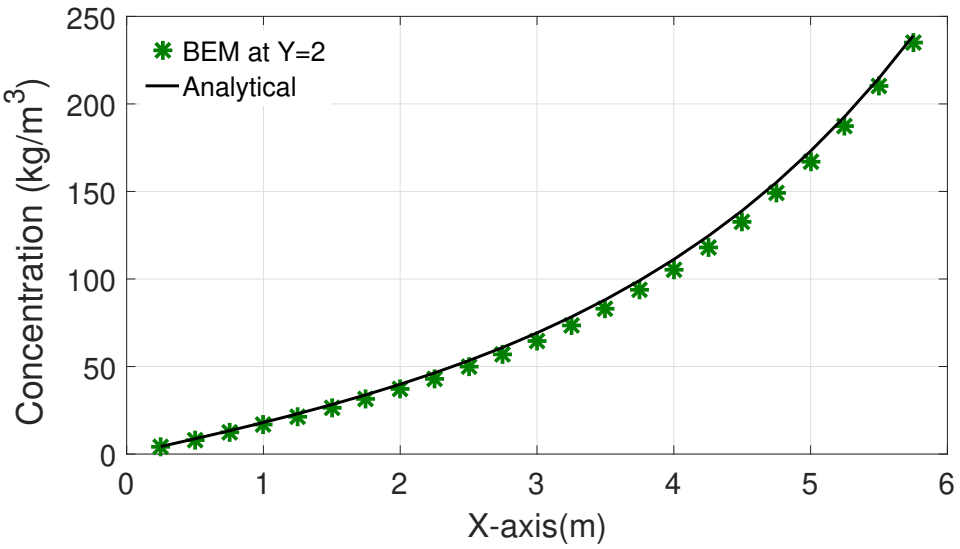

Figure 3.18: Variation of concentration profile ϕ along the horizontal line $y = 2$: comparison between the analytical (solid line) and numerical (star points) solutions

solution. The results exhibit a very good agreement with the analytical solutions.

In the second case, the results are plotted along the middle of the domain at $y = 2$ as shown in Fig. 3.20 for the velocity $v_x = 0.0055$. The simulated and the analytical results display good agreement in this test case. Next, the findings are plotted along the horizontal line at

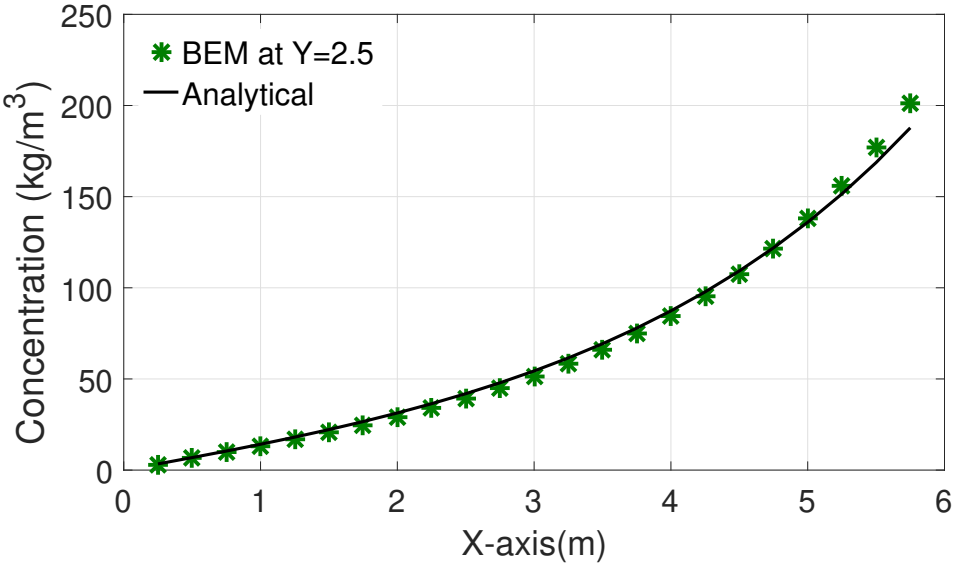

Figure 3.19: Variation of concentration profile ϕ along the horizontal line $y = 2.5$: comparison between the analytical (solid line) and numerical (star points) solutions

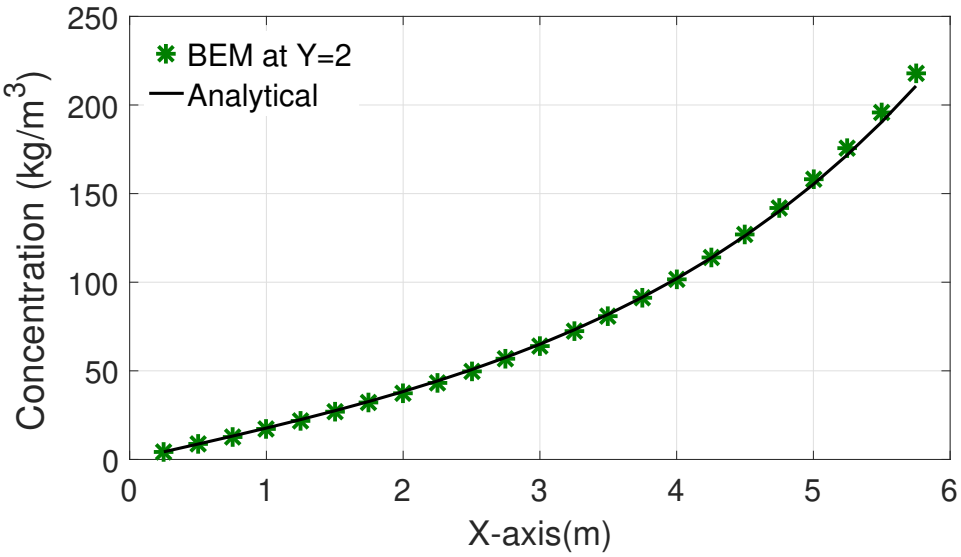

Figure 3.20: Variation of concentration profile ϕ along the horizontal line $y = 2$: comparison between the analytical (solid line) and numerical (star points) solutions

$y = 2.5$ as given in Fig. 3.21. Table 3.7 shows a comparison between the simulation and the analytical solutions for different positions along the middle of the y-axis, i.e. $y = 2$. The results for the numerical and the analytical solutions are in good agreement.

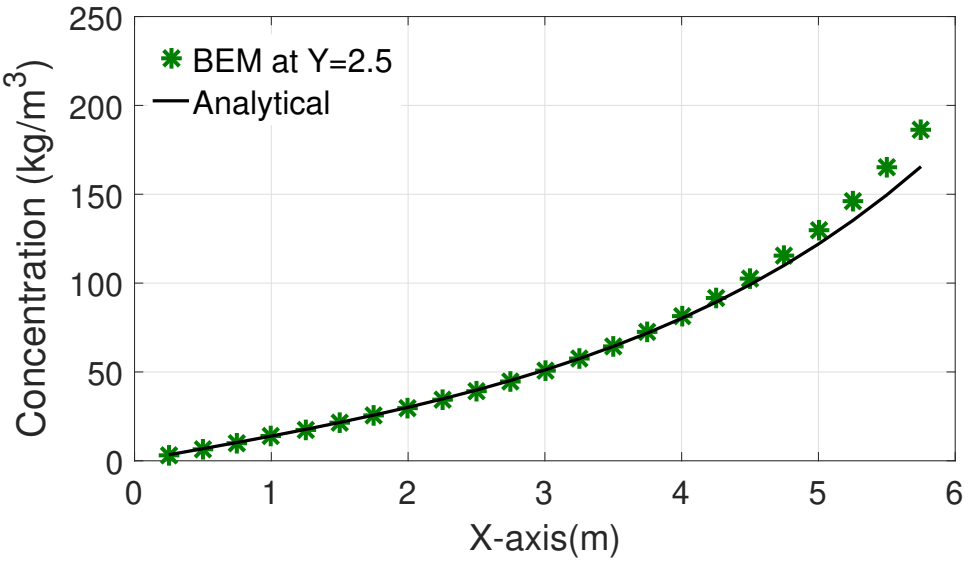

Figure 3.21: Variation of concentration profile ϕ along the horizontal line $y = 2.5$: comparison between the analytical (solid line) and numerical (star points) solutions

Table 3.7: Results of BEM for convection-diffusion-reaction problem at Pé $= 0.01$

x	BEM	Analytical
0.5	8.450	8.686
1.5	26.845	27.552
2.5	49.354	50.934
3.5	81.354	82.546
4.5	127.483	127.435
5.5	197.336	192.781

3.11 Summary and Discussions

In this chapter, simulations are presented for low, moderate and high Péclet numbers compared to the analytical solution for the corresponding problem with different numerical models. The results support the use of the proposed approach to solve steady-state convection-diffusion-reaction problems. Numerical performance and the accuracy of the numerical

scheme are then assessed. After validation of the numerical technique, results for different Péclet numbers are shown, concluding that the approach presented very good agreement between numerical and analytical solutions. It should be noted that, the highest velocity value in this chapter is 1.404×10^3. If the velocity field value is significant i.e. $v_x > 1.404 \times 10^3$, the domain discretisation is necessary to avoid the numerical oscillation and damping.

This chapter has presented an efficient integration scheme suitable for weakly singular integrals which appear in boundary element formulations for convection-diffusion-reaction problems with several positive and negative velocity fields. The weakly singular integral was evaluated by using Gauss quadrature with a cubic transformation developed by Telles [22], the Jacobian of which cancels the singularity. Therefore, powerful direct or iterative solvers can be implemented for an even increased efficiency.

Last but not least, results of applications have shown that the solutions do not display numerical problems of oscillations and damping of the wave front, common in many FDM and FEM formulations.

Chapter 4

DRBEM Modelling for Steady-State Convection-Diffusion-Reaction Problems with Variable Velocity Fields

4.1 Introduction

This chapter presents a dual reciprocity boundary element method (DRBEM) formulation for the solution of steady-state convection-diffusion-reaction problems with variable velocity field at low, moderate and high Péclet number. This scheme is based on utilising the fundamental solution of the convection-diffusion-reaction equation with constant coefficients. In this case, we decompose the velocity field into an average and a perturbation, with the latter being treated using a dual reciprocity approximation to convert the domain integrals arising in the boundary element formulation into equivalent boundary integrals. A proposed approach is implemented to treat the convective terms with variable velocity, for which the concentration is expanded as a series of functions. Three numerical experiments are included with available analytical solutions, to establish the validity of the approach and to demonstrate the efficiency of the proposed method.

The BEM has been applied to steady-state convection-diffusion-reaction problems with variable velocity by various researchers [8, 153, 115, 116, 119, 120, 122, 154, 155]. However,

the solution of this problem is still considered a big challenge, particularly for variable and high velocities. The BEM does have an inherent advantage over other numerical methods for the solution of convection-diffusion-reaction problems with constant velocity as the existing fundamental solution of the problem introduces the exact amount of upwind, contrary to finite element or finite-difference methods where the upwind is numerical [122]. The DRBEM represents an alternative for solving linear PDEs with variable coefficients [9, 8, 156, 1, 10]. The solution of problems involving variable coefficients is more difficult to achieve with the BEM as fundamental solutions are only available for a small number of cases, for coefficients with very simple variations in space. The approach adopted in this paper is to split the velocity field into an average and a perturbation; the average velocity (constant) is included in the fundamental solution, while the perturbation generates a domain integral which is treated with the DRBEM.

A brief outline of this chapter is as follows. Section 4.2 reviews the representation of convection-diffusion-reaction problems. Section 4.3 derives the boundary element formulation using the steady-state fundamental solution of the corresponding equation with constant velocity. In section 4.4, the DRM formulation is developed for 2D steady-state convection-diffusion-reaction problem, followed in section 4.5 by a description of the discretisation of the DRBEM formulation for this model. Handling the convective terms by expanding the relevant functions as a series is shown in section 4.6. Section 4.7 gives the description of the coordinate functions and the choice of three RBFs adopted in this work. Domain discretisation approach is discussed in section 4.8. Error indicators are shown in section 4.9. Comparison and discussion of the solution profiles for the present numerical experiments are presented as well as the computational aspects are included to demonstrate the performance of this approach in section 4.10. Finally, some conclusions and discussions are provided in the last section.

4.2 Convection-Diffusion-Reaction Equation

The 2D convection-diffusion-reaction problem over a bounded domain Ω in $\mathbb{R}^2$ with a boundary Γ, for isotropic materials, is governed by the following PDE:

$$D\nabla^2\phi(x,y) - v_x(x,y)\frac{\partial\phi(x,y)}{\partial x} - v_y(x,y)\frac{\partial\phi(x,y)}{\partial y} - k\phi(x,y) = 0,\ (x,y)\in\Omega. \tag{4.1}$$

In Eq.(4.1), ϕ represents the concentration of a substance, treated as a function of space. The velocity components v_x and v_y along the x and y directions assumed to vary in space. Also, D is the diffusivity coefficient and k represents the first-order reaction constant or adsorption coefficient. The boundary conditions are

$$\phi = \bar{\phi} \quad \text{over} \quad \Gamma_D \tag{4.2}$$

$$q = \frac{\partial\phi}{\partial n} = \bar{q} \quad \text{over} \quad \Gamma_N \tag{4.3}$$

where Γ_D and Γ_N are the Dirichlet and Neumann parts of the boundary with $\Gamma = \Gamma_D \cup \Gamma_N$ and $\Gamma_D \cap \Gamma_N = \emptyset$.

4.3 Boundary Element Formulation of Convection-Diffusion-Reaction Problems Using Steady-State Fundamental Solution

For the sake of obtaining an integral equation equivalent to the above PDE Eq.(4.1), a fundamental solution is necessary. However, fundamental solutions are only available for the case of constant velocity fields. Thus, the variable velocity components $v_x = v_x(x,y)$ and $v_y = v_y(x,y)$ are decomposed into average (constant) terms $\bar{v}_x$ and $\bar{v}_y$, and perturbations $P_x = P_x(x,y)$ and $P_y = P_y(x,y)$, such that

$$v_x(x,y) = \bar{v}_x + P_x(x,y),\ v_y(x,y) = \bar{v}_y + P_y(x,y). \tag{4.4}$$

This permits rewriting equation (4.1) as

$$D\nabla^2\phi - \bar{v}_x\frac{\partial\phi}{\partial x} - \bar{v}_y\frac{\partial\phi}{\partial y} - k\phi = P_x\frac{\partial\phi}{\partial x} + P_y\frac{\partial\phi}{\partial y}. \tag{4.5}$$

The above differential equation can now be transformed into the following equivalent integral equation

$$\phi(\xi) - D\int_\Gamma \phi^*\frac{\partial\phi}{\partial n}d\Gamma + D\int_\Gamma \phi\frac{\partial\phi^*}{\partial n}d\Gamma + \int_\Gamma \phi\phi^*\bar{v}_n d\Gamma = -\int_\Omega \left(P_x\frac{\partial\phi}{\partial x} + P_y\frac{\partial\phi}{\partial y}\right)\phi^* d\Omega \tag{4.6}$$

where $\bar{v}_n = \bar{\mathbf{v}}.\mathbf{n}$, n is the unit outward normal vector and the dot stands for scalar product. In the above equation, ϕ^* is the fundamental solution of the convection-diffusion-reaction equation with constant coefficients. For 2D problems, ϕ^* is of the form

$$\phi^*(\xi,\chi) = \frac{1}{2\pi D}e^{-\frac{\bar{v}.\mathbf{r}}{2D}}K_0(\mu\mathbf{r}),\ \mathbf{r} = |\xi - \chi|, \tag{4.7}$$

where

$$\mu = \left[\left(\frac{\bar{v}}{2D}\right)^2 + \frac{k}{D}\right]^{\frac{1}{2}} \tag{4.8}$$

in which ξ and χ are the source and field points, respectively, and r is the modulus of $\mathbf{r}$, the distance vector between the source and field points. The derivative of the fundamental solution with respect to the outward normal direction is given by

$$\frac{\partial\phi^*}{\partial n} = \frac{1}{2\pi D}e^{-\frac{\bar{v}.\mathbf{r}}{2D}}\left[-\mu K_1(\mu\mathbf{r})\frac{\partial\mathbf{r}}{\partial n} - \frac{\bar{v}_n}{2D}K_0(\mu\mathbf{r})\right]. \tag{4.9}$$

The exponential term is responsible for the inclusion of the correct amount of upwind into the formulation [122]. Eq.(4.6) is valid for source points ξ inside the domain Ω. A similar expression can be obtained, by a limit analysis, for source points ξ on the boundary Γ, in the

form

$$C(\xi)\,\phi(\xi) - D\int_{\Gamma}\phi^{*}\frac{\partial\phi}{\partial n}d\Gamma + D\int_{\Gamma}\phi\,\frac{\partial\phi^{*}}{\partial n}d\Gamma + \int_{\Gamma}\phi\,\phi^{*}\,\bar{v}_{n}\,d\Gamma = -\int_{\Omega}\left(P_{x}\frac{\partial\phi}{\partial x} + P_{y}\frac{\partial\phi}{\partial y}\right)\phi^{*}d\Omega, \tag{4.10}$$

in which $C(\xi)$ is a function of the external angle the boundary Γ makes at point ξ. For sake of clarify, more explanation has been comprehensively discussed in detail as shown in next section.

4.4 DRM Formulation for Steady-State Convection-Diffusion-Reaction Problem with Variable Velocity

In the present formulation, we concentrate on the implementation of the DRM based on the fundamental solution to the steady-state convection-diffusion-reaction equation. The basic idea is to expand the non-homogenous perturbation term on the right-hand side of Eq.(4.5) in the form

$$P_{x}\frac{\partial\phi}{\partial x} + P_{y}\frac{\partial\phi}{\partial y} = \sum_{k=1}^{M} f_{k}\,\alpha_{k}. \tag{4.11}$$

This finite sum contains a sequence of known functions $f_k = f_k(x,y)$, and a set of unknown coefficients α_k. Using this approximation, the domain integral in Eq.(4.10) can be approximated in the form

$$\int_{\Omega}\left(P_{x}\frac{\partial\phi}{\partial x} + P_{y}\frac{\partial\phi}{\partial y}\right)\phi^{*}d\Omega = \sum_{k=1}^{M}\alpha_{k}\int_{\Omega} f_{k}\phi^{*}d\Omega. \tag{4.12}$$

The next step is to consider that, for each function f_k, there exists a related function ψ_k which is a particular solution of the equation

$$D\nabla^{2}\psi - \bar{v}_{x}\frac{\partial\psi}{\partial x} - \bar{v}_{y}\frac{\partial\psi}{\partial y} - k\psi = f. \tag{4.13}$$

Thus, the domain integral can be recast in the form

$$\int_{\Omega}\left(P_x\frac{\partial\phi}{\partial x}+P_y\frac{\partial\phi}{\partial y}\right)\phi^* d\Omega=\sum_{k=1}^{M}\alpha_k\int_{\Omega}\left(D\nabla^2\psi_k-\bar{v}_x\frac{\partial\psi_k}{\partial x}-\bar{v}_y\frac{\partial\psi_k}{\partial y}-k\psi_k\right)\phi^* d\Omega. \tag{4.14}$$

Substituting Eq.(4.14) into (4.10), and utilising integration by parts in the domain integral of the resulting equation, we finally obtain a boundary integral equation of the form

$$c(\xi)\,\phi(\xi)-D\int_{\Gamma}\phi^*\frac{\partial\phi}{\partial n}d\Gamma+D\int_{\Gamma}\phi\frac{\partial\phi^*}{\partial n}d\Gamma+\int_{\Gamma}\phi\,\phi^*\bar{v}_n d\Gamma$$

$$=\sum_{k=1}^{M}\alpha_k\left[c(\xi)\,\psi_k(\xi)-D\int_{\Gamma}\phi^*\frac{\partial\psi_k}{\partial n}d\Gamma+D\int_{\Gamma}\psi_k\frac{\partial\phi^*}{\partial n}d\Gamma+\int_{\Gamma}\psi_k\phi^*\bar{v}_n d\Gamma\right]. \tag{4.15}$$

4.5 Space-Discretisation of the 2D Convection-Diffusion-Reaction Model

For the sake of simplicity in the presentation, this section will demonstrate the discretisation of the problem. To discretise the spatial domain, boundary element formulations were employed. From Appendix B, Eq.(4.15) can now be re-written in discretised form in which the integrals over the boundary are approximated by a summation of integrals over individual boundary elements, i.e.

$$C_i\phi_i-\sum_{j=1}^{N}D\int_{\Gamma_j}\phi^*\frac{\partial\phi}{\partial n}d\Gamma+D\sum_{j=1}^{N}\int_{\Gamma_j}\left(\frac{\partial\phi^*}{\partial n}+\frac{\bar{v}_n}{D}\phi^*\right)\phi\,d\Gamma$$

$$=\sum_{k=1}^{M}\alpha_k\left[C_i\psi_{ik}(\xi)-D\sum_{j=1}^{N}\int_{\Gamma_j}\phi^*\frac{\partial\psi_k}{\partial n}d\Gamma+D\sum_{j=1}^{N}\int_{\Gamma_j}\left(\frac{\partial\phi^*}{\partial n}+\frac{\bar{v}_n}{D}\phi^*\right)\psi_k d\Gamma\right], \tag{4.16}$$

where the index i means the values at the source point ξ and N elements have been employed. The functions $\phi, q=\partial\phi/\partial n, \psi$ and $\eta=\partial\psi/\partial n$ within each boundary element are approximated in this study using constant elements. It should be remarked that functions ψ and η

need not be approximated as they are known functions for a specified set f. However, doing so will greatly improve the computer efficiency of the technique with only a minor sacrifice in accuracy. Applying Eq.(4.16) to all boundary nodes using a collocation technique results in the following system of equations

$$H\phi - Gq = (H\psi - G\eta)\,\alpha. \tag{4.17}$$

As shown in the above system, the same matrices H and G are used on both sides. Both ψ and η are geometry-dependent square matrices (assuming, for simplicity, that the number of terms in expression (4.12) is equal to the number of boundary nodes), and ϕ, q and α are vectors of nodal values. The next step in the formulation is to find an expression for the unknown vector α. Applying Eq.(4.16) to all M nodes, it is possible to write the resulting set of equations in the following matrix form,

$$P_x \frac{\partial \phi}{\partial x} + P_y \frac{\partial \phi}{\partial y} = F\,\alpha, \tag{4.18}$$

where P_x and P_y can be understood as two diagonal matrices with components $P_x(x_i, y_i)$ and $P_y(x_i, y_i)$, respectively, while $\frac{\partial \phi}{\partial x}$ and $\frac{\partial \phi}{\partial y}$ are column vectors. Inverting expression (4.18), one arrives at

$$\alpha = F^{-1}\left(P_x \frac{\partial \phi}{\partial x} + P_y \frac{\partial \phi}{\partial y}\right). \tag{4.19}$$

Substituting into Eq.(4.17),

$$H\phi - Gq = (H\psi - G\eta)\,F^{-1}\left(P_x \frac{\partial \phi}{\partial x} + P_y \frac{\partial \phi}{\partial y}\right). \tag{4.20}$$

Defining a matrix S in the form

$$S = (H\psi - G\eta)\,F^{-1} \tag{4.21}$$

one can write Eq.(4.20) as

$$H\phi - Gq = S\left(P_x \frac{\partial \phi}{\partial x} + P_y \frac{\partial \phi}{\partial y}\right) \tag{4.22}$$

Once functions f_k are defined, matrix S can be established as this matrix depends on geometry only. Furthermore, the coefficients of matrices P_x and P_y are also known. Therefore, there remains to be found an expression relating the derivatives of ϕ to reduce Eq.(4.22) to a standard BEM form.

4.6 Handling Convective Terms

In this section, emphasis will be placed on convective terms. A mechanism must be established to relate the nodal values of ϕ to the nodal values of its derivatives. The function-expansion approach [141] has been implemented in this part of the work.
Assume that the function ϕ can be represented by

$$\phi(x,y) = \sum_{k=1}^{M} \Im_k(x,y)\,\beta_k. \tag{4.23}$$

where $\Im_k = \Im_k(x,y)$ are known functions and β_k unknown coefficients. The upper bound M stands for the total number of terms in the series i.e. $M = N + L$. This number L accounts for the points that are internal to the domain Ω. We now start by expanding the values of ϕ at an internal point by using expression (4.23). Differentiating it with respect to x and y produces

$$\frac{\partial \phi}{\partial x} = \sum_{k=1}^{M} \frac{\partial \Im_k}{\partial x}\beta_k \quad \text{and} \quad \frac{\partial \phi}{\partial y} = \sum_{k=1}^{M} \frac{\partial \Im_k}{\partial y}\beta_k. \tag{4.24}$$

Applying Eq.(4.23) at all M nodes, a set of equations is produced that can be represented in matrix form by

$$\phi = \Im\,\beta \tag{4.25}$$

with corresponding matrix equations for Eqs.(4.24) and (4.25) given as

$$\frac{\partial \phi}{\partial x} = \frac{\partial \Im}{\partial x} \Im^{-1} \phi \quad \text{and} \quad \frac{\partial \phi}{\partial y} = \frac{\partial \Im}{\partial y} \Im^{-1} \phi \tag{4.26}$$

Eq.(4.22) then takes the form

$$(H - P)\, \phi = Gq \tag{4.27}$$

where

$$P = S \left(P_x \frac{\partial \Im}{\partial x} + P_y \frac{\partial \Im}{\partial y} \right) \Im^{-1}. \tag{4.28}$$

The coefficients of the perturbation matrix P are all geometry-dependent only. Therefore, the boundary conditions can be implemented to Eq.(4.28) and the resulting system of algebraic equations solved by a direct or iterative scheme such as Gauss elimination and least squares method. It should mentioned that, normally the approximation of ϕ using constant boundary element is accurate but for the normal derivatives is less accurate and has an oscillation at the edges of the boundary which is typical for this kind of element.

4.7 The Choice of Radial Basis Functions

In recent years, the theory of radial basis functions (RBFs) has undergone intensive research and enjoyed considerable success as a technique for interpolating multivariable data and functions. A radial basis function, $\Psi\left(x - x_j\right) = \psi\left(\left\|x - x_j\right\|\right)$ depends upon the separation distances of a sub-set of data centres, $\left(x_j\right)_{j=\overline{1,N}}$. The distance, $\left\|x - x_j\right\|$, is usually taken to be the Euclidean metric, although other metrics are possible (for more details see Golberg and Chen [157]). The type of RBF used in the interpolation of the unknown variables normally plays an important role in determining the accuracy of the DRM [122]. Partridge *et al.* [8] have shown that a variety of functions can in principle be used as global interpolation functions f_k. The approach used by Wrobel and DeFigueiredo [116] was based on practical experience rather than formal mathematical analyses and motivated by a previous successful experience with axisymmetric diffusion problems in which a similar approach was used [22]. In the present work, decision has been made to follow [141] by starting with a simple form

of the particular solution ψ and find the related expression for function f by substitution directly into Eq.(4.17). The resulting expressions are

$$\psi_{Cubic} = r^3,$$

$$\eta_{Cubic} = 3\ r\ [(x-x_k)\ n_x + (y-y_k)\ n_y],$$

$$f_{Cubic} = 9Dr - 3r\ [(x-x_k)\ v_x + (y-y_k)\ v_y] - kr^3,$$

in which (x_k, y_k) and (x, y) are the coordinates of the k^{th} boundary or internal point and a general point, respectively. It is important to notice that the set of functions f produced depend not only on the distance r but also on the diffusivity D, velocity components v_x and v_y as well as the reaction rate k, therefore, it will behave differently when diffusion or convection is the dominating process.

The most popular RBFs are labelled as: $r^{2m-2}\log$ r (generalised thin plate spline), $\left(r^2+c^2\right)^{m/2}$ (generalised multiquadric) and $e^{-\beta r}$ (Gaussian) where m is an integer number and $r = \left\|x-x_j\right\|$. Duchon [83] derived the thin plate splines (TPS) as an optimum solution to the interpolation problem in a certain Hilbert space via the construction of a reproducing kernel. It is interesting to observe that Duchon's thin plate splines function with $m = 2$ corresponds to the fundamental solution commonly used in the BEM technique to solve biharmonic problems. The expressions for the TPS-RBF are as follows:

$$\psi_{TPS} = r^2 \log r,$$

$$\eta_{TPS} = [2\log(r)+1]\ [\{x-x_k\}\ n_x + \{y-y_k\}\ n_y],$$

$$f_{TPS} = -4D\ [\log(r)+1] + v_x\ [2\log(r)+1]\ (x-x_k) + v_y\ [2\log(r)+1]\ (y-y_k)$$

$$+kr^2\log(r).$$

Another popular RBF for the DRM is the multiquadric (MQ). However, despite MQs excellent performance, it contains a free parameter, c, often referred to as the shape parameter. When c is small the resulting interpolating surface is pulled tightly to the data points, forming a cone-

like basis functions. As c increases, the peak of the cone gradually flattens. The multiquadric functions with values of $m = 1$ and $c = 0$ are often referred to as conical functions and, with $m = 3$ and $c = 0$, as Duchon cubic. The related expressions for this RBF are as follows

$$\psi_{MQ} = \sqrt{c^2 + r^2},$$

$$\eta_{MQ} = \left(\frac{1}{\sqrt{c^2 + r^2}} \right) \left[\{x - x_k\} \, n_x + \{y - y_k\} \, n_y \right],$$

$$f_{MQ} = -D \left[(2\log(r) + 3) + (2\log(r) + 1) \right] + v_x \left[2\log(r) + 1 \right] (x - x_k)$$

$$+ v_y \left[2\log(r) + 1 \right] (y - y_k) + k\sqrt{c^2 + r^2}.$$

Even though TPS have been considered optimal in interpolating multivariate functions, they do only converge linearly, Powell [158]. On the other hand, the multiquadric (MQ) functions converge exponentially as shown by Madych and Nelson [82]. However, the tuning of the free parameter c can dramatically affect the quality of the solution obtained. Increasing the value of c will lead to a flatter RBF. This will, in general, improve the rate of convergence at the expense of increased numerical ill-conditioning of the resulting linear system [82]. Much effort has been made to search for ideal shape parameter c when utilising the multiquadric radial basis function. This is due to the lack of information on choosing the best shape parameter available in the literature, forcing the user having to make an 'ad-hoc' decision. It is important to note that the value of the multiquadric shape-parameter, c, has not been explicitly defined (see Table 4.1). After a process of investigation, the optimal value of the shape parameter for the current problems was found to be $c = 75$.

The radial basis functions presented in Table 4.1 have been examined in this paper. Thin-plate splines (TPS) and the multiquadric are conditionally positive definite functions (for more details see [159]).

4.7.1 Mathematical Derivation of the Cubic Radial Basis Function

In this section, we will explain the derivation of the cubic-RBF in which it is used for all numerical experiments in this chapter. The most widely used choices for the F_k when solving

Table 4.1: Radial Basis Functions

Name	Function
multiquadric MQ	$\left(r^2+c^2\right)^{1/2}$
Thin Plate Spline TPS	$r^2 \log(r)$
Cubic RBF	r^3

equations in involving the Laplace operator have led to ψ_k functions of the form

$$\psi = A\, r^3 \tag{4.29}$$

Where A is a constant and this was the approach followed here. In order to find out the functions F_k associated to these ψ_k through the convection-diffusion-reaction operator $\mathscr{L}$ one needs to apply this operator to the choice for ψ_k, i.e.

$$\mathscr{L}\left[A\, r_3^k\right] = F_K \tag{4.30}$$

For the sake of simplicity let us write the operator in 2D polar coordinates.

$$-D\left(\frac{\partial^2\psi}{\partial r^2}+\frac{1}{r}\frac{\partial\psi}{\partial r}-\frac{1}{r^2}\frac{\partial^2\psi}{\partial\theta^2}\right)+v_x\frac{\partial\psi}{\partial r}cos(\theta)-\frac{1}{r}sin(\theta)\frac{\partial\psi}{\partial\theta}+v_y\frac{\partial\psi}{\partial r}sin(\theta)$$

$$+\frac{1}{r}cos(\theta)\frac{\partial\psi}{\partial\theta}+k\,\psi = F \tag{4.31}$$

To evaluate F_k one has to obtain all the derivatives appearing in the operator, i.e.
(i) Derivatives with respect to r:

$$\frac{\partial\psi}{\partial r} = 3A\, r^3 \quad \text{Hence} \quad \frac{\partial^2\psi}{\partial r^2} = 6A\, r \tag{4.32}$$

(ii) Derivatives with respect to θ:

$$\frac{\partial \psi}{\partial \theta} = \frac{\partial^2 \psi}{\partial \theta^2} = 0 \tag{4.33}$$

and also the terms involving sine and cosine. On evaluating these terms one recalls that the derivatives under consideration is the derivative with respect to the field point. The terms will then take the form

$$\frac{\partial \psi}{\partial x} = \frac{\partial \psi}{\partial r}\frac{\partial r}{\partial x} = 3A\,r^2\frac{(x-x_k)}{r} = 3A\,r\,(x-x_k) \tag{4.34}$$

and similarly

$$\frac{\partial \psi}{\partial y} = \frac{\partial \psi}{\partial r}\frac{\partial r}{\partial y} = 3Ar^2\frac{(y-y_k)}{r} = 3A\,r\,(y-y_k) \tag{4.35}$$

where (x,y), (x_k,y_k) are coordinates of node and pole respectively into consideration. Replacing these results into Eq.(4.31) one will end up with an expression for F of the form:

$$F = -9DA\,r + 3A\,v_x\,r\,(x-x_k) + 3A\,v_y\,r\,(y-y_k) + kA\,r^3 \tag{4.36}$$

For the sake of completeness one should add a constant to the function F. This implies alterations to the function ψ that can be easily found. Suppose that the constant is B, then by inspection one can find that the particular solution ψ for an F defined as:

$$F = -9DA\,r + 3A\,v_x\,r\,(x-x_k) + 3A\,v_y\,r\,(y-y_k) + kA\,r^3 + B \tag{4.37}$$

is

$$\psi = \frac{B}{k} + A\,r^3 \tag{4.38}$$

Eqs.(4.37) and (4.38) respectively define the function F_k and ψ_k used throughout this work. Having established the functions used in this work for F_k and ψ_k one is then able to specifically determine the function η defined as:

$$\eta = \frac{\partial \psi}{\partial n} \tag{4.39}$$

Since ψ is only function of r it can be written that

$$\eta = \frac{\partial \psi}{\partial n}\frac{\partial r}{\partial n} \tag{4.40}$$

And once the expression for the normal derivative of the radius r is

$$\frac{\partial r}{\partial n} = \frac{\partial r}{\partial x}\frac{\partial x}{\partial n} + \frac{\partial r}{\partial y}\frac{\partial y}{\partial n} \tag{4.41}$$

Where the terms

$$\frac{\partial x}{\partial n} \quad \text{and} \quad \frac{\partial y}{\partial n} \tag{4.42}$$

are the direction cosines of the normal to the boundary at the field point considered, the expression for η takes the form

$$\eta = 3Ar^2\left[\frac{(x-x_k)}{r}\frac{\partial x}{\partial n} + \frac{(y-y_k)}{r}\frac{\partial y}{\partial n}\right]; \tag{4.43}$$

or

$$\eta = 3Ar\left[(x-x_k)\frac{\partial x}{\partial n} + (y-y_k)\frac{\partial y}{\partial n}\right]. \tag{4.44}$$

4.8 Domain Discretisation Approach

It is important to clarify that, when the velocity field is significant compared to the diffusivity (i.e., high Péclet numbers), the DRM approximation in the present form fails to properly

reproduce the perturbation terms and the accuracy of the solution degrades. In these situations, one must resort to domain discretisation. However, rather than integrating the domain terms in Eq.(4.10) directly, it is more convenient to perform an integration by parts to work with domain values of ϕ instead of its Cartesian derivatives. We start by writing the domain integral in equations (4.6) and (4.10) as

$$\int_{\Omega}\left(P_x\frac{\partial\phi}{\partial x}+P_y\frac{\partial\phi}{\partial y}\right)\phi^* d\Omega=\int_{\Gamma}\phi\,\phi^*\left(P_x n_x+P_y n_y\right)d\Gamma$$

$$-\int_{\Omega}\left[\left(\frac{\partial P_x}{\partial x}+\frac{\partial P_y}{\partial y}\right)\phi^*+P_x\frac{\partial\phi^*}{\partial x}+P_y\frac{\partial\phi^*}{\partial y}\right]\phi\,d\Omega. \tag{4.45}$$

Substituting the above into Eq.(4.10) gives

$$C\left(\xi\right)\phi\left(\xi\right)-D\int_{\Gamma}\phi^*\frac{\partial\phi}{\partial n}d\Gamma+D\int_{\Gamma}\phi\,\frac{\partial\phi^*}{\partial n}d\Gamma+\int_{\Gamma}\phi\,\phi^*\,\bar{v}_n d\Gamma$$

$$=\int_{\Omega}\left[\left(P_x\frac{\partial\phi}{\partial x}+P_y\frac{\partial\phi}{\partial y}\right)\phi^*+P_x\frac{\partial\phi^*}{\partial x}+P_y\frac{\partial\phi^*}{\partial y}\right]\phi d\Omega. \tag{4.46}$$

Notice that the boundary integral in Eq.(4.45) has been incorporated into the last integral on the left side of Eq.(4.10).

The term between brackets in the domain integral of Eq.(4.46) involves only known functions. Thus, by discretising the domain into cells, the application of Eq.(4.46) to all boundary nodes produces the system of equations

$$\mathbf{H}\phi_b-\mathbf{G}q_b=\mathbf{B}\phi_i \tag{4.47}$$

relating boundary values of ϕ and q and internal values of ϕ. This system has to be complemented by the application of Eq.(4.6) to the internal nodes.

4.9 Error Indicators

The accuracy of numerical solutions is usually improved by mesh refinement, as in FDM and the FEM. In our context there are two ways to present the solution convergence and accuracy, either by root mean square error or using average relative error. Our goal here is to study the convergence behaviour to show the accuracy and efficiency of the proposed method for which results are reported.

In order to estimate the simulation error throughout the numerical experiments, the root mean square norm is utilised as shown in Chapter 3. To obtain a more transparent measure of solution error, a well-known indicator has been used as an average relative error which is defined as

$$err(\phi) = \frac{1}{N}\sum_{i=1}^{N}\left|\frac{\phi_{i,numer} - \phi_{i,exact}}{\phi_{i,exact}}\right| \tag{4.48}$$

where i denotes a nodal value, $\phi_{i,exact}$ is the analytical solution, $\phi_{i,numer}$ is the numerical solution from the boundary element analysis and N is the total number of boundary and internal nodes, was computed for each analysis.

4.10 Numerical Applications and Discussions

The present section is concerned with the numerical application of the DRBEM for the solution of steady-state convection-diffusion-reaction problems with variable velocity. We shall examine several test examples to assess the accuracy and the performance of the proposed method.

4.10.1 Convection-Diffusion-Reaction Problem over Square Region with Mixed (Neumann-Dirichlet) Boundary Conditions and Linear Variable Velocity

This example, although 1D, is treated here as a 2D convection-diffusion-reaction problem with a variable velocity field in the x-direction. The velocity v_x is a linear function of x

expressed as

$$v_x(x,y) = kx + c_1,$$

where

$$c_1 = \ln\left(\frac{\phi_1}{\phi_0}\right) - \frac{k}{2}.$$

The problem geometry and discretisation are schematically described in Fig. 4.1. The problem is modelled as a square region with unit side length and mixed boundary conditions (Neumann-Dirichlet). There is no flux in the y-direction and the values $\phi_0 = 300$ and $\phi_1 = 10$ are specified at the faces $x = 0$ and $x = 1$, respectively, with the diffusivity coefficient taking the value $D = 1\left(m^2/s\right)$. The problem is discretised with 720 constant elements, 180 on each face, and 19 internal points. The exact solution of the problem is given by

$$\phi(x,y) = 300\exp\left(\frac{kx^2}{2} + c_1 x\right).$$

The plots of the variation of the concentration profile ϕ along the x-direction are presented

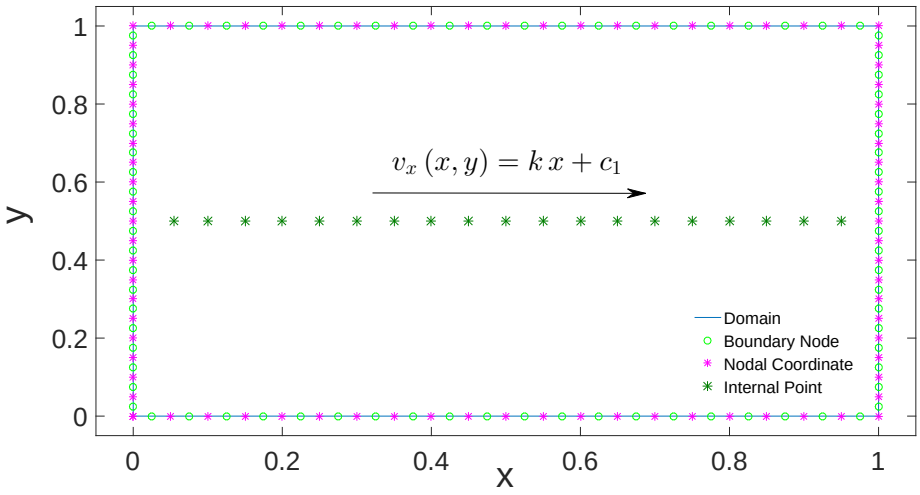

Figure 4.1: Domain discretisation with boundary conditions and internal nodes of square region with linear velocity problem

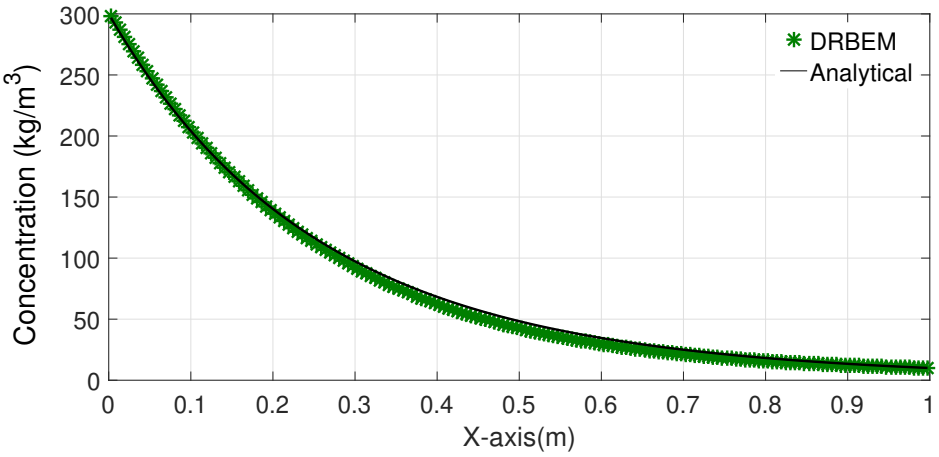

Figure 4.2: Variation of concentration profile ϕ along face $y = 0$ and $y = 1$, with $k = 1$ using TPS-RBF: comparison between the analytical (solid line) and numerical (star points) solutions

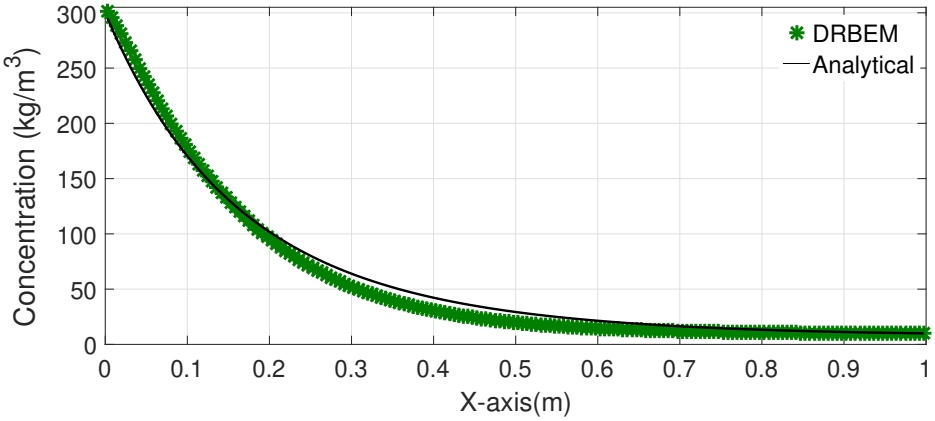

Figure 4.3: Variation of concentration profile ϕ along faces $y = 0$ and $y = 1$, with $k = 5$ using TPS-RBF: comparison between the analytical (solid line) and numerical (star points) solutions

in Fig. 4.2 to 4.5 for the cases $k = 1$ to $k = 100$. For $k = 1$ the velocity v_x varies from $v_x = -2.9012$ for $x = 1$ to $v_x = -3.9012$ for $x = 0$ while for $k = 5$, the total velocity v_x varies from $v_x = -0.9012$ for $x = 1$ to $v_x = -5.9012$ when $x = 0$. It can be noticed that the agreement with the analytical solution is very good. For the largest value of the reaction $k = 100$, the velocity v_x varies between $v_x = 46.5988$ for $x = 1$ and $v_x = -53.4012$ when $x = 0$. For all these cases the average velocity is considered to be $\bar{v}_x = -3.401$. It is obvious that, as the velocity increases, the concentration profile distribution becomes steeper and

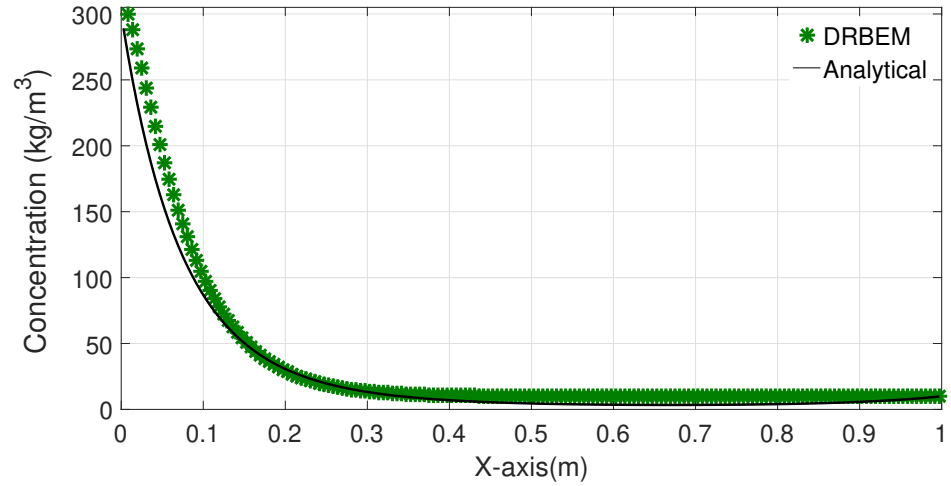

Figure 4.4: Variation of concentration profile ϕ along faces $y = 0$ and $y = 1$ with $k = 20$ using TPS-RBF: comparison between the analytical (solid line) and numerical (star points) solutions

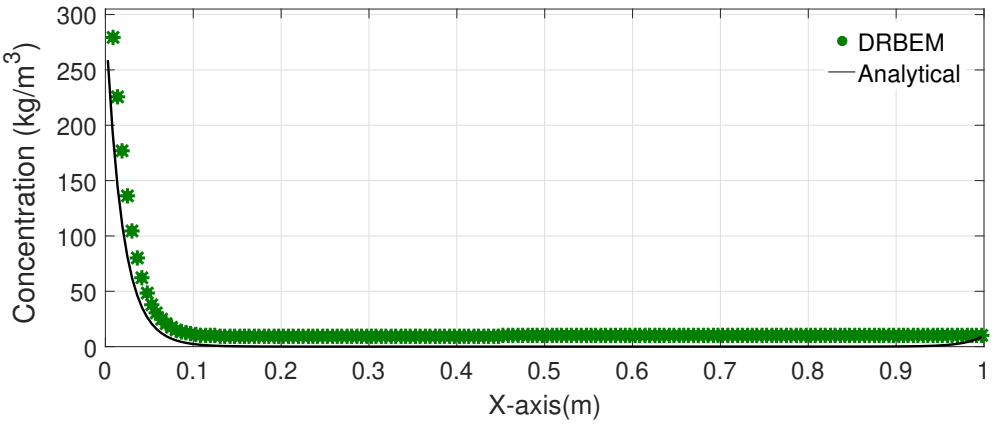

Figure 4.5: Variation of concentration profile ϕ along faces $y = 0$ and $y = 1$ with $k = 100$ using TPS-RBF: comparison between the analytical (solid line) and numerical (star points) solutions

more difficult to reproduce with numerical models. The maximum global Péclet number for this case study is 53.4012 for $k = 100$. The first case study considered $k = 1$ and an average velocity $\bar{v}_x = -3.901$ for all nodes. The results of the analyses using the three RBFs are shown in Table 4.2. The TPS and MQ-RBFs yield the most accurate results while the cubic-RBF is the least accurate. The relative errors for this test case using TPS are shown in Fig. 4.6 for $k = 5$. Moreover, another RMS error analysis has been done for different

Table 4.2: DRBEM results of ϕ for convection-diffusion-reaction with average velocity $\bar{v}_x = -3.901$

x	Cubic	MQ	TPS	Analytical
0.0	300	300	300	300
0.105	215.263	201.341	201.374	200.270
0.205	153.027	135.00	134.984	137.696
0.305	108.764	90.564	90.545	95.624
0.405	77.457	61.158	61.139	67.075
0.505	55.282	41.832	41.815	47.522
0.605	39.532	29.189	29.174	34.007
0.705	28.321	20.843	20.932	24.580
0.805	20.307	15.580	15.572	17.945
0.905	14.460	12.105	12.101	13.233
1.0	10	10	10	10

Table 4.3: RMS error for convection-diffusion-reaction with different reaction k values

$f = r^2 \log(r)$, Problem 1			
	$k = 1$	$k = 5$	$k = 20$
RMS error in ϕ	0.0730	0.1611	0.7623

reaction values using TPS as shown in Table 4.3. The RMS error increases with high k, which produces higher values of the Péclet number. The numerical evaluations of the modified Bessel functions of the second kind with zero and first orders K_0 and K_1, respectively, are performed by using the Matlab built-in functions.

To assess the convergence of the boundary concentrations with mesh refinement, Table 4.4 presents the RMS results using TPS-RBF. The results indicate convergence in the RMS norm.

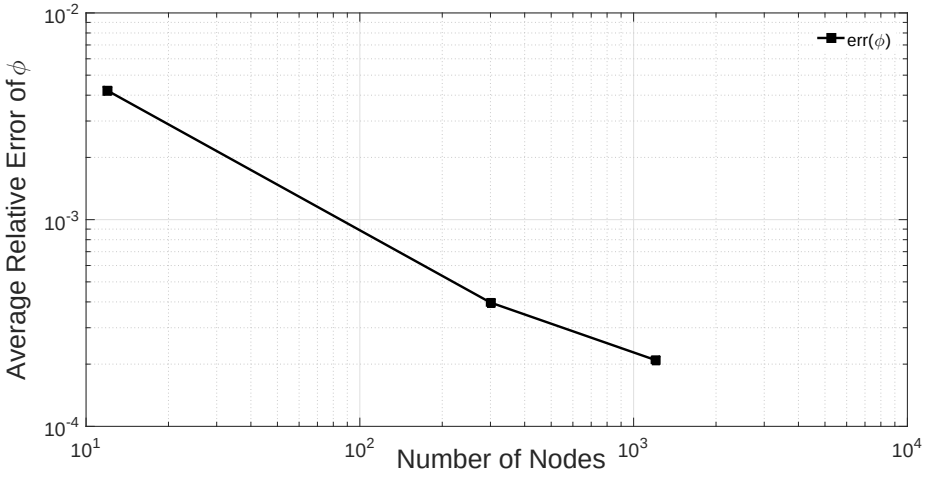

Figure 4.6: Average relative error $err(\phi)$ at internal nodes for 2D convection-diffusion-reaction problem with $k = 5$.

Table 4.4: RMS norm of DRBEM for convection-diffusion-reaction problem with different meshes

RMS error norm in ϕ, $f = r^2 \log(r)$, Problem 1			
Mesh size	$k = 1$	$k = 5$	$k = 10$
20	0.1294	0.3171	0.3354
40	0.1143	0.2736	0.2814
80	0.0987	0.2314	0.2283
100	0.0943	0.2195	0.2131
200	0.0834	0.1899	0.1737
400	0.0765	0.1708	0.1470
720	0.0730	0.1611	0.1328

4.10.2 Convection-Diffusion-Reaction Problem over a Unit Square Channel with Mixed (Neumann-Dirichlet) Boundary Conditions and Non-Linear Variable Velocity Field

In this second problem, the solution domain is taken to be the unit square $\Omega = (0,1) \times (0,1)$ as described in Fig. 4.7. The boundary is discretised with 160 constant elements, 40 on each face, and 209 internal points are adopted. A uni-directional velocity field in the x-direction depending on the coordinate y was defined by the expression

$$v_x(x,y) = A\,(y-B)^2.$$

The velocity field is now a second-order function of the y-coordinate, with A and B defined as constants; the values of the other coefficients are $D = 1$ and $k = 0$. The constant B defines the symmetry of the velocity field with respect to the coordinate y. If $B = 0.5$, the velocity and the concentration profiles are both symmetric. The analytical solution to this problem is given to be

$$\phi(x,y) = \bar{\phi} e^{A^{1/3}\left(A^{1/3} y\left(B-\frac{y}{2}\right)+x\right)}$$

with $\bar{\phi} = 300$.

The mixed boundary conditions (Neumann-Dirichlet) corresponding to the problem are defined as

$$\frac{\partial \phi}{\partial n}(x,0) = -300\, A^{\frac{2}{3}} B\, e^{A^{\frac{1}{3}} x}, \quad 0 \le x \le 1,$$

$$\phi(1,y) = 300\, e^{A^{\frac{1}{3}}\left(A^{\frac{1}{3}} y\left(B-\frac{y}{2}\right)+1\right)}, \quad 0 \le y \le 1,$$

$$\frac{\partial \phi}{\partial n}(x,1) = 300 A^{\frac{2}{3}}(B-1)\, e^{A^{\frac{1}{3}}\left(A^{\frac{1}{3}}\left(B-\frac{1}{2}\right)+x\right)}, \quad 0 \le x \le 1,$$

$$\phi(0,y) = 300 e^{A^{\frac{2}{3}} y\left(B-\frac{y}{2}\right)}, \quad 0 \le y \le 1.$$

The average velocity $\bar{v}_x = 0.0625$ is adopted at every node. The simulation results using

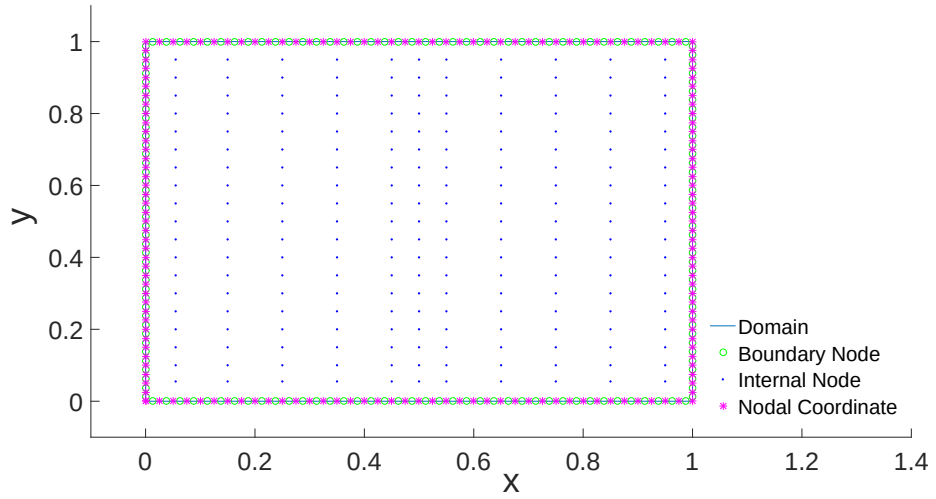

Figure 4.7: Geometry, discretisation, internal points and boundary conditions for two-dimensional problem with uni-directional velocity $v_x(y)$ and side lenght $1m$

Table 4.5: DRBEM results of ϕ for convection-diffusion-reaction with average velocity $\bar{v}_x = 0.0625$

x	Cubic	MQ	TPS	Analytical
0.15	348.505	352.465	348.438	348.550
0.25	385.185	390.817	385.120	385.207
0.35	425.715	432.487	425.651	425.720
0.45	470.507	477.825	470.416	470.493
0.55	520.009	527.268	519.860	519.975
0.65	574.718	581.322	574.491	574.662
0.75	635.188	640.580	634.902	635.100
0.85	702.301	705.738	701.765	701.894
0.95	775.985	777.993	775.891	775.712

the three different RBFs are compared with the analytical solution in Table 4.5. It can be seen that the Cubic and TPS RBFs provide results of the same level of accuracy, while

the MQ-RBF shows less accurate results in this case. Table 4.6 shows the RMS errors for different values of the parameter B using TPS, where it can be seen that the RMS is reduced as the value of B decreases. Table 4.7 shows the RMS error norm for different average

Table 4.6: RMS error for convection-diffusion-reaction with $A = 0.5$ and increasing values of B

$f = r^2 \log(r)$, Problem 2			
	$B = 1$	$B = 0.5$	$B = 0.25$
RMS error in ϕ	0.0225	0.0054	0.0016

velocities and mesh sizes. It can be noticed that the errors decrease with mesh refinement. The relative error in the RMS norm is of order 10^{-3} for small values of the average velocity and 10^{-2} for larger values of $\bar{v}_x$. The RMS errors for different average velocities $\bar{v}_x$ using

Table 4.7: RMS norm of DRBEM for convection-diffusion-reaction problem with different spatial meshes

RMS error norm in ϕ, $f = r^2 \log(r)$, Problem 2				
Mesh size	$\bar{v}_x = 0.0156$	$\bar{v}_x = 0.0313$	$\bar{v}_x = 0.25$	$\bar{v}_x = 0.5$
20	0.0027	0.0054	0.0146	0.0244
40	0.0018	0.0043	0.0152	0.0247
80	0.0017	0.0041	0.0150	0.0241
200	0.0016	0.0041	0.0139	0.0225
400	0.00159	0.0040	0.0129	0.0211
720	0.00158	0.0040	0.0121	0.0201

TPS are shown in Table 4.8.

Table 4.9 shows a comparison between five different values of the shape parameter c for MQ-RBF. It is clear that the results obtained are reasonable and laying at a similar level of accuracy, with slightly better results when the parameter $c = 75$ or 100. From another point

Table 4.8: RMS error for convection-diffusion-reaction with different values of average velocity $\bar{v}_x$

$f = r^2 \log(r)$, Problem 2			
	$\bar{v}_x = 0.0156$	$\bar{v}_x = 0.0313$	$\bar{v}_x = 0.25$
RMS error in ϕ	0.0016	0.0054	0.0089

Table 4.9: DRBEM results of ϕ for convection-diffusion-reaction problem using MQ-RBF with different values of the shape parameter c

x	$c = 100$	$c = 75$	$c = 50$	$c = 25$	$c = 5$	Analytical
0.05	320.825	321.342	322.438	326.857	322.725	319.348
0.3	413.973	415.212	417.832	428.255	416.120	410.051
0.5	505.360	506.786	509.797	521.762	507.024	500.838
0.7	615.378	616.557	619.052	629.031	617.490	611.727
0.9	749.037	749.577	750.727	755.392	751.101	747.162

of view, as the MQ function is flattened, it will be insensitive to the radial distance r, and the elements of matrix ψ become identical. Taking a very high value of the shape parameter c generates collocation matrices which are poorly conditioned and require high-precision arithmetic to solve accurately. Using a relatively high non-dimensional shape parameter of 75, the collocation matrices are sufficiently well conditioned to be solved using quad-precision arithmetic (see [81, 160, 161] for more details on the shape parameter c).

Case(i) : The Symmetric Case:

The first case is considered for which the computational domain is discretised into 200 constant elements and 209 internal points, for which Fig. 4.8 shows the variation of the concentration profile ϕ along the horizontal faces $y = 0$ and $y = 1$ for the case $A = 0.5$ and $B = 0.5$, compared to the analytical solution. Figs. 4.9 and 4.10 display the variation of the normal heat flux along the vertical faces $x = 1$ and $x = 0$, respectively, using the same value of the parameters A and B, and compared to the analytical solution.

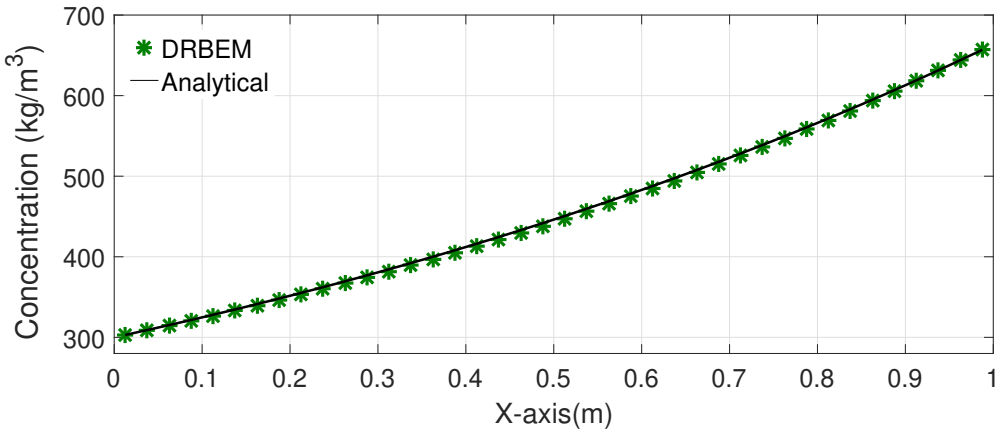

Figure 4.8: Variation of concentration profile ϕ along faces $y = 0$ and $y = 1$ using TPS-RBF: comparison between the analytical (solid line) and numerical (star points) solutions

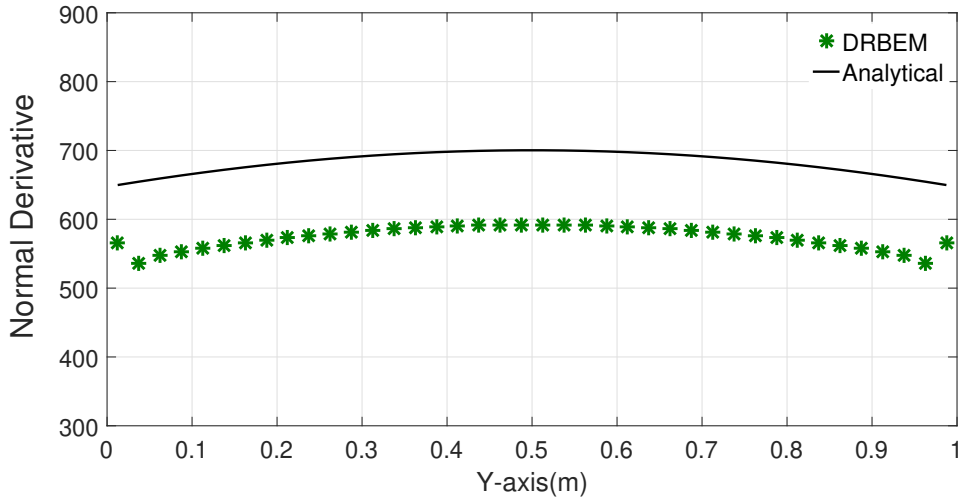

Figure 4.9: Variation of normal flux q along face $x = 1$ using TPS-RBF: comparison between the analytical (solid line) and numerical (star points) solutions

Case(ii) : Non − Symmetric Cases:

The second case is implemented using the same previous discretisation but with different values for the parameters A and B. Fig. 4.11 shows the results for the concentration profile ϕ along the faces $y = 0$ and $y = 1$ for the case $A = 0.2$, $B = 4$. Figs. 4.12 and 4.13 show the variation of the normal flux along the vertical faces $x = 0$ and $x = 1$, respectively, for this case, compared to the analytical solution. Next, the value of B is considered to be $B = 0.4$. Fig. 4.14 shows the variation of the concentration ϕ along the horizontal faces $y = 0$

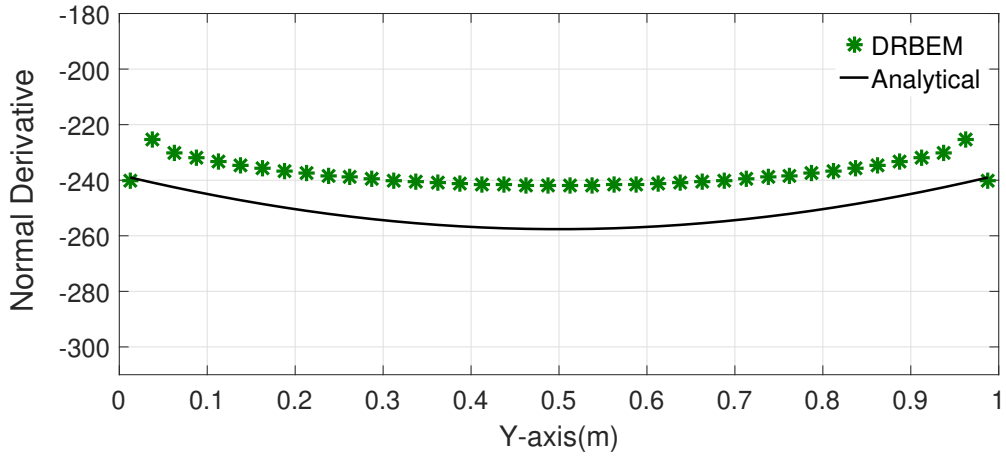

Figure 4.10: Variation of normal flux q along face $x = 0$ using TPS-RBF: comparison between the analytical (solid line) and numerical (star points) solutions

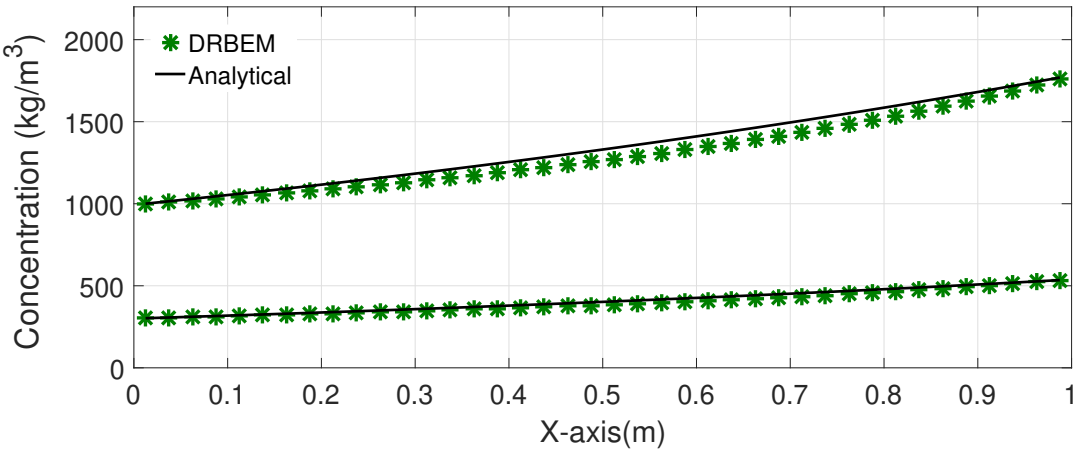

Figure 4.11: Variation of concentration profile ϕ along faces $y = 0$ and $y = 1$ using TPS-RBF: comparison between the analytical (solid line) and numerical (star points) solutions

and $y = 1$ for the case of $A = 0.895$, which presents an excellent agreement with the exact solution. Figs. 4.15 and 4.16 show the distribution of the normal flux along the vertical faces $x = 0$ and $x = 1$, respectively, in comparison with the analytical solution. The oscillations near the boundaries are typical of the use of constant elements. Different scales are used in these figures due to the difference in magnitude of the fluxes. The relative error for the present study is plotted in Fig. 4.17, for the case $A = 0.25$ and $B = 0.25$ with only 16 internal nodes and using TPS-RBF, which shows very accurate results even though using few internal nodes.

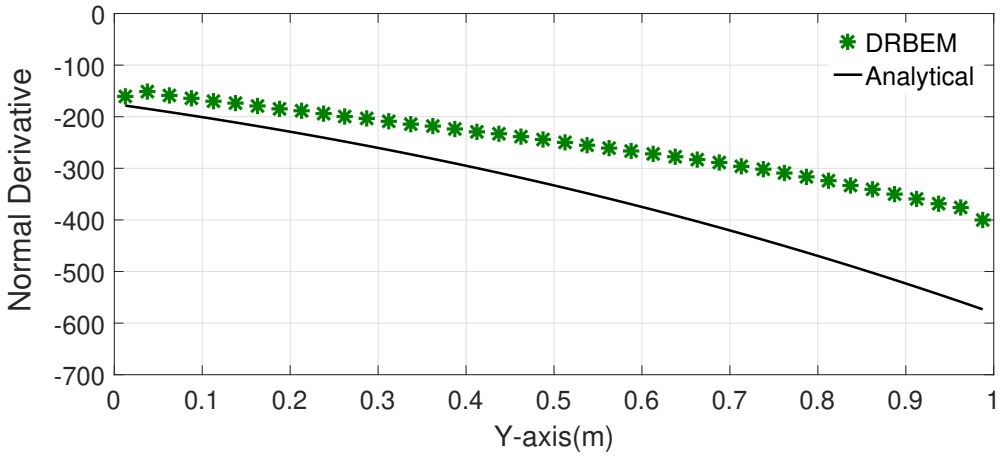

Figure 4.12: Variation of normal flux q along face $x = 0$ using TPS-RBF: comparison between the analytical (solid line) and numerical (star points) solutions

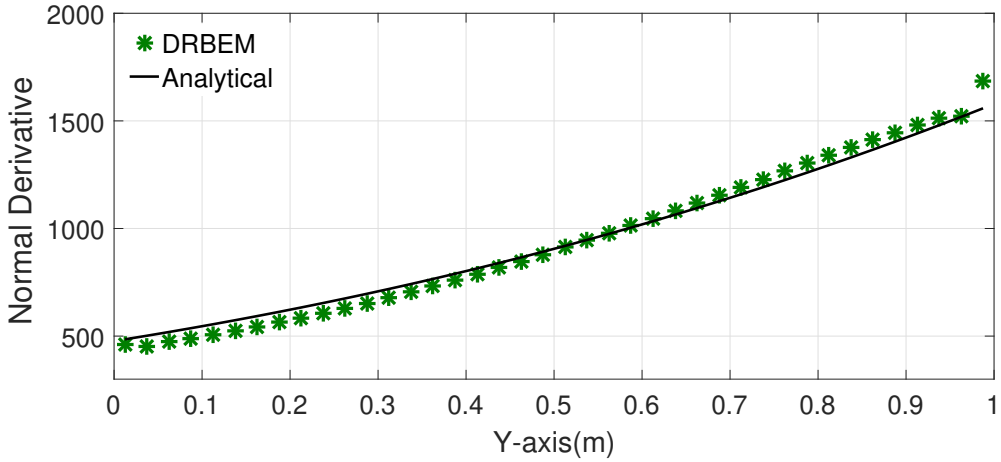

Figure 4.13: Variation of normal flux q along face $x = 1$ using TPS-RBF: comparison between the analytical (solid line) and numerical (star points) solutions

4.10.3 Convection-Diffusion-Reaction Problem over a Square-Shaped Body with Mixed (Neumann-Dirichlet) Boundary Conditions and Non-Linear Variable Velocity Field

In the last example, the cross-section is considered to be square with unit side length. This case study considers a uni-directional velocity field in the x-direction depending on the

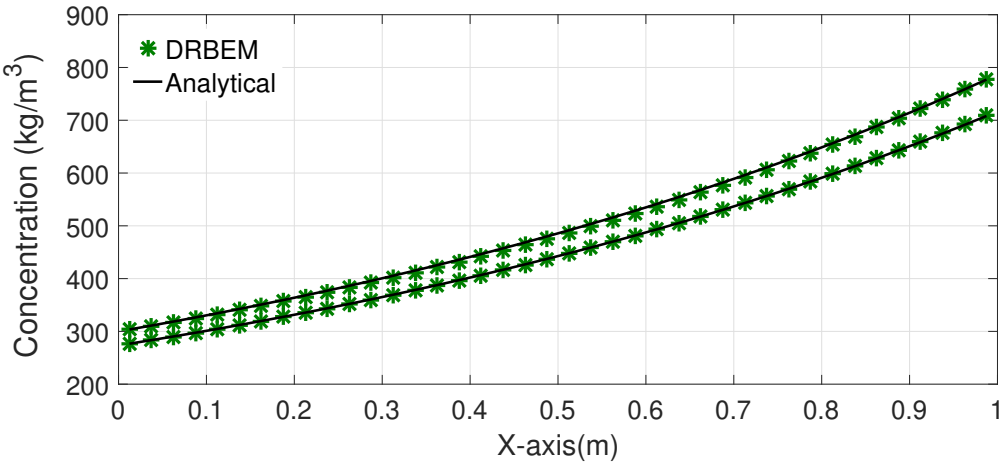

Figure 4.14: Variation of concentration profile ϕ along faces $y = 0$ and $y = 1$ using TPS-RBF: comparison between the analytical (solid line) and numerical (star points) solutions

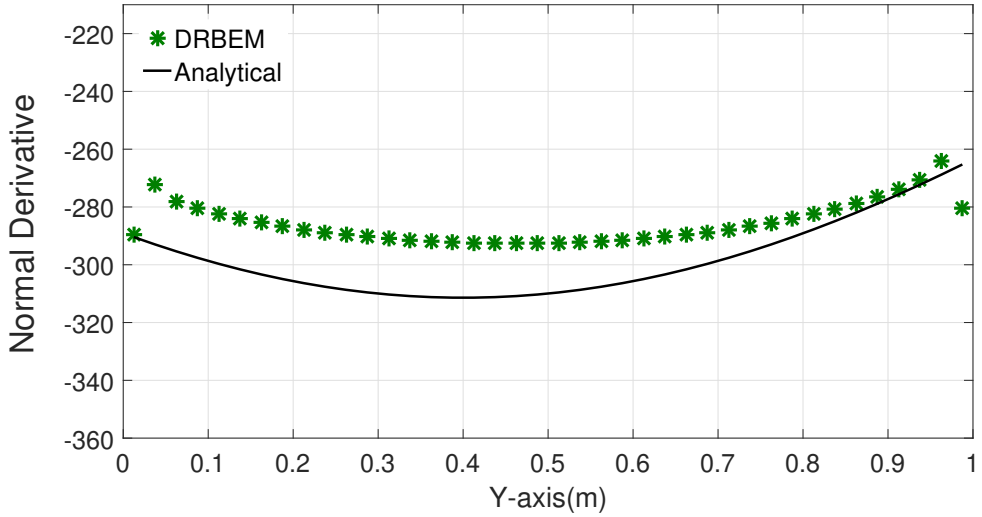

Figure 4.15: Variation of normal flux q along face $x = 0$ using TPS-RBF: comparison between the analytical (solid line) and numerical (star points) solutions

y-direction to take the following expression

$$v_x(x,y) = \frac{\lambda^2}{C_2}(y-B)^2 \tag{4.49}$$

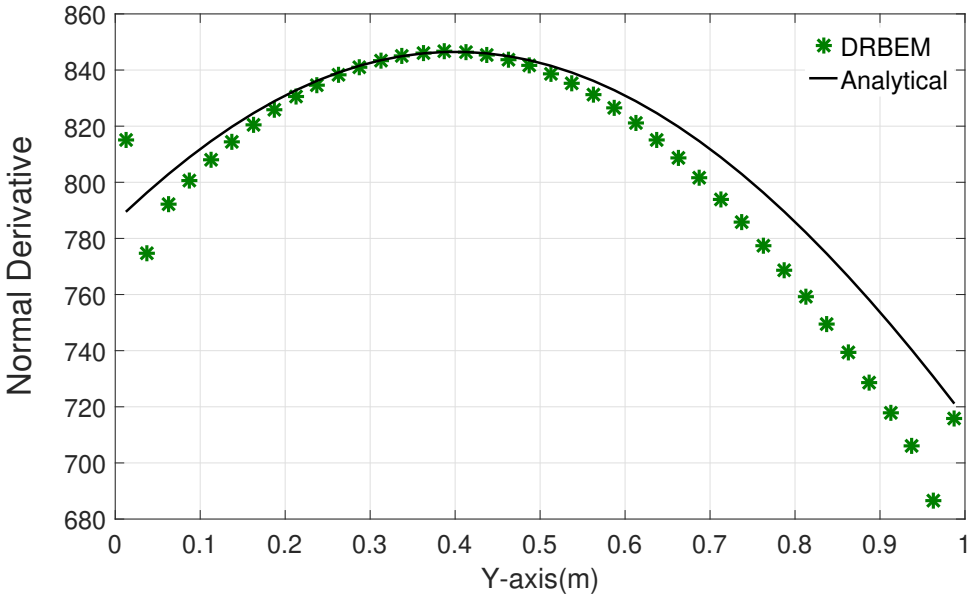

Figure 4.16: Variation of normal flux q along face $x = 1$ using TPS-RBF: comparison between the analytical (solid line) and numerical (star points) solutions

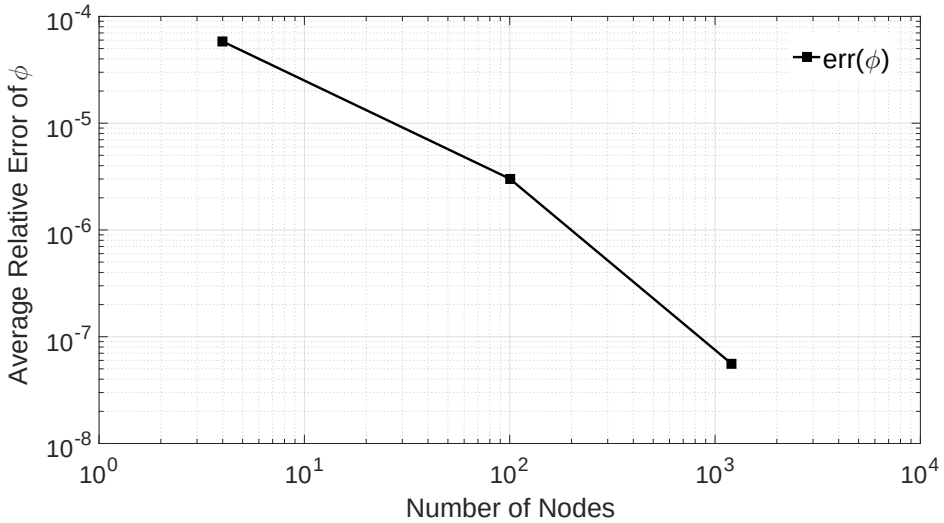

Figure 4.17: Average relative error $err(\phi)$ for 2D convection-diffusion-reaction problem at selected internal points with $k = 0$.

with $\lambda = k - C_2^2$. The v_y component is again equal to zero and consequently the equation to be solved reduces to

$$D\nabla^2\phi - \frac{\lambda^2}{C_2}(y-B)^2\frac{\partial\phi}{\partial x} - k\phi = 0, \tag{4.50}$$

subject to mixed boundary conditions (Neumann-Dirichlet) which can be defined as follows:

$$\frac{\partial \phi}{\partial n}(x,0) = 300\,\lambda\,B\,e^{(C_2 x)}, \quad 0 \le x \le 1,$$

$$\phi(1,y) = 300\,e^{\left(\frac{\lambda}{2}y^2 - \lambda B y + C_2\right)}, \quad 0 \le y \le 1,$$

$$\frac{\partial \phi}{\partial n}(x,1) = 300\,\lambda\,(1-B)\,e^{\lambda\left(\left(\frac{1}{2}-B\right)+C_2 x\right)}, \quad 0 \le x \le 1,$$

$$\phi(0,y) = 300\,e^{\left(\frac{\lambda}{2}y^2 - \lambda B y\right)}, \quad 0 \le y \le 1.$$

The analytical solution to the above problem is

$$\phi(x,y) = 300\exp\left[\frac{\lambda}{2}y^2 - \lambda B y + C_2 x\right]. \tag{4.51}$$

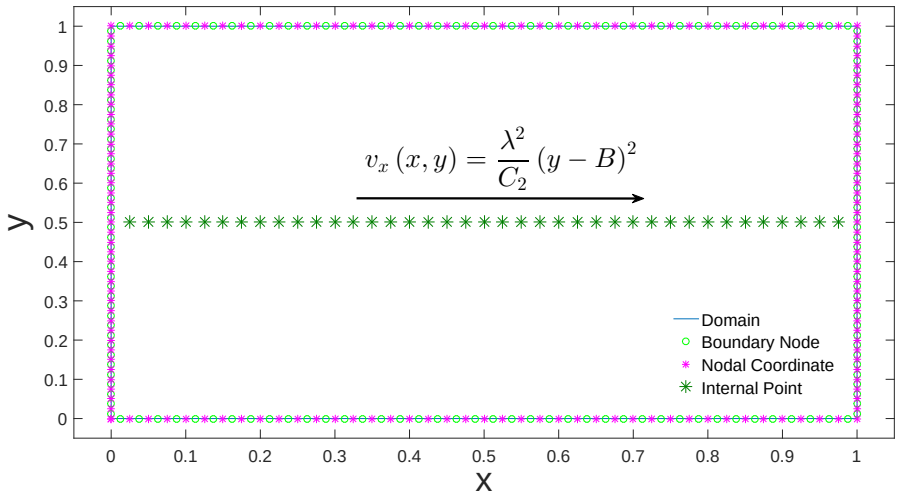

Figure 4.18: Domain discretisation of square-shaped body, internal points and boundary conditions with non-linear velocity problem

This example was studied for different average velocity values. The numerical solution when $\bar{v}_x = -1.8654$ is tabulated in Table 4.10, using the three RBFs. Once again, the best results are obtained with the TPS-RBF. The value of the constant B defines the symmetry of the velocity field with respect to the coordinate y. If $B = 0.5$ the velocity field and the

Table 4.10: DRBEM results of ϕ for convection-diffusion-reaction with average velocity $\bar{v}_x = -1.8654$

x	Cubic	MQ	TPS	Analytical
0.1	195.202	183.104	181.458	182.147
0.2	134.721	135.445	133.692	129.631
0.3	92.136	99.775	97.985	92.257
0.4	62.328	73.271	71.500	65.658
0.5	41.463	53.621	51.915	46.727
0.6	26.762	39.041	37.443	33.255
0.7	16.219	28.183	26.735	23.667
0.8	8.378	20.041	18.788	16.843
0.9	2.189	13.860	12.846	11.987

concentration profiles are both symmetric. The value of the constant C_2 is given by

$$C_2 = \ln\left[\frac{\phi(1,0)}{\phi(0,0)}\right]$$

with the values $\phi(0,0) = 300$ and $\phi(1,0) = 10$. Figure 4.18 presents the problem geometry,

Table 4.11: RMS error for convection-diffusion-reaction with increasing reaction k values

$f = r^2 \log(r)$, Problem 3			
	$k = 5$	$k = 7.337$	$k = 10$
RMS error in ϕ	0.2873	0.2422	0.3335

discretisation and internal nodes. The problem is discretised with 160 constant elements, 40 on each face, and 39 internal points. The RMS errors for different reaction values k using TPS-RBF are shown in Table 4.11. The relative error at different points inside the domain

with $k = 9.724$, $B = 1.4222$ and using TPS-RBF is displayed in Fig. 4.19.

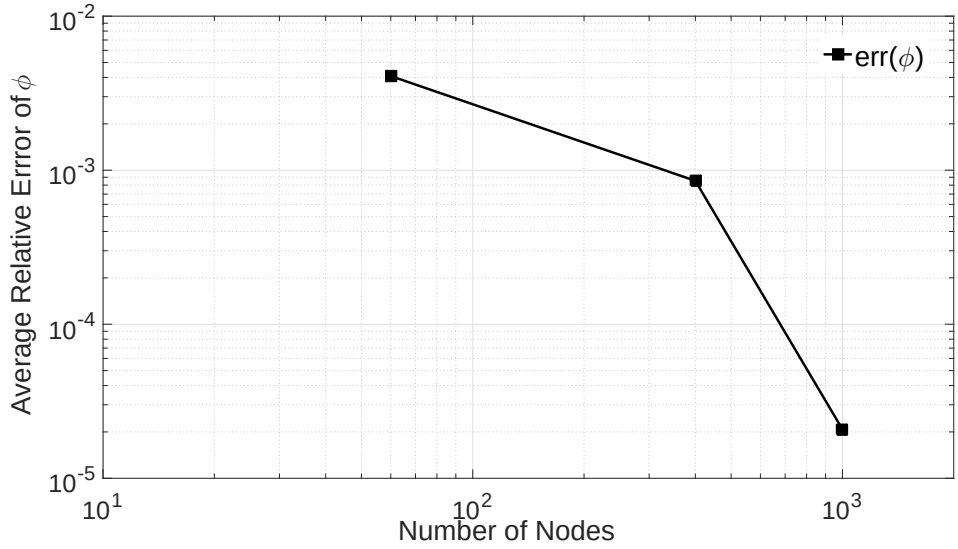

Figure 4.19: Average relative error $err(\phi)$ for 2D convection-diffusion-reaction problem at selected internal nodes with $k = 9.724$.

Case(i) : Non − Symmetric Cases:

Figure 4.20 shows the concentration profile ϕ at the middle of channel, where the value of B was considered as $B = 0.222$ and the average velocity value, $\bar{v}_x = -1.8654$, with total velocity field $v_x = -1.8654$ at $y = 0$ and $v_x = -22.9099$ at $y = 1$, and $k = 0.222$. Figure

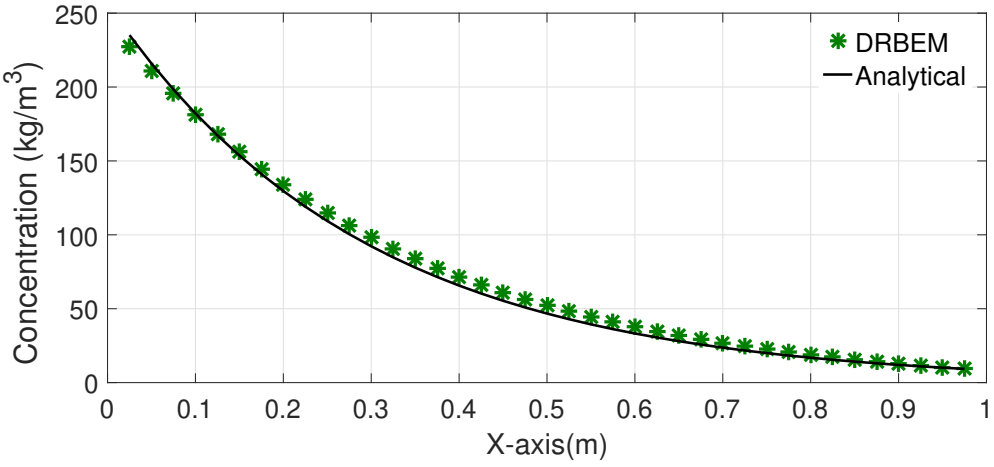

Figure 4.20: Variation of concentration profile ϕ along the middle line of the computational domain using TPS-RBF: comparison between analytical (solid line) and numerical (star points) solutions

4.21 represents the concentration profile when $k = 1$ along the bottom face $y = 0$ for the case $B = 0.125$ compared to the analytical solution. This gives velocity values of $v_x = -0.5131$ at $y = 0$ and $v_x = -25.1409$ at $y = 1$. Figure 4.22 shows simulation and exact solutions utilising

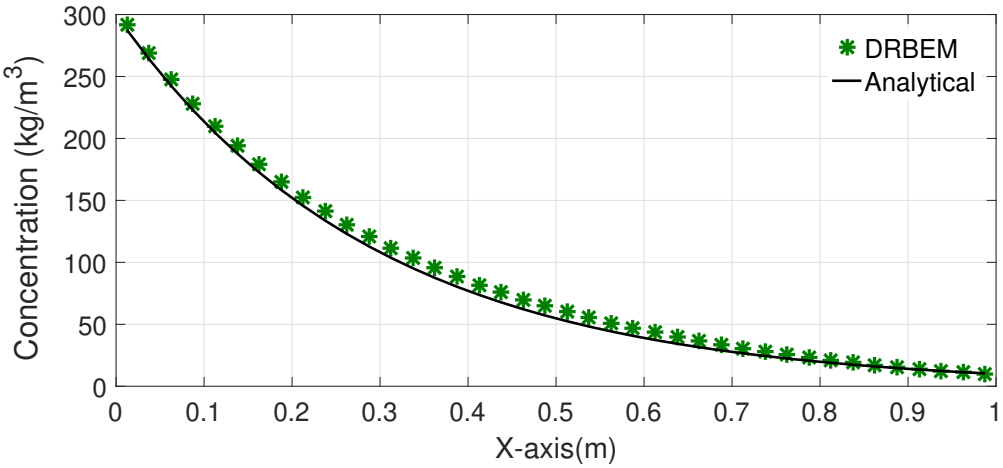

Figure 4.21: Variation of concentration profile ϕ along the bottom horizontal face using TPS-RBF: comparison between analytical (solid line) and numerical (star points) solutions

the value of $B = 1.4222$ and $k = 9.724$. This gives velocity values of $v_x = -2.0225$ at $y = 0$ and $v_x = -0.1782$ at $y = 1$. Next, Fig. 4.23 shows a comparison between simulation and

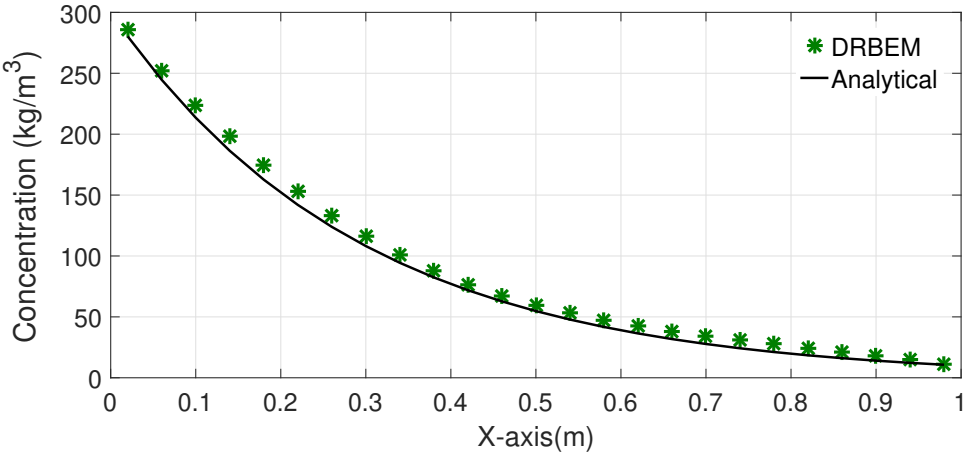

Figure 4.22: Variation of concentration profile ϕ along the bottom horizontal face using TPS-RBF: comparison between analytical (solid line) and numerical (star points) solutions

exact solutions by utilising $k = 50$. The value of B was considered as $B = 1.6$ to make the concentration ϕ and the velocity profiles highly non-symmetric. This gives velocity values

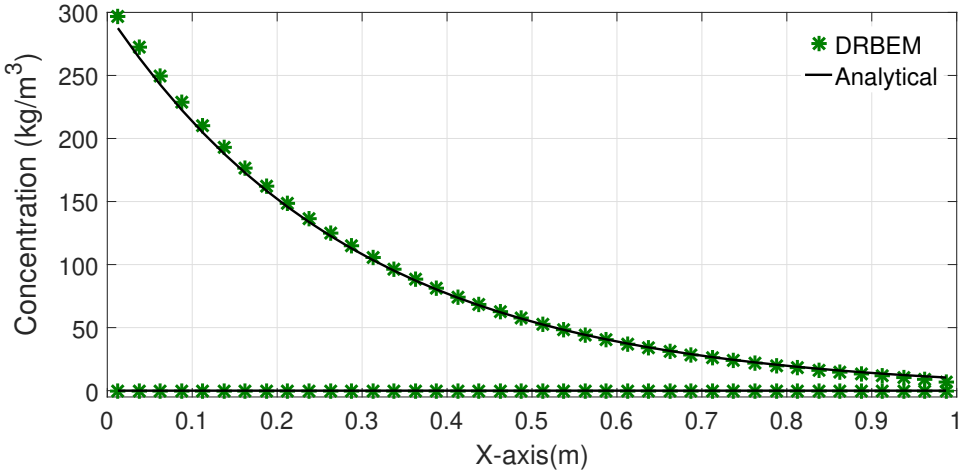

Figure 4.23: Variation of concentration profile ϕ along the horizontal faces: comparison between analytical (solid line) and numerical (star points) solutions

of $v_x = -1.1117 \times 10^3$ at $y = 0$ and $v_x = -156.334$ at $y = 1$. Figs. 4.24 and 4.25 show the variation of the normal flux q along the vertical faces $x = 1$ and $x = 0$, respectively. It

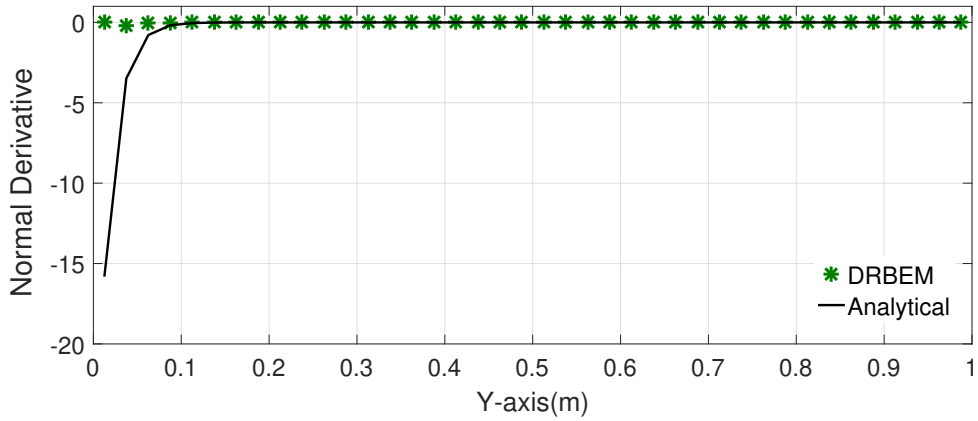

Figure 4.24: Variation of normal flux q along the horizontal face $x = 1$: comparison between analytical (solid line) and numerical (star points) solutions

should be stressed that the maximum global Péclet number in this case Pé $= 1.1117 \times 10^3$.

Next, the value of B was increased to $B = 2$, where the velocity $v_x = -212.178$ at $y = 0$ and $v_x = -53.0445$ at $y = 1$, whereas the reaction value was increased to $k = 25$. The results using TPS are in excellent agreement with the analytical solution, as shown in Fig. 4.26. The maximum global Péclet number in this case is Pé $= 212.178$. Figure 4.27 shows the variation

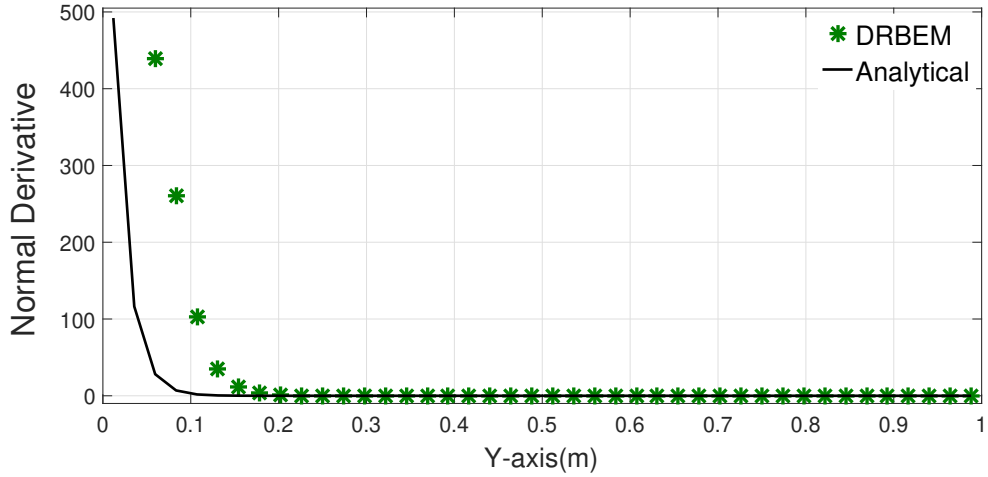

Figure 4.25: Variation of normal flux q along the horizontal face $x = 0$: comparison between analytical (solid line) and numerical (star points) solutions

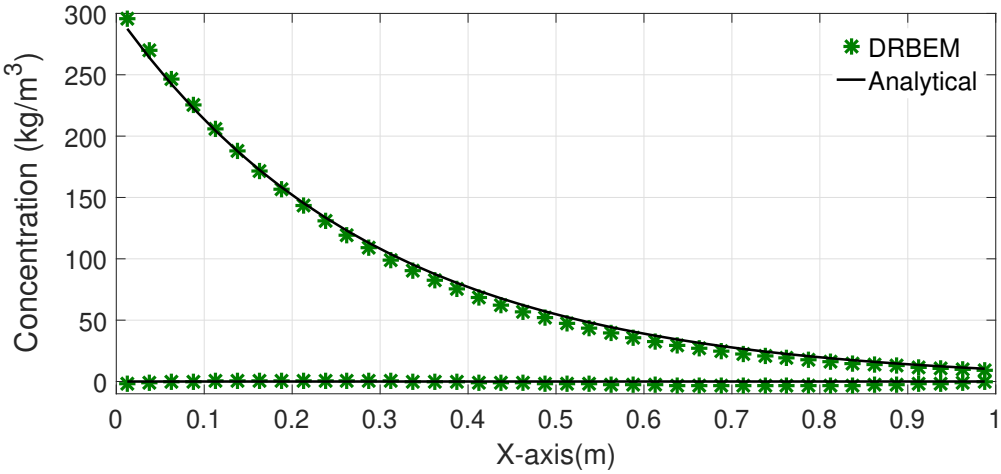

Figure 4.26: Variation of concentration profile ϕ along the horizontal faces: comparison between analytical (solid line) and numerical (star points) solutions

of the normal flux along the vertical face $x = 1$. It is seen that the visible oscillations near the edges are typical of the implementation of constant boundary elements.

Case(ii) : Symmetric Case:

The last value of the parameter B was considered to be $B = 0.5$, where the velocity v_x and the concentration profiles become symmetric. It is found that the DRBEM gives good results with reaction value $k = 125$ as displayed in Fig. 4.28.

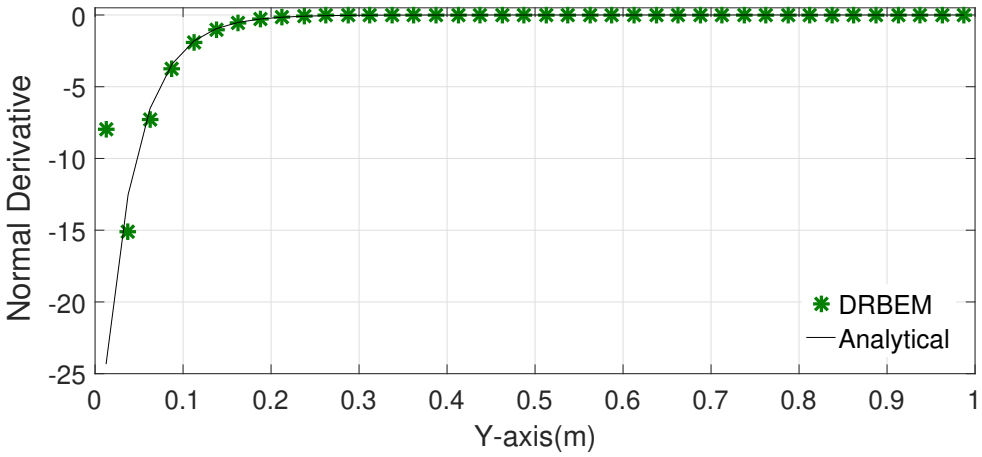

Figure 4.27: Variation of normal flux q along the vertical face $x = 1$: comparison between analytical (solid line) and numerical (star points) solutions

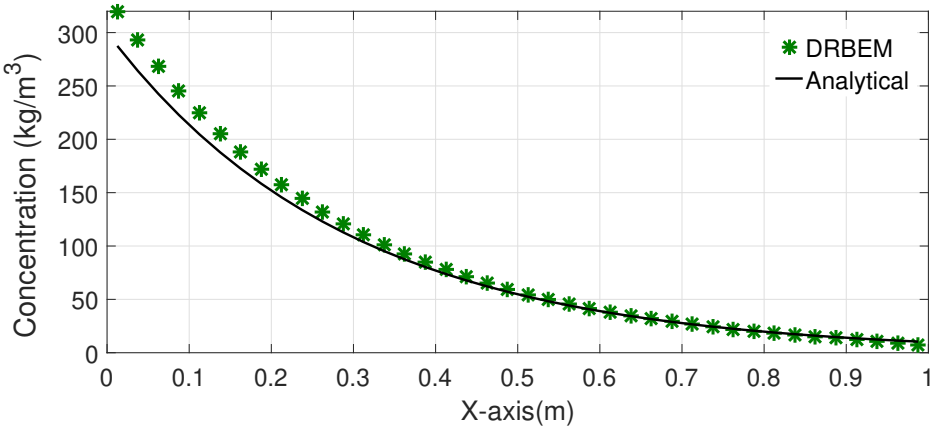

Figure 4.28: Variation of concentration profile ϕ along the symmetrical horizontal faces: comparison between analytical (solid line) and numerical (star points) solutions

4.11 Summary and Discussions

In this chapter, a BEM formulation for two-dimensional steady-state convection-diffusion-reaction problems with variable velocity field is presented, employing the fundamental solution of the corresponding equation with constant coefficients and a dual reciprocity approximation of the perturbation velocity. The DRBEM is used to transform the domain integrals appearing in the BEM formulations into equivalent boundary integrals, thus retaining the boundary-only character of the standard BEM. A proposed approach is implemented to

treat the convective terms. Numerical applications are included to demonstrate the validity of the proposed technique, and its accuracy was evaluated by applying it to three tests with different velocity fields. We can note a distinct advantage of the present approach, which demonstrates very good accuracy even for high reaction values which increase the Péclet number for the cases studied. It is obvious that, as the velocity increases, the concentration distribution becomes steeper and more difficult to reproduce with numerical models. However, all BEM solutions are still accurate for a high Péclet number Pé = 10^3.

We have made an extensive investigation for the last case studied by considering many different values of the reaction coefficient k, up to $k = 125$. We derived and implemented three RBFs and tested them with different types of problems, and we have found that the thin-plate spline radial basis function is the most accurate among these RBFs for our problems. It is, however, worth stressing that the small visible oscillations of the normal fluxes in all test cases are common and distinctive of the use of constant boundary elements. Discretisation errors of the boundary elements solutions are estimated to show the accuracy and effectiveness of the present method.

Previous applications of the BEM to convection-diffusion problems have shown that the BEM appears to be relatively free from oscillations and damping of the numerical solutions, which is typical of standard FDM and FEM techniques. However, since the BEM formulation requires the evaluation of singular integrals, oscillations may develop at high values of Pé if this integration is not properly carried out. Qiu *et al.* [119] developed a numerical technique for all BEM at high values of Pé that isolates the singular integration problem and describe the measures taken and a scheme to optimise the integration. They also show that for higher values of the Péclet number, the system matrix becomes more sparse and diagonally dominant. Thus, powerful direct or iterative solvers can be implemented for an even increased efficiency.

For convection-dominated problems domain discretisation is necessary, and a more convenient equation for numerical treatment is derived in this chapter through integration by parts as in section 4.7. The numerical techniques implemented in this chapter can also be applied to transient problems, as discussed in the next chapter.

Chapter 5

DRBEM Modelling for Transient Convection-Diffusion-Reaction Problems with Constant Velocity Fields

5.1 Introduction

The great advantage of applying the BEM to solve engineering problems resides on its requirement of boundary-only discretisation, which implies saving in computer time and manpower in pre and post-processing. For problems governed by differential equations with known fundamental solutions an integral equation involving variables only on the boundary of the region under study was derived in Chapter 3. It is not always simple to obtain a boundary-only expression for more complicated problems such as the ones to be tackled in this chapter, which are governed by the transient convection-diffusion-reaction equation. In this chapter it will be shown how the BEM formulation can be extended to deal with transient problems using the same fundamental solution of the steady-state case and approximating the resulting domain integral involving the time derivative by a dual reciprocity technique.

The DRBEM, initially applied to transient heat conduction problems by Wrobel *et al.* [162], interprets the time derivative in the diffusion equation as a body force and employs the

fundamental solution to the corresponding steady-state equation to generate a boundary integral equation. When the steady-state fundamental solution is used in the DRBEM to approximate transient convection-diffusion problems, other techniques should be employed to approximate the solution's functional dependence on the temporal variables. Aral and Tang [124] used the fundamental solution of the Laplace equation, but made use of a secondary reduction process, called SR-BEM, to arrive at a boundary-only formulation. They presented the results of transient convection-diffusion problems with or without first-order chemical reaction for low to moderate Péclet numbers. Martin [163] proposed a Schwartz waveform relaxation algorithm for the unsteady diffusive-convective equation, which uses domain decomposition methods and applies the iterative algorithm directly to the time-dependent problem. Partridge and Sensale [164] have used the method of fundamental solutions with dual reciprocity and subdomain approach to solve convection-diffusion problems. The time integration scheme is the FDM with a relaxation procedure, which is iterative in nature and needs a carefully selected time increment.

We use the fundamental solution to the steady-state convection-diffusion-reaction equation and transform the domain integral arising from the time derivative term using a set of co-ordinate functions and particular solutions which satisfy the associated non-homogeneous steady-state convection-diffusion-reaction problem. Further, only a simple set of cubic RBF has been previously used in this formulation. We consider two other sets of coordinate functions, non-augmented thin plate spline (TPS) and multiquadric (MQ), and analyse their performance in conjunction with the time integration algorithms for convection-diffusion-reaction problems.

A brief outline of the rest of this chapter is as follows. Section 5.2 describes the mathematical model governing by the transient convection-diffusion-reaction problem with constant velocity. Section 5.3 derives the DRBEM formulation of the governing equation employing the steady-state fundamental solution of the corresponding equation. In section 5.4, the time discretisation for the problem will be presented, then, a two-level time marching procedure for the proposed model is implemented in section 5.5. Section 5.6 compares and investigates the solution profiles for the present numerical experiments with the analytical solution of

the tested cases, with computational aspects included to demonstrate the performance of the proposed approach. Finally, a summary and discussions are provided in section 5.7.

5.2 Transient Convection-Diffusion-Reaction Equation

5.2.1 The Mathematical Model

The standard BEM approach is used for equations for which a fundamental solution can be found for the adjoint operator, and this enables one to write an integral equation involving variables just on the boundary, such as shown in Chapter 3 for the steady-state case. The DRM instead can be used as an alternative approach for situations in which the fundamental solution of the complete operator is not available, as in Chapter 4, or is too complicated or inefficient to be used in practice.

In the case of the transient convection-diffusion equation without decay or reaction, there is a time-dependent fundamental solution given by:

$$\Phi^*(\xi,x,\tau,t)=\frac{\mathscr{H}(\tau-t)}{[4\pi D(\tau-t)]^{\frac{d}{2}}}\exp\left[-\frac{v.\mathbf{r}}{2D}-\frac{|v|^2(\tau-t)}{4D}-\frac{|\mathbf{r}|^2}{4D(\tau-t)}\right], \tag{5.1}$$

where $\mathbf{r}=|\xi-\chi|$, d is the number of spatial dimensions and $\mathscr{H}[\ ]$ stands for the Heaviside step function. This fundamental solution is valid only when the velocity v is constant in space and time [33]. The utilisation of this fundamental solutions leads to a boundary-only integral equation for which the time integration is relatively time consuming, and therefore impractical for the solution of large scale engineering problems.

5.2.2 The Governing Equation

If one is dealing with a transient problem in a reactive medium in which a first-order chemical reaction occurs, two additional terms appear in Eq.(3.1) to account for the time dependence

and decay of the species. In such a case, Eq.(3.2) takes the form:

$$-D\nabla^2\phi\,(x,y,t)+v_x\frac{\partial\phi\,(x,y,t)}{\partial x}+v_y\frac{\partial\phi\,(x,y,t)}{\partial y}+k\phi\,(x,y,t)=\frac{\partial\phi\,(x,y,t)}{\partial t}, \tag{5.2}$$

where $\phi\,(x,y,t)$ is a potential (temperature or concentration) x and y are spatial coordinates, v_x, v_y are components of the velocity vector, D is the diffusivity constant or dispersion coefficient, k represents the first-order reaction coefficient and ∇^2 is the Laplacian operator already defined in Eq.(3.2). The boundary conditions can be of the Dirichlet, Neumann and Robin types.

In Eq.(5.2), $\phi\,(x,y,t)$ represents the concentration of a substance in this chapter, handled as a function of space and time. The velocity components v_x and v_y along the x and y directions are assumed to be constant.

The boundary conditions are

$$\phi=\bar{\phi}\quad\text{over}\quad\Gamma_D \tag{5.3}$$

$$q=\frac{\partial\phi}{\partial n}=\bar{q}\quad\text{over}\quad\Gamma_N, \tag{5.4}$$

where Γ_D and Γ_N are the Dirichlet and Neumann parts of the boundary with $\Gamma=\Gamma_D\cup\Gamma_N$, and $\Gamma_D\cap\Gamma_N=\emptyset$. The initial condition over the domain Ω is

$$\phi\,(x,y,0)=\phi_0\,(x,y)\,,\ (x,y)\in\Omega. \tag{5.5}$$

In trying to obtain a boundary integral formulation for the equation Eq.(5.2) one can follow the same approach as in Chapter 3. This starts by defining a linear operator $\mathscr{L}$ in a domain Ω with boundary Γ as in Eq.(3.4). This allow to write the equation as

$$\mathscr{L}\,[\phi]=\frac{\partial\phi}{\partial t}. \tag{5.6}$$

Using the same arbitrary weighting function Φ^* and integrating over the whole domain produces

$$\int_\Omega \mathscr{L}[\phi]\,\Phi^* d\Omega = \int_\Omega \frac{\partial \phi}{\partial t}\Phi^* d\Omega. \tag{5.7}$$

The integration by parts twice of the left-hand side of this equation produces terms absolutely identical to the ones of Eq.(3.25) in the steady-state case which now, for the transient case, becomes

$$\int_\Omega \mathscr{L}[\phi]\,\Phi^* d\Omega = \int_\Omega \mathscr{L}^*[\Phi^*]\,\phi d\Omega - D\int_\Gamma \Phi^* \nabla\phi.n\, d\Gamma$$

$$+D\int_\Gamma \phi \nabla\Phi^*.n\, d\Gamma + \int_\Gamma (\phi\Phi^*)\, v.n\, d\Gamma = \int_\Omega \frac{\partial \phi}{\partial t}\Phi^* d\Omega. \tag{5.8}$$

The above equation can be recast as

$$\int_\Omega \mathscr{L}^*[\Phi^*]\,\phi\, d\Omega + D\int_\Gamma (-\Phi^*\nabla\phi.n + \phi\nabla\Phi^*.n)\, d\Gamma + \int_\Gamma (\phi\Phi^*)\, v.n\, d\Gamma = \int_\Omega \frac{\partial \phi}{\partial t}\Phi^* d\Omega. \tag{5.9}$$

If one chooses the same weighting function $\Phi^*(\xi, x)$ as for the steady-state case one has, after the limiting process of taking the domain integral to the boundary, that

$$C(\xi)\,\phi(\xi) + \int_\Gamma \left(D\frac{\partial \Phi^*}{\partial n} + v_n\Phi^*\right)\phi\, d\Gamma - D\int_\Gamma \Phi^* \frac{\partial \phi}{\partial n} d\Gamma = \int_\Omega \frac{\partial \phi}{\partial t}\Phi^* d\Omega. \tag{5.10}$$

As can be seen, this equation still contains a domain integral and one has to propose a scheme to reduce the integral to the boundary. The approach used here is the DRBEM.

5.3 DRBEM Formulation for the 2D Transient Convection-Diffusion-Reaction Problem

In order to be able to solve an equation like Eq.(5.1) in which the non-homogeneous term is a function not only of position, but also of the potential derivative with respect to time, one has to expand $\frac{\partial \phi}{\partial t}$ as a series of functions. These functions are such that, for each of them, a particular solution of the convection-diffusion-reaction equation can be found. For the case under consideration, this choice of the functions will be made in a later section.

The basic idea is to expand the function $\frac{\partial \phi}{\partial t}$ as a sum of functions F_k, dependent only on geometry, multiplied by some coefficients α_k function of time

$$\frac{\partial \phi\left(x,t\right)}{\partial t} = \sum_{k=1}^{M} F_k\left(x\right)\, \alpha_k\left(t\right), \tag{5.11}$$

where M stands for the total number of terms in the series.

As the intention is to remove the domain integration, the functions F_k have to be chosen in such a way that, firstly, the expansion represents properly the function, and secondly, one can find functions ψ_k so that

$$\mathscr{L}\left[\psi_k\right] = F_k \tag{5.12}$$

such that the integral over the domain can be transformed into a boundary integral expression, as it will be shown in what follows.

The right-hand-side of Eq.(5.10) can be written, after substitution of expression Eq.(5.11), as

$$\int_{\Omega} \frac{\partial \phi}{\partial t} \Phi^* d\Omega = \int_{\Omega} \sum_{k=1}^{M} F_k\left(x\right)\, \alpha_k\left(t\right)\, \Phi^* d\Omega, \tag{5.13}$$

and also recast as:

$$\int_{\Omega} \frac{\partial \phi}{\partial t} \Phi^* d\Omega = \sum_{k=1}^{M} \alpha_k\left(t\right) \int_{\Omega} F_k\left(x\right) \Phi^* d\Omega, \tag{5.14}$$

This in view of Eq.(5.12), can be written as,

$$\int_{\Omega} \frac{\partial \phi}{\partial t} \Phi^* d\Omega = \sum_{k=1}^{M} \alpha_k(t) \int_{\Omega} \mathscr{L}[\psi_k] \Phi^* d\Omega. \tag{5.15}$$

Let us consider now a single term of the summation, for the sake of simplicity.
Looking back at the results of Eq.(3.25), one can easily see that the integration on the right-hand-side of this equation can be written as

$$\int_{\Omega} \mathscr{L}[\psi_k] \Phi^* d\Omega = \int_{\Omega} \mathscr{L}^*[\Phi^*] \psi_k \, d\Omega - D \int_{\Gamma} \Phi^* \nabla \psi_k . n \, d\Gamma$$

$$+ D \int_{\Gamma} \psi_k \nabla \Phi^* . n \, d\Gamma + \int_{\Gamma} (\psi_k \Phi^*) v . n \, d\Gamma. \tag{5.16}$$

Making use of Eq.(3.36) one ends up with:

$$\int_{\Omega} \mathscr{L}[\psi_k] \Phi^* d\Omega = C(\xi) \psi_k(\xi) + \int_{\Gamma} \left(D \frac{\partial \Phi^*}{\partial n} + v_n \Phi^* \right) \psi_k \, d\Gamma - D \int_{\Gamma} \Phi^* \frac{\partial \psi_k}{\partial n} d\Gamma, \tag{5.17}$$

where ξ is the source point under consideration and the constant $C(\xi)$ depends on its location in the domain, whether inside, outside or on the boundary. It is important to recall that this equation relates the integral of one of the values of the same function $\psi_k(x)$ and its normal derivative $\frac{\partial \psi_k}{\partial n}$ on the boundary. It is also important to keep in mind that these are known functions, therefore, easily evaluated everywhere. Replacing the results of this equation into Eq.(5.15) one has

$$\int_{\Omega} \frac{\partial \phi}{\partial t} \Phi^* d\Omega = \sum_{k=1}^{M} \alpha_k \left[C(\xi) \psi_k(\xi) + \int_{\Gamma} \left(D \frac{\partial \Phi^*}{\partial n} + v_n \Phi^* \right) \psi_k \, d\Gamma - D \int_{\Gamma} \Phi^* \frac{\partial \psi_k}{\partial n} d\Gamma \right]. \tag{5.18}$$

and substituting this into Eq.(5.10), it produces

$$C(\xi) \phi(\xi) + \int_{\Gamma} \left(D \frac{\partial \Phi^*}{\partial n} + v_n \Phi^* \right) \phi \, d\Gamma - D \int_{\Gamma} \Phi^* \frac{\partial \phi}{\partial n} d\Gamma$$

$$= \sum_{k=1}^{M} \alpha_k \left\{ C(\xi)\,\psi_k(\xi) + \int_\Gamma \left(D\frac{\partial \Phi^*}{\partial n} + v_n \Phi^* \right) \psi_k \, d\Gamma - D \int_\Gamma \Phi^* \frac{\partial \psi_k}{\partial n} \, d\Gamma \right\}. \tag{5.19}$$

5.4 Time-Discretisation for 2D Convection-Diffusion-Reaction Problem

As one can see only boundary integrals appear in the Eq.(5.19). If one uses the integrand kernels defined in Eqs.(3.85) and (3.86), it is possible to write Eq.(5.19) as:

$$C(\xi)\,\phi(\xi) - \sum_{j=1}^{N} \int_{\Gamma_j} G(\xi, x) \frac{\partial \phi}{\partial n}(x)\, d\Gamma(x) + \sum_{j=1}^{N} \int_{\Gamma_j} H(\xi, x)\,\phi(x)\, d\Gamma(x) =$$

$$\sum_{k=1}^{M} \alpha_k \left[C(\xi)\,\psi_k(\xi, p_k) - \sum_{j=1}^{N} \int_{\Gamma_j} G(\xi, x) \frac{\partial \psi_k(x, p_k)}{\partial n} d\Gamma(x) + \sum_{j=1}^{N} \int_{\Gamma_j} H(\xi, x)\,\psi_k(x, p_k)\, d\Gamma(x) \right], \tag{5.20}$$

where p_k stands for the k-th reference point used in the expansion in terms of functions F_k. At this point it is convenient to notice a few important properties related to the functions ψ_k and $\frac{\partial \psi_k}{\partial n}$.

Firstly, they are known functions associated though the operator $\mathscr{L}$ to the functions F_k of our own choice, therefore easily evaluated anywhere in the domain. Secondly, it is interesting when evaluating the integrals involving ψ_k and $\frac{\partial \psi_k}{\partial n}$ to assume the same type of discretisation as for the evaluation of ϕ and $\frac{\partial \phi}{\partial n}$ in Chapter 3, in ordr to be able to re-use matrices G and H. Applying the discretisation procedure of Chapter 3 in which the boundary is discretised into N elements it is possible to write that

$$C_i \phi_i - \sum_{j=1}^{N} \int_{\Gamma_j} G(\xi, x) \frac{\partial \phi}{\partial n} d\Gamma(x) + \sum_{j=1}^{N} \int_{\Gamma_j} H(\xi, x)\,\phi(x)\, d\Gamma(x)$$

$$= \sum_{k=1}^{M} \alpha_k \left[C_k \psi_k - \sum_{j=1}^{N} \int_{\Gamma_j} G(\xi, x) \frac{\partial \psi}{\partial n} d\Gamma + \sum_{j=1}^{N} \int_{\Gamma_j} H(\xi, x) \psi \, d\Gamma(x) \right]. \tag{5.21}$$

Defining

$$\frac{\partial \psi}{\partial n} = \eta \quad \text{and} \quad q = \frac{\partial \phi}{\partial n}. \tag{5.22}$$

one can write

$$C_i \phi_i + \sum_{j=1}^{N} H_{ij} \phi_j - \sum_{j=1}^{N} G_{ij} q_j = \sum_{k=1}^{M} \alpha_k \left[C_i \psi_{ik} + \sum_{j=1}^{N} H_{ij} \psi_{jk} - \sum_{j=1}^{N} G_{ij} \eta_{jk} \right]. \tag{5.23}$$

As seen in the previous chapter, every node i will generate an equation like the above. It is also assumed that the number of points M exceeds the number of boundary nodes N by L units. Therefore, an equation like (5.23) applies at every point.
The system of equation in matrix form produces the following expression

$$H\phi - Gq = [H\psi - G\eta]\,\alpha. \tag{5.24}$$

The influence matrices H and G have the dimension $M \times M$, i.e. $(N+L) \times (N+L)$ and so do the matrices η and ψ. The vectors ϕ and q are column vectors of $(N+L)$ components. For the sake of clarity, the above schematic form can be described as follows:

- The matrices ψ and η relate influences of points to points, as can be easily identified from Eqs.(5.20) and (5.23). These points can be located either on the boundary or internal to the domain.
- The sub-matrices marked bb are related to the influence boundary-to-boundary points.
- Those marked ib account for the influence internal-to-boundary points, and again in the matrices ψ and η account for the influence internal points to points located on the boundary.
- The sub-matrices marked 00:

- In matrices H_{00} and G_{00} account for boundary-to-internal points influence, but in fact are just an augmentation of the matrices to conform their dimensions to the mathematical operations.

- In matrix η, having in mind that it contains by definition the normal derivatives of the ψ_k functions, they must be zero for the same reasons mentioned above for the matrix G.

- In the vector q, they would account for normal fluxes at internal points which are meaningless.

- The sub-matrices II stand for the unit sub-matrix of the matrix H and account for the internal points self-influence, i.e those points where the coefficient $C(\xi) = 1$.

- The sub-matrix marked ii accounts for the influence internal-to-internal points.

$$\begin{bmatrix} H_{bb} & H_{00} \\ H_{ib} & H_{II} \end{bmatrix} \begin{Bmatrix} \phi_N \\ \phi_L \end{Bmatrix} - \begin{bmatrix} G_{bb} & G_{00} \\ G_{ib} & G_{00} \end{bmatrix} \begin{Bmatrix} q_N \\ q_0 \end{Bmatrix} =$$

$$\begin{bmatrix} \begin{bmatrix} H_{bb} & H_{00} \\ H_{ib} & H_{II} \end{bmatrix} \begin{bmatrix} \psi_{bb} & \psi_{ib} \\ \psi_{ib} & \psi_{ii} \end{bmatrix} - \begin{bmatrix} G_{bb} & G_{00} \\ G_{ib} & G_{00} \end{bmatrix} \begin{bmatrix} \eta_{bb} & \eta_{ib} \\ \eta_{00} & \eta_{00} \end{bmatrix} \end{bmatrix} \begin{Bmatrix} \alpha_N \\ \alpha_L \end{Bmatrix}$$

It is very important to remember the fact that all the matrices in Eq.(5.12) have size $(N+L)\times(N+L)$.

Bearing in mind Eq.(5.11) can be written as

$$\alpha = F^{-1}\dot{\phi} \tag{5.25}$$

when replaced into Eq.(5.24) it produces

$$H\phi - Gq = [H\psi - G\eta]\, F^{-1}\dot{\phi}. \tag{5.26}$$

Calling

$$S = [H\psi - G\eta]\, F^{-1} \tag{5.27}$$

then Eq.(5.26) takes the form

$$S\dot{\phi} = H\phi - Gq, \tag{5.28}$$

which expresses in a concise form the functional relationship between the variable ϕ and its temporal derivative at all points in space.

5.5 Time Marching Scheme for Transient Convection-Diffusion-Reaction Problem with Constant Velocity

In this section, a time marching technique will be implemented to handle the time-derivative part of the governing equation. Therefore, in order to predict the value of ϕ at any time level, one has to integrate the above equation with respect to time in an interval (t_0, t_1). This produces

$$S\int_{t_0}^{t_1} \dot{\phi}\, dt = H\int_{t_0}^{t_1} \phi\, dt - G\int_{t_0}^{t_1} q\, dt \tag{5.29}$$

while the first integral could be directly integrated in the form

$$\int_{t_0}^{t_1} \dot{\phi}\, dt = \phi\,(t_1) - \phi\,(t_0)\,. \tag{5.30}$$

The other two terms are not so easy, as one does not know the functional dependence on time of ϕ and q. That being so, two additional assumptions are necessary to overcome the problem. Let us assume a linear variation of ϕ and q within the time interval $t \in (t_0, t_1)$ according to

$$\begin{cases} \phi(t) = \left(1-\theta_\phi\right)\phi(t_0) + \theta_\phi\,\phi(t_1), \\ q(t) = \left(1-\theta_q\right) q(t_0) + \theta_q\, q(t_1), \end{cases} \tag{5.31}$$

where θ_ϕ and θ_q are parameters which position the values of ϕ and q between time levels m and $m+1$; and take values in the interval $0 \leqslant \theta_\phi, \theta_q \leq 1$.

Replacing Eqs.(5.30) and (5.31) into Eq.(5.29) one has that:

$$S\left[\phi(t_1) - \phi(t_0)\right] = H\int_{t_0}^{t_1}\left[\left(1-\theta_\phi\right)\phi(t_0) + \theta_\phi\,\phi(t_1)\right]dt$$

$$-G\int_{t_0}^{t_1}\left[\left(1-\theta_q\right)q(t_0) + \theta_q\, q(t_1)\right]dt. \tag{5.32}$$

Once $q(t_i)$, $\phi(t_i)$, $i = 0$ are constant, the integrations can be carried out producing

$$S\left[\phi(t_1) - \phi(t_0)\right] = H\left[\left(1-\theta_\phi\right)\phi(t_0) + \theta_\phi\,\phi(t_1)\right](t_1 - t_0)$$

$$-G\left[\left(1-\theta_q\right)q(t_0) + \theta_q\, q(t_1)\right](t_1 - t_0). \tag{5.33}$$

Dividing this equation by $\Delta t = (t_1 - t_0)$ and after some rearrangement one can write

$$\left[\frac{1}{\Delta t}S - \theta_\phi H\right]\phi(t_1) + \theta_q G q(t_1) = \left[\frac{1}{\Delta t}S + \left(1-\theta_\phi\right)H\right]\phi(t_0) - \left(1-\theta_q\right)G q(t_0). \tag{5.34}$$

The right-hand-side of the above equation is known, and it contains the initial conditions of the problem. Thus, to be able to predict the value of ϕ at any time, one needs to impose prescribed boundary conditions for ϕ or q at this time t_1.

The evolution on time can then be made in a step-by-step way according to the recurrence

formula

$$\left[\frac{1}{\Delta t}S-\theta_{\phi}H\right]\phi^{m+1}+\theta_{q}Gq^{m+1}=\left[\frac{1}{\Delta t}S+\left(1-\theta_{\phi}\right)H\right]\phi^{m}-\left(1-\theta_{q}\right)Gq^{m}. \qquad (5.35)$$

where $\phi^m = \phi(t_m)$. Equation (5.35) represents the DRBEM discretisation of the algebraic equations.

If one makes the value of Δt constant then the matrices

$$A=\left[\frac{1}{\Delta t}S-\theta_{\phi}H\right] \quad \text{and} \quad B=\left[\frac{1}{\Delta t}S+\left(1-\theta_{\phi}\right)H\right] \qquad (5.36)$$

need to be calculated only once, as the matrices S, H and G are time invariant influence coefficient matrices and therefore dependent only on the geometry of the problem. Once evaluated they can be stored and used in the recurrence procedure that consequently will consist of only matrix additions and products. Upon introducing the boundary conditions, the resulting linear algebraic system can be solved by utilising a standard procedure such as Gauss elimination, LU decomposition or least square method.

5.6 Numerical Applications and Discussions

To study the performance of the proposed strategies, we consider six examples with known analytical solutions. All numerical computations have been performed using constant elements. To assess the accuracy of the DRBEM based scheme for different types of problems, we have chosen representative problems with Dirichlet and mixed boundary conditions. Numerical outcomes with this scheme are compared with the corresponding analytical solutions. The reaction coefficient value is zero in for all tests.

5.6.1 Transient Convection-Diffusion-Reaction Problem over a Rectangular Region with Mixed Boundary Conditions

In this problem, the convection-diffusion-reaction is modelled as a rectangular channel with 140 elements distributed as 30 constant elements for each vertical side of the domain and 40 for each the horizontal faces, while imposing 39 internal nodes along the centre of the computational region.

The mathematical model is given by

$$D\nabla^2\phi - v_x\frac{\partial\phi}{\partial x} - v_y\frac{\partial\phi}{\partial y} = \frac{\partial\phi}{\partial t}, \quad 0 \le x \le 1, 0 \le y \le 0.7, t > 0. \tag{5.37}$$

The geometry is considered to be $[1, 0.7]$, as shown in Fig. 5.1. The initial condition is:

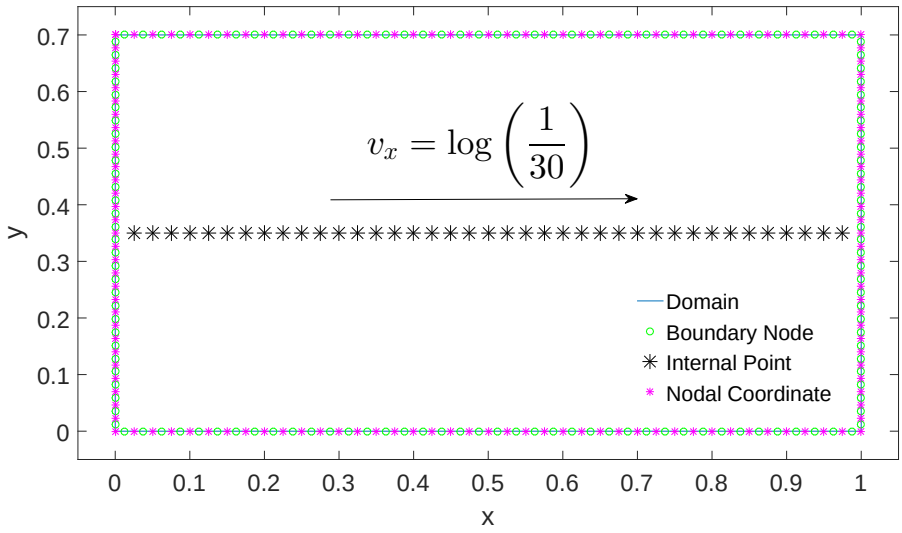

Figure 5.1: DRBEM discretisation of the 2D transient convection-diffusion-reaction model with the internal points.

$$\phi(x, y, 0) = 0 \tag{5.38}$$

The mixed boundary conditions (Dirichlet-Neumann) under consideration are defined as:

$$\begin{cases} \phi(0,y,t) = 300, \quad 0 \leq y \leq 0.7, t > 0 \\ \phi(1,y,t) = 10, \quad 0 \leq y \leq 0.7, t > 0 \\ \frac{\partial \phi}{\partial n}(x,0,t) = 0, \quad 0 \leq x \leq 1, t > 0 \\ \frac{\partial \phi}{\partial n}(x,0.7,t) = 0, \quad 0 \leq x \leq 1, t > 0 \end{cases}$$

The steady-state analytical solution is provided as follows:

$$\phi(x,y) = 300 \exp\left[x \log\left(\frac{1}{30}\right)\right] \tag{5.39}$$

This problem is analysed as transient with both the velocity and diffusion coefficient set to be constants as $v_x = \log\left(\frac{1}{30}\right)$, $v_y = 0$, $D = 1$ while the reaction coefficient value is $k = 0$. Figure 5.2 shows a comparison of the numerical and the analytical solutions after 100 time-steps of $\Delta t = 0.08s$ along the bottom face of the computational domain, i.e. $y = 0$, utilising the TPS-RBF.

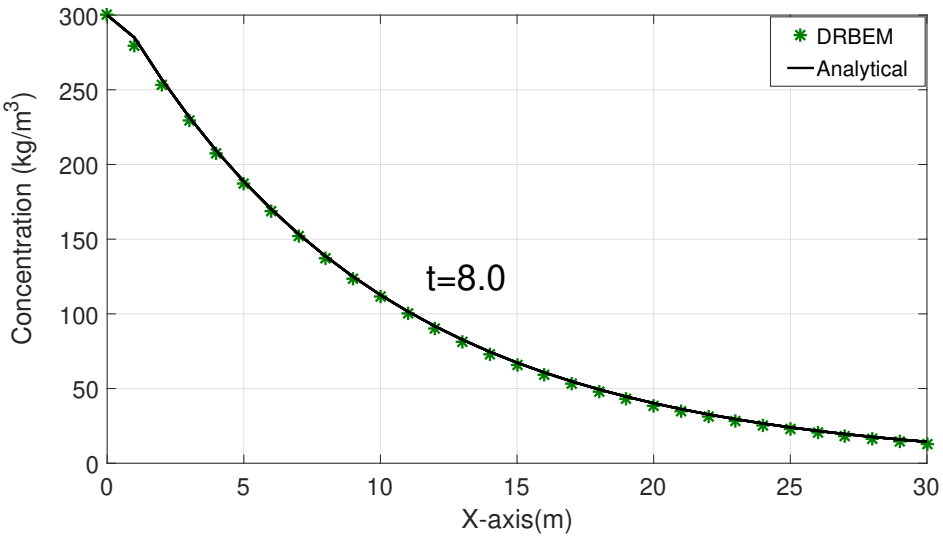

Figure 5.2: Concentration profiles distribution along the bottom face $y = 0$ with $\Delta t = 0.08$ using TPS-RBF: comparison of analytical (solid line) and numerical solutions (star points).

Next, Fig. 5.3 shows the numerical and the analytical solutions for internal points distributed

along the central face of the computational domain, $y = 0.5$, also using the TPS-RBF. After 100 time steps with $\Delta t = 0.08s$, the present solution approaches the steady-state case, with very good agreement with the analytical solution.

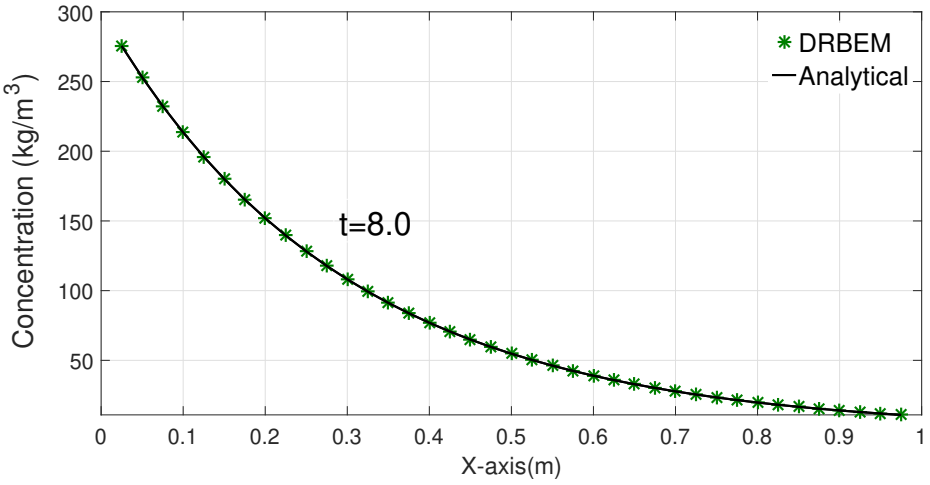

Figure 5.3: Concentration profiles distribution along the centre of the domain $y = 0.5$ with $\Delta t = 0.08$ using TPS-RBF: comparison of analytical (solid line) and numerical solutions (star points).

5.6.2 Transient Convection-Diffusion-Reaction Problem over a Rectangular Channel with Time-Dependent Boundary Conditions

We next consider 2D convection-diffusion-reaction problems with time-dependent boundary conditions for testing the accuracy of our proposed procedure. The mathematical model is as follows:

$$D\nabla^2\phi - \frac{\partial \phi}{\partial x} - \frac{\partial \phi}{\partial y} = \frac{\partial \phi}{\partial t}, \quad 0 \leq x \leq 1, 0 \leq y \leq 0.2, t > 0. \tag{5.40}$$

This problem is performed with time-dependent boundary conditions to the left and right sides of the computational domain, respectively,

$$\begin{cases} \phi(0,y,t) = \frac{1}{\sqrt{4t+1}} \exp\left[-\frac{(-1-v_x t)^2}{D(4t+1)}\right], \\ \phi(1,y,t) = \frac{1}{\sqrt{4t+1}} \exp\left[-\frac{(-v_x t)^2}{D(4t+1)}\right], \\ \frac{\partial \phi}{\partial n}(x,0,t) = 0, \\ \frac{\partial \phi}{\partial n}(x,1,t) = 0. \end{cases}$$

The initial condition is given by:

$$\phi(x,y,0) = \exp\left[-\frac{x^2}{D}\right]. \tag{5.41}$$

The analytical solution for this problem is expressed as follows:

$$\phi(x,y,t) = \frac{1}{\sqrt{4t+1}} \exp\left[-\frac{(x-1-v_x t)^2}{D(4t+1)}\right]. \tag{5.42}$$

The numerical solution of the problem is compared to the analytical one considering $v_y = 0$, $v_x = 0.001\,(m/s)$, $k = 0$ and $D = 1\left(m^2/s\right)$ with constant time increments of $\Delta t = 0.25$, 0.5 and 1, respectively. The problem is schematically described in Fig. 5.4 with 140 collocation points, with 30 elements distributed along each vertical faces and 40 for each the horizontal side. In addition, 39 internal nodes are imposed along the central line of the corresponding domain.

For the boundary element analysis, the problem is modelled as a two-dimensional channel of dimensions $[1m \times 0.2m]$. A fully implicit scheme has been implemented for modelling the time derivative term.

The results of simulations are shown in Fig. 5.5 for $\Delta t = 0.25s$ at different time levels for the internal points at the centre of the computational domain using TPS-RBF. The concentration results show very good agreement between the numerical and the analytical solutions. Next, Fig. 5.6 shows results for $\Delta t = 0.5$ at different time levels for the internal points at the central

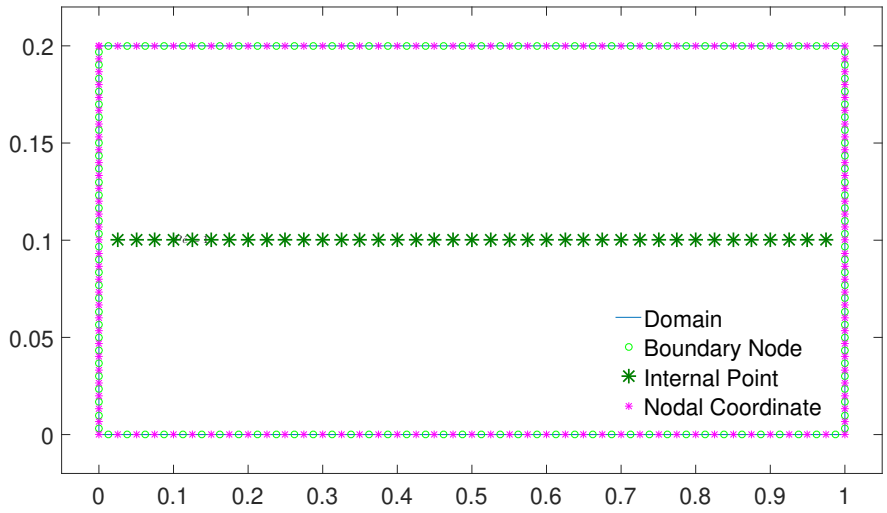

Figure 5.4: Discretisation for 2D transient convection-diffusion-reaction model with 39 internal points.

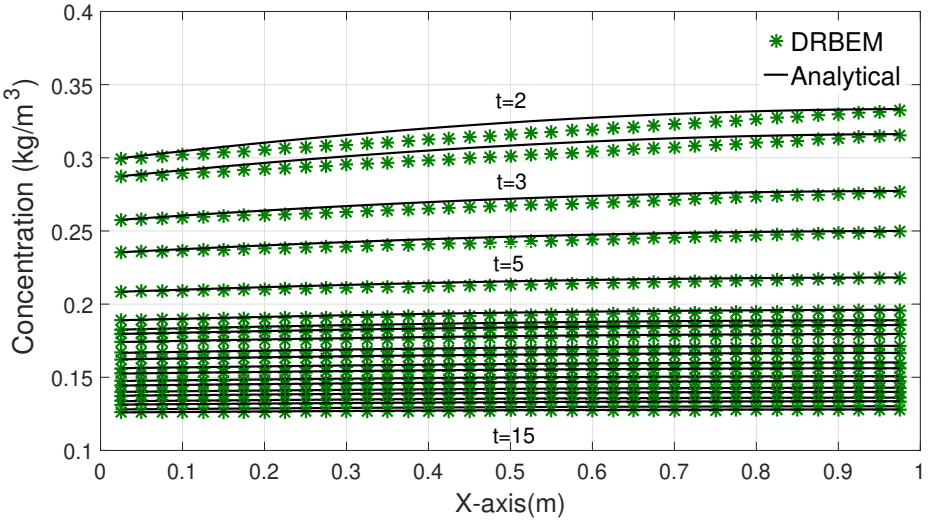

Figure 5.5: Concentration profiles at the central line $y = 0.5$ with $\Delta t = 0.25$ using TPS-RBF: comparison of analytical (solid line) and numerical solutions (star points).

line of the computational domain. Another simulation for this transient transport problem is plotted for $\Delta t = 1s$ at different time levels along the central line of the computational domain for internal points using TPS-RBF as displayed in Fig. 5.7. Table 5.1 shows the RMS error norm for different Péclet numbers and mesh sizes. It can be noticed that the errors decrease with mesh refinement. The relative error in the RMS norm is of order 10^{-6} for small values

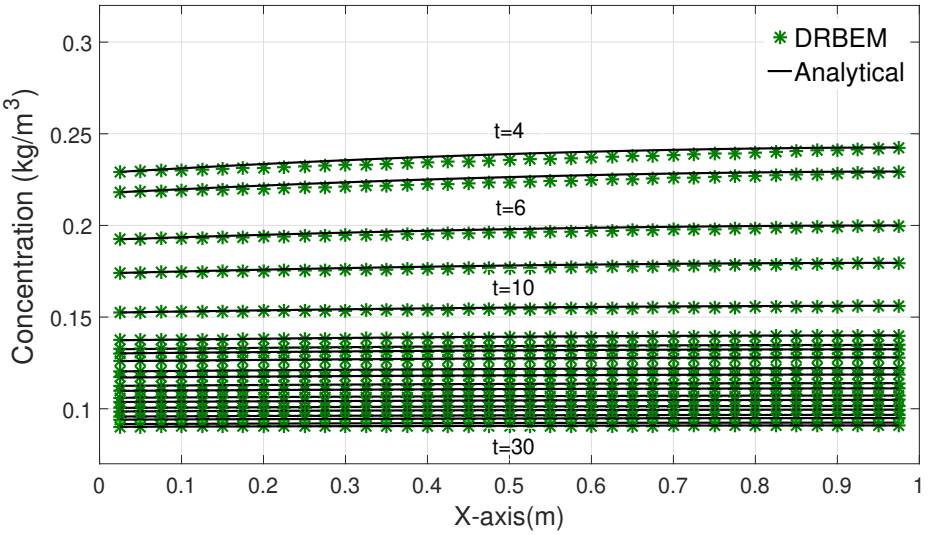

Figure 5.6: Concentration profiles at the central line $y = 0.5$ with $\Delta t = 0.5s$ using TPS-RBF: comparison of analytical (solid line) and numerical solutions (star points).

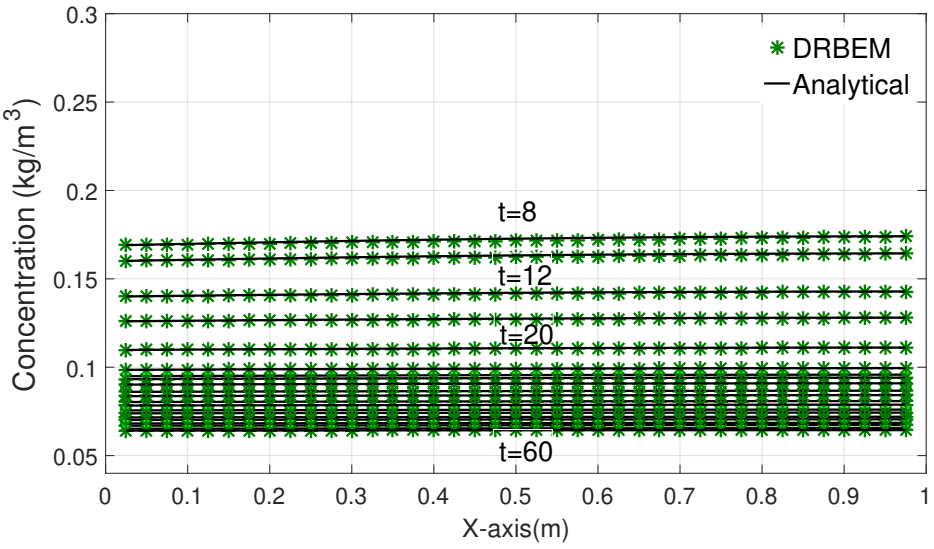

Figure 5.7: Concentration profiles at the central line $y = 0$ with $\Delta t = 1$ using TPS-RBF: comparison of analytical (solid line) and numerical solutions (star points).

of the velocity and of the order 10^{-2} for larger values of Pé.

Table 5.2 presents the RMS results at time $t = 2.5$ with $\Delta t = 0.5s$ using TPS-RBF. The results indicate good convergence in the RMS norm. As seen in Table 5.3, cubic and TPS RBFs produce similar results, with good agreement with the analytical solution. In this case

Table 5.1: RMS error norm of DRBEM for convection-diffusion-reaction problem with different spatial meshes

RMS error norm in ϕ, $f = r^2 \log(r)$, Problem 2				
Mesh size	Pé $= 0.001$	Pé $= 0.01$	Pé $= 0.1$	Pé $= 1$
14	5.974×10^{-4}	1.744×10^{-5}	6.300×10^{-3}	8.710×10^{-2}
36	5.014×10^{-4}	1.465×10^{-5}	5.300×10^{-3}	7.300×10^{-2}
72	4.120×10^{-4}	1.204×10^{-5}	4.400×10^{-3}	6.000×10^{-2}
100	3.681×10^{-4}	1.113×10^{-5}	3.900×10^{-3}	5.360×10^{-2}
200	2.807×10^{-4}	8.234×10^{-6}	3.000×10^{-3}	4.090×10^{-2}

Table 5.2: RMS norm of DRBEM for convection-diffusion-reaction problem with different meshes

RMS error norm in ϕ, $f = r^2 \log(r)$, Problem 2			
Mesh size	$D = 1$	$D = 5$	$D = 10$
14	1.744×10^{-5}	0.5495	1.2363
36	1.465×10^{-5}	0.4169	1.0392
72	2.362×10^{-5}	0.3797	0.8542
100	1.080×10^{-5}	0.3393	0.7634
140	9.517×10^{-6}	0.2990	0.6727
200	8.234×10^{-6}	0.2587	0.5822

study, it is apparent that the accuracy is reduced with MQ-RBF. In Table 5.4 the error at time $t = 10$ using TPS-RBF for Pé =0.01 is seen to reduce as Δt decreases, as expected. The time evolution of the concentration at selected internal points using TPS is shown in Fig. 5.8. It can be seen that the proposed DRBEM achieves an excellent agreement with the analytical solutions, in which the maximum relative error in the RMS norm is 4.2903×10^{-4}.

Table 5.3: Results for convection-diffusion-reaction at $t = 5$ for $\Delta t = 0.5$

x	Cubic	MQ	TPS	Analytical
0.1	0.2101	0.2082	0.2091	0.2098
0.25	0.2126	0.2087	0.2106	0.2137
0.50	0.2158	0.2106	0.2131	0.2155
0.75	0.2177	0.2137	0.2157	0.2175
0.95	0.2182	0.2172	0.2177	0.2181

Table 5.4: RMS error norm of DRBEM for decreasing Δt

$\theta = 1$, $f = r^2 \log(r)$, Problem 2			
	$\Delta t = 2$	$\Delta t = 1$	$\Delta t = 0.5$
RMS error in ϕ	3.591×10^{-4}	2.430×10^{-4}	1.2044×10^{-5}

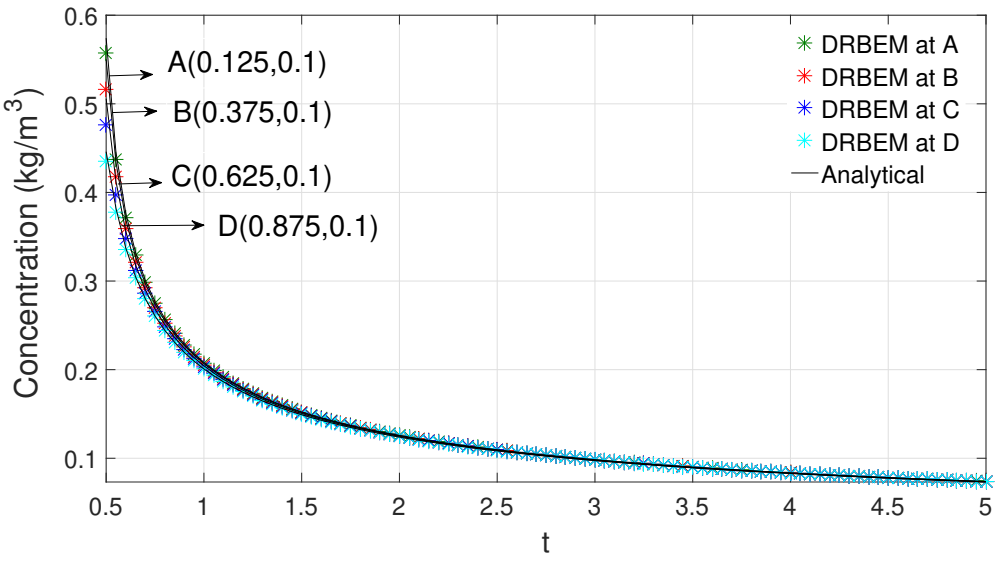

Figure 5.8: Concentration profiles with time at selected internal points using TPS-RBF: comparison of analytical (solid line) and numerical solutions (star points).

5.6.3 Transient Convection-Diffusion-Reaction Problem over a Square Domain with Time-Dependent Boundary Conditions

The dimensions of the domain for this problem are $[0,1] \times [0,1]$ with the time-dependent Dirichlet type boundary conditions. The mathematical model is as follows:

$$D\nabla^2\phi - \frac{\partial \phi}{\partial x} - \frac{1}{2}\frac{\partial \phi}{\partial y} = \frac{\partial \phi}{\partial t}, \quad 0 \leq x \leq 1, 0 \leq y \leq 1, t > 0. \tag{5.43}$$

The geometry is discretised with 120 constant boundary elements and 19 equally spaced internal points as shown in Fig. 5.9. The velocity field is given by $v_x = 1$ and $v_y = 0.5$, respectively. The diffusivity is $D = 1$ and the reaction value is $k = 0$. In this case study,

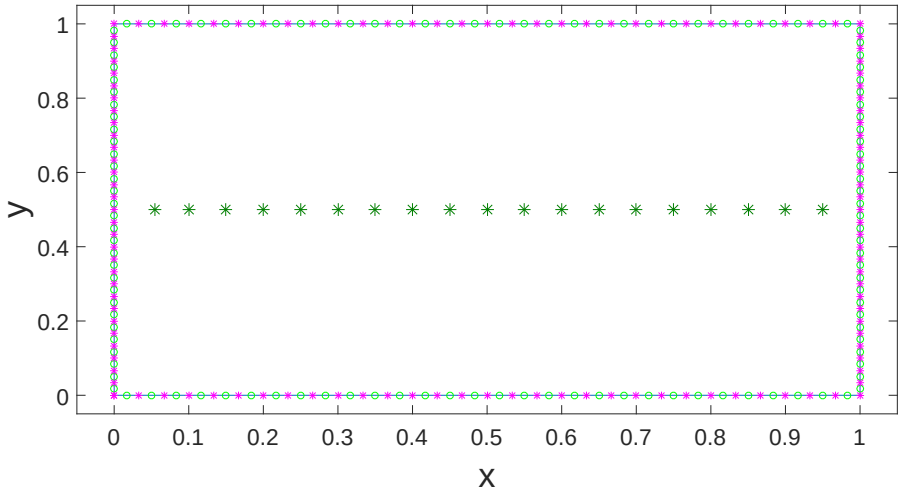

Figure 5.9: Schematic diagram of the problem representation the geometry, discretisation and the internal points.

large time increments (e.g. $\Delta t = 0.5, 2.0$) were utilised. The problem is modelled with the non-zero initial condition:

$$\phi(x,y,0) = \exp\left[\left(-(x+1/4)^2 + y^2\right)/4\right] \tag{5.44}$$

and the time-dependent Dirichlet-type boundary conditions are chosen as:

$$\begin{cases} \phi(0,y,t) = \exp\left[\left(-(1/4-t)^2+(y-t/2)^2\right)/(4(1+t))\right], \quad 0<y<1, \\ \phi(1,y,t) = \exp\left[\left(-(5/4-t)^2+(y-t/2)^2\right)/(4(1+t))\right], \quad 0<y<1, \\ \phi(x,0,t) = \exp\left[\left(-((x-t+1)/4)^2+(t/2)^2\right)/(4(1+t))\right], \quad 0<x<1, \\ \phi(x,1,t) = \exp\left[\left(-((x-t+1)/4)^2+(1-t/2)^2\right)/(4(1+t))\right], \quad 0<x<1. \end{cases}$$

The analytical solution is represented by

$$\phi(x,y,t) = \frac{1}{1+t}\exp\left[\frac{-(x-t+1/4)^2+(y-t/2)^2}{4(1+t)}\right]. \tag{5.45}$$

Figure 5.10 shows the numerical and analytical solutions for internal points distributed at the central line of the computational domain for several time-levels using TPS-RBF. After 54 time steps with $\Delta t = 0.5\,s$, the present solution reaches the steady-state case, in very good agreement with the analytical solution. Next, Fig. 5.11 shows the numerical and analytical

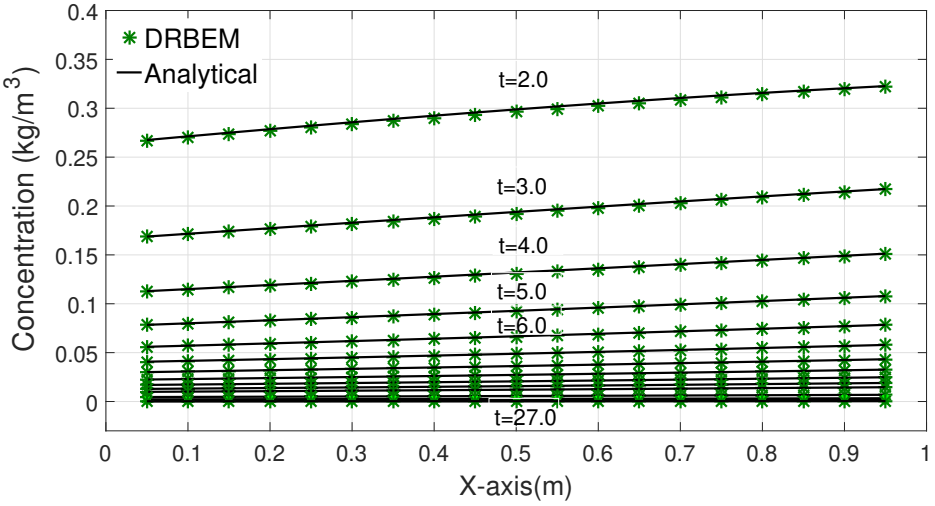

Figure 5.10: Concentration profiles at $y = 0.5$ with $\Delta t = 0.5$ using TPS-RBF: comparison of analytical (solid line) and numerical solutions (star points).

solutions at the middle of the channel at several time-levels using TPS-RBF, with $\Delta t = 2.0$. When time is continued up to 27 time steps, the numerical solution reaches the steady-state

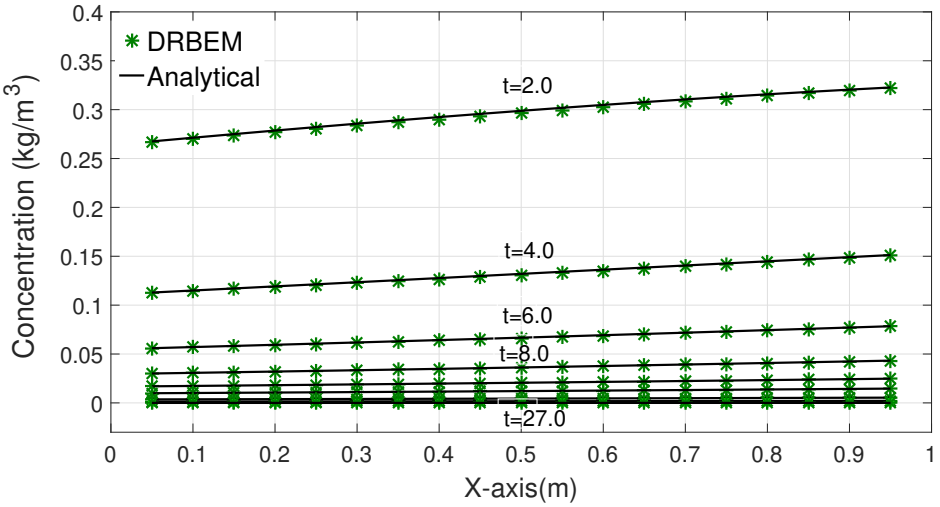

Figure 5.11: Concentration profiles at $y = 0.5$ with $\Delta t = 2.0$ using TPS-RBF: comparison of analytical (solid line) and numerical solutions (star points).

solution. In addition, other RBFs still remain in reasonably good agreement with the exact solution. The solutions are obtained up to steady state, which is reached when the absolute difference between the solutions of two consecutive time levels is less than 10^{-5}.

As seen in Table 5.5, all the RBFs produce results with good agreement with the analytical solution, although the TPS results are slightly more accurate at this time. In Table 5.6, the accuracy of the results is of the order 10^{-4} for all the RBFs.

Table 5.7 gives the RMS error norm for different values of Péclet number and various spatial

Table 5.5: Results for convection-diffusion-reaction at $t = 2.5$ for $\Delta t = 0.5$

x	Cubic	MQ	TPS	Analytical
0.1	0.2161	0.2100	0.2130	0.2138
0.25	0.2283	0.2157	0.2219	0.2235
0.50	0.2458	0.2283	0.2369	0.2390
0.75	0.2568	0.2408	0.2487	0.2505
0.95	0.2653	0.2610	0.2632	0.2636

Table 5.6: DRBEM results of ϕ for convection-diffusion-reaction at $t = 27$ for $\Delta t = 0.5$

x	Cubic	MQ	TPS	Analytical
0.1	2.845×10^{-4}	2.845×10^{-4}	2.839×10^{-4}	2.845×10^{-4}
0.25	3.055×10^{-4}	3.055×10^{-4}	3.042×10^{-4}	3.055×10^{-4}
0.50	3.437×10^{-4}	3.437×10^{-4}	3.417×10^{-4}	3.437×10^{-4}
0.75	3.862×10^{-4}	3.862×10^{-4}	3.845×10^{-4}	3.862×10^{-4}
0.95	4.237×10^{-4}	4.237×10^{-4}	4.231×10^{-4}	4.237×10^{-4}

Table 5.7: RMS norm of DRBEM for convection-diffusion-reaction problem with different spatial meshes

RMS error norm of ϕ, $f = r^2 \log(r)$, Problem 3				
Mesh size	Pé $= 1$	Pé $= 10$	Pé $= 50$	Pé $= 100$
20	5.186×10^{-4}	1.540×10^{-2}	4.940×10^{-2}	5.420×10^{-2}
40	1.877×10^{-4}	1.250×10^{-2}	4.020×10^{-2}	4.400×10^{-2}
80	1.447×10^{-4}	9.600×10^{-3}	3.100×10^{-2}	3.400×10^{-2}
120	1.216×10^{-4}	8.100×10^{-3}	2.630×10^{-2}	2.870×10^{-2}
200	9.633×10^{-5}	6.500×10^{-3}	2.080×10^{-2}	2.290×10^{-2}
400	6.892×10^{-5}	4.700×10^{-3}	1.510×10^{-2}	1.650×10^{-2}

mesh sizes at time $t = 13.5$ with time-step value $\Delta t = 0.5$. It can be noticed that the errors decrease with mesh refinement. The relative error in the RMS norm is of order 10^{-5} for small values of the Péclet number and 10^{-2} for higher values of Pé.

The time evolution of the concentration ϕ up to $t = 27$ and with $v_x = 1$ and $v_y = 0.5$ is shown in Fig. 5.12. It can be seen that the proposed DRBEM achieves an excellent agreement between the present results and the corresponding analytical solutions, in which the maximum relative error is 10^{-5}.

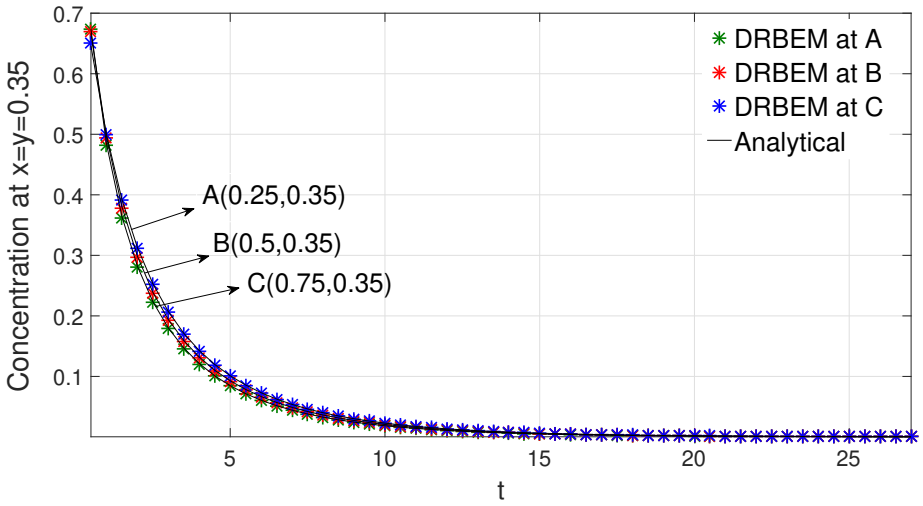

Figure 5.12: Concentration profiles distribution at selected internal nodes using TPS-RBF: comparison of analytical (solid line) and numerical solutions (star points).

5.6.4 Transient Convection-Diffusion-Reaction with Irregular Domain and Time-Dependent Boundary Conditions

In this case, the method is extended to a 2D convection-diffusion-reaction problem in an amoeba-like irregular shape domain Ω. Fig. 5.13 shows the geometrical discretisation of the problem, which is defined parametrically as

$$\Gamma = \left\{ (\rho \cos\theta, \rho(\theta) \sin\theta) : \rho = e^{sin\,\theta} \sin^2(2\theta) + e^{cos\,\theta} \cos^2(2\theta), 0 \leq \theta \leq 2\pi \right\}. \quad (5.46)$$

The initial and boundary conditions are given as follows:

$$\phi(x,y,0) = \pi\left(e^{-x} + e^{-y}\right), \quad (x,y) \in \Omega,$$

$$\phi(\rho,\theta,t) = \pi\left(e^{-\rho\,cos(\theta)} + e^{-\rho\,sin(\theta)}\right) e^{-t}. \quad (5.47)$$

where

$$\rho = e^{sin\,\theta} sin^2(2\theta) + e^{cos\,\theta} cos^2(2\theta), \quad 0 \le \theta \le 2\pi. \tag{5.48}$$

The analytical solution of the problem is given by

$$\phi(x,y,t) = \pi\left(e^{-x} + e^{-y}\right) e^{-t}, \quad (x,y,t) \in \Gamma, \quad x\,(0,\infty). \tag{5.49}$$

where $D = 1$ and $(v_x, v_y) = (-2, 0)$. To solve this problem numerically, the time increment

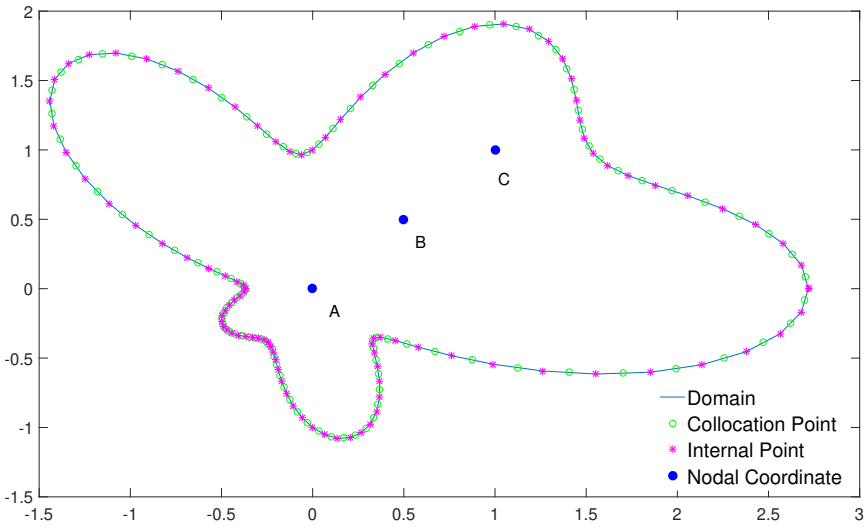

Figure 5.13: Discretisation of amoeba-like irregular domain with distribution of boundary nodes and internal nodes for convection-diffusion-reaction model

is initially taken as $\Delta t = 0.05$ with 3 internal points uniformly distributed inside the computational domain and 50 constant elements distributed on the boundary. The time evolution of the concentration profile ϕ at points $A\,(0,0)$, $B\,(0.5,0.5)$ and $C\,(1,1)$ is displayed in Fig. 5.14. It can be seen that the proposed DRBEM achieves an excellent agreement between the present results and the corresponding analytical solutions.

Next, Fig. 5.15 displays the results for the same three internal nodes and negative velocity values $v_x = -1$ and $v_y = -1$ using TPS-RBF with $\Delta t = 0.05$. Figure 5.16 shows the results for the three internal nodes and negative velocity values $v_x = -1$ and $v_y = -1$ using TPS-RBF

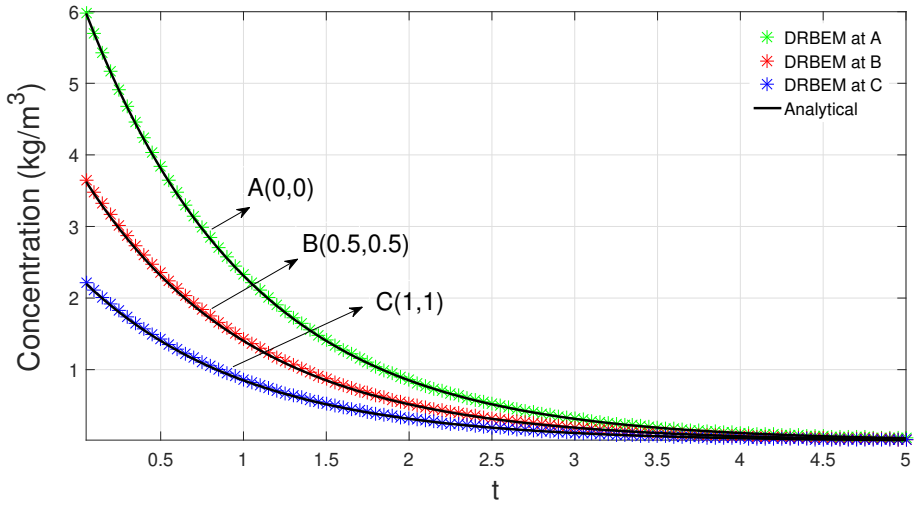

Figure 5.14: Concentration profiles at internal nodes using TPS-RBF: comparison of analytical (solid line) and numerical solutions (star points).

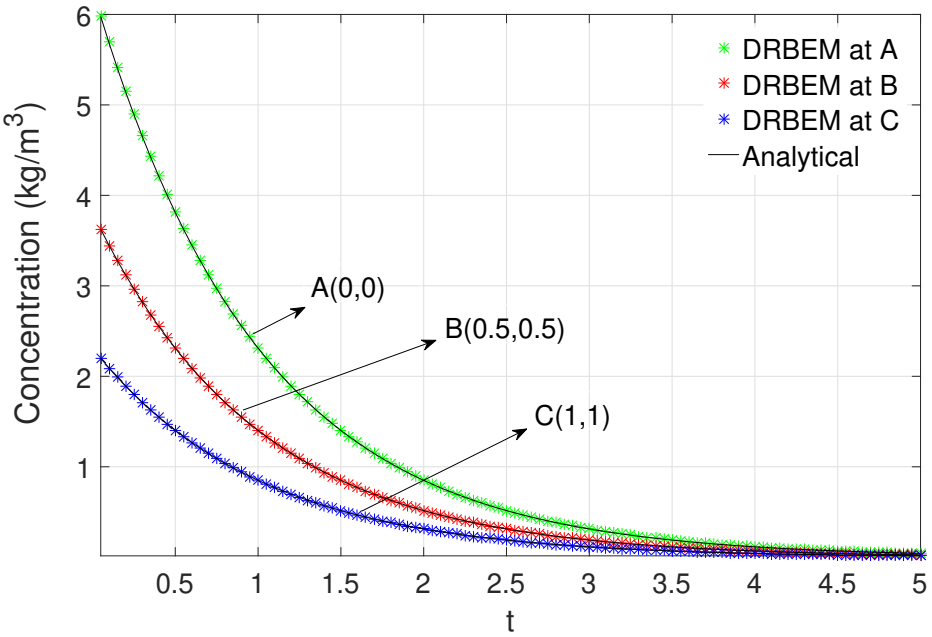

Figure 5.15: Concentration profiles at internal nodes using TPS-RBF: comparison of analytical (solid line) and numerical solutions (star points).

with a smaller time-step $\Delta t = 0.005$. It can be observed that the predicted concentration profiles agree very well with the corresponding analytical solutions at different times and internal points.

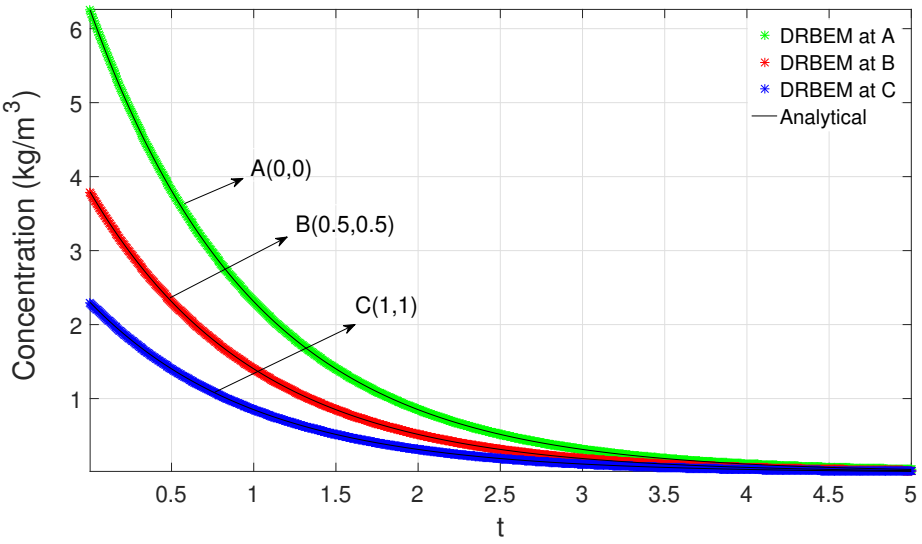

Figure 5.16: Concentration profiles at internal nodes using TPS-RBF: comparison of analytical (solid line) and numerical solutions (star points).

5.6.5 Transient Convection-Diffusion-Reaction Problem over a Semi-Infinite Rectangular Channel with Mixed Boundary Conditions

Let us now consider the test problem of convection-diffusion-reaction for a long bar of length L moving with constant velocity v_x along the x-axis, with specified concentration at its left edge, i.e. boundary conditions are chosen as:

$$\frac{\partial \phi}{\partial n}(x, y = 0, t) = 0;\ 0 \leq x \leq 20$$

$$\frac{\partial \phi}{\partial n}(x = 20, y, t) = 0;\ 0 \leq y \leq 1$$

$$\frac{\partial \phi}{\partial n}(x, y = 1, t) = 0;\ 0 \leq x \leq 20$$

$$\phi(x = 0, y, t) = \phi_0 = 300\ \left(kg/m^3\right);\ 0 \leq y \leq 1, \quad t > 0.$$

The initial conditions are chosen as the analytical value of Eq.(5.50) at $t = 0$:

$$\phi(x, y, t = 0) = \phi_i = 0$$

The analytical solution [145] of this transport problem over a semi-infinite rectangular channel is:

$$\phi(x,y,t) = \phi_i + (\phi_0 - \phi_i) A(x,t), \tag{5.50}$$

where

$$A(x,t) = \frac{1}{2}\text{erfc}\left[\frac{(x - v_x t)}{2(Dt)^{1/2}}\right] + \frac{1}{2}\exp\left(\frac{v_x x}{D}\right)\text{erfc}\left[\frac{(x + v_x t)}{2(Dt)^{1/2}}\right], \tag{5.51}$$

and erfc is the complementary error function. The geometry as a rectangular channel with dimension $[20m \times 1m]$ was discretised as represented in Fig. 5.17. We only show solutions

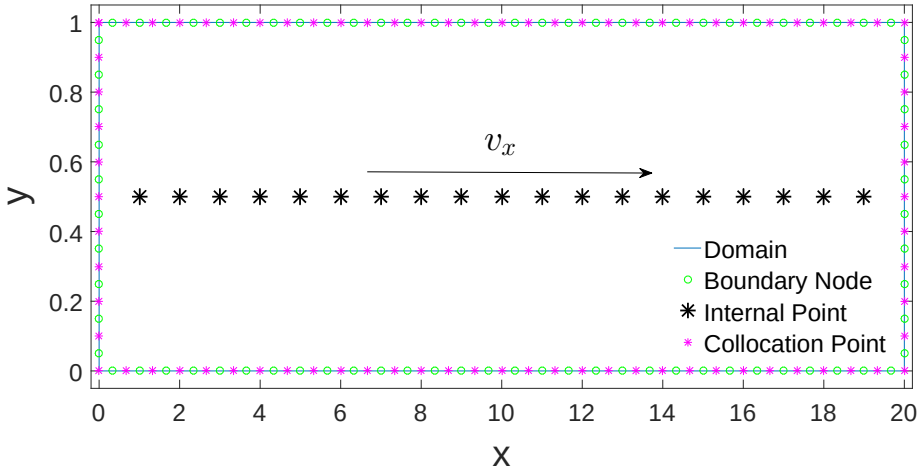

Figure 5.17: Schematic diagram of the problem representation of the geometry, discretisation and internal points.

with the cubic RBF in this section, as it produced the most accurate results for the problem under consideration.

This problem is divided into two cases:

First case study : rectangular channel in x and y-directions without rotating the problem domain. This case is examined with two types of boundary conditions as follows:

Case(**i**): Neumann boundary conditions at the right wall.

As a first case, the above problem will be considered a bounded one consisting of 19 equally spaced interior points and 80 constant elements distributed as 10 elements on each vertical faces and 30 for the horizontal face. The boundary conditions are mixed (Dirichlet-Neumann). We solved this problem by imposing a zero flux at $x = 20$ instead of the condition

$\frac{\partial \phi(\infty,y,t)}{\partial x} = 0.$

In this way, we are able to analyse the process until the concentration front starts to reach the end cross-section at $x = 20$. In the numerical simulation with a fully implicit scheme, a diffusion coefficient $D = 1\ \left(m^2/s\right)$, a velocity field $v_x = 0.6\ (m/s)$, reaction coefficient $k = 0$, and a time step $\Delta t = 0.025s$ were used. Comparison between the analytical solution and our numerical results for Pé=12 is given in Fig. 5.18, showing excellent agreement. Comparison between the analytical and simulation results at Pé=100 is given in Fig. 5.19, also showing an excellent agreement.

Next, the time step value is decreased to $\Delta t = 0.005s$ to present the solution convergence for a smaller time-step value. The obtained results of the time evolution of the concentration profile ϕ along the bottom side of the computational domain, i.e. $y = 0$ are displayed in Figs. 5.20 and 5.21, from which we observe an excellent agreement with the analytical solution.

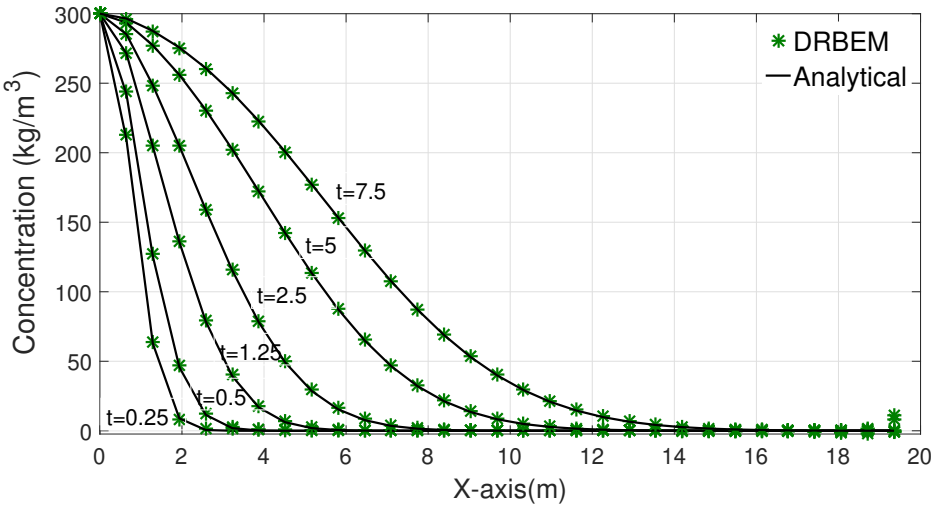

Figure 5.18: Concentration profiles at Pé=12 using Cubic-RBF: comparison of analytical (solid line) and numerical solutions (star points) at the bottom side.

Case(**ii**): Dirichlet boundary conditions at the right wall.

As a second case, instead of defining zero flux at the end of the cross-section, we impose zero concentration, i.e. $\phi\,(20,y,t) = 0$. In this case, we use the same diffusion coefficient as well as the same mesh, and consider the Péclet number Pé=400. Again, a fully implicit scheme has been implemented, however, the time step value is $\Delta t = 0.00125$. Comparison

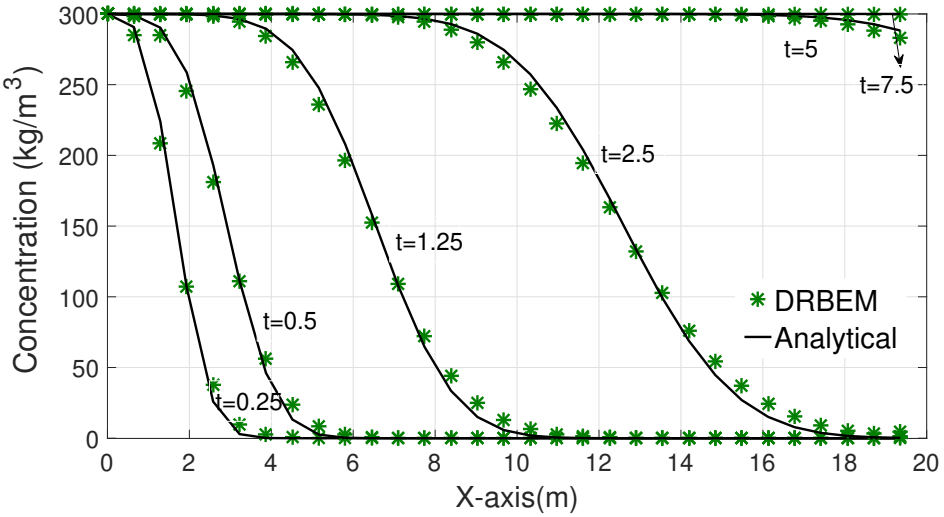

Figure 5.19: Concentration profiles at Pé=100 using Cubic-RBF: comparison of analytical (solid line) and numerical solutions (star points) at the bottom side.

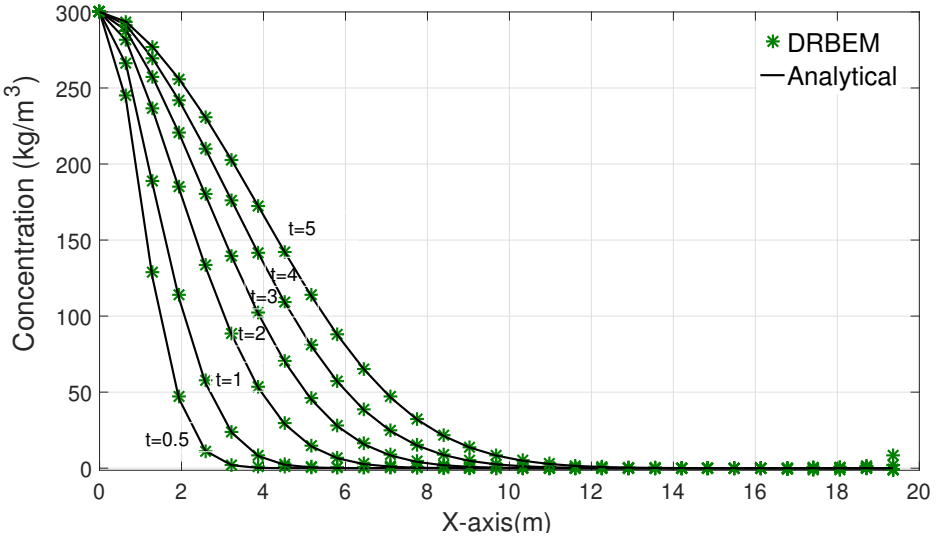

Figure 5.20: Concentration profiles at Pé=20 using Cubic-RBF: comparison of analytical (solid line) and numerical solutions (star points) at the bottom side.

between numerical and analytical solutions for this case is shown in Fig. 5.22. As can be observed, excellent results were obtained. As before, in this case the solution was stopped before the concentration front reaches the auxiliary contour.

Figure 5.23 shows the solutions for Pé=600 with the same time-step value $\Delta t = 0.00125$. The comparison of the analytical and numerical results indicates that the proposed method

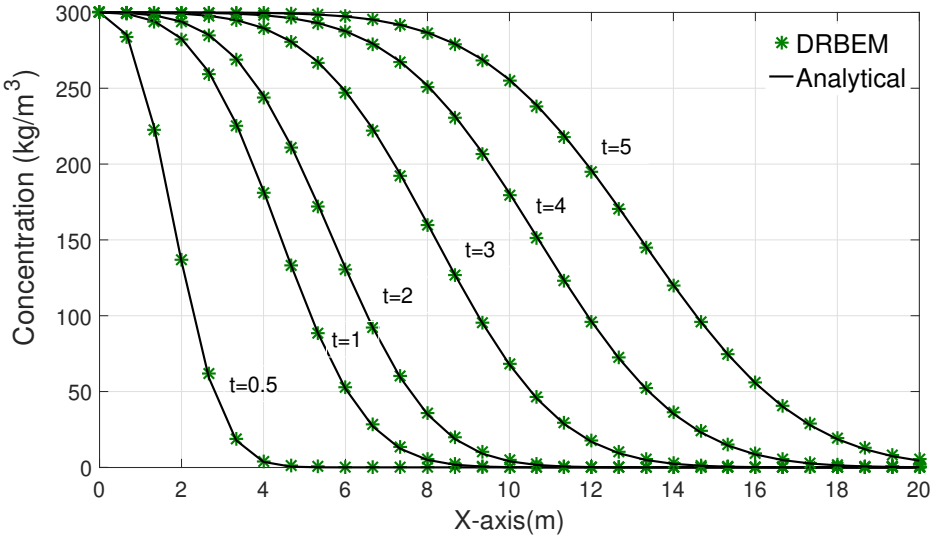

Figure 5.21: Concentration profiles at Pé=50 using Cubic-RBF: comparison of analytical (solid line) and numerical solutions (star points) at the bottom side.

can accurately predict the time evolution characteristics of convection-diffusion-reaction problems.

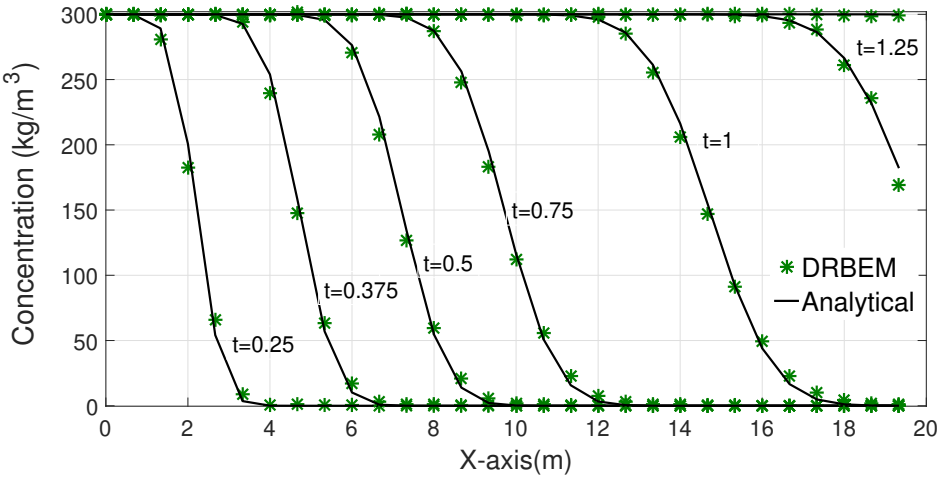

Figure 5.22: Concentration profiles at Pé=400 using Cubic-RBF: comparison of analytical (solid line) and numerical solutions (star points) at the bottom face.

Second case study : the same rectangular channel is considered but now rotated by the inclination angle $\theta = \pi/8$, as shown in Fig. 5.24. The problem is solved in the original (x,y) coordinate system using the same initial and boundary conditions but now defined in

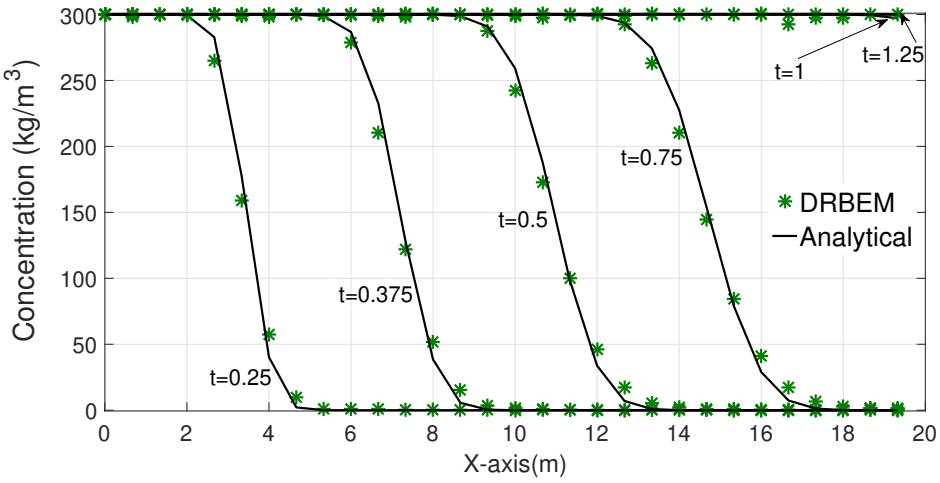

Figure 5.23: Concentration profiles at Pé=600 using Cubic-RBF: comparison of analytical (solid line) and numerical solutions (star points) at the bottom face.

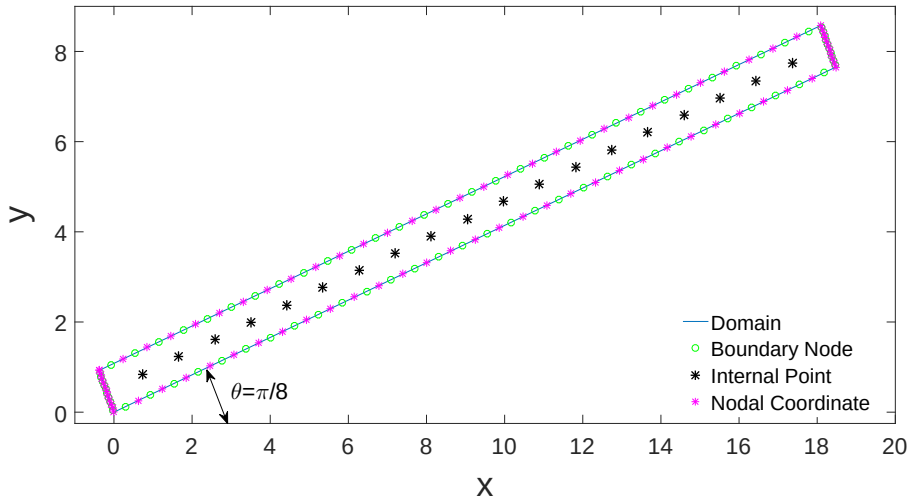

Figure 5.24: Schematic representation of the rotated rectangle domain, discretisation and the internal points.

the inclined geometry. In this way, the new velocity field is constituted by the components $\acute{v}_x = v_x.\cos\theta$ and $\acute{v}_y = v_y.\sin\theta$. The diffusivity coefficient value is $D = 1$ and the reaction coefficient $k = 0$.

Case(**i**): Neumann boundary conditions at the right wall.

Figure 5.25 displays the numerical and the analytical solutions with time-step $\Delta t = 0.00125s$. In this particular case the velocity field along the x-axis is considered to be $\acute{v}_x = 5.5432$ and

$\acute{v}_y = 2.29610$. The Péclet number is Pé=120 in this test case. Figure 5.26 presents the results

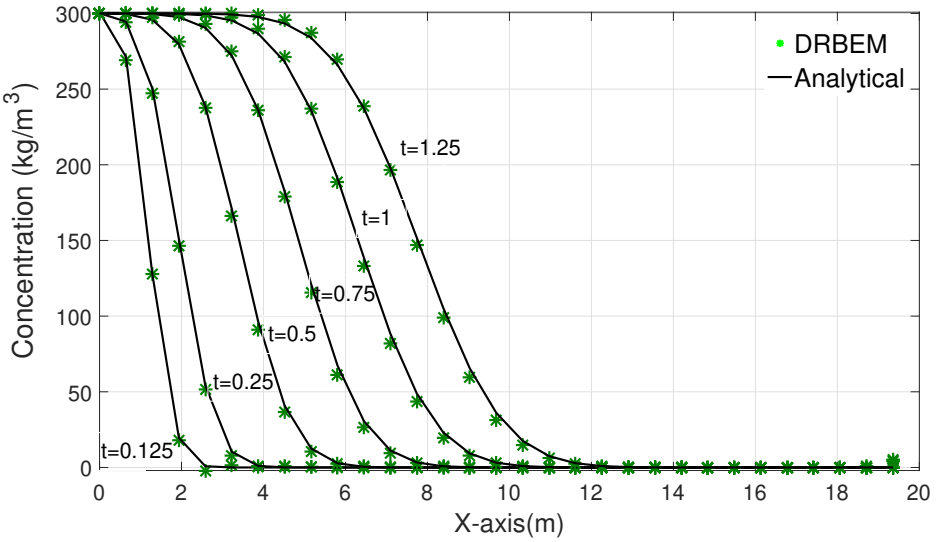

Figure 5.25: Concentration profiles at Pé=120 using Cubic-RBF: comparison of analytical (solid line) and numerical solution s(star points) at the bottom face.

along the centre line of the channel $y = 0.5$, i.e. along an inclined line at an angle $\theta = \pi/8$. The velocity field along the x-axis is considered to be $\acute{v}_x = 9.2388$ and $\acute{v}_y = 3.8268$.

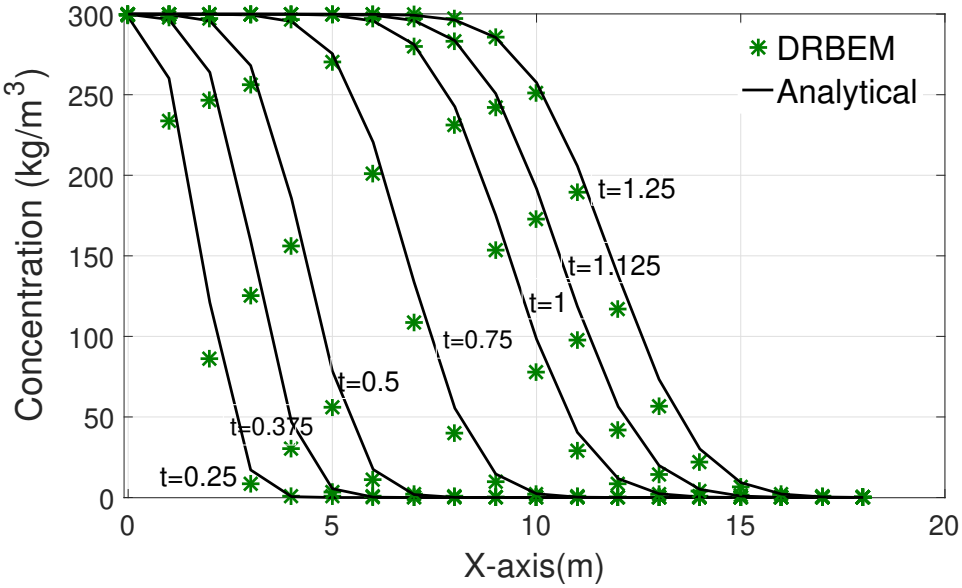

Figure 5.26: Concentration profiles at the central line with Pé=200 using Cubic-RBF: comparison of analytical (solid line) and numerical solutions (star points).

Case(**ii**): Dirichlet boundary conditions at the right wall.

Figure 5.27 displays the numerical and the analytical solutions with time-step $\Delta t = 0.00125s$ and Pé=400. The velocity field along the x-axis is considered to be $\acute{v}_x = 18.4776$ and $\acute{v}_y = 7.6536$.

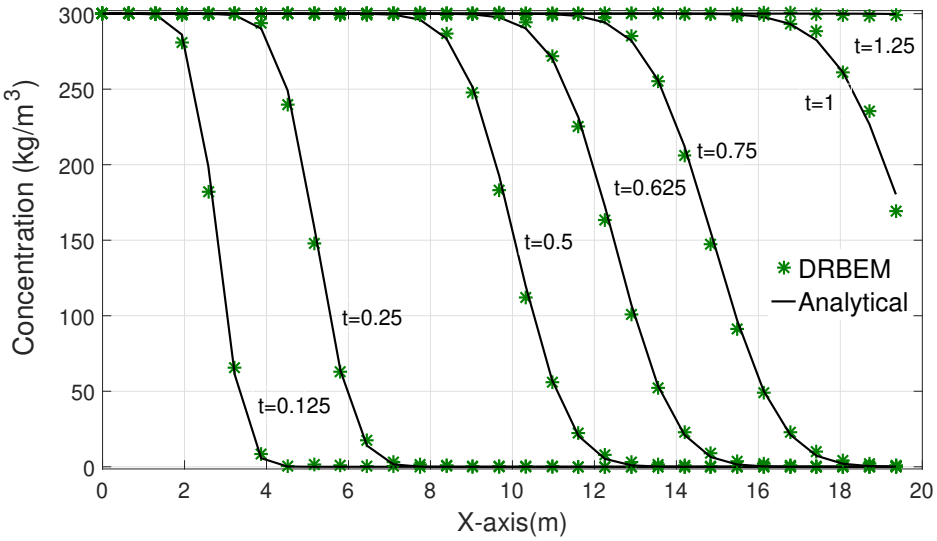

Figure 5.27: Concentration profiles at the central line with Pé=400 using Cubic-RBF: comparison of analytical (solid line) and numerical solutions (star points).

5.6.6 Transient Convection-Diffusion-Reaction with Square Channel and Constant Boundary Conditions

This test example is a transport problem with constant diffusion coefficient $D = 1\ \left(m^2/s\right)$, reaction coefficient $k = 0$ and convection velocity components $v_x = 5$ and $v_y = 0\ (m/s)$. The computational area is considered to be a square discretised into 120 constant boundary elements, with 30 elements along each side and using 19 internal nodes distributed at the centre line of the channel. Only a longitudinal convective term is considered, i.e.

$$\frac{\partial \phi}{\partial t} = D\nabla^2\phi - v_x \frac{\partial \phi}{\partial x}, \quad 0 \leq x \leq 1, 0 \leq y \leq 1, t > 0. \tag{5.52}$$

The analytical solution for this test case is expressed in the following form:

$$\phi(x,y,t) = 2\sum_{n=1}^{\infty} \frac{n\pi}{\lambda_n} \left[1 - \exp(-\lambda_n t)\right] \exp\left(\frac{\text{Pé}\, x}{2}\right) \sin(n\pi x) \tag{5.53}$$

where

$$\lambda_n = \left(\frac{\text{Pé}}{2}\right)^2 + n^2\pi^2. \tag{5.54}$$

The above series expansion works for low Pé number cases. The problem is subject to the mixed boundary conditions:

$$\begin{cases} \phi(0,y,t) = 1, \quad 0 \le y \le 1, \quad t > 0, \\ \phi(1,y,t) = 0, \quad 0 \le y \le 1, \quad t > 0, \\ \frac{\partial \phi}{\partial n}(x,0,t) = 0, \quad 0 \le x \le 1, \quad t > 0, \\ \frac{\partial \phi}{\partial n}(x,1,t) = 0, \quad 0 \le x \le 1, \quad t > 0. \end{cases}$$

and the initial condition

$$\phi(x,y,0) = 0, \quad (x,y) \in [0,1] \times [0,1]. \tag{5.55}$$

The problem is schematically described in Fig. 5.28 below. Figure 5.29 presents the simulated results for the internal points along the central line of the domain with Pé $= 5$ using cubic-RBF. Figure 5.30 shows time evolution the results for three internal nodes using cubic-RBF. From this figure, it can be observed that the predicted concentration profiles agree very well with the corresponding analytical solutions at different times and internal points. This indicates that the proposed method can accurately predict the time evolution characteristics of transient convection-diffusion-reaction problems.

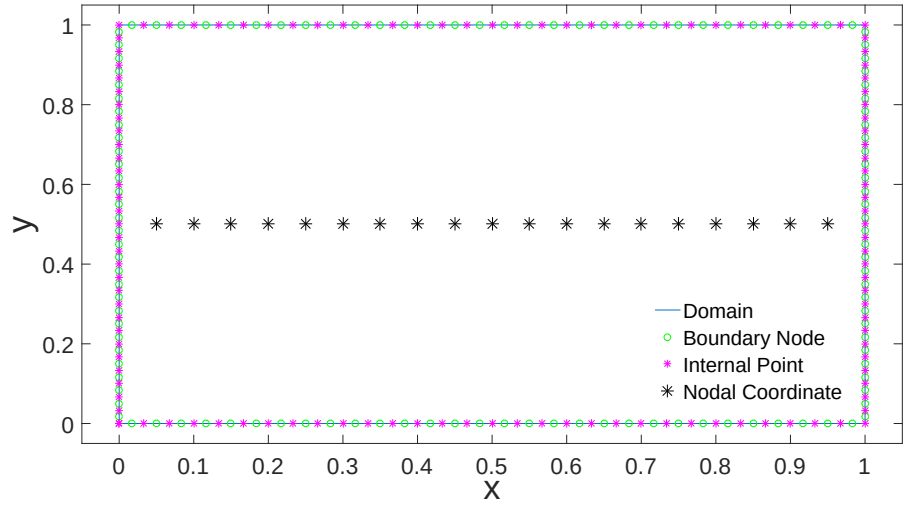

Figure 5.28: Discretisation for 2D transient convection-diffusion-reaction model with internal points.

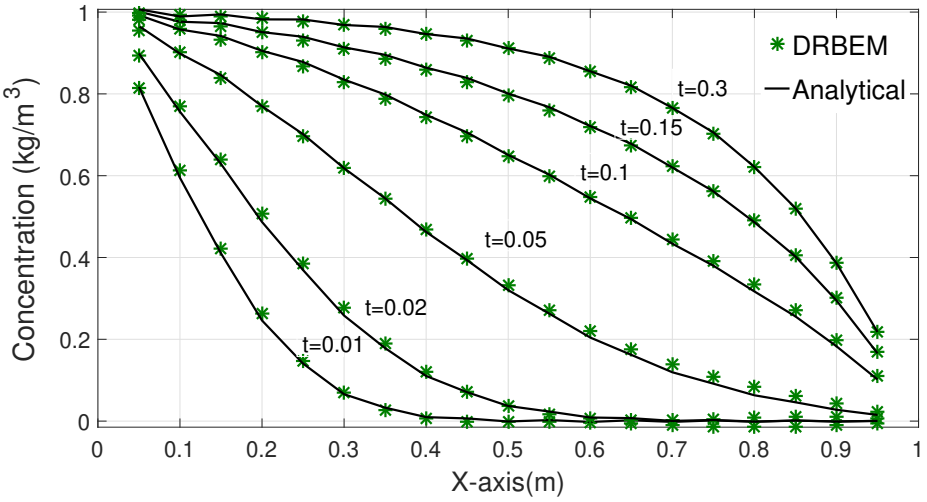

Figure 5.29: Concentration profiles at $y = 0.5$ with $\Delta t = 0.001$ using Cubic-RBF: comparison of analytical (solid line) and numerical solutions (star points)

5.7 Summary and Discussions

In this chapter, two-dimensional transient convection-diffusion-reaction problems with constant velocity were investigated and validated using the DRBEM scheme. The backward FDM formulation is used for modelling the time-derivative part showing very good behaviour in all cases with good convergence for the proposed scheme. The results of several analyses

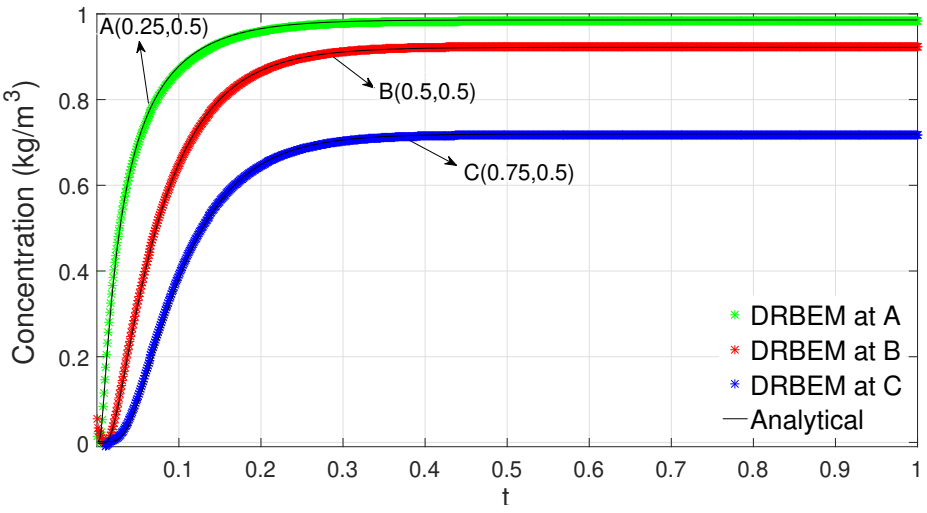

Figure 5.30: Concentration profiles distribution at selected internal points with Pé $= 5$ using Cubic-RBF: comparison of analytical (solid line) and numerical solution (star points).

using constant boundary elements showed good agreement with the corresponding analytical solutions, with no oscillations or smoothing of sharp fronts for the range of Péclet number studied.

It is obvious that, as the velocity increases, the concentration profile becomes more difficult to reproduce with numerical models. However, all BEM solutions are still in good agreement for high Péclet number. We have made a comprehensive investigation of different test cases by considering many different domains and boundary condition types. We have implemented three RBFs and tested them with different types of problems. To ascertain the robustness and effectiveness of the proposed method, the figures demonstrated convergent behaviour for the simulated results in all cases studied and various Péclet numbers with very small order of the relative error in the RMS norm.

Chapter 6

DRBEM Modelling for Transient Convection-Diffusion-Reaction Problems with Variable Velocity Fields

6.1 Introduction

The solution of convection-diffusion-reaction problems is a difficult task for all numerical methods because of the nature of the governing equation, which includes first-order and second-order partial derivatives in space [8, 155, 9, 1, 10]. The convection-diffusion equation is the basis of many physical and chemical phenomena, and its use has also spread in economics, financial forecasting and other fields [165].

It should be stressed that this chapter will describe a new formulation of the DRBEM for 2D transient convection-diffusion-reaction problems with variable velocity. The formulation decomposes the velocity field into an average and a perturbation part, with the latter being treated using a dual reciprocity approximation to convert the domain integrals arising in the boundary element formulation into equivalent boundary integrals. The integral representation formula for the convection-diffusion-reaction problem with variable velocity is obtained from the Green's second identity, using the fundamental solution of the corresponding steady-state equation with constant coefficients. A FDM is used to simulate the time evolution procedure

for solving the resulting system of equations. Numerical applications are included for three different benchmark examples for which analytical solutions are available, to establish the validity of the proposed approach and to demonstrate its efficiency. Finally, results obtained show that the DRBEM results are in excellent agreement with the analytical solutions and do not present oscillations or damping of the wave front, as it appears in other numerical techniques.

A brief outline of the rest of this chapter is as follows. Section 6.2 reviews the mathematical representation of the transient convection-diffusion-reaction problem with variable velocity. Section 6.3 derives the boundary element formulation of the governing equation using the steady-state fundamental solution of the corresponding equation. In sections 6.4 and 6.5, the DRBEM formulation and its discretisation are developed for the 2D transient convection-diffusion-reaction problem. A two-level time marching procedure for the proposed model is implemented in section 6.6. Section 6.7 gives the description of the coordinate functions and the choice of the three radial basis functions. Section 6.8 compares and investigates the solution profiles for the present numerical experiments with the analytical solution of the tested cases. Computational aspects are included to demonstrate the performance of the approach in section 6.9. Finally, some conclusions and remarks are provided in the last section.

6.2 Transient Convection-Diffusion-Reaction Equation

The 2D transient convection-diffusion-reaction problem over a domain Ω in $\mathbb{R}^2$ bounded by a boundary Γ, for isotropic materials, is governed by the following PDE:

$$D\nabla^2\phi\,(x,y,t) - v_x\,(x,y)\,\frac{\partial\phi\,(x,y,t)}{\partial x} - v_y\,(x,y)\,\frac{\partial\phi\,(x,y,t)}{\partial y} - k\,\phi\,(x,y,t) = \frac{\partial\phi\,(x,y,t)}{\partial t},$$

$$(x,y) \in \Omega \quad t > 0. \tag{6.1}$$

In Eq.(6.1), ϕ represents the concentration of a substance, treated as a function of space and time. The velocity components v_x and v_y along the x and y directions and assumed to vary

in space. Besides, D is the diffusivity coefficient and k represents the first-order reaction constant or adsorption coefficient. The boundary conditions are given by Eqs.(4.2) and (4.3). The initial condition over the domain Ω is

$$\phi\left(x,y,t=0\right)=\phi_0\left(x,y\right),\ \left(x,y\right)\in\Omega \tag{6.2}$$

6.3 Boundary Element Formulation of Transient Convection-Diffusion-Reaction Problems Using Steady-State Fundamental Solution

For the sake of obtaining an integral equation equivalent to the above PDE Eq.(6.1), a fundamental solution is necessary. However, fundamental solutions are only available for the case of constant velocity fields. At this stage, the variable velocity components $v_x=v_x(x,y)$ and $v_y=v_y(x,y)$ are decomposed into average (constant) terms $\bar{v}_x$ and $\bar{v}_y$, and perturbations $P_x=P_x\left(x,y\right)$ and $P_y=P_y\left(x,y\right)$, such that

$$v_x\left(x,y\right)=\bar{v}_x+P_x\left(x,y\right),\ v_y\left(x,y\right)=\bar{v}_y+P_y\left(x,y\right). \tag{6.3}$$

Now, we can re-write Eq.(6.1) to take the form

$$D\nabla^2\phi-\bar{v}_x\left(x,y\right)\frac{\partial\phi}{\partial x}-\bar{v}_y\left(x,y\right)\frac{\partial\phi}{\partial y}-k\,\phi=\frac{\partial\phi}{\partial t}+P_x\frac{\partial\phi}{\partial x}+P_y\frac{\partial\phi}{\partial y}. \tag{6.4}$$

Next, one can transform the differential equation (6.4) into an equivalent integral equation as follows [110]

$$\begin{aligned}&\phi\left(\xi\right)-D\int_{\Gamma}\phi^*\frac{\partial\phi}{\partial n}\,d\Gamma+D\int_{\Gamma}\phi\,\frac{\partial\phi^*}{\partial n}\,d\Gamma+\int_{\Gamma}\phi\,\phi^*\,\bar{v}_n\,d\Gamma\\&=-\int_{\Omega}\left[\frac{\partial\phi}{\partial t}+\left(P_x\frac{\partial\phi}{\partial x}+P_y\frac{\partial\phi}{\partial y}\right)\right]\phi^*\,d\Omega,\quad\xi\in\Omega.\end{aligned} \tag{6.5}$$

In the above equation, ϕ^* is the fundamental solution of the steady-state convection-diffusion-reaction equation with constant coefficients. A similar expression can be obtained, by implementing Green's second identity and a limit analysis, for source points ξ on the boundary Γ, in the form

$$C(\xi)\,\phi(\xi) - D\int_{\Gamma}\phi^*\frac{\partial\phi}{\partial n}\,d\Gamma + D\int_{\Gamma}\phi\,\frac{\partial\phi^*}{\partial n}\,d\Gamma + \int_{\Gamma}\phi\,\phi^*\,\bar{v}_n\,d\Gamma$$

$$= -\int_{\Omega}\frac{\partial\phi}{\partial t}\,\phi^*\,d\Omega - \int_{\Omega}\left(P_x\frac{\partial\phi}{\partial x} + P_y\frac{\partial\phi}{\partial y}\right)\phi^*\,d\Omega, \quad \xi\in\Gamma. \tag{6.6}$$

6.4 DRBEM Formulation for Transient Convection-Diffusion-Reaction Problems

In this section, we will discuss the transformation of the domain integral in Eqs.(6.5) and (6.6), and the DRBEM will be implemented twice to approximate the two domain integrals appearing in this formulation, first the domain integral of the time derivative, and second the domain integral related to the velocity perturbation parts. Now, we start by expanding the time-derivative $\frac{\partial\phi}{\partial t}$ in the form

$$\frac{\partial\phi(x,y,t)}{\partial t} = \sum_{i=1}^{n} f_i(x,y)\,\alpha_{1,i}(t). \tag{6.7}$$

The above series involves a set of known coordinate functions f_i and a set of unknown time-dependent coefficients $\alpha_{1,i}$. With this approximation, the first domain integral in Eq.(6.6) becomes

$$\int_{\Omega}\frac{\partial\phi}{\partial t}\phi^*\,d\Omega = \sum_{i=1}^{n}\alpha_{1,i}\int_{\Omega} f_i\phi^*\,d\Omega. \tag{6.8}$$

The next step is to consider that, for each function f_i, there exists a related function ψ_i which is a particular solution of the equation:

$$D\nabla^2\psi - v_x\frac{\partial\psi}{\partial y} - v_y\frac{\partial\psi}{\partial x} - k\psi = f. \tag{6.9}$$

Now, the domain integral (6.8) can be recast in the form:

$$\int_\Omega \frac{\partial\phi}{\partial t}\,\phi^* d\Omega = \sum_{k=1}^{M}\alpha_{1,k}\int_\Omega\left(D\nabla^2\psi_k - \bar{v}_x\frac{\partial\phi_k}{\partial y} - \bar{v}_y\frac{\partial\phi_k}{\partial x} - k\psi_k\right)\phi^* d\Omega. \tag{6.10}$$

Substituting expression (6.10) into (6.6), and applying integration by parts to the right side of the resulting equation and doing some simplifications, one finally arrives at a boundary integral equation of the form

$$C(\xi)\,\phi(\xi) - D\int_\Gamma \phi^*\frac{\partial\phi}{\partial n}d\Gamma + D\int_\Gamma \phi\frac{\partial\phi^*}{\partial n}d\Gamma + \int_\Gamma \phi\,\phi^*\,\bar{v}_n d\Gamma$$

$$= \sum_{k=1}^{M}\alpha_{1,k}\left[C(\xi)\,\psi_k(\xi) - D\int_\Gamma \phi^*\frac{\partial\psi_k}{\partial n}d\Gamma + D\int_\Gamma\left[\left(\frac{\partial\phi^*}{\partial n} + \frac{\bar{v}_n}{D}\phi^*\right)\psi_k\right]d\Gamma\right]$$

$$-\int_\Omega\left(P_x\frac{\partial\phi_k}{\partial x} + P_y\frac{\partial\phi_k}{\partial y}\right)\phi^* d\Omega, \quad \xi\in\Gamma. \tag{6.11}$$

6.5 Space-Time Discretisation of the 2D Convection-Diffusion-Reaction Model

To discretise the spatial domain, boundary elements were employed. The integrals over the boundary are approximated by a summation of integrals over individual boundary elements.

For the numerical solution of the problem, Eq.(6.11) is discretised in the form

$$C_i\,\phi_i - D\sum_{j=1}^{N}\int_{\Gamma_j}\phi^*\,\frac{\partial\phi}{\partial n}\,d\Gamma + D\sum_{j=1}^{N}\int_{\Gamma_j}\left(\frac{\partial\phi^*}{\partial n}+\frac{\bar{v}_n}{D}\,\phi^*\right)\phi\,d\Gamma =$$

$$= \sum_{k=1}^{M}\alpha_{1,k}\left[C_i\,\psi_{ik}(\xi) - D\sum_{j=1}^{N}\int_{\Gamma_j}\phi^*\frac{\partial\psi_k}{\partial n}\,d\Gamma + D\sum_{j=1}^{N}\int_{\Gamma_j}\left[\left(\frac{\partial\phi^*}{\partial n}+\frac{\bar{v}_n}{D}\,\phi^*\right)\psi_k\,d\Gamma\right]\right]$$

$$-\int_{\Omega}\left(P_x\,\frac{\partial\phi_k}{\partial x} + P_y\,\frac{\partial\phi_k}{\partial y}\right)\phi^*\,d\Omega, \tag{6.12}$$

where the index i means the values at the source point ξ and N elements have been employed. The domain integral on the right-hand-side prevents us from obtaining a boundary-only equation.

Now, in order to obtain a boundary integral which is equivalent to the domain integral in expressions (6.11) and (6.12), a dual reciprocity approximation is implemented [155]. Applying this to the domain integral of Eq.(6.12), the expression will be expanded in the form

$$P_x(x,y)\,\frac{\partial\phi}{\partial x} + P_y(x,y)\,\frac{\partial\phi}{\partial y} = \sum_{k=1}^{N}\alpha_{2,k}(t)\,f_k. \tag{6.13}$$

Expression (6.13) contains two diagonal matrices $P_x = \left(P_x(x_i,y_i)\,\kappa_{i,j}\right)_{i,j=\overline{1,M}}$ and $P_y = \left(P_y(x_i,y_i)\,\kappa_{i,j}\right)_{i,j=\overline{1,M}}$ while $\frac{\partial\phi}{\partial x} = \left(\frac{\partial\phi(x_i,y_i,t)}{\partial x}\right)^T_{i=\overline{1,M}}$ and $\frac{\partial\phi}{\partial y} = \left(\frac{\partial\phi(x_i,y_i,t)}{\partial x}\right)^T_{i=\overline{1,M}}$ are column vectors and $\kappa_{i,j}$ is the Kronecker delta symbol. Integrating Eq.(6.13) we obtain

$$\int_{\Omega}\left(P_x\frac{\partial\phi}{\partial x}+P_y\frac{\partial\phi}{\partial y}\right)\phi^*d\Omega = \sum_{k=1}^{M}\alpha_{2,k}(t)\int_{\Omega}f_k\,\phi^*d\Omega. \tag{6.14}$$

Now, substituting Eq.(6.14) into (6.12), we obtain

$$C_i\,\phi_i - D\sum_{j=1}^{N}\int_{\Gamma_j}\phi^*\,\frac{\partial\phi}{\partial n}\,d\Gamma + D\sum_{j=1}^{N}\int_{\Gamma_j}\left(\frac{\partial\phi^*}{\partial n}+\frac{\bar{v}_n}{D}\,\phi^*\right)\phi\,d\Gamma$$

$$= \sum_{k=1}^{M}\alpha_{1,k}\left[C_i\,\psi_{ik}\,(\xi) - D\sum_{j=1}^{N}\int_{\Gamma_j}\phi^*\frac{\partial\psi_k}{\partial n}\,d\Gamma + D\sum_{j=1}^{N}\int_{\Gamma_j}\left[\left(\frac{\partial\phi^*}{\partial n}+\frac{\bar{v}_n}{D}\,\phi^*\right)\psi_k\,d\Gamma\right]\right]$$

$$-\sum_{j=1}^{M}\alpha_{2,j}\,(t)\int_{\Omega} f_k\,\phi^*\,d\Omega. \tag{6.15}$$

The next step is to consider that, for each function f_k, there exists a related function ψ_k which represents the particular solution as in Eq.(6.9). We get

$$\int_{\Omega}\left(P_x\frac{\partial\phi}{\partial x}+P_y\frac{\partial\phi}{\partial y}\right)\phi^*\,d\Omega = \sum_{k=1}^{M}\alpha_{2,k}\int_{\Omega}\left(D\nabla^2\psi_k-\bar{v}_x\frac{\partial\phi_k}{\partial y}-\bar{v}_y\frac{\partial\phi_k}{\partial x}-k\psi_k\right)\phi^*\,d\Omega. \tag{6.16}$$

Substituting Eq.(6.16) into expression (6.11), and applying integration by parts to the domain integral of the resulting equation, one finally arrives at a boundary integral equation of the form

$$C_i\,\phi_i - D\sum_{j=1}^{N}\int_{\Gamma_j}\phi^*\,\frac{\partial\phi}{\partial n}\,d\Gamma + D\sum_{j=1}^{N}\int_{\Gamma_j}\left(\frac{\partial\phi^*}{\partial n}+\frac{\bar{v}_n}{D}\,\phi^*\right)\phi\,d\Gamma$$

$$= \sum_{k=1}^{M}\alpha_{1,k}\left[C_i\,\psi_{ik}\,(\xi) - D\sum_{j=1}^{N}\int_{\Gamma_j}\phi^*\frac{\partial\psi_k}{\partial n}\,d\Gamma + D\sum_{j=1}^{N}\int_{\Gamma_j}\left[\left(\frac{\partial\phi^*}{\partial n}+\frac{\bar{v}_n}{D}\,\phi^*\right)\psi_k\,d\Gamma\right]\right]$$

$$-\sum_{k=1}^{N}\alpha_{2,k}\left[C_i\psi_{ik} - D\sum_{j=1}^{N}\int_{\Gamma_j}\phi^*\,\frac{\partial\psi_k}{\partial n}\,d\Gamma + \sum_{j=1}^{N}\int_{\Gamma_j}\left(\frac{\partial\phi^*}{\partial n}+\frac{\bar{v}_n}{D}\phi^*\right)\psi_k\,d\Gamma\right]. \tag{6.17}$$

Applying Eq.(6.17) to all boundary nodes using a collocation technique, taking into account the previous functions, results in the following system of algebraic equations:

$$H\phi - Gq = (H\psi - G\eta)\,\alpha_1(t) + (H\psi - G\eta)\,\alpha_2(t). \tag{6.18}$$

In the above system, the same matrices H and G are used on both sides. Matrices ψ and η are also geometry-dependent square matrices (assuming, for simplicity, that the number of terms in Eq.(6.7) is equal to the number of boundary nodes), and ϕ, q, and α are vectors of nodal values. The next step in the formulation is to find an expression for the unknown vectors α. By applying expression (6.7) to all boundary nodes and inverting it and Eq.(6.13), one arrives at:

$$\alpha_1 = F^{-1}\frac{\partial \phi}{\partial t} \tag{6.19}$$

and

$$\alpha_2 = F^{-1}\left(P_x(x,y)\,\frac{\partial \phi}{\partial x} + P_y(x,y)\,\frac{\partial \phi}{\partial y}\right) \tag{6.20}$$

which, substituted into (6.18) results in:

$$H\phi - Gq = (H\psi - G\eta)\,F^{-1}\frac{\partial \phi}{\partial t} + (H\psi - G\eta)\,F^{-1}\left(P_x\frac{\partial \phi}{\partial x} + P_y\frac{\partial \phi}{\partial y}\right) \tag{6.21}$$

Calling:

$$C = (H\psi - G\eta)\,F^{-1} \tag{6.22}$$

gives

$$H\phi - Gq = C\frac{\partial \phi}{\partial t} + C\left(P_x\frac{\partial \phi}{\partial x} + P_y\frac{\partial \phi}{\partial y}\right). \tag{6.23}$$

Next, we shall explain how to deal with the convective terms in Eq.(6.23).

6.6 Handling Convective Terms

In the present section, emphasis will be placed on the treatment of the convective terms. A mechanism must be established to relate the nodal values of ϕ to the nodal values of its derivatives. The approach will be discussed in detail in the next subsection.

6.6.1 The Function-Expansion Approach

This approach will start by expanding the values of ϕ at an internal point by using expression below:

$$\phi = \sum_{k=1}^{M} \Im_k \beta_k \tag{6.24}$$

where β_k are constants. Now, by differentiating it with respect to x and y produces

$$\frac{\partial \phi}{\partial x} = \sum_{k=1}^{M} \frac{\partial \Im_k}{\partial x} \beta_k \quad \text{and} \quad \frac{\partial \phi}{\partial y} = \sum_{k=1}^{M} \frac{\partial \Im_k}{\partial y} \beta_k \tag{6.25}$$

Applying Eq.(6.24) at all M nodes, a set of equations is produced that can be represented in matrix form by

$$\phi = \Im \, \beta \tag{6.26}$$

with corresponding matrix equations for expressions (6.25) given as

$$\frac{\partial \phi}{\partial x} = \frac{\partial \Im}{\partial x} \Im^{-1} \phi \quad \text{and} \quad \frac{\partial \phi}{\partial y} = \frac{\partial \Im}{\partial y} \Im^{-1} \phi \tag{6.27}$$

Therefore, substituting Eq.(6.27) into Eq.(6.23), the new expression will be,

$$(H - P)\, \phi - Gq = C \frac{\partial \phi}{\partial t} \tag{6.28}$$

where

$$P = C \left(P_x \frac{\partial \Im}{\partial x} + P_y \frac{\partial \Im}{\partial y} \right) \Im^{-1} \tag{6.29}$$

The coefficients of the diagonal perturbation matrix P are all geometry-dependent only. The differential algebraic system (6.28) in time has a form similar to the one obtained using the

FEM and hence, can be solved by any standard time integration algorithm by incorporating suitable modifications to account for its *mixed nature*. The system (6.28) can be integrated in time using time marching procedures [9]. It should be stressed that the coefficients of matrices H, G and C all depend on geometry only, thus they can be computed once and stored. In the forthcoming section, we shall explain how to solve this kind of algebraic system.

6.7 Time Marching Schemes for the DRBEM Formulation

This section will show how to handle the linear algebraic system (6.28) adopting time marching schemes [8, 166, 167]. A finite difference approximation for the time derivative term is given by:

$$\frac{\partial \phi}{\partial t} = \frac{\phi^{i+1} - \phi^{i}}{\Delta t}, \tag{6.30}$$

$$\phi(t) = \left(1-\theta_{\phi}\right)\phi^{i} + \theta_{\phi}\phi^{i+1}, \quad q(t) = \left(1-\theta_{q}\right)q^{i} + \theta_{q}q^{i+1}, \tag{6.31}$$

Next, employing a general two-level time integration scheme for solution of Eq.(6.28), the following discrete form is obtained:

$$\left[\frac{1}{\Delta t}C + \theta_{\phi}\{H-P\}\right]\phi^{m+1} - \theta_{q}Gq^{m+1} = \left[\frac{1}{\Delta t}C - \left\{\left(1-\theta_{\phi}\right)(H-P)\right\}\right]\phi^{m} + \left(1-\theta_{q}\right)Gq^{m}, \tag{6.32}$$

where ϕ^{m+1} and q^{m+1} represent the potential and flux at the $(m+1)^{th}$ time step, Δt is the time step, ϕ^{m} and q^{m} are the potential and flux at the m^{th} time step, and θ is a parameter that determines if the method is explicit $\left(\theta_{\phi}, \theta_{q} = 0\right)$ or implicit $\left(\theta_{\phi}, \theta_{q} = 1\right)$. Several tests were done here to choose the best values for θ and we decided to select the backward difference scheme $\theta_{\phi} = 1$ and $\theta_{q} = 1$. In the time marching computation, the unknown quantities ϕ^{m} are updated at each time step by the new values obtained after solving Eq.(6.32). At the first time step, the concentration ϕ and heat flux q at all boundary and internal points are specified with initial values. The computation ends when all time steps are fulfilled [98, 9] or a steady

state is reached. The right side of Eq.(6.32) is known at all times. Upon introducing the boundary conditions at time $(m+1)\Delta t$, the left side of the equation can be rearranged and the resulting system solved by using standard direct procedures such as Gauss elimination, least squares and LU decomposition method. More details of the element properties, interpolation functions, time integration and equation system formulation used in this paper are described in Brebbia *et al.* [10].

6.8 Numerical Experiments and Discussions

The present section is concerned with the numerical application of the DRBEM for the solution of 2D transient convection-diffusion-reaction problems with variable velocity. We shall examine some test examples to assess the robustness and accuracy of this new proposed formulations. For the validation and the performance of the proposed procedure, three standard test problems with known analytical solution are considered.

6.8.1 Transient Convection-Diffusion-Reaction Problem over a Square Channel with Time-dependent Dirichlet Boundary Conditions and Tangential Velocity Field

In the first example, the domain is considered to be square with dimensions $[1m \times 1m]$. We focus on solutions predicted all over the domain by using 19 internal nodes and fixed values of $D = 1\ m^2/s$, $k = 0$, and variable velocity as follows:

$$v_x(x,y) = \tan(x), \tag{6.33}$$
$$v_y(x,y) = \tan(y).$$

The test results are obtained for Eq.(6.1) with the following initial and boundary conditions. The initial condition is chosen as the analytical value of Eq.(6.35) at $t = 0$:

$$\phi(x,y,t=0) = \sin(x) + \sin(y). \tag{6.34}$$

Boundary conditions are chosen as:

$$\begin{cases} \phi\left(x=0,y,t\right)=\left(\sin\left(y\right)\right)e^{-2t}, & \phi\left(x=1,y,t\right)=\left(\sin\left(1\right)+\sin\left(y\right)\right)e^{-2t}, \\ \phi\left(x,y=0,t\right)=\left(\sin\left(x\right)\right)e^{-2t}, & \phi\left(x,y=1,t\right)=\left(\sin\left(x\right)+\sin\left(1\right)\right)e^{-2t}. \end{cases}$$

The analytical solution fis given by:

$$\phi\left(x,y,t\right)=\left(\sin\left(x\right)+\sin\left(y\right)\right)e^{-2t}. \tag{6.35}$$

Figure 6.1 shows the geometrical mesh of the BEM model over a square channel. The

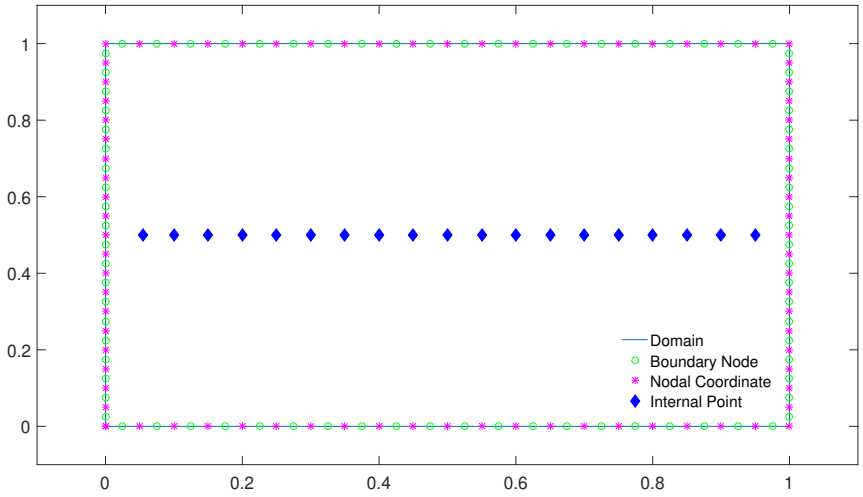

Figure 6.1: Geometrical mesh of convection- diffusion problem with side length $1m$.

boundary is discretised into 50 equally spaced constant elements per side. The analytical and the numerical solutions of this problem are shown in Fig. 6.2 at several time levels utilising the MQ-RBF and implementing a fully implicit scheme when $\theta = 1$ and time-step $\Delta t = 0.05$. The result is obtained for the time evolution of the concentration profile along the centre line of the domain. Comparison between the above analytical solution and the numerical results show an excellent agreement.

Figures 6.3 and 6.4 consider the results using the thin-plate spline TPS-RBF and Cubic RBF

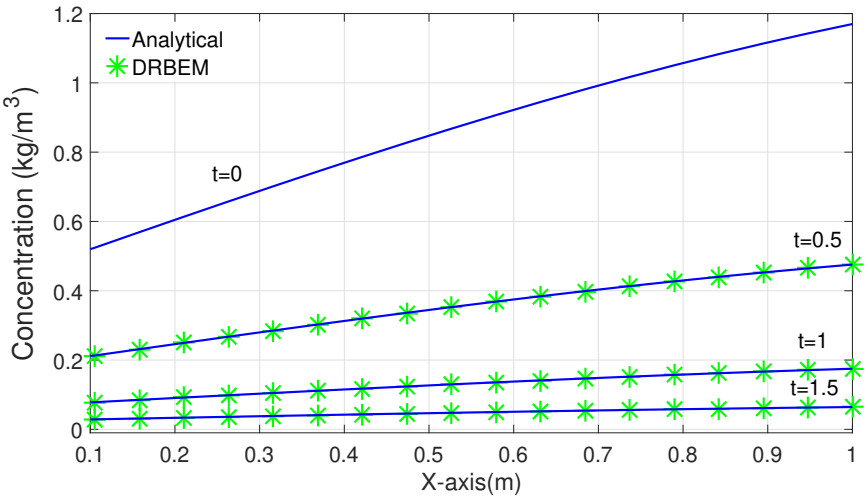

Figure 6.2: Concentration profile for every 10 time steps using MQ-RBF: comparison between the analytical (solid line) and numerical (star points) solutions.

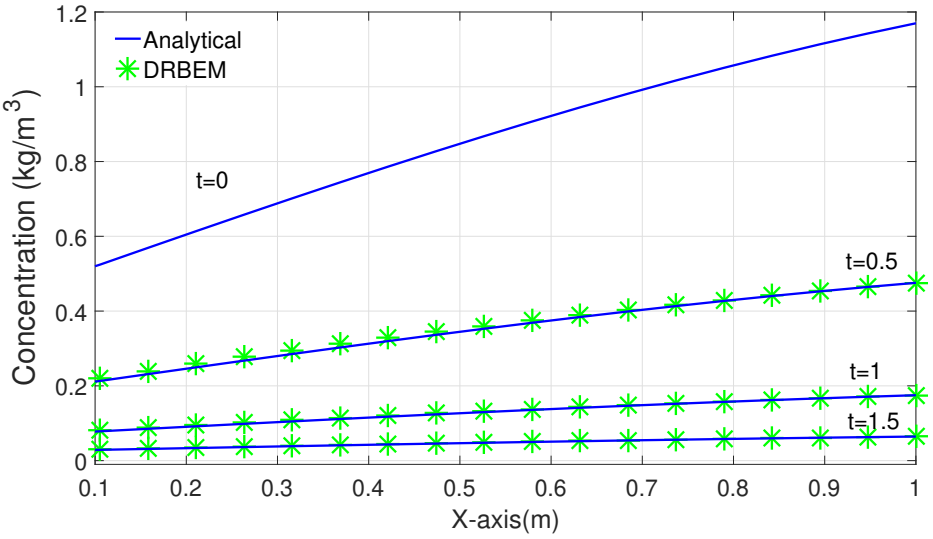

Figure 6.3: Concentration profile for every 10 time steps using TPS-RBF: comparison between the analytical (solid line) and numerical (star points) solutions.

also with time-step $\Delta t = 0.05\,s$. Similar results as for the MQ-RBF have been obtained in both cases. Figure 6.5 shows the time evolution of the concentration distribution in comparison with the analytical solution along the centre line of the computational domain i.e., $x = y = 0.5$ using the backward-difference procedure and TPS-RBF. Table 6.1 shows a comparison between the three different RBFs with time-step value $\Delta t = 0.05\,s$ at time

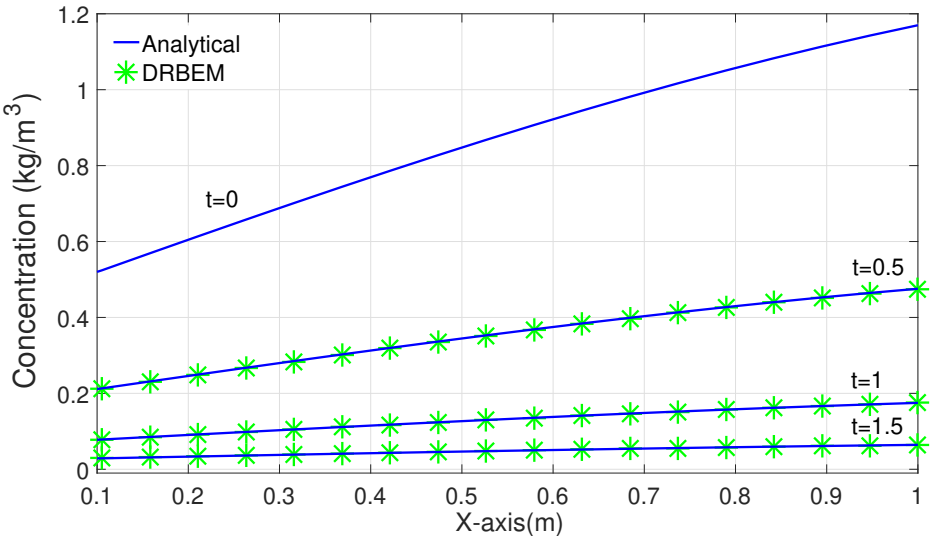

Figure 6.4: Concentration profile for every 10 time steps using Cubic-RBF: comparison between the analytical (solid line) and numerical (star points) solutions.

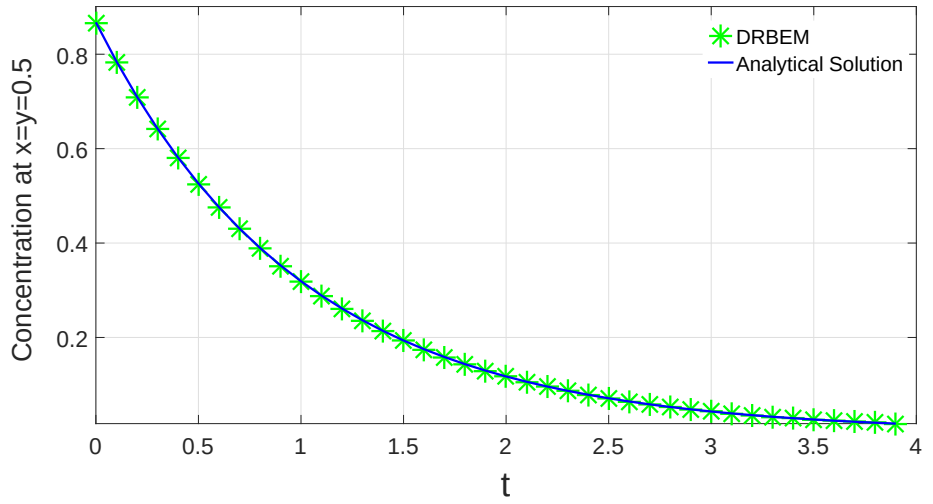

Figure 6.5: Concentration distribution with time using TPS-RBF: comparison of analytical (solid line) and numerical solution (star points) for at $x = y = 0.5$.

level $t = 0.5$. It can be seen that the results obtained by the MQ, TPS and cubic RBFs are reasonably similar. In order to estimate the simulation error, the root mean square norm is utilised as shown in Table 6.2. In this Table the error is seen to reduce as Δt decreases, as expected. Table 6.3 shows a comparison between five different values of the shape parameter c for MQ-RBF with time-step value $\Delta t = 0.05\,s$ at time level $t = 0.5$. It is clear that the

Table 6.1: DRBEM results of ϕ for convection-diffusion-reaction at $t = 0.5$ for $\Delta t = 0.05$

x	Cubic	MQ	TPS	Analytical
0.055	0.1962	0.1939	0.2000	0.1965
0.15	0.2304	0.2285	0.2395	0.2313
0.25	0.2662	0.2680	0.2773	0.2673
0.35	0.3013	0.3020	0.2951	0.3025
0.50	0.3515	0.3490	0.3601	0.3527
0.60	0.3829	0.3847	0.3893	0.3840
0.75	0.4259	0.4258	0.4287	0.4271
0.85	0.4517	0.4509	0.4535	0.4527
0.95	0.4751	0.4759	0.4756	0.4756

Table 6.2: RMS error of DRBEM at $t = 2$ for decreasing Δt

$\theta = 1$, $f = r^2 \log(r)$, Problem 1			
	$\Delta t = 0.1$	$\Delta t = 0.05$	$\Delta t = 0.025$
RMS error in ϕ	0.0091	0.0067	0.0058

results obtained are reasonable and laying at same level of accuracy when the parameter $c = 75$ or 100. On the other hand, the results appear to lose their accuracy for smaller values of c.

From another point of view, taking a very high value of the shape parameter c creates collocation matrices which are poorly conditioned and require high-precision arithmetic to solve accurately. Using a relatively high non-dimensional shape parameter of 75, the collocation matrices are sufficiently well conditioned to be solved using quad-precision arithmetic (see [160, 161, 2] for more details on the shape parameter c).

Table 6.3: Results for convection-diffusion-reaction problem using MQ-RBF with different values of the shape parameter c

x	$c = 100$	$c = 75$	$c = 50$	$c = 25$	$c = 5$	Analytical
0.055	0.1970	0.1939	0.1861	0.1852	0.3752	0.1965
0.25	0.2678	0.2680	0.2468	0.2284	1.4938	0.2673
0.50	0.3524	0.3490	0.3185	0.3025	-3.5933	0.3527
0.75	0.4268	0.4258	0.3984	0.3909	-7.3263	0.4271
0.95	0.4759	0.4759	0.4708	0.4662	-1.6469	0.4756

6.8.2 Transient Convection-Diffusion-Reaction Problem over a Square Channel with Time-Dependent Dirichlet Boundary Conditions and Cosenoidal Velocity Field

In order to further demonstrate the capability of the present numerical scheme for the solution of convection-diffusion-reaction with varying velocity values, the following problem is considered, where the velocities v_x and v_y are defined as:

$$v_x(x,y) = \cos(\pi y), \quad v_y(x,y) = \text{-}\cos(\pi x) \tag{6.36}$$

The problem geometry, discretisation and interior nodes are schematically described in Fig. 6.1. The problem is modeled as square-shaped region, Dirichlet boundary conditions, and 19 internal nodes have been set at the middle line of the computational channel. Test results of this case study are obtained for Eq.(6.1) with the following initial and boundary conditions. The initial condition is chosen as the analytical value of the Eq.(6.38) at $t = 0$:

$$\phi(x,y,0) = \sin(\pi x) + \sin(\pi y) \tag{6.37}$$

Boundary conditions are chosen as:

$$\begin{cases} \phi\left(x=0,y,t\right)=\phi\left(x=1,y,t\right)=\sin\left(\pi y\right)e^{-D\pi^2 t}, \\ \phi\left(x,y=0,t\right)=\phi\left(x,y=1,t\right)=\sin\left(\pi x\right)e^{-D\pi^2 t}. \end{cases}$$

For the sake of convenience, we assume the diffusivity coefficient takes the value $D=1$, the reaction coefficient $k=0$. The problem is discretised into 200 equally spaced constant elements, 50 on each face. The analytical solution of the problem is given by

$$\phi\left(x,y,t\right)=\left(\sin\left(\pi x\right)+\sin\left(\pi y\right)\right)e^{-D\pi^2 t}. \tag{6.38}$$

Figure 6.6 shows the analytical and the numerical solutions of this problem using the cubic-RBF and implementing the fully implicit scheme when $\theta=1$ and time-step $\Delta t=0.005\,s$. The

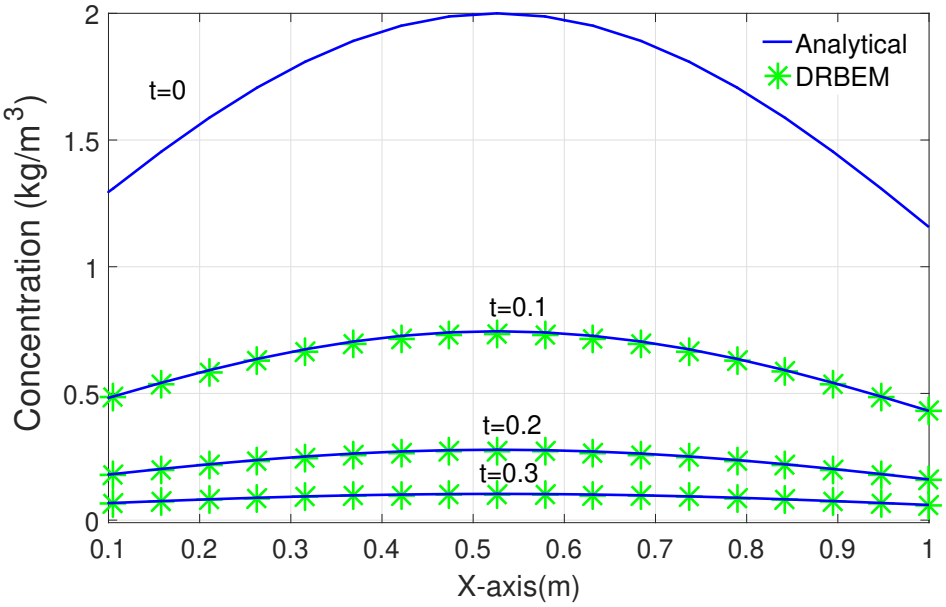

Figure 6.6: Concentration profile for every 20 time steps using Cubic-RBF: comparison between the internal analytical (solid line) and numerical (star points) solutions.

results are obtained for the time evolution of the concentration profile along the centre line of the domain. The comparison between the above analytical solution and our numerical result shows excellent agreement. Figure 6.7 represents the numerical and exact solutions using

the MQ-RBF, while Fig. 6.8 shows the numerical and exact solutions using the TPS-RBF, both with the same time-step $\Delta t = 0.005\,s$. Figure 6.9 illustrates the time evolution of ϕ

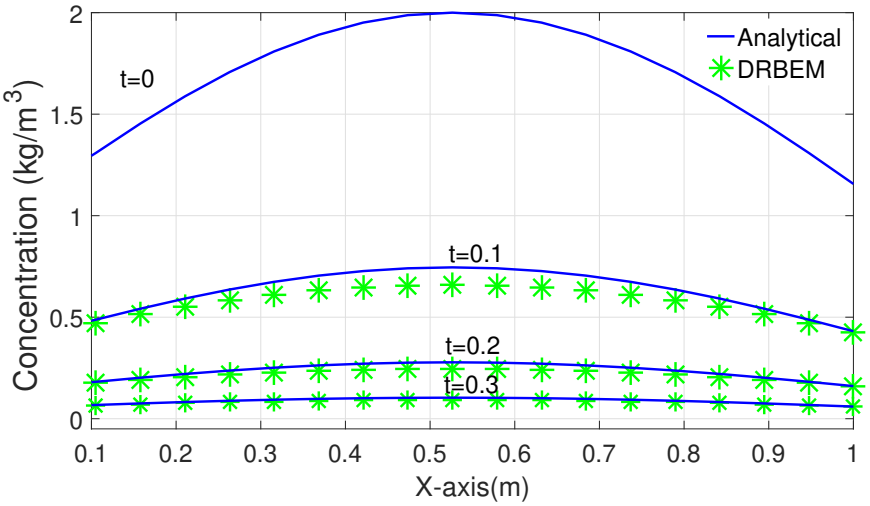

Figure 6.7: Concentration profile for every 20 time steps using MQ-RBF: comparison between the analytical (solid line) and numerical (star points) solutions.

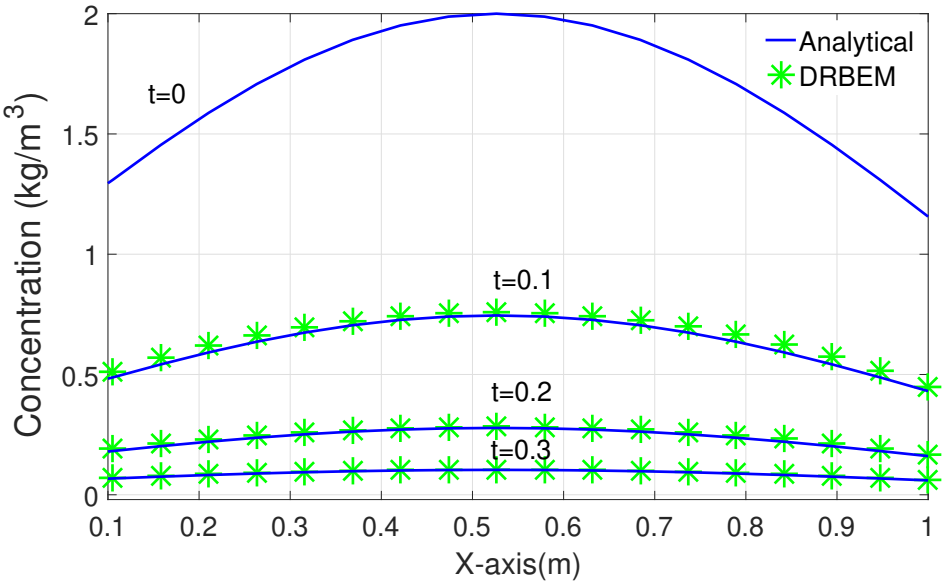

Figure 6.8: Concentration profile for every 20 time steps using TPS-RBF: comparison between the analytical (solid line) and numerical (star points) solutions.

at $x = y = 0.5$ along with the corresponding analytical solution using the thin-plate spline RBF. The numerical approximation for the propagation of ϕ with time is in close agreement

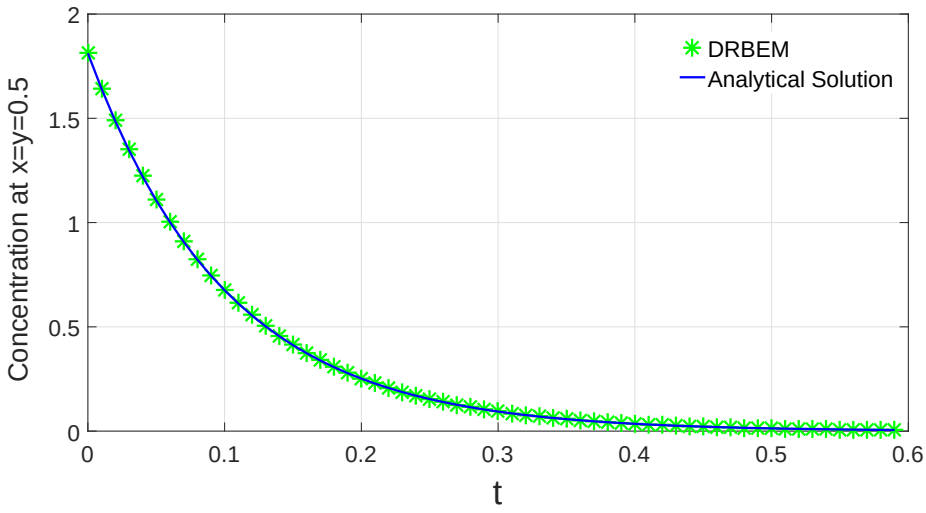

Figure 6.9: Concentration distribution of bounded domain: comparison for various time steps evolution of ϕ at $x = y = 0.5$.

with the analytical solution. The numerical error produced by the present numerical scheme decreases with propagating time. This guarantees the required numerical stability in the convection-diffusion problem. Thus, the salient properties of numerical solution for the consistency, stability, and accuracy are well treated in the present numerical experiments. As seen in table 6.4, the thin-plate spline and the cubic RBFs produce similar results, with good agreement with the analytical solution. In this case study, it is apparent that the accuracy is reduced with MQ-RBF. In table 6.5, the accuracy of the results for the best combination of parameters, $\Delta t = 0.005$ and $f = r^2 \log(r)$, is better than 0.01%.

6.8.3 Transient Convection-Diffusion-Reaction Problem over Rectangular Region with Mixed (Neumann-Dirichlet) Boundary Conditions

As a final example, we investigate a convection-diffusion-reaction problem with linear reaction term. The velocity field is considered to be along the longitudinal direction and all the coefficients in the governing equation are constant. The numerical and analytical solutions are compared for different time steps Δt and reaction coefficient k. The geometry is

Table 6.4: Results for convection-diffusion-reaction at $t = 0.1$ for $\Delta t = 0.005$

x	Cubic	MQ	TPS	Analytical
0.055	0.434	0.428	0.444	0.436
0.15	0.536	0.513	0.541	0.541
0.25	0.627	0.583	0.633	0.636
0.35	0.694	0.632	0.690	0.704
0.50	0.733	0.660	0.722	0.745
0.60	0.716	0.647	0.709	0.727
0.75	0.628	0.583	0.637	0.636
0.85	0.536	0.513	0.553	0.541
0.95	0.429	0.423	0.439	0.431

Table 6.5: RMS error of DRBEM at $t = 2$ for decreasing Δt

$\theta = 1$, $f = r^2 \log(r)$, Problem 2			
	$\Delta t = 0.01$	$\Delta t = 0.005$	$\Delta t = 0.0025$
RMS error in ϕ	0.0153	0.0115	0.0097

considered to be $[0.7m \times 1m]$ as shown in Fig. 6.10. Potential values are imposed at the ends of the cross-section, i.e., at $x = 0$, $\phi = 300$ and at $x = 1$, $\phi = 10$. On the sides parallel to x, the zero lateral fluxes $q = 0$, the problem thus having mixed Neumann-Dirichlet boundary conditions:

$$\begin{cases} \frac{\partial \phi}{\partial n}(x,0,t) = \frac{\partial \phi}{\partial n}(x,0.7,t) = 0, \quad 0 \leq x \leq 1, \quad t > 0, \\ \phi(0,y,t) = 300, \, \phi(1,y,t) = 10, \quad 0 \leq y \leq 0.7, \quad t > 0. \end{cases}$$

and the initial conditions is $\phi(x,y,0)=0$ at all points at $t=0$. The values of the reaction parameter k are assumed to be $k=1,5,10,20$, and $40\,s^{-1}$, $v_y=0$ while v_x is considered to vary according to the formula:

$$v_x(x,y)=kx+\log\left(\frac{10}{300}\right)x-\frac{k}{2}. \tag{6.39}$$

The steady-state solution is given in [164]

$$\phi(x,y)=300\exp\left[\frac{k}{2}x^2+\log\left(\frac{10}{300}\right)x-\frac{k}{2}x\right]. \tag{6.40}$$

In the numerical simulation with a fully implicit scheme, a diffusion coefficient $D=1\left(m^2/s\right)$, a variable velocity $v_x\,(m/s)$ as described in Eq.(6.39), and a time step $\Delta t=0.05\,s$ were used. Comparison between the above analytical solution and our numerical results are given in figures below, showing excellent agreement.

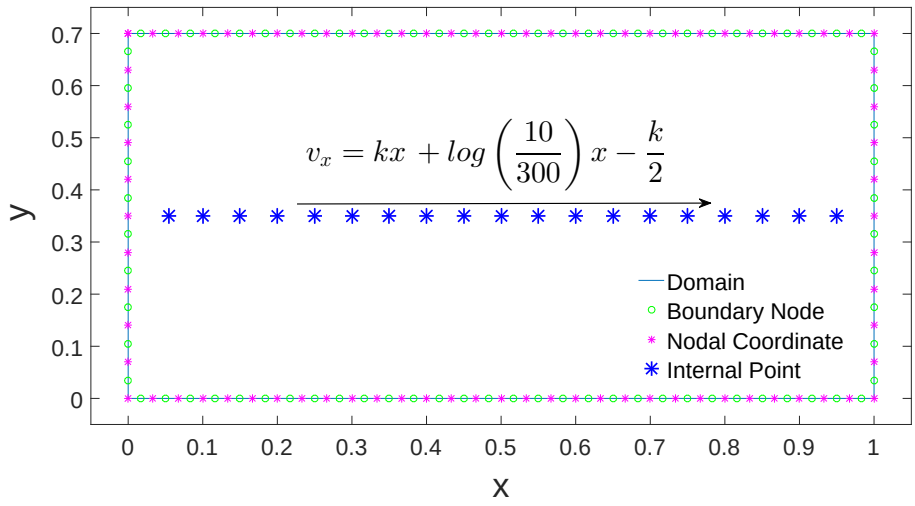

Figure 6.10: Schematic representation of the rectangular channel model with side length $1m$.

Case(i) : The first case is considered with the reaction value $k=1$, which is analysed considering the computational domain discretised into 80 constant elements and using 19 internal points with a time step $\Delta t=0.05\,s$. For the DRBEM model, only the TPS-RBF

has been applied in all cases. Figure 6.11 shows the exact and numerical solutions, with 10 constant elements along the vertical sides and 30 along each horizontal side.

Case(**ii**) : In the second case, the contribution of the reactive term in Eq.(6.1) is increased to $k = 5$. In Fig. 6.11, results are compared for the same time-stepping scheme considered in the previous case with $\Delta t = 0.05$, at $t = 2$ by which time the solution has converged to a steady-state. The results are still very reasonable for the discretisation employed, which is the same as for $k = 1$.

Case(**iii**) : For this case, the contribution of the reactive term in Eq.(6.1) is increased to $k = 10$. Figure 6.11 displays the results time for the same time-stepping scheme considered in the previous case with $\Delta t = 0.05$, at $t = 2$ by which time the solutions have converged to a steady- state.

Case(**iv**) : To see the effect of increasing the value of k, the reaction coefficient is now $k = 20$. In this case, the maximum global Péclet number is equal to 10 (see, Fig. 6.12).

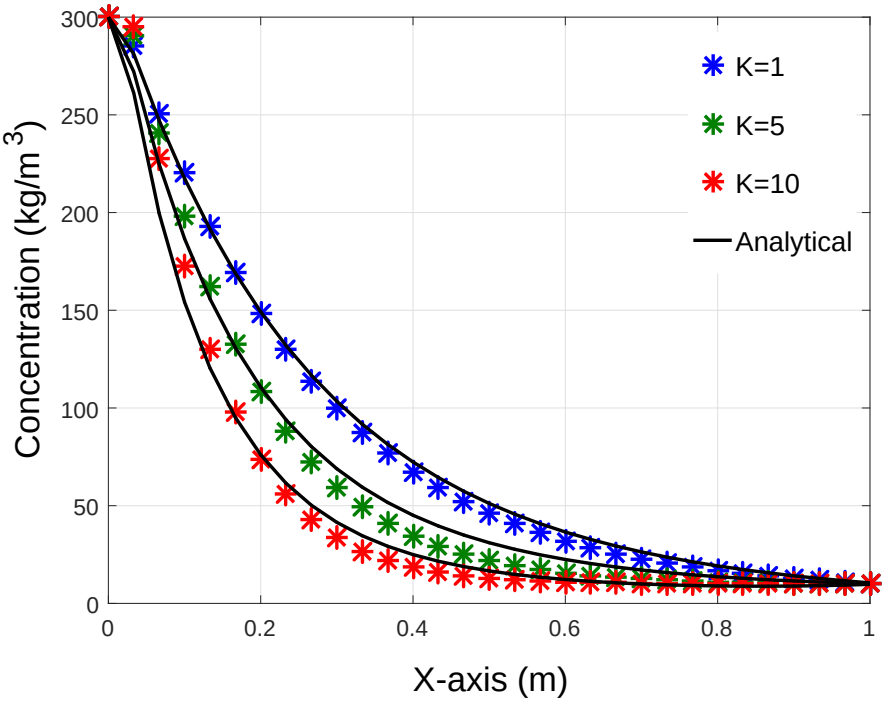

Figure 6.11: Concentration profile ϕ distribution for bounded domain with different values of reaction k: Comparison between the analytical (solid line) and numerical (star points) solutions, for every 5 time steps, Problem 3.

Case(**iv**) : The final test considers the reaction coefficient $k = 40$. A plot of the variation of the concentration ϕ along the x-axis is presented in Fig. 6.12. In this case, the maximum global Péclet number is 20. It is obvious that the agreement with the corresponding analytical solution is still very good.

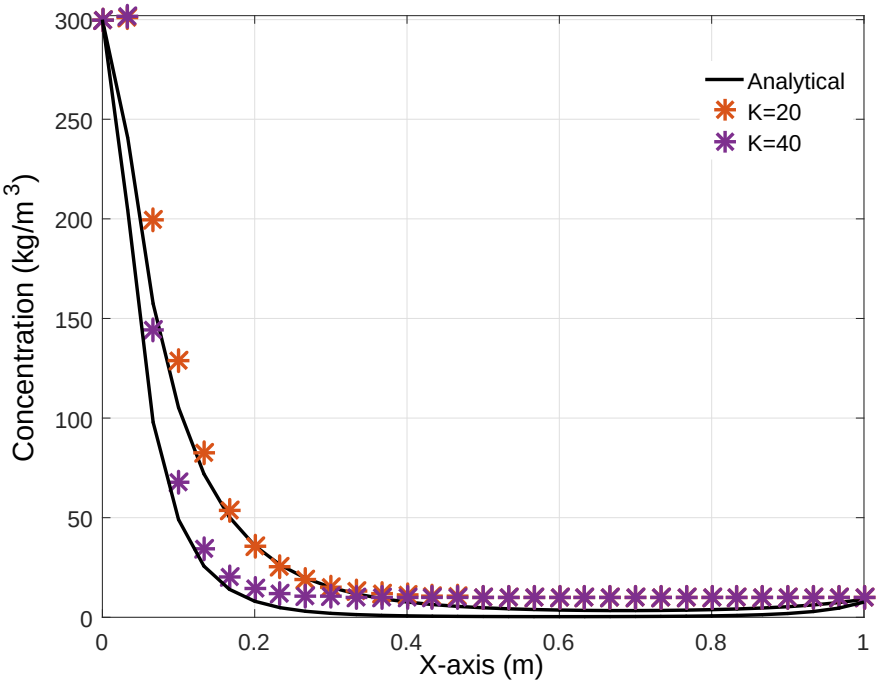

Figure 6.12: Comparison between the analytical (solid line) and numerical (star points) solutions, for different values of the reaction k.

6.9 Summary and Discussions

In this chapter, we present a novel formulation of the DRBEM for solving 2D transient convection-diffusion-reaction problems with spatial variable velocity field. This new formulation for this type of problems has been implemented to handle the time derivative part and the variable velocity field. The fundamental solution of the corresponding steady-state equation with constant coefficients has been utilised. The DRBEM is used to transform the domain integrals appearing in the BEM formulations into equivalent boundary integrals, thus retaining the boundary-only character of the standard BEM. This formulation is expected to

be stable at low Péclet numbers (i.e. diffusion-dominated problems). Numerical applications for 2D time-dependent problems are demonstrated to show the validity of the proposed technique, and its accuracy was evaluated by applying it to three tests with different velocity fields. Moreover, numerical results show that the DRBEM does not present oscillations or damping of the wave front as may appear in other numerical techniques.

In the empirical analysis section, the results presented in section 9 show the versatility of the method to solve time-dependent convection-diffusion-reaction problems involving variable velocity fields. The first-order time derivative of the potential is approximated by employing a backward finite difference scheme. We can note a distinct advantage of the present approach, which demonstrates very good accuracy even for high reaction values which increase the Péclet number for the cases studied. It is obvious that, as the velocity increses, the concentration distribution becomes steeper and more difficult to reproduce with numerical models. However, all BEM solutions are still in good agreement for moderate Péclet number $(\text{Pé} = 10)$ and $(\text{Pé} = 20)$, but oscillations appear for high Péclet number; thus, more refined discretisations are required. We have made an extensive investigation for the last case studied by considering many different values of the reaction coefficient k. For all these various values of k the backward time-stepping scheme produces very good results in general. We have derived and implemented three RBFs and tested them with different types of problems, and we have found that the TPS is the most accurate among these RBFs for our problems.

Chapter 7

RIBEM Modelling for Non-Homogeneous Convection-Diffusion-Reaction Problems with Variable Source Term

7.1 Introduction

A simple and robust transformation technique, called the radial integration method (RIM), was developed by Gao [85] which not only can transform any complicated domain integral to the boundary without using particular solutions, but can also remove various singularities appearing in the domain integrals [168, 84].

Based on the RIM, the RIBEM was developed and applied to handle a wide range of engineering and mathematical problems including non-homogeneous steady-state and transient heat conduction problems, acoustics problems, diffusion problems, elastoplasticity and other mechanical problems [85, 168–171, 99, 172].

Yang and Gao [98] proposed a new boundary element technique to handle transient heat conduction problems, for which the RIM is implemented to transfer the domain integral associated with the time derivative of temperatures, and the radial integral is evaluated

numerically. The RIM can be applied to the combination of power series expansion operated on the parameter plane of intrinsic coordinates [173] or for the projection plane of global coordinates [174, 175], for which it can evaluate all types of singular boundary integrals numerically [103].

Recently, Feng [176] proposed a new type of single integral equation technique to solve transient heat conduction problems in multi-media with variable thermal properties. The same author has also derived an interface integral equation method to solve general multi-media mechanical problems by considering the discontinuity of the stress-strain constitutive relationship during the transformation from elastic to plastic regions [177]. Feng also proposed a new BEM formulation without initial stresses for solving two and three-dimensional elastoplastic problems [178].

Yang *et al*. [179, 101] successfully derived a series of analytical expressions for evaluating radial integrals, which are utilised in the RIM for converting the domain integrals into equivalent boundary integrals. By using these analytical expressions, the computation time spent in the numerical calculation of radial integrals can be considerably reduced. This technique has been implemented to handle non-homogeneous heat conduction, non-homogeneous elasticity and thermoelasticity problems. However, in the derivation of the analytical radial integral expressions, some special circumstances may appear which will influence the accuracy of the results [103].

The RIBEM was successfully derived and implemented for the free vibration analysis of anisotropic plates [180], and to thermoelasticity, elastic inclusion problems, creep damage mechanics problems, transient heat conduction problems, and viscous flow problems [181, 172, 182, 98, 183]. Owing to the advantages of the RIM, mainly that particular solutions are not required and various domain integrals appearing in the same integral equation can be dealt with simultaneously, RIM-based BEM have gained considerable attention from many BEM researchers [184–186].

The radial integral in the RIBEM formulation is usually calculated by utilising Gaussian quadrature, which requires it to be computed at each Gaussian point of the boundary element under consideration. Evaluating the radial integrals numerically, especially for a 3D non-

linear and large-scale non-homogeneous problem, is highly time-consuming and this will lead to a reduction of the performance and the efficiency of this numerical method [178, 183]. This chapter presents a new formulation of the RIBEM for convection-diffusion-reaction problems with source terms.

A brief outline of this chapter is as follows: Section 7.2 shows the representation of the non-homogeneous convection-diffusion-reaction equation with source term. Section 7.3 derives the boundary element formulation of the governing equation using the fundamental solution of the corresponding equation without a source. In section 7.4, the RIM formulation is developed for the 2D non-homogeneous convection-diffusion-reaction problem with source term, followed in section 7.5 by domain integrals with weakly-singular integrand for this model. Space discretisation of the RIBEM formulation for the corresponding problem is discussed in section 7.6, while section 7.7 gives a description of the assembly of the RIBEM system. Section 7.8 compares and discusses the solution profiles for the present numerical experiments with the analytical solution of the tested cases. Some error indicators were used to represent the error and the solution behaviour. Computational aspects are included to demonstrate the performance of this approach in section 7.9. Finally, some conclusions and remarks are provided in the last section.

7.2 Non-homogeneous Convection-Diffusion-Reaction Problem with Source Term

Our mathematical model, i.e. non-homogeneous 2D convection-diffusion-reaction problem with source term over a domain Ω in $\mathbb{R}^2$ bounded by Γ, for isotropic materials, is governed by the following PDE:

$$D\nabla^2\phi\left(x,y\right)-v_x\frac{\partial\phi\left(x,y\right)}{\partial x}-v_y\frac{\partial\phi\left(x,y\right)}{\partial y}-k\,\phi\left(x,y\right)=S\left(x,y\right),\quad \left(x,y\right)\in\Omega. \tag{7.1}$$

In Eq.(7.1), ϕ represents the concentration of a substance, treated as a function of space. The velocity components v_x and v_y along the x and y directions are assumed to be constant in

space. Besides, D is the diffusivity coefficient, k represents the first-order reaction constant or adsorption coefficient and $S(x,y)$ represents the source term. The boundary conditions are

$$\phi = \bar{\phi} \quad \text{over} \quad \Gamma_D \tag{7.2}$$

$$q = \frac{\partial \phi}{\partial n} = \bar{q} \quad \text{over} \quad \Gamma_N \tag{7.3}$$

where Γ_D and Γ_N are the Dirichlet (essential) and Neumann (natural) parts of the boundary with $\Gamma = \Gamma_D \cup \Gamma_N$, and $\Gamma_D \cap \Gamma_N = \emptyset$.

7.3 Boundary Element Formulation of Non-Homogeneous Convection-Diffusion-Reaction Problems with Source Term

The transport of ϕ in the presence of a reaction term is governed by the 2D convection-diffusion-reaction Eq.(7.1). The variable ϕ can be interpreted as temperature for heat transfer problems, concentration for dispersion problems, etc, and will be herein referred to as a concentration. For the sake of obtaining an integral equation equivalent to the PDE (7.1), a fundamental solution of Eq.(7.1) is necessary. Equation (7.1) can be transformed into an equivalent integral equation by applying a weighted residual technique. Starting with the weighted residual statement:

$$\int_{\Omega} \left(D\nabla^2 \phi(x,y) - v_x \frac{\partial \phi(x,y)}{\partial x} - v_y \frac{\partial \phi(x,y)}{\partial y} - k\,\phi(x,y) \right) \phi^* d\Omega = \int_{\Omega} S(x,y)\,\phi^* d\Omega \tag{7.4}$$

and integrating by parts twice the Laplacian and once the first-order derivatives, the following equation is obtained:

$$\phi(\xi) = D \int_{\Gamma} \phi^* \frac{\partial \phi}{\partial n} d\Gamma - D \int_{\Gamma} \phi\, \frac{\partial \phi^*}{\partial n} d\Gamma - \int_{\Gamma} \phi\, \phi^*\, \bar{v}_n\, d\Gamma - \int_{\Omega} S(x,y)\,\phi^*\, d\Omega. \tag{7.5}$$

In the above equation, ϕ^* is the fundamental solution of the convection-diffusion-reaction equation without source term. Expression (7.5) is valid for source points ξ inside the domain Ω. A similar expression can be obtained, by a limit analysis, for source points ξ on the boundary Γ, in the form

$$c(\xi)\,\phi(\xi) = D\int_{\Gamma}\phi^*\frac{\partial\phi}{\partial n}\,d\Gamma - D\int_{\Gamma}\phi\,\frac{\partial\phi^*}{\partial n}\,d\Gamma - \int_{\Gamma}\phi\,\phi^*\,\bar{v}_n\,d\Gamma - \int_{\Omega}S(x,y)\,\phi^*\,d\Omega, \quad (7.6)$$

as shown in Appendix A.

7.4 The Radial Integration Method for Transforming General Domain Integrals to the Boundary

Given a 2D domain Ω bounded by a boundary Γ, define a Cartesian coordinate system (χ_1,χ_2) and a polar coordinate system (r,θ) with origin at the source point $\xi=(\xi_1,\xi_2)$. The relationships between the Cartesian and polar coordinate systems are:

$$\begin{cases} r_1 = \chi(1) - \xi(1) = r\cos(\theta), \\ r_2 = \chi(2) - \xi(2) = r\sin(\theta), \end{cases} \quad (7.7)$$

where $0 \le \theta \le 2\pi$ and r is the distance between the source point ξ and a field point χ. The relationship between a differential domain in the Cartesian system and the polar system is given by

$$d\Omega = d\chi_1\,d\chi_2 = J\,dr\,d\theta = r\,dr\,d\theta, \quad (7.8)$$

where $J = |\partial(\chi(1),\chi(2))/\partial(r,\theta)| = r$ is the Jacobian. We can notice from Fig. 7.1 that when the field point is located on the boundary, we can obtain the following relation [3]

$$r\,d\theta = d\Gamma\,cos\varphi = d\Gamma\,\frac{r_i n_i}{r}, \quad (7.9)$$

where φ is the angle between the normal of the differential arc $rd\theta$ with radius r with the differential boundary Γ with outward normal n_i, with the summation subscript i taking the values 1 to 2. Substituting Eq.(7.9) in (7.8) and re-arranging, we obtain

$$d\Omega = r\,dr\,ds, \quad \text{where} \quad ds = \frac{1}{r}\frac{\partial r}{\partial n}d\Gamma \tag{7.10}$$

for which the following expressions are employed

$$\frac{\partial r}{\partial n} = r_{,i}n_i, \quad r_{,i} = \frac{\partial r}{\partial \chi_i} = \frac{r_i}{r} = \frac{(\chi_i - \xi_i)}{r}, \quad r_{,i}r_{,i} = 1 \tag{7.11}$$

From Fig.7.1 when the field point is located on the boundary, we can obtain the following relation [187]. Now, a function in Cartesian coordinates can be written in polar coordinates

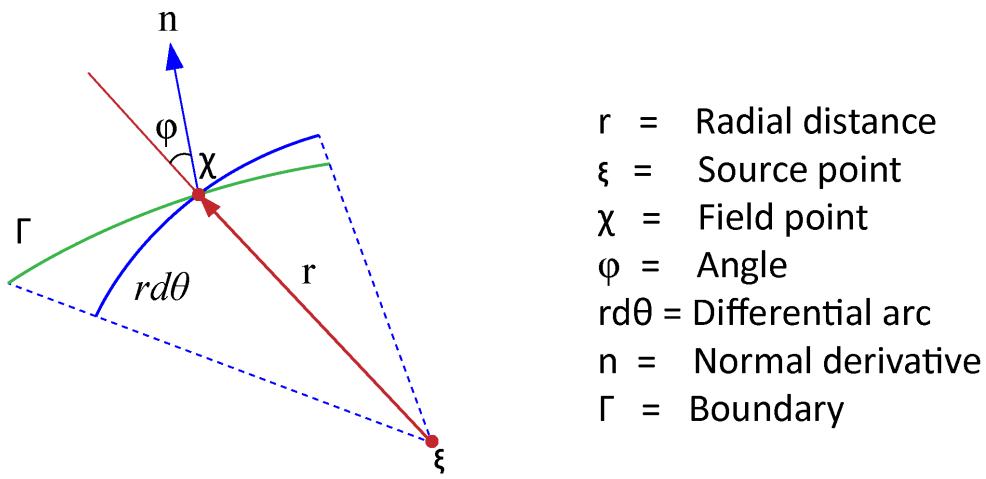

Figure 7.1: Relationship between differential elements $rd\theta$ and $d\Gamma$

and integrated as follows:

$$\int_\Omega f(\chi)\,d\Omega = \int_s \left\{ \int_0^{r(\chi)} f(\chi)\,r^\alpha dr \right\} ds(\chi) = \int_s F(\chi)\,ds(\chi), \tag{7.12}$$

where

$$F(\chi) = \int_0^{r(\chi)} f(\chi)\, r^{\alpha} dr. \tag{7.13}$$

In Eqs.(7.12) and (7.13), $\alpha = 1$ for the 2D case and $\alpha = 2$ for the 3D case. The symbol $r(\chi)$ means the variable r takes values on the boundary Γ (see Fig. 7.1). Substituting expression (7.10) into (7.12), we obtain

$$\int_{\Omega} f(\chi)\, d\Omega = \int_{\Gamma} \frac{1}{r^{\alpha}} \frac{\partial r}{\partial n} F(\chi)\, d\Gamma(\chi). \tag{7.14}$$

The following notes are crucial for the RIM, especially for Eqs.(7.13) and (7.14):

- Although the derivation is in a polar coordinate system, the variables are now written in the Cartesian coordinate system.
- The equations are valid for a source point ξ located at both internal and boundary nodes.
- The most attractive feature of the RIM is that the transformation (7.14) is very simple and has similar forms for both 2D and 3D. It can remove various singularities appearing in domain integrals since r^{α} is included in the radial integral in expression (7.13).
  In order to transform a domain integral to a boundary one, the main task is to calculate the radial integral in Eq.(7.14), which can be done analytically for simple kernels. We have written a simple Matlab code for analytical integration of Eq.(7.14) which can integrate many given functions $f(\chi)$, however, for complicated functions, numerical integration techniques are required [168, 84].
- In order to evaluate the RIM in Eq.(7.13), the coordinates $\chi(1)$, $\chi(2)$ in $f(\chi)$ need to be expressed in terms of the distance r using:

$$\chi_i = \xi_i + r_{,i}\, r, \quad i = 1,2. \tag{7.15}$$

  where the quantities ξ_i and $r_{,i}$ are constants for the radial integral in Eq.(7.13).

- Weak singularities involved in the integrand $f(\chi)$ have been transformed to the boundary. Consequently, no singularities exist at internal nodes for such integrands.
- Expression (7.14) can be computed using constant, linear and higher order boundary elements in the same way as in the standard BEM.

7.5 RIM Formulation for Domain Integrals with Weakly-Singular Integrand

It is known that, in a domain integral, if the integrand includes the term $1/r^{\alpha}$, then when $n \leq \alpha$ $(\alpha = 1)$ in 2D and $(\alpha = 2)$ in 3D, this integrand is weakly singular as the source point approaches the field point. For such an integrand, Eq.(7.13) shows that the singularity is explicitly eliminated after multiplying by the term r^{α}. After integrating Eq.(7.13), $F(\chi)$ will include a term r^m where m is equal to or greater than 1. This makes the transformed boundary integral (7.14) weakly singular when the source point approaches the boundary. For strongly singular integrands $f(\chi)$, which includes $1/r^n$ with $n > 1$, Eq.(7.13) cannot omit the singularity completely. However, for some special functions, for example the strain kernels in elastoplastic integral equations, the idea of differentiating Eqs.(7.13) and (7.14) can be utilised to remove the strong singularities [187].

From Eqs.(7.13) and (7.14), we can see that the key task for the transformation of domain to boundary integrals is the evaluation of the radial integral (7.13). For most kernel functions involved in domain integrals in BEM for mechanical and potential problems, Eq.(7.13) can be analytically integrated. For some very complicated functions, it may be difficult to do this. In that case, numerical integration techniques, such as Gaussian quadrature, may be used to compute the radial integral for every field point χ. To use Gaussian quadrature, the following variable transformation is required:

$$r = \frac{r(\chi)}{2}\zeta + \frac{r(\chi)}{2}, \quad -1 \leq \zeta \leq 1. \tag{7.16}$$

When the source term $S(x,y)$ is variable, then the RIM can be implemented to transform the domain integral appearing in Eq.(7.5). The radial integral can be evaluated by direct implementation (analytically) as described in section 4 when the source term is constant whilst for variable source terms, numerical integration will be implemented. Using Eqs.(7.15) and (7.16), the radial integral (7.13) can be expressed as:

$$F(\chi) = \int_{-1}^{+1} f(\chi(\zeta)) \left(\frac{r(\chi)}{2}\zeta + \frac{r(\chi)}{2} \right)^{\alpha} \frac{r(\chi)}{2} d\zeta$$

$$= \left(\frac{r(\chi)}{2} \right)^{\alpha+1} \sum_{n=1}^{N_g} (1+\zeta_n)^{\alpha} f(\chi(\zeta_n)) w_n$$

where N_g is the number of Gaussian points, ζ_n are the Gaussian point coordinates and w_n is the associated weight. In this work, 60 Gauss points are used for increased accuracy.

7.6 Space-Discretisation of the Radial Integration Boundary Element Formulation for Convection-Diffusion-Reaction Model with Source Term

For numerical solution of the problem, Eq.(7.6) can be written in discretised form in which the integrals over the boundary are approximated by a summation of integrals over individual boundary elements, i.e.

$$c_i \phi_i = D \sum_{j=1}^{N} \int_{\Gamma_j} \phi^* \frac{\partial \phi}{\partial n} d\Gamma - D \sum_{j=1}^{N} \int_{\Gamma_j} \left(\frac{\partial \phi^*}{\partial n} + \frac{v_n}{D} \phi^* \right) \phi \, d\Gamma$$

$$- \sum_{j=1}^{N} \int_{\Gamma_j} \left[\frac{1}{r} \frac{\partial r}{\partial n} \left(\frac{r}{2} \right)^2 \sum_{n=1}^{N_g} (1+\xi_n) f(\chi(\xi_n)) w_n \right] \phi^* d\Gamma \tag{7.17}$$

where the index i stands for values at the source point ξ_i, N_g is the number of integration points and N the number of boundary elements. In the above expression, it can be noticed that:

$$\frac{\partial \phi^*}{\partial n} + \frac{v_n}{D}\phi^* = \frac{1}{2\pi D}\exp\left(\frac{-v.r}{2D}\right)\left[-\mu K_1(\mu r)\frac{\partial r}{\partial n} + \frac{v_n}{2D}K_0(\mu r)\right]. \tag{7.18}$$

Next, the constant functions ϕ and $\frac{\partial \phi}{\partial n}$ within each element are approximated by their nodal values. Therefore, the following expression is obtained

$$c_i\phi_i = \sum_{j=1}^{N}\left(G_{ij}q_j - H_{ij}\phi_j\right) + B_j. \tag{7.19}$$

Note that the coefficients of the two influence matrices can be represented as:

$$G_{ij} = D\int_{\Gamma_j}\phi^* d\Gamma \tag{7.20}$$

and

$$H_{ij} = D\int_{\Gamma_j}\left(\frac{\partial \phi^*}{\partial n} + \frac{v_n}{D}\phi^*\right)d\Gamma \tag{7.21}$$

with

$$B_j = \int_{\Gamma_j}\left(\frac{1}{r}\frac{\partial r}{\partial n}\left(\frac{r}{2}\right)^2\sum_{n=1}^{N_g}(1+\xi_n)\,f(\chi(\xi_n))\,w_n\right)\phi^*\,d\Gamma. \tag{7.22}$$

The above expression (7.19) involves N values of ϕ and $q = \frac{\partial \phi}{\partial n}$, half of which are prescribed as boundary conditions. In order to calculate the remaining unknowns, it is necessary to generate N equations. This can be done by using a simple collocation technique, i.e. by making the equation be satisfied at the N nodal points. The c_i values have been incorporated into the diagonal coefficients of matrix H. After introducing the boundary conditions, the system is reordered and solved by a direct method, for instance, Gauss elimination or LU

decomposition. The result is a system of equations of the form:

$$\mathbf{H}\phi = \mathbf{G}q + \mathbf{B}, \tag{7.23}$$

where B is the term representing the radial integral for the source term as in Eq.(7.5). Evaluation of the coefficients of matrices H, G and vector B is carried out numerically. It should be noted that the diagonal coefficients of matrix G have a weak singularity of the logarithmic type, and are calculated using the self-adaptive scheme of Telles [22]. The coefficients H_{ii} can be calculated, in the absence of the reaction term, by noting that a consistent solution for a prescribed uniform concentration along the boundary can be obtained if matrix H is singular, i.e.

$$H_{ii} = -\sum_{j=1}^{N} H_{ij} \ (i \neq j) \tag{7.24}$$

However, when $k \neq 0$, there is a flux when a uniform concentration is applied (or, in other words, the zero flux state cannot be achieved for a uniform concentration distribution). In this case, the coefficients H_{ii} have to be evaluated explicitly [110]. These terms are composed of two parts, one being a sum of integrals of the form H_{ij} and the other the free term c_i. The former also possesses a logarithmic singularity, and is calculated using Telles' scheme [22]. The free terms c_i depend only on geometry, and have the same values as for Laplace's equation [141].

7.7 Numerical Experiments and Results

The present section is concerned with numerical tests of the RIBEM for the solution of 2D non-homogeneous convection-diffusion-reaction problems with constant and variable source terms. We shall examine four case studies with known analytical solutions to quantitatively and qualitatively assess the accuracy and the robustness of the proposed formulation. All numerical computations were coded using Matlab® 2016a Version 9.

7.7.1 Experiment 1: Non-Homogeneous Convection-Diffusion-Reaction Problem over a Square-Shaped Region with Constant Source Term

In this test, a two-dimensional transport problem with constant source term has been examined to analyse the validity of the present formulation. This problem deals with a square cross-section with unit dimensions. We assume the diffusivity $D = 1\left(m^2/s\right)$, the reaction value $k = 0\,(1/s)$, and velocity component $v_y = 0\,(m/s)$. We shall consider the cases where $S = 1$, 10, 100 and 500.

The mixed boundary condition are as follows: For vertical faces, i.e. $x = 0$ and $x = 1$, Dirichlet boundary conditions are imposed:

$$\phi\,(0,y) = 0, \quad \phi\,(1,y) = 1, \quad 0 \leq y \leq 1.$$

and zero fluxes (Neumann boundary conditions) for the horizontal faces, i.e. $y = 0$ and $y = 1$:

$$\frac{\partial \phi}{\partial n}\,(x,0) = \frac{\partial \phi}{\partial n}\,(x,1) = 0, \quad 0 \leq x \leq 1.$$

The analytical solution of the problem is given by

$$\phi\,(x,y) = \phi_0 + \frac{S}{v_x}x + \frac{\phi_L - \phi_0 - (SL/v_x)}{\exp\left(\frac{v_x L}{D}\right) - 1}\left[\exp\left(\frac{v_x L x}{D}\right) - 1\right]. \tag{7.25}$$

The geometry is discretised into 120 equally-spaced constant elements, 30 on each side as shown in Fig.7.2.

Positive Velocity

The concentration ϕ at boundary nodes along the faces $y = 0$ and $y = 1$ is investigated. Figure 7.3 displays the numerical and analytical solutions along the bottom and the top sides of the channel for $S = 5$ and $v_x = 10$. Next, Fig. 7.4 presents RIBEM and analytical solutions for $S = 10$ and $v_x = 30$. Figure 7.5 presents the numerical and analytical solutions for $S = 50$ and $v_x = 15$. Figure 7.6 shows the numerical and exact solutions for $S = 500$ and $v_x = 20$.

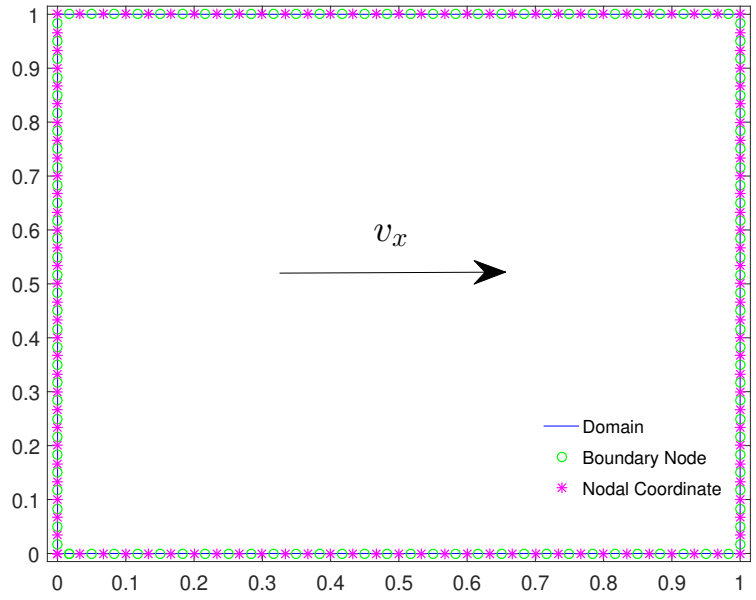

Figure 7.2: Geometry and model discretisation with unit side length

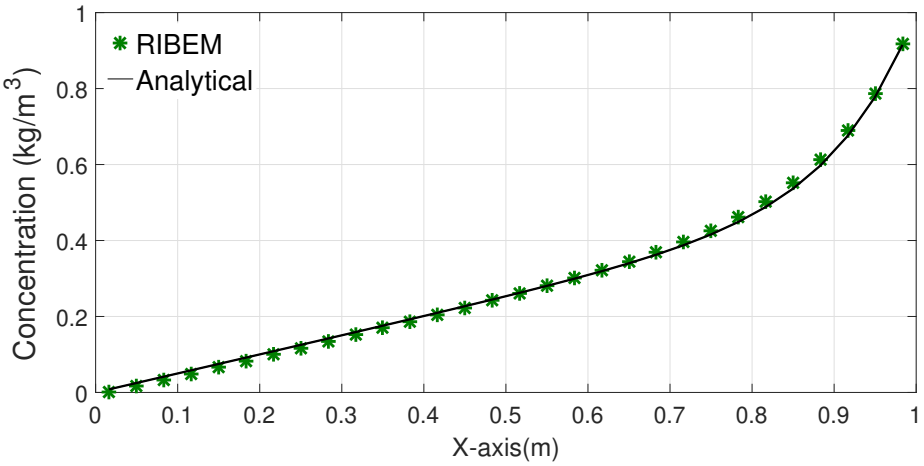

Figure 7.3: Variation of concentration profile ϕ along faces $y = 0$ and $y = 1$ for $S = 5$, $v_x = 10$: comparison between the analytical (solid line) and numerical (star points) solutions

The Péclet number in this case is Pé $= 20$. Figure 7.7 presents the solution for $S = 100$ and $v_x = 500$. Figure 7.8 shows the variation of the concentration profile along the horizontal faces for a high value of the source term $S = 500$ and velocity $v_x = 500$, compared to the analytical solution, in which case the Péclet number is Pé $= 500$. All figures display the expected behaviour for the concentration profiles at different Péclet numbers and with various

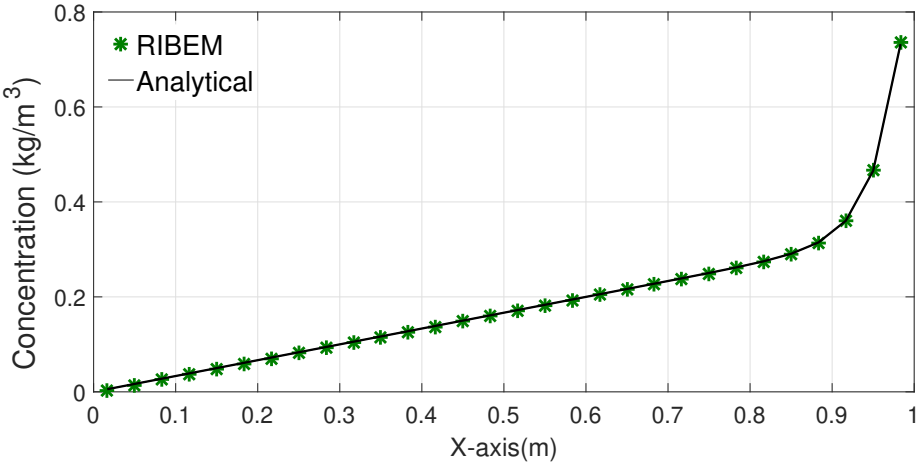

Figure 7.4: Variation of concentration profile ϕ along faces $y = 0$ and $y = 1$ for $S = 10$, $v_x = 30\,(m/s)$: comparison between the analytical (solid line) and numerical (star points) solutions

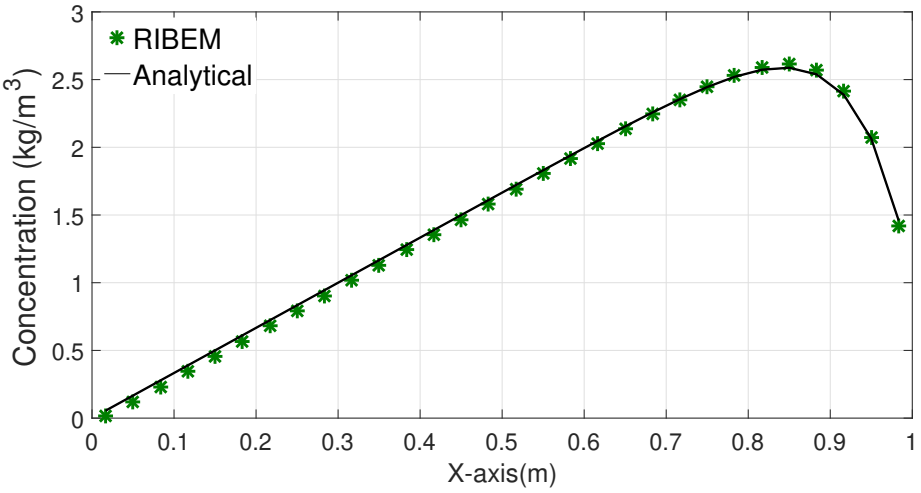

Figure 7.5: Variation of concentration profile ϕ along faces $y = 0$ and $y = 1$ for $S = 50$, $v_x = 15$: comparison between the analytical (solid line) and numerical (circle points) solutions

source term values, showing an excellent agreement with the analytical results.

To examine the variation of the concentration profiles at different positions at the bottom face, Table 7.1 shows the numerical and analytical solutions for $S = 50$ and $v_x = 50$.

To assess the error of the boundary concentrations with mesh refinement, Table 7.2 presents the absolute error for RMS. The accuracy of the results for the RIBEM is good as the absolute error in RMS error norm is of the order 10^{-3}. The simulation and the analytical solutions on

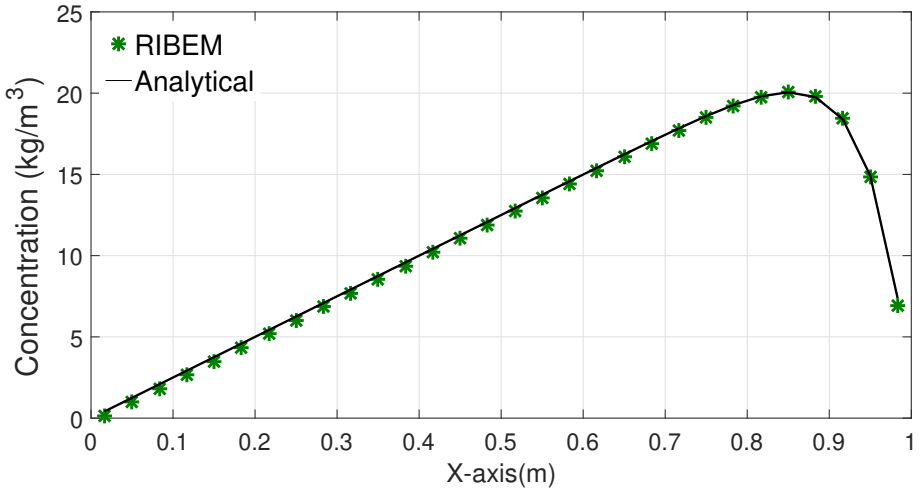

Figure 7.6: Variation of concentration profile ϕ along faces $y = 0$ and $y = 1$ for $S = 500$, $v_x = 20$: comparison between the analytical (solid line) and numerical (star points) solutions

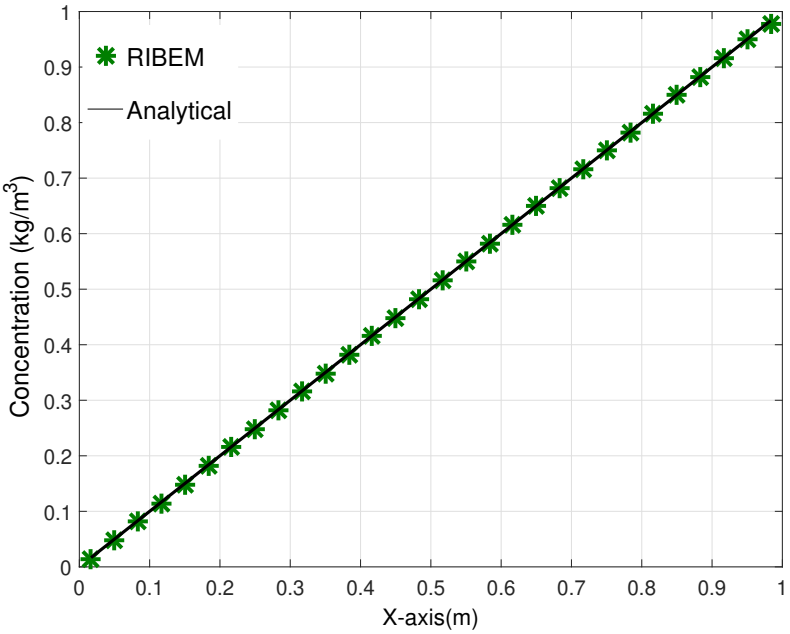

Figure 7.7: Variation of concentration profile ϕ along faces $y = 0$ and $y = 1$ for $S = 100$, $v_x = 500$: comparison between the analytical (solid line) and numerical (star points) solutions

two-dimensional refined meshes are computed with good agreement. The calculated error are cast in the RMS error norm and are plotted in Fig. 7.9. This calculation represents the global error solution for this case study.

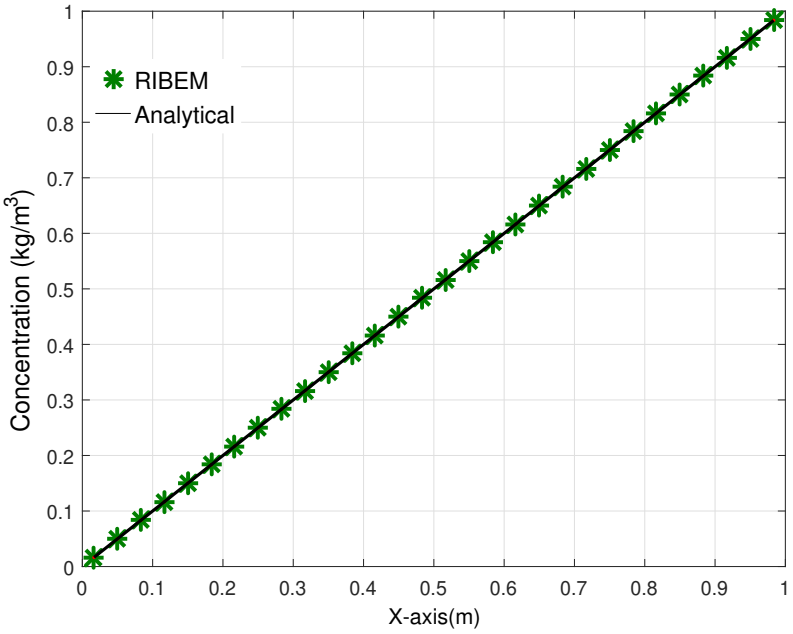

Figure 7.8: Variation of concentration profile ϕ along faces $y = 0$ and $y = 1$ for $S = 500$, $v_x = 500$: comparison between the analytical (solid line) and numerical (star points) solutions

Table 7.1: RIBEM results of ϕ for convection-diffusion-reaction problem at Pé $= 50$

x	RIBEM	Analytical
0.1	0.1124	0.1167
0.2	0.2131	0.2167
0.3	0.3136	0.3167
0.4	0.4139	0.4167
0.5	0.5141	0.5167
0.6	0.6143	0.6167
0.7	0.7144	0.7167
0.8	0.8146	0.8167
0.9	0.9151	0.9167

Table 7.2: RMS norm of RIBEM for convection-diffusion-reaction problem with different values of Péclet number.

Péclet number, RMS error norm in ϕ, Experiment 1			
Mesh size	Pé $= 15$	Pé $= 20$	Pé $= 25$
	$\|\|e_\phi\|\|_{RMS}$	$\|\|e_\phi\|\|_{RMS}$	$\|\|e_\phi\|\|_{RMS}$
20	6.4×10^{-3}	3.6×10^{-3}	2.2×10^{-3}
40	5.5×10^{-3}	3.3×10^{-3}	2.2×10^{-3}
80	4.8×10^{-3}	2.9×10^{-3}	2.0×10^{-3}
100	4.8×10^{-3}	2.7×10^{-3}	1.9×10^{-3}
200	4.4×10^{-3}	2.5×10^{-3}	1.6×10^{-3}
400	4.3×10^{-3}	2.4×10^{-3}	1.5×10^{-3}

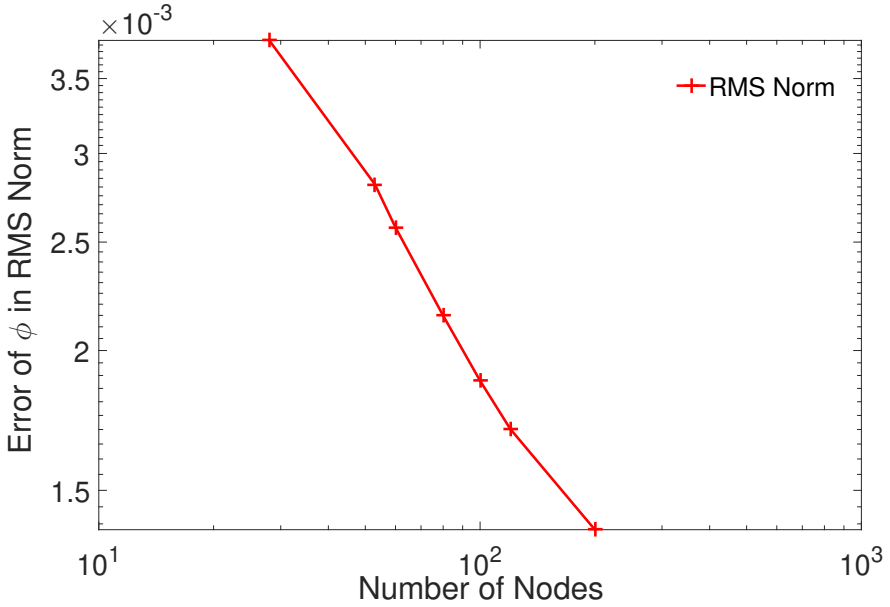

Figure 7.9: RMS Error Norm: RIBEM results with spatial meshes for the concentration ϕ with increasing nodes at Pé $= 1$ for experiment 1.

Negative Velocity

We now solve this problem with negative velocities to provide further validation of the proposed scheme. Figure 7.10 displays the solutions for $S = 10$ and $v_x = -10$. In Fig. 7.11

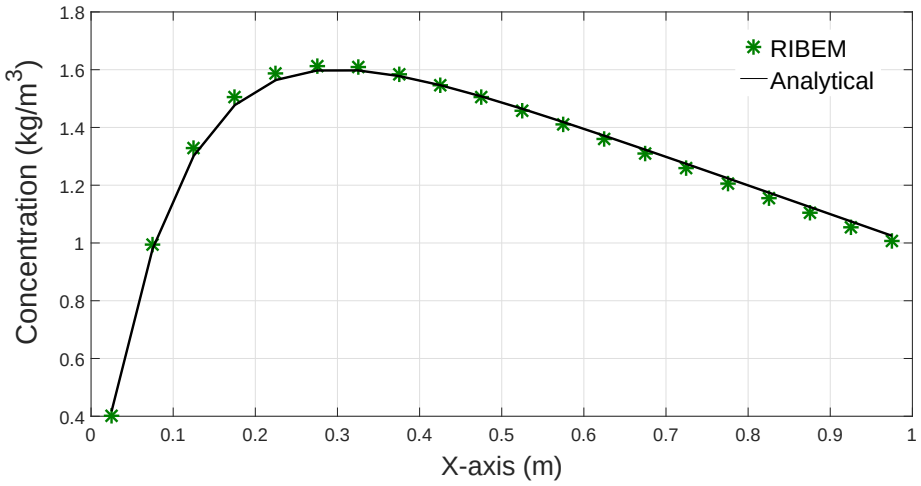

Figure 7.10: Variation of concentration profile ϕ along faces $y = 0$ and $y = 1$ for $S = 10$, $v_x = -10$: comparison between the analytical (solid line) and numerical (star points) solutions

the velocity has been increased to $v_x = -80$ and $S = 80$. The Péclet number in this case is 80. Then, the value of S is considered as 100 to make the velocity and the concentration profiles

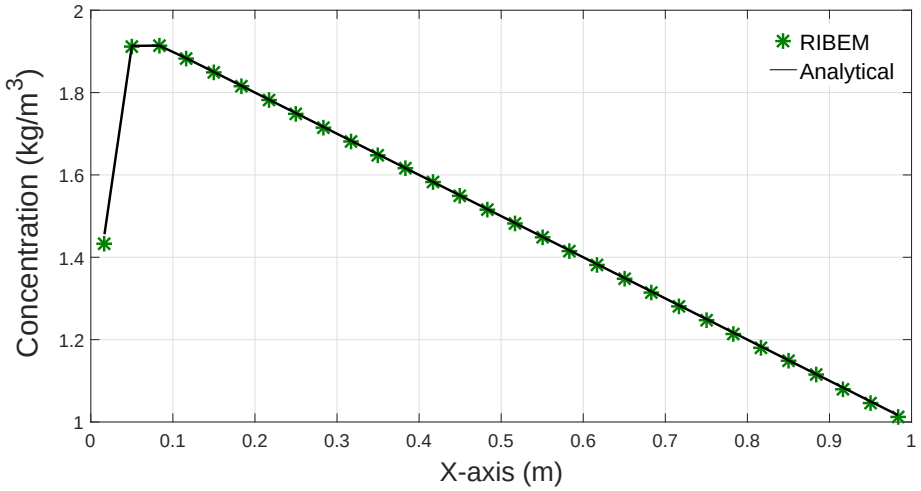

Figure 7.11: Variation of concentration profile ϕ along faces $y = 0$ and $y = 1$ for $S = 80$, $v_x = -80$: comparison between the analytical (solid line) and numerical (star points) solutions

significantly sharp in the opposite direction. Figure 7.12 compares the BEM and analytical solutions for this case. Once again, the results show very good agreement for a Péclet number in this case equal to 50. Finally, Fig. 7.13 presents the solutions for a higher value of the source coefficient $S = 500$ with $v_x = -20$. Throughout this section, the figures for negative

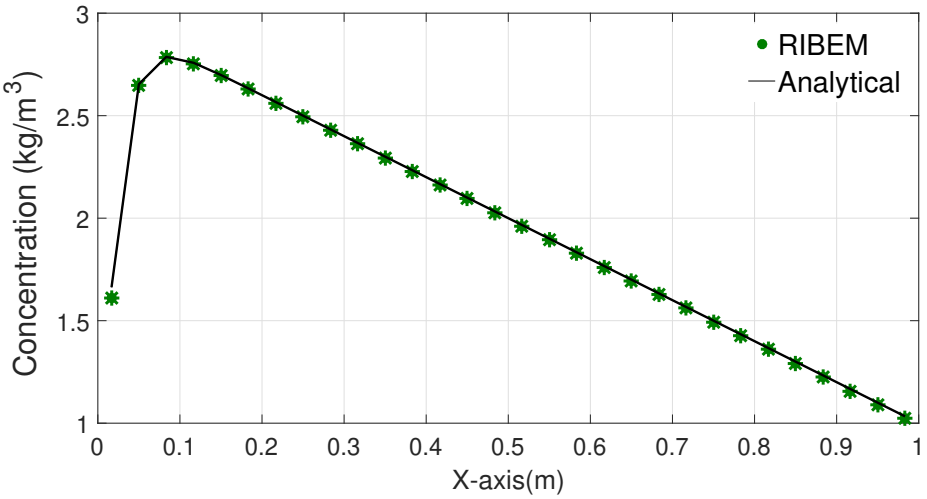

Figure 7.12: Variation of concentration profile ϕ along face $y = 0$ and $y = 1$ for $S = 100$, $v_x = -50$: comparison between the analytical (solid line) and numerical (star points) solutions

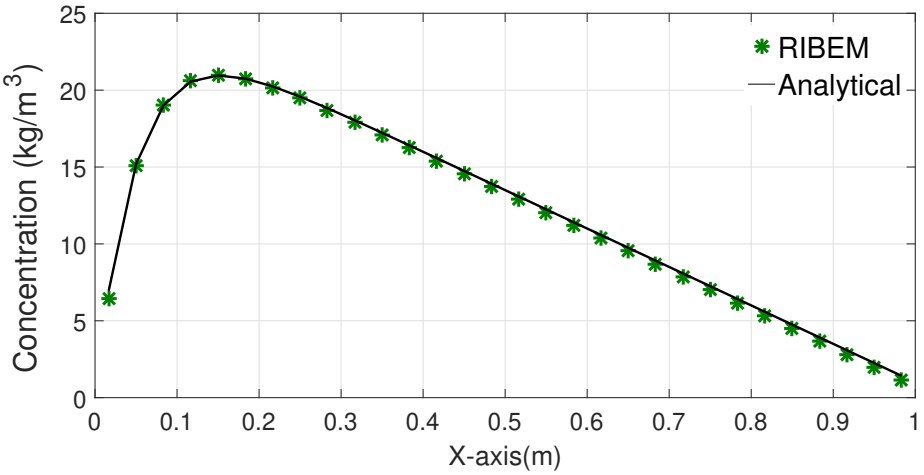

Figure 7.13: Variation of concentration profile ϕ along faces $y = 0$ and $y = 1$ for $S = 500$, $v_x = -20$: comparison between the analytical (solid line) and numerical (star points) solutions

velocities show very good agreement between the numerical and the analytical solutions, for the concentration profile results at different values of the Péclet number and with different source term values. We observe that the numerical solutions are non-oscillatory and are in good agreement with the analytical solutions in all cases. To assess the error of the boundary concentration ϕ with spatial mesh refinement, we present RMS error norm with different

mesh sizes at different values of Péclet number, as shown in Table 7.2 and Fig. 7.9. The results with these various element sizes indicate small RMS.

7.7.2 Experiment 2: Non-Homogeneous Convection-Diffusion-Reaction Problem over a Square Channel and Exponential Diffusivity-Dependent Source Term

Consider a convection-diffusion-reaction problem with a variable source term, subject to mixed boundary conditions:

$$\phi(0,y) = 1, \quad \phi(1,y) = 0, \quad 0 \leq y \leq 1,$$

$$\frac{\partial \phi}{\partial n}(x,0) = \frac{\partial \phi}{\partial n}(x,1) = 0, \quad 0 \leq x \leq 1.$$

The source term varies in the form:

$$S(x,y) = \frac{2\,\mathrm{e}^{1/D}}{\left[D\,\mathrm{e}^{x/D}\left(\mathrm{e}^{1/D}-1\right)\right]} \tag{7.26}$$

The analytical solution of the problem is given by

$$\phi(x,y) = \frac{\exp(\frac{-x}{D}) - \exp(\frac{-1}{D})}{1-\exp(\frac{-1}{D})}. \tag{7.27}$$

This case study is discretised into 120 equally spaced constant elements, 30 on each side as shown in Fig. 7.2. Figure 7.14 presents the solution with velocity $v_x = 10$ and diffusivity value $D = 100$. Table 7.3 shows a comparison between the simulation and the analytical solutions at different positions at the bottom side for Pé $= 0.1$. To compute the global solution error, the RMS error norm is used for this case study. Figure 7.15 demonstrates the solution at velocity value $v_x = 0.05$ and diffusivity coefficient $D = 100$. Table 7.4 shows a comparison between the simulation and the analytical solutions with diffusivity value $D = 100$ and various values of $v_x = 0.1, 1, 10$. To assess the solution of the concentration ϕ with spatial mesh refinement, we present RMS error norm with different element sizes for

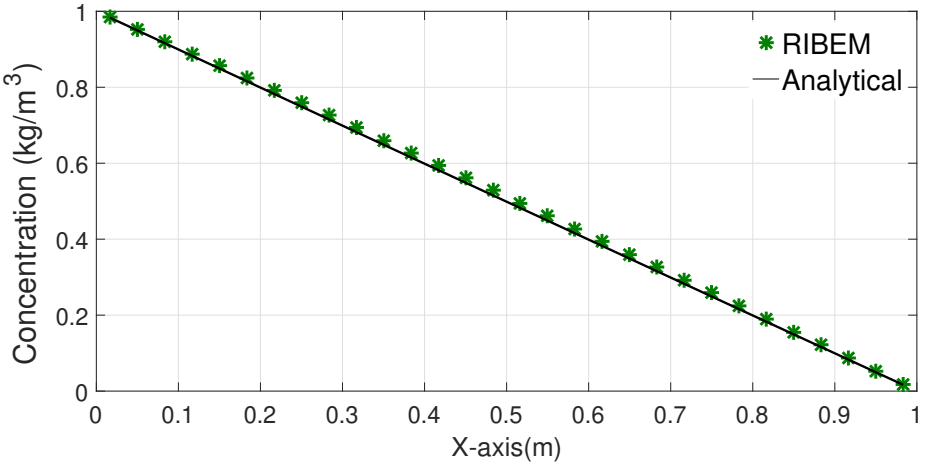

Figure 7.14: Variation of concentration profile ϕ along faces $y = 0$ and $y = 1$: comparison between the analytical (solid line) and numerical (star points) solutions

Table 7.3: RIBEM results of ϕ for convection-diffusion-reaction problem at Pé $= 0.1$

x	RIBEM	Analytical
0.1	0.8883	0.8828
0.2	0.7912	0.7825
0.3	0.6932	0.6823
0.4	0.5944	0.5821
0.5	0.4947	0.4821
0.6	0.3940	0.3822
0.7	0.2925	0.2823
0.8	0.1900	0.1826
0.9	0.0864	0.0830

different Péclet numbers in Table 7.4. The accuracy of the results for the RIBEM is excellent as the RMS relative error norm is of the order 10^{-2} to 10^{-5} in this test case.

To analyse the error of the proposed numerical method, Fig. 7.15 depicts the RMS absolute error of the numerical results at different meshes, obtained by using the proposed RIBEM

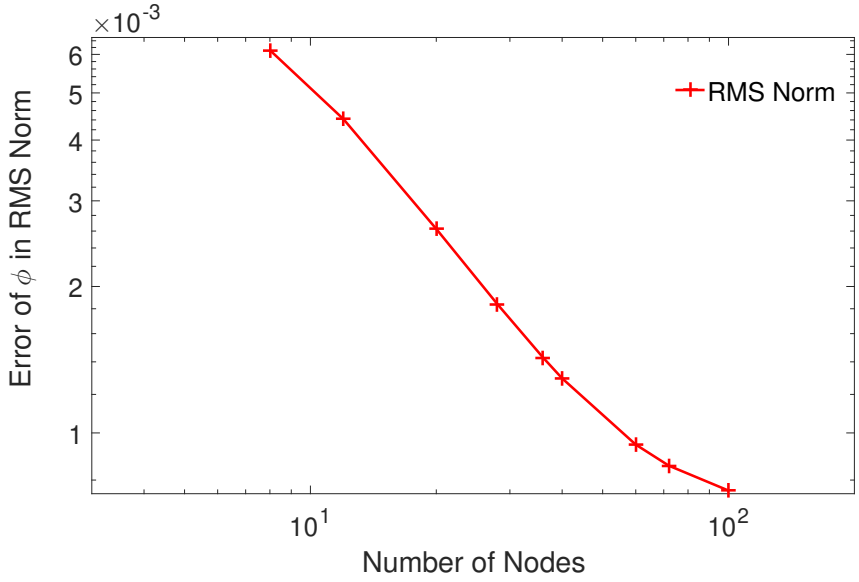

Figure 7.15: RMS Error Norm: RIBEM results with spatial meshes of the concentration ϕ with increasing nodes at Pé $= 0.01$ for experiment 2.

Table 7.4: RMS norm of RIBEM for convection-diffusion-reaction problem with different values of Péclet number.

Péclet number, RMS error norm in ϕ, Experiment 2			
Mesh size	Pé $= 0.001$	Pé $= 0.01$	Pé $= 0.1$
	$\|\|e_\phi\|\|_{RMS}$	$\|\|e_\phi\|\|_{RMS}$	$\|\|e_\phi\|\|_{RMS}$
20	2.5×10^{-3}	2.6×10^{-3}	6.9×10^{-3}
40	1.1×10^{-3}	1.3×10^{-3}	6.6×10^{-3}
80	4.5×10^{-4}	8.1×10^{-4}	6.5×10^{-4}
100	3.4×10^{-4}	7.6×10^{-4}	6.5×10^{-3}
200	1.5×10^{-4}	6.9×10^{-4}	6.5×10^{-3}
400	1.0×10^{-4}	6.8×10^{-4}	6.5×10^{-3}

with respect to the number of boundary elements, where the results were yielded at 120 calculation points uniformly-spaced over the relevant domain. The RMS error obtained with

various choices of spatial meshes for the boundary concentration ϕ, with different element sizes at different values of the Péclet number, is presented in Table 7.4 and Fig. 7.15.

7.7.3 Experiment 3: Non-Homogeneous Convection-Diffusion-Reaction Problem over a Square Domain with Sinusoidal (Cosenoidal) Source Term

Next, we consider another problem whose domain is defined as a unit square. We consider the case where the source term $\mathrm{S}(x,y) = 3\sin(x) - \cos(x)$. The test case is discretised into 120 equally spaced constant elements, 30 on each side as shown in Fig. 7.2. Therefore, the non-homogeneous 2D convection-diffusion-reaction problem can be re-written as

$$D\nabla^2\phi - v_x\frac{\partial\phi}{\partial x} - v_y\frac{\partial\phi}{\partial y} - k\,\phi = 3\sin(x) - \cos(x) \tag{7.28}$$

subject to the mixed boundary conditions: For vertical faces, i.e. $x = 0$ and $x = 1$, non-homogeneous Dirichlet boundary conditions are imposed

$$\phi(0,y) = 0, \quad \phi(1,y) = \sin(1) \quad 0 \le y \le 1,$$

$$\frac{\partial\phi}{\partial n}(x,0) = \frac{\partial\phi}{\partial n}(x,1) = 0, \quad 0 \le x \le 1.$$

The analytical solution of the problem is given by

$$\phi(x,y) = \sin(x). \tag{7.29}$$

Figure 7.16 shows the simulation and the exact solutions using $v_x = -1$, $k = 0$ and $D = 1$. Then, Fig. 7.17 presents the solutions using $v_x = -4$ and $D = 5$. It can be seen that the simulation and the exact solutions are at a very good level of accuracy. Figure 7.18 displays the numerical solution for the concentration profile ϕ by using $v_x = -50$ and $D = 100$. Next, Fig. 7.19 shows the simulation and the exact solutions using $v_x = -5$, $D = 10$ and $k = 2$.
To evaluate the global solution error, the RMS error norm is shown in Fig. 7.20 for coarse and

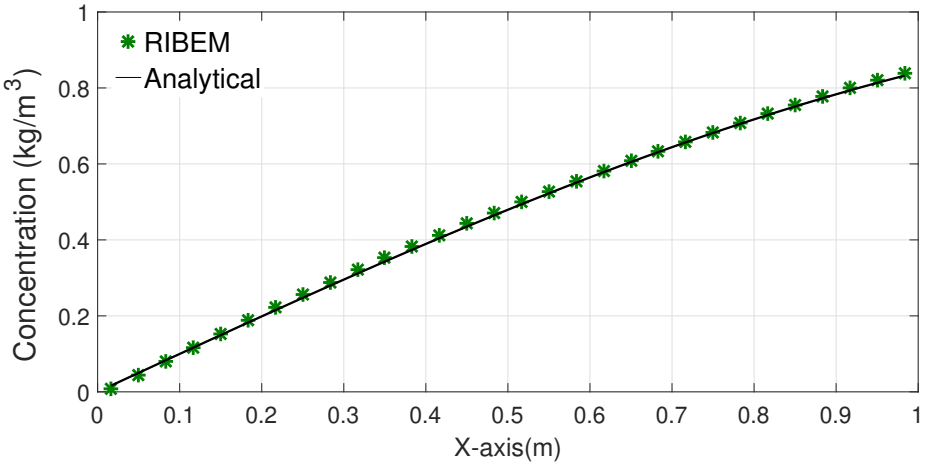

Figure 7.16: Variation of concentration profile ϕ along faces $y = 0$ and $y = 1$ for $v_x = -1$, $D = 1$: comparison between the analytical (solid line) and numerical (star points) solutions

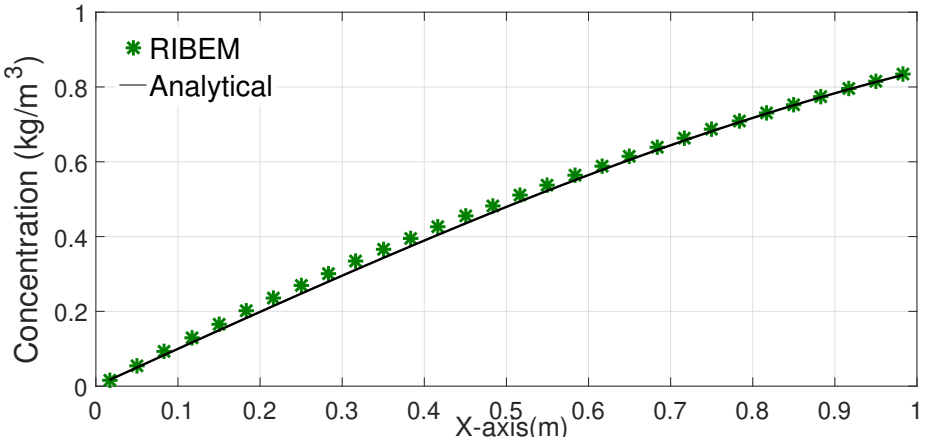

Figure 7.17: Variation of concentration profile ϕ along faces $y = 0$ and $y = 1$ for $v_x = -4$, $D = 5$: comparison between the analytical (solid line) and numerical (star points) solutions

refined meshes. These error measures are computed for $v_x = -1$, $D = 1$ and $k = 0$. The plots show that the numerical solutions obtained from the present method capture the characteristic feature of the analytical solution even for coarse meshes.

Table 7.5 shows a comparison between the simulation and the analytical solutions where $v_x = -1$, $D = 1$, $k = 0$. This table shows the same level of accuracy at different positions along the face $y = 0$.

In addition, to show the error of the boundary concentration ϕ with spatial mesh refinement, we present the RMS errors with different element sizes for different Péclet numbers in Table

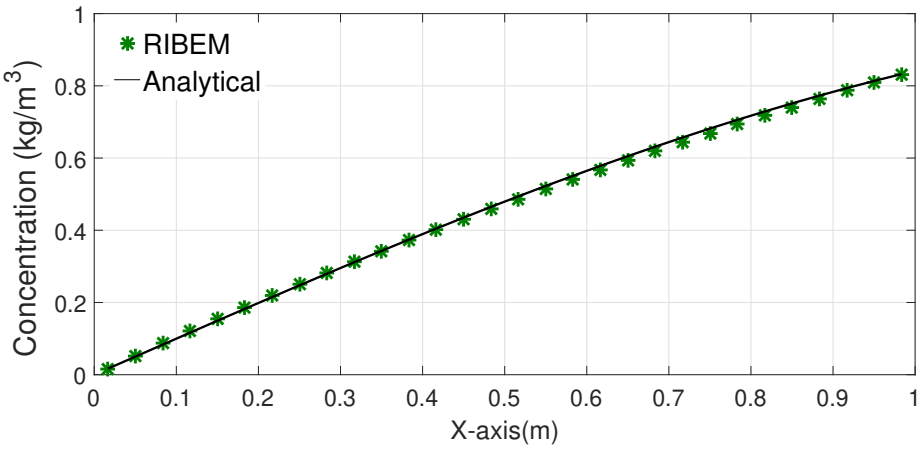

Figure 7.18: Variation of concentration profile ϕ along faces $y = 0$ and $y = 1$ for $v_x = -50$, $D = 100$: comparison between the analytical (solid line) and numerical (star points) solutions

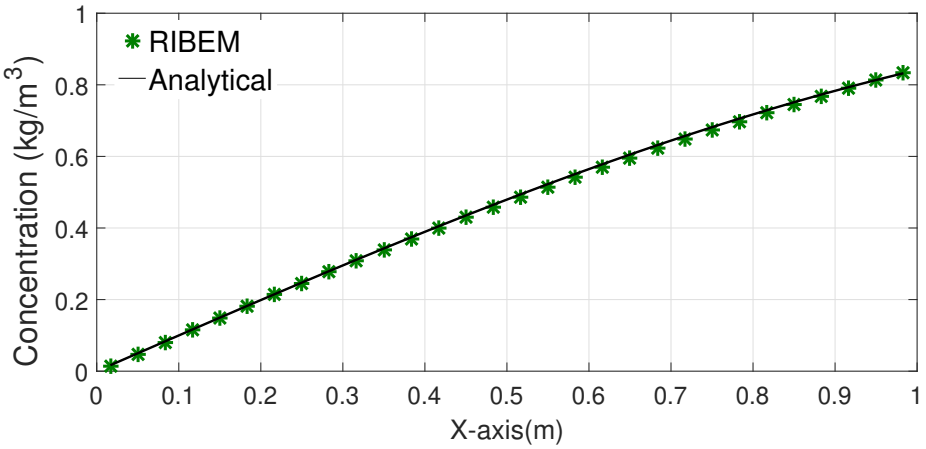

Figure 7.19: Variation of concentration profile ϕ along faces $y = 0$ and $y = 1$ for $v_x = -5$, $D = 10$ and $k = 2$: comparison between the analytical (solid line) and numerical (star points) solutions

7.6. The accuracy of the results for the RIBEM is excellent using a high value of diffusivity $D = 100$, as the RMS errors are of order 10^{-2} to 10^{-3} for all values of the Péclet number. The RMS errors obtained for the boundary concentration ϕ, with different mesh sizes at different values of the Péclet number, are presented in Table 7.6 and Fig. 7.20. It can be seen that the errors are reduced with continuous mesh refinement for low Péclet number. Further, for all spatial mesh refinement, the RIBEM for problem 3 produced an accurate behaviour of the boundary concentration even with a small number of boundary elements.

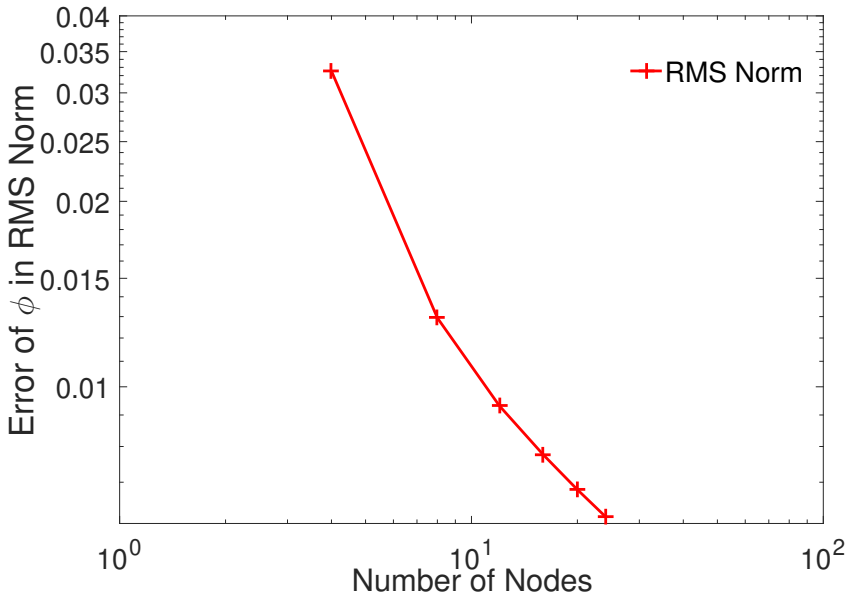

Figure 7.20: RMS Error Norm: RIBEM results with spatial meshes of the concentration ϕ with increasing nodes at Pé $= 1$ for experiment 3.

Table 7.5: RIBEM results of ϕ for convection-diffusion-reaction problem at Pé $= 1$

x	RIBEM	Analytical
0.1	0.1168	0.1164
0.2	0.2220	0.2150
0.3	0.3207	0.3114
0.4	0.4131	0.4047
0.5	0.4997	0.4940
0.6	0.5814	0.5783
0.7	0.6586	0.6569
0.8	0.7315	0.7289
0.9	0.7995	0.7936

Table 7.6: RMS norm of RIBEM for convection-diffusion-reaction problem with different values of Péclet number.

Péclet number, RMS error norm in ϕ, Experiment 3			
Mesh size	Pé $= 0.001$	Pé $= 0.01$	Pé $= 0.1$
	$\|e_\phi\|_{RMS}$	$\|e_\phi\|_{RMS}$	$\|e_\phi\|_{RMS}$
20	0.0839	0.0658	0.1026
40	0.0734	0.0593	0.0452
80	0.0694	0.0569	0.0442
100	0.0687	0.0565	0.0440
200	0.0678	0.0559	0.0438
400	0.0674	0.0557	0.0437

7.7.4 Experiment 4: Two-dimensional Non-Homogeneous Convection-Diffusion-Reaction Problem over a Square Panel with Parabolic Source Term

This problem has been modelled as two-dimensional over a unit square, $\Omega = \{(x_1, x_2) : x_1, x_2 \in (0,1)\}$. The last tested case is a non-homogeneous 2D convection-diffusion-reaction problem described by

$$D\nabla^2\phi - v_x\frac{\partial\phi}{\partial x} - v_y\frac{\partial\phi}{\partial y} - k\,\phi = -2\left(3x^2+1\right). \tag{7.30}$$

We assume the diffusivity is $D = 1$, reaction coefficient $k = 2$, and the constant velocity components are $v_x = 6$ and $v_y = 0$. The analysis is conducted with a discretisation of 120 equally spaced constant elements, 30 on each face. The boundary conditions are imposed as follows:

$$\frac{\partial\phi}{\partial n}(x,0) = \frac{\partial\phi}{\partial n}(x,1) = 0, \quad 0 \le x \le 1.$$

$$\phi(1,y) = 5.5, \quad \phi(0,y) = 0.5, \quad 0 \leq y \leq 1.$$

The analytical solution of the problem can be expressed as

$$\phi(x,y) = \exp(3x)\left[\left(\frac{-7\exp(-3)+6\cosh\sqrt{5}}{\sinh\left(\sqrt{5}\right)}\right)\sinh\left(\sqrt{5}x\right) - 6\cosh\left(\sqrt{5}x\right)\right]$$

$$+\frac{3}{2}x^2 + \frac{9}{2}x + \frac{13}{2}. \tag{7.31}$$

Table 7.7 shows that the current simulation results are in good agreement with the analytical

Table 7.7: RIBEM results of ϕ for convection-diffusion-reaction problem at Pé $= 6$.

x	RIBEM	Analytical
0.1	0.5166	0.5098
0.2	0.5409	0.5265
0.3	0.5802	0.5592
0.4	0.6478	0.6236
0.5	0.7690	0.7483
0.6	0.9923	0.9835
0.7	1.4081	1.4165
0.8	2.1842	2.1971
0.9	3.6157	3.5807

solution. This present Table provides the solutions at different positions at the bottom side of the domain. The simulation errors are presented in Table 7.8, in which it can observed that RMS error norm has been calculated for the present method. We can see the absolute error of this experiment is small and solution behaviour of this approach is excellent at different values of the Péclet number. Moreover, it is worth noting that the results obtained with the

Table 7.8: RMS norm of RIBEM for convection-diffusion-reaction problem with different values of Péclet number.

Péclet number, RMS error norm in ϕ, Experiment 4			
Mesh size	Pé $= 4$	Pé $= 6$	Pé $= 10$
	$\|e_\phi\|_{RMS}$	$\|e_\phi\|_{RMS}$	$\|e_\phi\|_{RMS}$
12	0.3703	0.0379	0.3602
40	0.3309	0.0306	0.3094
80	0.3269	0.0288	0.3118
100	0.3263	0.0285	0.3127
200	0.3252	0.0283	0.3145
400	0.3249	0.0283	0.3152

RIBEM are accurate with all choices of spatial meshes.

The simulation and the analytical solutions on a 2D refined mesh computed with very good agreement. The calculated errors are cast in the RMS error norm and are plotted against mesh size in Fig. 7.21. To compare the global solution error, the RMS error norm is shown in Fig. 7.21 for coarse and refined spatial meshes at low Péclet number, i.e. Pé $= 6$. Further, the solution behaviour shown in Fig. 7.21 indicates that we can have a good numerical solution with the RIBEM scheme. Figure 7.22 presents the solution using $v_x = 6$, $D = 1$ and $k = 2$. This plot shows the concentration profiles of ϕ along both horizontal faces, i.e. $y = 0$ and $y = 1$, where the predicted results for the concentration agree quite well with the corresponding analytical solutions. Figure 7.23 shows the simulated and the analytical solutions by considering $v_x = 10$, $D = 1.5$ and $k = 0.5$. From these figures, it can be seen that the proposed method can accurately predict the numerical solution for the convective-diffusive-reactive problem with source term.

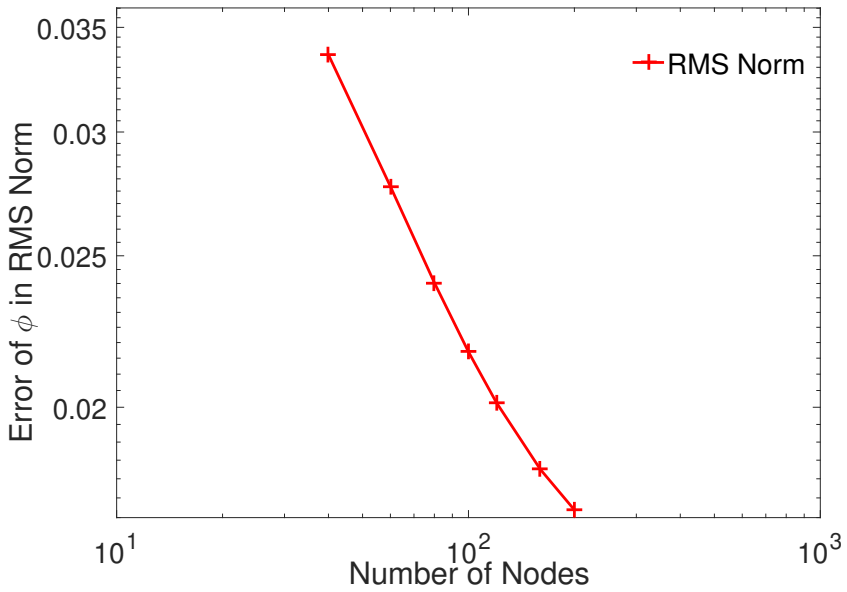

Figure 7.21: RMS Error Norm: RIBEM results with spatial meshes for the concentration ϕ with increasing nodes at at Pé $= 6$ for experiment 4.

7.8 Summary and Discussions

A new formulation of the radial integration boundary element method (RIBEM) is developed for the two-dimensional non-homogeneous convection-diffusion-reaction problem with source term. The fundamental solution of the corresponding problem without source term is implemented in this work. The formulation is the first attempt to solving two-dimensional convection-diffusion-reaction problems with constant and variable source terms in which the BEM modelling described does not require any internal points and internal cells. The domain integral involved is transformed into equivalent boundary integral using the radial integral method (RIM), and a boundary-only integral equation formulation is achieved.

Numerical applications for 2D non-homogeneous problems are demonstrated to show the validity of the proposed technique, and its accuracy was evaluated by applying it to four tests with different velocity fields. Moreover, numerical results show that the RIBEM does not present oscillations or damping of the wave front as may appear in other numerical techniques.

The results presented in section 8 show the versatility of the RIBEM approach to solve non-

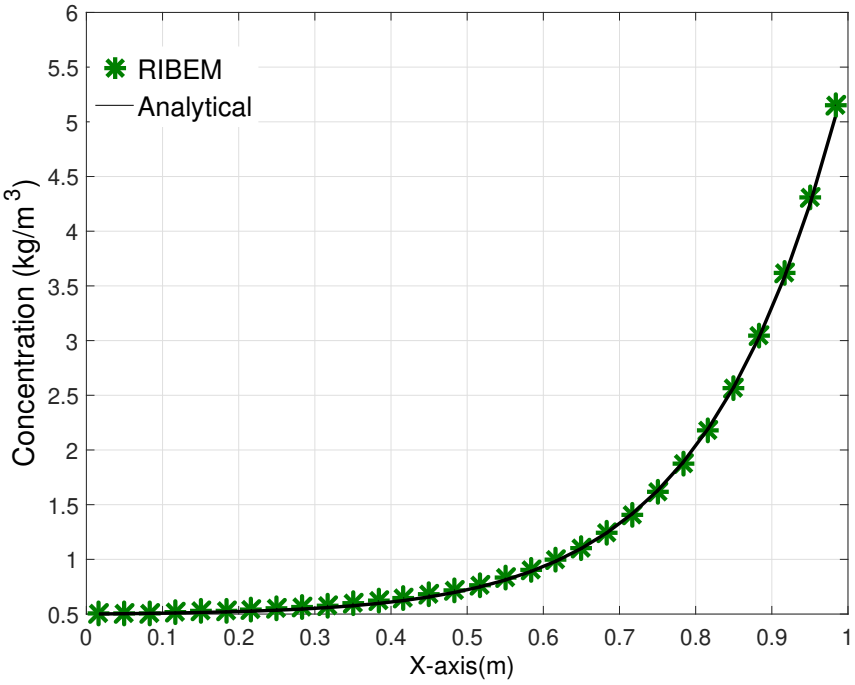

Figure 7.22: Variation of concentration profiles ϕ along faces $y = 0$ and $y = 1$ with $v_x = 6$, $D = 1$ and $k = 2$: comparison between the analytical (solid line) and numerical (star points) solutions

homogeneous convection-diffusion-reaction problems involving variable source terms. We can note a distinct advantage of the present approach, which shows very good accuracy for different types of source terms. It is obvious that, as the velocity increases, the concentration distribution becomes steeper and more difficult to reproduce with numerical models.

The absolute errors in the RMS have been investigated in all case studies for the proposed technique. Analytical solutions are employed to examine the accuracy of the present method. Several numerical tests have been carried out to assess the performance and demonstrate the capacity to handle a wide range of situations in the context of convection-diffusion-reaction problems with source term.

Finally, the accuracy of this novel contribution shows promise, but future work needs to clarify the expected and achieved convergence rates.

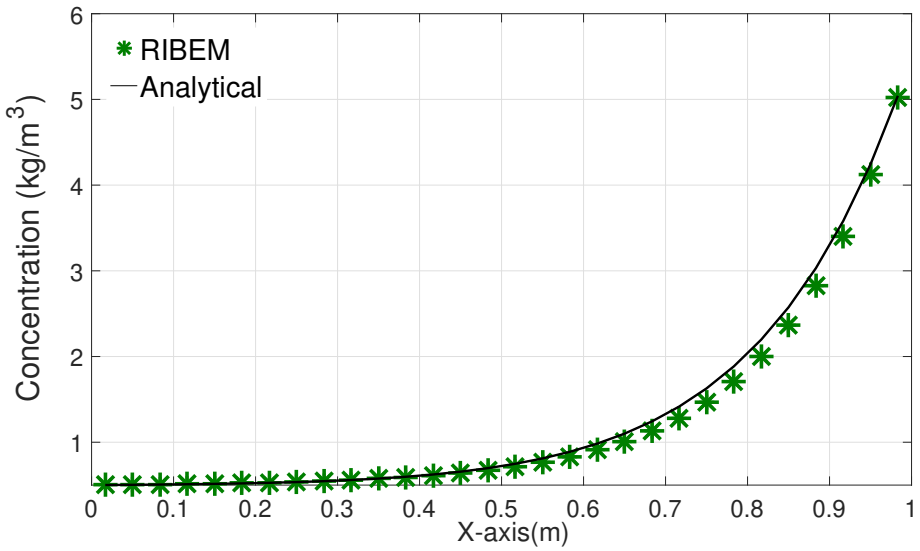

Figure 7.23: Variation of concentration profiles ϕ along faces $y = 0$ and $y = 1$ with $v_x = 10$, $D = 1.5$ and $k = 0.5$: comparison between the analytical (solid line) and numerical (star points) solutions

Chapter 8

Conclusions and Future Works

8.1 Conclusions and Discussions

This chapter outlines the main contributions of the research programme; what has been done, the difficulties encountered, decisions made and how results from examples have represented these findings. This chapter also outlines the research objectives stated in Chapter 1 and shows how these objectives have been met and how they have led to further ideas and work.

Two-dimensional steady-state and transient convection-diffusion-reaction problems with constant and variable velocity have been studied numerically using several newly developed numerical methods. The proposed numerical techniques for the problems are considered the main feature of this thesis.

The significant novelty of this thesis lies in the development of two numerical schemes, namely DRBEM and RIBEM, that have allowed to handle different types of convection-diffusion-reaction problems with variable velocity. Through systematic numerical experimentation, several key features of the DRBEM formulation were revealed under the conditions mentioned above, which had not been reported before. This detailed analysis will increase the overall understanding of the boundary element method combining two powerful techniques, DRM and RIM, for problems described by the convection-diffusion-reaction equation.

In the initial part of this research, the BEM formulation is developed to analyse the steady-

state convection-diffusion-reaction problem with constant velocity. A boundary-only integral equation was obtained in which the singular integrals were calculated applying a transformation proposed by Telles [22], the Jacobian of which becomes zero at the singular point thus smoothing the singularity of the kernel. The accurate evaluation of the singular integrals is particularly important for the case in which a chemical reaction is taking place. As conservation laws no longer hold, they cannot be applied to evaluate the diagonal terms of the influence matrix where the singularity is stronger, avoiding this calculation. The results of several analyses using constant boundary elements showed very good agreement with corresponding analytical solutions, with no oscillations or smoothing of sharp fronts.

A study of the range of Péclet numbers for which the model still produces oscillation-free solutions was carried out, resulting in a higher upper bound for the Péclet number than that reported in the literature for other methods and other approaches.

Problems with variable velocity fields were studied in Chapter 4 in a very generalised manner. The approach devised to solve the steady-state convection-diffusion-reaction problems can be used either if the velocity is a known function of space variables, or if it is given at a number of sample points from experiments or field measurements.

The fundamental solution used was the one for the constant velocity equation with the variable velocity field represented as a sum of a constant value plus a perturbation. The perturbation was moved to the right-hand-side of the equation and the non-homogeneous term generated was treated by the DRM.

A function-expansion approach was utilised to handle the convective terms involving the perturbations. This technique expands the concentration as a series of function. Several functions were tested for the expansion and again the physical parameters of the problem were taken into account in the choice of the functions. The technique was applied to several examples and the results compared to analytical solutions displaying very good agreement.

From the mathematical point of view, more formal studies are required related to the characteristics of the DRM approximation in order to make the choice of the expansion functions more consistent related to the physical problems.

The concentration fields have been evaluated for different benchmark problems showing

very good solution. We have made an extensive investigation for the last case studied by considering many different values of the reaction coefficient k, up to $k = 125$. We derived and implemented three radial basis functions and tested them with different types of problems, and we have found that the thin-plate spline radial basis function is the most accurate among these RBFs for our problems. It is, however, worth stressing that the small visible oscillations of the normal fluxes at the vertical faces in all test cases are common and distinctive for constant boundary elements. Discretisation errors of the boundary elements solutions are estimated using two different indicators to show the accuracy and effectiveness of the present method.

The numerical techniques implemented in this paper can also be applied to transient problems, as discussed in [188]. Transient convection-diffusion-reaction problems with constant velocity are studied in Chapter 5. A developed approach to tackle the problem is devised by making use of the DRM.

The DRM, in the present case, is applied using the fundamental solution of the corresponding problem with constant coefficients, and approximating convective terms using a series expansion. Several functions were tested based on previous choices reported in the literature. The best ones, according to their ability to produce well-conditioned matrices and accurate solutions, were used for the expansion. Besides, the physical parameters of the problem were included in these functions used for the expansion of the non-homogeneous term, providing improved results. The results of several examples showed good agreement with analytical solutions, again producing oscillation-free solutions for the range of Péclet numbers studied. The time derivative term has been approximated using the FDM. Among several techniques the backward-difference scheme was the best one, showing very good solution for transient problems. The transient concentration fields have been evaluated for different benchmark problems showing very good solution behaviour and good convergence.

Chapter 6 presents a novel formulation of the DRBEM for solving 2D transient convection-diffusion-reaction problems with spatial variable velocity field. This new formulation for this type of problem has been implemented to handle the time derivative term and the variable velocity field. The fundamental solution of the corresponding steady-state equation with

constant coefficients has been utilised. The DRBEM is used to transform the domain integrals appearing in the BEM formulations into equivalent boundary integrals, thus retaining the boundary-only character of the standard BEM. Numerical applications for 2D time-dependent problems are demonstrated to show the validity of the proposed technique, and its accuracy was evaluated by applying it to three tests with different velocity fields.

In the empirical analysis section, the results presented show the versatility of the method to solve time-dependent convection-diffusion-reaction problems involving variable velocity fields. The first-order time derivative of the potential is approximated by employing a backward FDM. We can note a distinct advantage of the present approach, which demonstrates very good accuracy even for high values of the reaction coefficient which increase the Péclet number for the cases studied. It is obvious that, as the velocity increases, the concentration distribution becomes steeper and more difficult to reproduce with numerical models.

We have made an extensive investigation for the last case studied by considering many different values of the reaction coefficient k. For all these various values of k, the backward time-stepping scheme produces very good results in general. We have derived and implemented three RBFs and tested them with different types of problems, and we have found that the thin-plate spline is the most accurate among these RBFs for our problems.

Finally, a new formulation of the RIBEM is developed in Chapter 7 for the 2D non-homogeneous convection-diffusion-reaction problem with source term. The fundamental solution of the corresponding problem without source term is implemented in this work. The formulation is the first attempt to solving two-dimensional convection-diffusion-reaction problems with constant and variable source terms in which the BEM modelling described does not require any internal points and internal cells.

The domain integral involved is transformed into equivalent boundary integrals using the RIM, and a boundary-only integral equation formulation is achieved. Numerical applications for 2D non-homogeneous problems are demonstrated to show the validity of the proposed technique, and its accuracy was evaluated by applying it to four tests with different source terms. Moreover, numerical results show that the RIBEM does not present oscillations or damping of the wave front as may appear in other numerical techniques. The results pre-

sented in section 8 show the versatility of the RIBEM approach to solve non-homogeneous convection-diffusion-reaction problems involving variable source terms.
The absolute errors in RMS have been investigated in all case studies for the proposed technique. Analytical solutions are employed to examine the accuracy of the present method. Several numerical tests have been carried out to assess the performance and demonstrate the capacity to handle a wide range of situations in the context of convection-diffusion-reaction problems with source terms.

8.2 Difficulties Encountered

One of the problems encountered in the BEM is the evaluation of singular integrals which occur when the integration and source points coincide. Chapter 4 concentrates on a number of methods of handling this singularity. Telles method was considered the most suitable and this was used throughout the investigation of problems using the DRBEM.
The derivation and implementation of the RBFs are also considered to be a difficult task, especially as they have been derived from the fundamental solution of the corresponding equation, i.e. convection-diffusion-reaction. In conclusion, this thesis provides a detailed analysis of several key topics that have been previously unexplored.
Convection-diffusion-reaction problems are encountered in several industrial processes and, through increased understanding of their physics, these processes can be made more efficient and more reliable. Efficient numerical methods were developed to allow a better understanding of these problems, providing insight into their governing mechanisms.

8.3 Future Works and Recommendations

During the course of this work, it became apparent that there are several related areas of research and extensions to the current methods that are worthy of study. However, due to time constraints, not all of these areas could be investigated.
This section highlights extensions and possible new research directions for the current work,

based on developments of the numerical methods and the original mathematical models. It will be significant to outline the possible applications of the developed models and algorithms. More practical problems can now be solved using this technique. Additional research effort should be made in order to extend the formulation to steady-state convection-diffusion-reaction problems with variable velocity, diffusivity and reaction coefficient in 2D and 3D spaces. Moreover, transient cases with variable coefficients can also be implemented, even in multi-zone domain problems. A powerful numerical formulation of the BEM can be implemented to solve convection-diffusion-reaction problems at very high Péclet number.

Another strategy for developing our work is by employing other RBF functions such as augmented TPS, inverse multiquadric, etc, which will be derived and implemented in the near future. A RIBEM numerical scheme is also under consideration and development for more complicated types of problems with variable velocity, reaction or diffusivity terms, both for steady-state and transient convection-diffusion-reaction problems. Furthermore, the source term could be a non-linear function of concentration.

The application of the RIBEM to convection-diffusion-reaction problems in this thesis can be considered as the first attempt to handle this type of problem. The RIBEM is an excellent alternative to the DRBEM, but it certainly needs a considerable amount of work to develop the mathematical formulation and its numerical implementation. We demonstrated that the RIBEM works well for convection-diffusion-reaction problems with constant/variable source terms. The results are promising but future work will be needed to understand the expected and achieved convergence rates. More complicated equations will be studied in future work including variable velocity, diffusivity, reaction coefficient and concentration-dependent terms.

Finally, additional efforts will be made to improve the solution for the heat flux q by using discontinuous linear, quadratic or higher order elements.

References

[1] M. Aliabadi, *The Boundary Element Method: Applications in Solids and Structures*. John Wiley & Sons, Chichester, 2002.

[2] J. Zhou and G. Chen, *Boundary Element Methods with Applications to Nonlinear Problems: 2nd edition*. Atlantis Press, 2015.

[3] O. C. Zienkiewicz and R. L. Taylor, *The Finite Element Method: Solid Mechanics*, vol. 2. Butterworth-Heinemann, 2000.

[4] I. Koutromanos, *Fundamentals of Finite Element Analysis: Linear Finite Element Analysis*. John Wiley & Sons, Chichester, 2018.

[5] D. Soares Jr and L. C. Wrobel, "A coupled BEM/FEM formulation for drop interaction in Stokes flows with flexible and slip confining boundaries," *Engineering Analysis with Boundary Elements*, vol. 77, pp. 112–122, 2017.

[6] J. Peiró and S. Sherwin, "Finite difference, finite element and finite volume methods for partial differential equations," in *Handbook of Materials Modeling*, pp. 2415–2446, Springer, 2005.

[7] W. Toutip, *The Dual Reciprocity Boundary Element Method for Linear and Non-Linear Problems*. PhD thesis, University of Herfordshire, 2001.

[8] P. W. Partridge, C. A. Brebbia, and L. C. Wrobel, *The Dual Reciprocity Boundary Element Method*. Computational Mechanics Publication, Southampton, 1992.

[9] L. C. Wrobel, *The Boundary Element Method, Applications in Thermo-Fluids and Acoustics*. John Wiley & Sons, Chichester, 2002.

[10] C. A. Brebbia, J. C. F. Telles, and L. C. Wrobel, *Boundary Element Techniques: Theory and Applications in Engineering*. Springer Science & Business Media, 2012.

[11] F. J. Sayas, *Introduction to the boundary element method. A case study: the Helmholtz equation, Lecture Notes, Third Summer School, University of Concepción, Chile*. 2006.

[12] S. Li and W. K. Liu, *Meshfree Particle Methods*. Springer Science & Business Media, 2007.

[13] A. Arnold, O. Lenz, S. Kesselheim, R. Weeber, F. Fahrenberger, D. Roehm, P. Košovan, and C. Holm, "Meshfree methods for partial differential equations VI," *Lecture Notes in Computational Science and Engineering*, vol. 89, pp. 1–23, 2013.

[14] G. Fairweather and A. Karageorghis, "The method of fundamental solutions for elliptic boundary value problems," *Advances in Computational Mathematics*, vol. 9, no. 1-2, p. 69, 1998.

[15] M. Golberg and C. Chen, "The method of fundamental solutions for potential, Helmholtz and diffusion problems," *Boundary Integral Methods-Numerical and Mathematical Aspects*, pp. 103–176, 1998.

[16] V. Kupradze and M. A. Aleksidze, "The method of functional equations for the approximate solution of certain boundary value problems," *USSR Computational Mathematics and Mathematical Physics*, vol. 4, no. 4, pp. 82–126, 1964.

[17] R. Mathon and R. L. Johnston, "The approximate solution of elliptic boundary-value problems by fundamental solutions," *SIAM Journal on Numerical Analysis*, vol. 14, no. 4, pp. 638–650, 1977.

[18] S. Mukherjee and Y. X. Mukherjee, *Boundary Methods: Elements, Contours, and Nodes*. CRC Press, 2005.

[19] D. Levin, "The approximation power of moving least-squares," *Mathematics of Computation*, vol. 67, no. 224, pp. 1517–1531, 1998.

[20] H. Wendland, "Local polynomial reproduction and moving least squares approximation," *IMA Journal of Numerical Analysis*, vol. 21, no. 1, pp. 285–300, 2001.

[21] S.-H. Park and S.-K. Youn, "The least-squares meshfree method," *International Journal for Numerical Methods in Engineering*, vol. 52, no. 9, pp. 997–1012, 2001.

[22] J. C. F. Telles, "A self-adaptive co-ordinate transformation for efficient numerical evaluation of general boundary element integrals," *International Journal for Numerical Methods in Engineering*, vol. 24, no. 5, pp. 959–973, 1987.

[23] C. A. Brebbia and J. Dominguez, *Boundary Elements: An Introductory Course*. WIT press, 1994.

[24] C. A. Brebbia, *The Boundary Element Method for Engineers*. Pentech Press, 1978.

[25] A. H.-D. Cheng and D. T. Cheng, "Heritage and early history of the boundary element method," *Engineering Analysis with Boundary Elements*, vol. 29, no. 3, pp. 268–302, 2005.

[26] J. Lachat and J. Watson, "Effective numerical treatment of boundary integral equations: A formulation for three-dimensional elastostatics," *International Journal for Numerical Methods in Engineering*, vol. 10, no. 5, pp. 991–1005, 1976.

[27] Y. Gu, W. Wang, L. Zhang, and X. Feng, "An enriched radial point interpolation method (e-RPIM) for analysis of crack tip fields," *Engineering Fracture Mechanics*, vol. 78, no. 1, pp. 175–190, 2011.

[28] P. K. Banerjee and R. Butterfield, *Boundary Element Methods in Engineering Science*, vol. 17. McGraw-Hill, London, 1981.

[29] F. Paris and J. Canas, *Boundary Element Method Fundamentals and Applications*. Oxford University Press, Oxford, 1997.

[30] C. Brebbia and J. Dominguez, "Boundary element methods for potential problems," *Applied Mathematical Modelling*, vol. 1, no. 7, pp. 372–378, 1977.

[31] M. Ikeuchi and K. Onishi, "Boundary element solutions to steady convective diffusion equations," *Applied Mathematical Modelling*, vol. 7, no. 2, pp. 115–118, 1983.

[32] L. C. Wrobel and C. A. Brebbia, *Boundary Element Methods in Heat Transfer*. Computational Mechanics Publications, 1992.

[33] Y. Tanaka, T. Honma, and I. Kaji, "Transient solutions of a three-dimensional convective diffusion equation using mixed boundary elements," in *Advanced Boundary Element Methods*, pp. 417–425, Springer, 1988.

[34] M. Enokizono and S. Nagata, "Convection-diffusion analysis at high Péclet number by the boundary element method," *IEEE Transactions on Magnetics*, vol. 28, no. 2, pp. 1651–1654, 1992.

[35] I. Zagar, L. Škerget, and A. Alujevic, "Diffusion-convection problems using boundary-domain integral formulation for non-uniform flows," *WIT Press, Southampton*, vol. 9, 1994.

[36] Y. Shi and P. Banerjee, "Boundary element methods for convective heat transfer," *Computer Methods in Applied Mechanics and Engineering*, vol. 105, no. 2, pp. 261–284, 1993.

[37] H. Zakerdoost and H. Ghassemi, "Dual reciprocity boundary element method for steady state convection-diffusion-radiation problems," *International Journal of Partial Differential Equations and Applications*, vol. 2, no. 4, pp. 68–71, 2014.

[38] A. Rap, L. Elliott, D. Ingham, D. Lesnic, and X. Wen, "The inverse source problem for the variable coefficients convection-diffusion equation," *Inverse Problems in Science and Engineering*, vol. 15, no. 5, pp. 413–440, 2007.

[39] R. Cholewa, A. J. Nowak, and L. C. Wrobel, "Application of BEM and sensitivity analysis to the solution of the governing diffusion–convection equation for a continuous casting process," *Engineering Analysis with Boundary Elements*, vol. 28, no. 4, pp. 389–403, 2004.

[40] P. J. Roache, *Computational Fluid Dynamics*. Hermosa Publishers, 1972.

[41] T. J. Hughes, "A multidimentional upwind scheme with no crosswind diffusion," *Finite Element Methods for Convection Dominated Flows, AMD 34*, 1979.

[42] I. Christie, D. F. Griffiths, A. R. Mitchell, and O. C. Zienkiewicz, "Finite element methods for second order differential equations with significant first derivatives," *International Journal for Numerical Methods in Engineering*, vol. 10, no. 6, pp. 1389–1396, 1976.

[43] P. Huyakorn, "Solution of steady-state, convective transport equation using an upwind finite element scheme," *Applied Mathematical Modelling*, vol. 1, no. 4, pp. 187–195, 1977.

[44] J. Heinrich, P. Huyakorn, O. Zienkiewicz, and A. Mitchell, "An 'upwind' finite element scheme for two-dimensional convective transport equation," *International Journal for Numerical Methods in Engineering*, vol. 11, no. 1, pp. 131–143, 1977.

[45] J. Heinrich and O. Zienkiewicz, "Quadratic finite element schemes for two-dimensional convective-transport problems," *International Journal for Numerical Methods in Engineering*, vol. 11, no. 12, pp. 1831–1844, 1977.

[46] I. Christie and A. Mitchell, "Upwinding of high order Galerkin methods in conduction-convection problems," *International Journal for Numerical Methods in Engineering*, vol. 12, no. 11, pp. 1764–1771, 1978.

[47] R. Gallagher, O. Zienkiewicz, J. Oden, M. Morandi Cecchi, and C. Taylor, *Finite Elements in Fluids. Volume 7*. John Wiley & Sons, 1988.

[48] T. J. Hughes, *Finite Element Methods for Convection Dominated Flows*. American Society of Mechanical Engineers, 1979.

[49] M. P. Anderson and J. A. Cherry, "Using models to simulate the movement of contaminants through groundwater flow systems," *Critical Reviews in Environmental Science and Technology*, vol. 9, no. 2, pp. 97–156, 1979.

[50] J. Donea, "A Taylor–Galerkin method for convective transport problems," *International Journal for Numerical Methods in Engineering*, vol. 20, no. 1, pp. 101–119, 1984.

[51] J. Donea, S. Giuliani, H. Laval, and L. Quartapelle, "Time-accurate solution of advection-diffusion problems by finite elements," *Computer Methods in Applied Mechanics and Engineering*, vol. 45, no. 1-3, pp. 123–145, 1984.

[52] J. Donea, L. Quartapelle, and V. Selmin, "An analysis of time discretization in the finite element solution of hyperbolic problems," *Journal of Computational Physics*, vol. 70, no. 2, pp. 463–499, 1987.

[53] G. Carey and B.-N. Jiang, "Least-squares finite element method for first-order hyperbolic systems," *International Journal for Numerical Methods in Engineering*, vol. 26, pp. 81–93, 1988.

[54] N.-S. Park and J. A. Liggett, "Taylor–least-squares finite element for two-dimensional advection-dominated unsteady advection–diffusion problems," *International Journal for Numerical Methods in Fluids*, vol. 11, no. 1, pp. 21–38, 1990.

[55] C.-C. Yu and J. C. Heinrich, "Petrov-Galerkin methods for the time-dependent convective transport equation," *International Journal for Nmerical Methods in Engineering*, vol. 23, no. 5, pp. 883–901, 1986.

[56] J. Westerink and D. Shea, "Consistent higher degree Petrov–Galerkin methods for the solution of the transient convection–diffusion equation," *International Journal for Numerical Methods in Engineering*, vol. 28, no. 5, pp. 1077–1101, 1989.

[57] C. Li, "Least-squares characteristics and finite elements for advection–dispersion simulation," *International Journal for Numerical Methods in Engineering*, vol. 29, no. 6, pp. 1343–1358, 1990.

[58] T. J. Hughes, W. K. Liu, and A. Brooks, "Finite element analysis of incompressible viscous flows by the penalty function formulation," *Journal of Computational Physics*, vol. 30, no. 1, pp. 1–60, 1979.

[59] B. Leonard, "A survey of finite differences of opinion on numerical muddling of the incomprehensible defective confusion equation," *Finite Element Methods for Convection Dominated Flows*, vol. 34, pp. 1–10, 1979.

[60] P. M. Gresho and R. L. Lee, "Don't suppress the wiggles—they're telling you something!," *Computers & Fluids*, vol. 9, no. 2, pp. 223–253, 1981.

[61] I. Brunton, *Solving Variable Coefficient Partial Differential Equations Using the Boundary Element Method*. PhD thesis, University of Auckland, New Zealand, 1996.

[62] W.-T. Ang, *A Beginner's Course in Boundary Element Methods*. Universal-Publishers, 2007.

[63] M. A. Jaswon and G. T. Symm, *Integral Equation Methods in Potential Theory and Elastostatics*. Academic Press, London, 1977.

[64] J. T. Katsikadelis, *Boundary Elements: Theory and Applications*. Elsevier, 2002.

[65] P. Hunter and A. Pullan, "FEM/BEM Notes," *Department of Engineering Science, The University of Auckland, New Zeland*, 2001.

[66] J. Gomez and H. Power, "A multipole direct and indirect BEM for 2D cavity flow at low Reynolds number," *Engineering Analysis with Boundary Elements*, vol. 19, no. 1, pp. 17–31, 1997.

[67] S. E. Zarantonello and B. Elton, "Domain decomposition, boundary integrals, and wavelets," in *Wavelet Applications in Signal and Image Processing III*, vol. 2569, pp. 866–876, International Society for Optics and Photonics, 1995.

[68] R. D. Ciskowski and C. A. Brebbia, *Boundary Element Methods in Acoustics*. Springer, 1991.

[69] A. A. Becker, *The Boundary Element Method in Engineering: A Complete Course*. McGraw-Hill, 1992.

[70] L. Škerget, H. Power, and V. Popov, *Domain Decomposition Techniques for Boundary Elements: Application to Fluid Flow*, vol. 21. WIT press, 2007.

[71] J. Iljaž, L. C. Wrobel, M. Hriberšek, and J. Marn, "Subdomain BEM formulations for the solution of bio-heat problems in biological tissue with melanoma lesions," *Engineering Analysis with Boundary Elements*, vol. 83, pp. 25–42, 2017.

[72] J. Iljaž and L. Škerget, "Blood perfusion estimation in heterogeneous tissue using BEM based algorithm," *Engineering Analysis with Boundary Elements*, vol. 39, pp. 75–87, 2014.

[73] S. E. Mikhailov, "Analysis of united boundary-domain integro-differential and integral equations for a mixed BVP with variable coefficient," *Mathematical Methods in the Applied Sciences*, vol. 29, no. 6, pp. 715–739, 2006.

[74] O. Chkadua, S. Mikhailov, and D. Natroshvili, "Analysis of direct boundary-domain integral equations for a mixed BVP with variable coefficient, I: Equivalence and invertibility," *Journal of Integral Equations and Applications*, pp. 499–543, 2009.

[75] O. Chkadua, S. Mikhailov, and D. Natroshvili, "Analysis of direct boundary-domain integral equations for a mixed BVP with variable coefficient, II: Solution regularity and asymptotics," *Journal of Integral Equations and Applications*, pp. 19–37, 2010.

[76] A. Pomp, *The Boundary-Domain Integral Method for Elliptic Systems, with Applications in Shells, Vol. 1683 of Lecture Notes in Mathematics*. Springer, Berlin-Heidelberg-New York, 1998.

[77] C. Miranda, *Partial Differential Equations of Elliptic Type*, vol. 2. Springer Science & Business Media, 2012.

[78] D. Nardini and C. Brebbia, "A new approach to free vibration analysis using boundary elements," *Applied Mathematical Modelling*, vol. 7, no. 3, pp. 157–162, 1983.

[79] M. Zerroukat and L. C. Wrobel, "A boundary element method for multiple moving boundary problems," *Journal of Computational Physics*, vol. 138, no. 2, pp. 501–519, 1997.

[80] B. Šarler and G. Kuhn, "Dual reciprocity boundary element method for convective-diffusive solid-liquid phase change problems, part 1. formulation," *Engineering Analysis with Boundary Elements*, vol. 21, no. 1, pp. 53–63, 1998.

[81] A. H.-D. Cheng, "Multiquadric and its shape parameter–A numerical investigation of error estimate, condition number, and round-off error by arbitrary precision computation," *Engineering Analysis with Boundary Elements*, vol. 36, no. 2, pp. 220–239, 2012.

[82] W. Madych and S. Nelson, "Multivariate interpolation and conditionally positive definite functions. II," *Mathematics of Computation*, vol. 54, no. 189, pp. 211–230, 1990.

[83] J. Duchon, "Splines minimizing rotation-invariant semi-norms in Sobolev spaces," *Constructive Theory of Functions of Several Variables*, pp. 85–100, 1977.

[84] X.-W. Gao, "The radial integration method for evaluation of domain integrals with boundary-only discretization," *Engineering Analysis with Boundary Elements*, vol. 26, no. 10, pp. 905–916, 2002.

[85] X.-W. Gao, "A boundary element method without internal cells for two-dimensional and three-dimensional elastoplastic problems," *Journal of Applied Mechanics*, vol. 69, no. 2, pp. 154–160, 2002.

[86] V. Takhteyev and C. Brebbia, "Analytical integrations in boundary elements," *Engineering Analysis with Boundary Elements*, vol. 7, no. 2, pp. 95–100, 1990.

[87] J. T. Katsikadelis, *The Boundary Element Method for Engineers and Scientists: Theory and Applications*. Academic Press, 2016.

[88] B. F. Zalewski, *Uncertainties in the Solutions to Boundary Element Method: An Interval Approach*. PhD thesis, Case Western Reserve University, 2008.

[89] H. Power and L. C. Wrobel, *Boundary Integral Methods in Fluid Mechanics*. Computational Mechanics Publications, 1995.

[90] M. Schanz and O. Steinbach, *Boundary Element Analysis: Mathematical Aspects and Applications*, vol. 29. Springer Science & Business Media, 2007.

[91] A. Nowak, "The multiple-reciprocity method. A new approach for transforming BEM domain integral to the boundary," *Engineering Analysis Boundary Elements*, vol. 6, pp. 164–167, 1989.

[92] A. Neves and C. Brebbia, "The multiple reciprocity boundary element method in elasticity: A new approach for transforming domain integrals to the boundary," *International Journal for Numerical Methods in Engineering*, vol. 31, no. 4, pp. 709–727, 1991.

[93] Y. Ochiai and T. Kobayashi, "Initial stress formulation for elastoplastic analysis by improved multiple-reciprocity boundary element method," *Engineering Analysis with Boundary Elements*, vol. 23, no. 2, pp. 167–173, 1999.

[94] M. Itagaki, "Boundary element methods applied to two-dimensional neutron diffusion problems," *Journal of Nuclear Science and Technology*, vol. 22, no. 7, pp. 565–583, 1985.

[95] W. Tang, *Transforming domain into boundary integrals in BEM: A generalized approach*, vol. 35. Springer Science & Business Media, 2012.

[96] J. Azevedo and C. Brebbia, "An efficient technique for reducing domain integrals to the boundary," *Boundary Elements X*, vol. 1, pp. 347–361, 1988.

[97] D. Nardini and C. A. Brebbia, "A new approach to free vibration analysis using boundary elements," *Applied Mathematical Modelling*, vol. 7, no. 3, pp. 157–162, 1983.

[98] K. Yang and X.-W. Gao, "Radial integration BEM for transient heat conduction problems," *Engineering Analysis with Boundary Elements*, vol. 34, no. 6, pp. 557–563, 2010.

[99] X.-W. Gao, B.-J. Zheng, K. Yang, and C. Zhang, "Radial integration BEM for dynamic coupled thermoelastic analysis under thermal shock loading," *Computers & Structures*, vol. 158, pp. 140–147, 2015.

[100] W.-A. Yao, H.-X. Yao, and B. Yu, "Radial integration BEM for solving non-fourier heat conduction problems," *Engineering Analysis with Boundary Elements*, vol. 60, pp. 18–26, 2015.

[101] K. Yang, H.-F. Peng, M. Cui, and X.-W. Gao, "New analytical expressions in radial integration BEM for solving heat conduction problems with variable coefficients," *Engineering Analysis with Boundary Elements*, vol. 50, pp. 224–230, 2015.

[102] B. Yu, W.-A. Yao, X.-W. Gao, and S. Zhang, "Radial integration BEM for one-phase solidification problems," *Engineering Analysis with Boundary Elements*, vol. 39, pp. 36–43, 2014.

[103] W.-Z. Feng, K. Yang, M. Cui, and X.-W. Gao, "Analytically-integrated radial integration BEM for solving three-dimensional transient heat conduction problems," *International Communications in Heat and Mass Transfer*, vol. 79, pp. 21–30, 2016.

[104] H.-F. Peng, M. Cui, K. Yang, and X.-W. Gao, "Radial integration BEM for steady convection-conduction problem with spatially variable velocity and thermal conductivity," *International Journal of Heat & Mass Transfer*, vol. 126, pp. 1150–1161, 2018.

[105] M. Ikeuchi, M. Sakakihara, and K. Onishi, "Constant boundary element solution for steady-state convective diffusion equation in three dimensions," *IEICE Transactins (1976-1990)*, vol. 66, no. 6, pp. 373–376, 1983.

[106] M. Ikeuchi, "Further Development of boundary elements in steady convective diffusion problems," *Numerical Methods in Laminar and Turbulent Flow IV*, 1985.

[107] N. Okamoto, "Boundary element method for chemical reaction system in convective diffusion," *Numerical Methods in Laminar and Turbulent Flow IV*, 1985.

[108] A. Taigbenu and J. A. Liggett, "An integral solution for the diffusion-advection equation," *Water Resources Research*, vol. 22, no. 8, pp. 1237–1246, 1986.

[109] N. Okamoto, "Analysis of convective diffusion problem with first-order chemical reaction by boundary element method," *International Journal for Numerical Methods in Fluids*, vol. 8, no. 1, pp. 55–64, 1988.

[110] L. C. Wrobel and D. B. DeFigueiredo, "Numerical analysis of convection-diffusion problems using the boundary element method," *International Journal of Numerical Methods for Heat & Fluid Flow*, vol. 1, no. 1, pp. 3–18, 1991.

[111] M. M. Grigor'ev, "A boundary element method for the solution of convective diffusion and Burgers' equations," *International Journal of Numerical Methods for Heat & Fluid Flow*, vol. 4, no. 6, pp. 527–552, 1994.

[112] Y. Tanaka, T. Honma, and I. Kaji, "Mixed boundary element solution for three-dimensional convection-diffusion problem with a velocity profile," *Applied Mathematical Modelling*, vol. 11, no. 6, pp. 402–410, 1987.

[113] M. M. Aral and Y. Tang, "A boundary-only procedure for transient transport problems with or without first-order chemical reaction," *Applied Mathematical Modelling*, vol. 13, no. 3, pp. 130–137, 1989.

[114] D. Nardini and C. Brebbia, "The solution of parabolic and hyperbolic problems using an alternative boundary element formulation," *Boundary Elements VII*, pp. 3–87, 1985.

[115] P. Partridge and C. Brebbia, "Computer implementation of the BEM dual reciprocity method for the solution of general field equations," *International Journal for Numerical Methods in Biomedical Engineering*, vol. 6, no. 2, pp. 83–92, 1990.

[116] L. C. Wrobel and D. DeFigueiredo, "A dual reciprocity boundary element formulation for convection-diffusion problems with variable velocity fields," *Engineering Analysis with Boundary Elements*, vol. 8, no. 6, pp. 312–319, 1991.

[117] A. Gupta, C. L. Chan, and A. Chandra, "BEM formulation for steady-state conduction-convection problems with variable velocities," *Numerical Heat Transfer, Part B Fundamentals*, vol. 25, no. 4, pp. 415–432, 1994.

[118] A. Rap, L. Elliott, D. Ingham, D. Lesnic, and X. Wen, "DRBEM for cauchy convection-diffusion problems with variable coefficients," *Engineering Analysis with Boundary Elements*, vol. 28, no. 11, pp. 1321–1333, 2004.

[119] Z. Qiu, L. C. Wrobel, and H. Power, "An evaluation of boundary element schemes for convection-diffusion problems," *WIT Transactions on Modelling and Simulation*, vol. 1, 1993.

[120] Z. Qiu, L. C. Wrobel, and H. Power, "Numerical solution of convection–diffusion problems at high Péclet number using boundary elements," *International Journal for Numerical Methods in Engineering*, vol. 41, no. 5, pp. 899–914, 1998.

[121] G. L. Young, K. A. McDonald, A. Palazoglu, and W. Ford, "Boundary element solutions for free boundary convection-diffusion problems," *Numerical Heat Transfer*, vol. 21, no. 3, pp. 299–311, 1992.

[122] J. Ravnik and L. Škerget, "A gradient free integral equation for diffusion–convection equation with variable coefficient and velocity," *Engineering Analysis with Boundary Elements*, vol. 37, no. 4, pp. 683–690, 2013.

[123] K. M. Singh and M. Tanaka, "On exponential variable transformation based boundary element formulation for advection–diffusion problems," *Engineering Analysis with Boundary Elements*, vol. 24, no. 3, pp. 225–235, 2000.

[124] M. M. Aral and Y. Tang, "A boundary-only procedure for transient transport problems with or without first-order chemical reaction," *Applied Mathematical Modelling*, vol. 13, no. 3, pp. 130–137, 1989.

[125] T. Honma and Y. Tanaka, "Transient solutions of two-dimension convective diffusion equation using regular boundary element method," *IEEE Transactions on Magnetics*, vol. 23, no. 5, pp. 3293–3295, 1987.

[126] A. Chandra, C. L. Chan, and J. Lim, "A BEM approach for transient conduction-convection in machining processes," in *Advances in Boundary Element Techniques*, pp. 55–79, Springer, 1993.

[127] C. Cunha, J. Carrer, M. Oliveira, and V. Costa, "A study concerning the solution of advection–diffusion problems by the boundary element method," *Engineering Analysis with Boundary Elements*, vol. 65, pp. 79–94, 2016.

[128] J. Lim, C. Chan, and A. Chandra, "A BEM analysis for transient conduction—convection problems," *International Journal of Numerical Methods for Heat & Fluid Flow*, vol. 4, no. 1, pp. 31–45, 1994.

[129] F. Wang, W. Chen, A. Tadeu, and C. G. Correia, "Singular boundary method for transient convection–diffusion problems with time-dependent fundamental solution," *International Journal of Heat and Mass Transfer*, vol. 114, pp. 1126–1134, 2017.

[130] Y. Gu, W. Chen, and X.-Q. He, "Singular boundary method for steady-state heat conduction in three dimensional general anisotropic media," *International Journal of Heat and Mass Transfer*, vol. 55, no. 17-18, pp. 4837–4848, 2012.

[131] S. J. DeSilva, C. L. Chan, A. Chandra, and J. Lim, "Boundary element method analysis for the transient conduction–convection in 2-D with spatially variable convective velocity," *Applied Mathematical Modelling*, vol. 22, no. 1, pp. 81–112, 1998.

[132] J. Ravnik and L. Škerget, "Integral equation formulation of an unsteady diffusion–convection equation with variable coefficient and velocity," *Computers & Mathematics with Applications*, vol. 66, no. 12, pp. 2477–2488, 2014.

[133] B. Pan, B. Li, and Y. Ruan, "A boundary element method for steady state convection-diffusion problems with or without phase change," *WIT Transactions on Modelling and Simulation*, vol. 16, 1997.

[134] N. Bozkaya and M. Tezer-Sezgin, "Time-domain BEM solution of convection–diffusion-type MHD equations," *International Journal for Numerical Methods in Fluids*, vol. 56, no. 11, pp. 1969–1991, 2008.

[135] K. M. Singh and M. Tanaka, "Dual reciprocity boundary element analysis of transient advection-diffusion," *International Journal of Numerical Methods for Heat & Fluid Flow*, vol. 13, no. 5, pp. 633–646, 2003.

[136] A. Peratta and V. Popov, "Numerical stability of the BEM for advection-diffusion problems," *Numerical Methods for Partial Differential Equations*, vol. 20, no. 5, pp. 675–702, 2004.

[137] L. M. Romero and F. G. Benitez, "A boundary element numerical scheme for the two-dimensional convection–diffusion equation," *International Journal for Numerical Methods in Engineering*, vol. 76, no. 13, pp. 2063–2090, 2008.

[138] R. Pettres and L. A. de Lacerda, "Numerical analysis of an advective diffusion domain coupled with a diffusive heat source," *Engineering Analysis with Boundary Elements*, vol. 84, pp. 129–140, 2017.

[139] H. Fendoğlu, C. Bozkaya, and M. Tezer-Sezgin, "DBEM and DRBEM solutions to 2D transient convection-diffusion-reaction type equations," *Engineering Analysis with Boundary Elements*, vol. 93, pp. 124–134, 2018.

[140] N. Samec and L. Škerget, "Integral formulation of non-steady convective diffusion problem with high source term value," *WIT Press*, vol. 21, 1998.

[141] D. B. DeFigueiredo, *Boundary Element Analysis of Convection-Diffusion Problems*. PhD Thesis, Wessex Institute of Technology: Southampton, England, 1990.

[142] L. Škerget, A. Alujevic, and C. Brebbia, "Analysis of laminar flows with separation using BEM," in *:Boundary Elements VII; Proceedings of the Seventh International Conference, Como, Italy*, vol. 2, pp. 9–23, 1985.

[143] H. Carslaw and J. Jaeger, *Conduction of Heat in Solids: Oxford Science Publications*. Oxford, 1959.

[144] W. J. Wnek and E. G. Fochtman, "Mathematical model for fate of pollutants in near-shore waters," *Environmental Science & Technology*, vol. 6, no. 4, pp. 331–337, 1972.

[145] M. T. Van Genuchten and W. Alves, "Analytical solutions of the one-dimensional convective-dispersive solute transport equation," tech. rep., United States Department of Agriculture, Economic Research Service, 1982.

[146] C.-C. Yu and J. C. Heinrich, "Petrov—Galerkin method for multidimensional, time-dependent, convective-diffusion equations," *International Journal for Numerical Methods in Engineering*, vol. 24, no. 11, pp. 2201–2215, 1987.

[147] Y. Tanaka and T. Honma, "A boundary element analysis for convective diffusion problems adjacent to diffusion domains," *Applied Mathematical Modelling*, vol. 13, no. 2, pp. 115–121, 1989.

[148] J. P. Davim, *Tribology in Manufacturing Technology*. Springer, 2012.

[149] W. Kaplan, *Advanced Mathematics for Engineers*. Addison-Wesley World Student Series, 1981.

[150] M. Abramowitz and I. Stegun, *Handbook of Mathematical Functions*. Dover, New York, 1972.

[151] A. H. Stroud and D. Secrest, *Gaussian Quadrature Formulas*. Prentice-Hall, 1966.

[152] A. J. Davies, *Aspects of the Boundary Integral Equation Method and Its Implementation on a Distributed Array Processor*. PhD thesis, Imperial College, 1989.

[153] D. DeFigueiredo and L. C. Wrobel, "A boundary element analysis of convective heat diffusion problems," *Advanced Computational Methods in Heat Transfer*, vol. 1, pp. 229–38, 1990.

[154] A. Shiva and H. Adibi, "A numerical solution for advection-diffusion equation using dual reciprocity method," *Numerical Methods for Partial Differential Equations*, vol. 29, no. 3, pp. 843–856, 2013.

[155] S. A. Al-Bayati and L. C. Wrobel, "DRBEM formulation for convection-diffusion-reaction problems with variable velocity," *In: D. J. Chappell, (editor), Eleventh UK Conference on Boundary Integral Methods (UKBIM 11), Nottingham Trent University Press*, pp. p. 5–14, 2017.

[156] C. Bustamante, H. Power, and W. Florez, "An efficient accurate local method of approximate particular solutions for solving convection–diffusion problems," *Engineering Analysis with Boundary Elements*, vol. 47, pp. 32–37, 2014.

[157] M. Golberg and C. Chen, "The theory of radial basis functions applied to the BEM for inhomogeneous partial differential equations," *Boundary Elements Communications*, vol. 5, no. 2, pp. 57–61, 1994.

[158] M. Powell, "The uniform convergence of thin plate spline interpolation in two dimensions," *Numerische Mathematik*, vol. 68, no. 1, pp. 107–128, 1994.

[159] P. Orsini, H. Power, and M. Lees, "The Hermite radial basis function control volume method for multi-zones problems; A non-overlapping domain decomposition algorithm," *Computer Methods in Applied Mechanics and Engineering*, vol. 200, no. 5, pp. 477–493, 2011.

[160] D. Stevens, H. Power, C. Meng, D. Howard, and K. Cliffe, "An alternative local collocation strategy for high-convergence meshless PDE solutions, using radial basis functions," *Journal of Computational Physics*, vol. 254, pp. 52–75, 2013.

[161] D. Stevens and H. Power, "The radial basis function finite collocation approach for capturing sharp fronts in time dependent advection problems," *Journal of Computational Physics*, vol. 298, pp. 423–445, 2015.

[162] L. C. Wrobel, C. A. Brebbia, and D. Nardini, "The dual reciprocity boundary element formulation for transient heat conduction," *Finite Elements in Water Resources VI*, pp. 801–811, 1986.

[163] V. Martin, "An optimized Schwarz waveform relaxation method for the unsteady convection diffusion equation in two dimensions," *Applied Numerical Mathematics*, vol. 52, no. 4, pp. 401–428, 2005.

[164] P. W. Partridge and B. Sensale, "The method of fundamental solutions with dual reciprocity for diffusion and diffusion–convection using subdomains," *Engineering Analysis with Boundary Elements*, vol. 24, no. 9, pp. 633–641, 2000.

[165] K. W. Morton, *Numerical Solution of Convection-Diffusion Problems*. Chapman & Hall, London, 1996.

[166] L. Cao, Q.-H. Qin, and N. Zhao, "Application of DRM-Trefftz and DRM-MFS to transient heat conduction analysis," *Recent Patents on Space Technology*, vol. 2, pp. 41–50, 2010.

[167] E. Divo and A. J. Kassab, "Transient non-linear heat conduction solution by a dual reciprocity boundary element method with an effective posteriori error estimator," in *ASME 2004 International Mechanical Engineering Congress and Exposition*, pp. 77–86, American Society of Mechanical Engineers, 2004.

[168] X.-W. Gao, "A meshless BEM for isotropic heat conduction problems with heat generation and spatially varying conductivity," *International Journal for Numerical Methods in Engineering*, vol. 66, no. 9, pp. 1411–1431, 2006.

[169] M. Al-Jawary and L. C. Wrobel, "Radial integration boundary integral and integro-differential equation methods for two-dimensional heat conduction problems with variable coefficients," *Engineering Analysis with Boundary Elements*, vol. 36, no. 5, pp. 685–695, 2012.

[170] M. Cui, H.-F. Peng, B.-B. Xu, X.-W. Gao, and Y. Zhang, "A new radial integration polygonal boundary element method for solving heat conduction problems," *International Journal of Heat and Mass Transfer*, vol. 123, pp. 251–260, 2018.

[171] S. Qu, S. Li, H.-R. Chen, and Z. Qu, "Radial integration boundary element method for acoustic eigenvalue problems," *Engineering Analysis with Boundary Elements*, vol. 37, no. 7-8, pp. 1043–1051, 2013.

[172] E. Albuquerque, P. Sollero, and W. Portilho de Paiva, "The radial integration method applied to dynamic problems of anisotropic plates," *International Journal for Numerical Methods in Biomedical Engineering*, vol. 23, no. 9, pp. 805–818, 2007.

[173] X.-W. Gao, "An effective method for numerical evaluation of general 2D and 3D high order singular boundary integrals," *Computer Methods in Applied Mechanics and Engineering*, vol. 199, no. 45-48, pp. 2856–2864, 2010.

[174] X.-W. Gao, W.-Z. Feng, K. Yang, and M. Cui, "Projection plane method for evaluation of arbitrary high order singular boundary integrals," *Engineering Analysis with Boundary Elements*, vol. 50, pp. 265–274, 2015.

[175] M. Cui, W.-Z. Feng, X.-W. Gao, and K. Yang, "High order projection plane method for evaluation of supersingular curved boundary integrals in BEM," *Mathematical Problems in Engineering*, vol. 2016, 2016.

[176] W.-Z. Feng and X.-W. Gao, "An interface integral equation method for solving transient heat conduction in multi-medium materials with variable thermal properties," *International Journal of Heat and Mass Transfer*, vol. 98, pp. 227–239, 2016.

[177] X.-W. Gao, W.-Z. Feng, B.-J. Zheng, and K. Yang, "An interface integral equation method for solving general multi-medium mechanics problems," *International Journal for Numerical Methods in Engineering*, vol. 107, no. 8, pp. 696–720, 2016.

[178] W.-Z. Feng, X.-W. Gao, J. Liu, and K. Yang, "A new BEM for solving 2D and 3D elastoplastic problems without initial stresses/strains," *Engineering Analysis with Boundary Elements*, vol. 61, pp. 134–144, 2015.

[179] K. Yang, W.-Z. Feng, H.-F. Peng, and J. Lv, "A new analytical approach of functionally graded material structures for thermal stress BEM analysis," *International Communications in Heat and Mass Transfer*, vol. 62, pp. 26–32, 2015.

[180] B. Zheng, X. Gao, and C. Zhang, "Radial integration BEM for vibration analysis of two-and three-dimensional elasticity structures," *Applied Mathematics and Computation*, vol. 277, pp. 111–126, 2016.

[181] E. Albuquerque, P. Sollero, and P. Fedelinski, "Free vibration analysis of anisotropic material structures using the boundary element method," *Engineering Analysis with Boundary Elements*, vol. 27, no. 10, pp. 977–985, 2003.

[182] X.-W. Gao, "Boundary element analysis in thermoelasticity with and without internal cells," *International Journal for Numerical Methods in Engineering*, vol. 57, no. 7, pp. 975–990, 2003.

[183] K. Yang, X.-W. Gao, and Y.-F. Liu, "Using analytical expressions in radial integration BEM for variable coefficient heat conduction problems," *Engineering Analysis with Boundary Elements*, vol. 35, no. 10, pp. 1085–1089, 2011.

[184] K. Yang, J. Wang, J.-M. Du, H.-F. Peng, and X.-W. Gao, "Radial integration boundary element method for nonlinear heat conduction problems with temperature-dependent conductivity," *International Journal of Heat and Mass Transfer*, vol. 104, pp. 1145–1151, 2017.

[185] C. Zhang, M. Cui, J. Wang, X. Gao, J. Sladek, and V. Sladek, "3D crack analysis in functionally graded materials," *Engineering Fracture Mechanics*, vol. 78, no. 3, pp. 585–604, 2011.

[186] H.-F. Peng, Y.-G. Bai, K. Yang, and X.-W. Gao, "Three-step multi-domain BEM for solving transient multi-media heat conduction problems," *Engineering Analysis with Boundary Elements*, vol. 37, no. 11, pp. 1545–1555, 2013.

[187] X.-W. Gao and T. G. Davies, "An effective boundary element algorithm for 2D and 3D elastoplastic problems," *International Journal of Solids and Structures*, vol. 37, no. 36, pp. 4987–5008, 2000.

[188] J. Duchon, "Splines minimizing rotation-invariant semi-norms in Sobolev spaces," *Constructive Theory of Functions of Several Variables*, pp. 85–100, 1977.

Appendix A

The Limiting Process

Starting from Eq.(3.34) one places the source point at the position ξ on the boundary Γ of the domain Ω, and augments the domain Ω by a circular portion Ω_ε (or spherical if we are in 3D) of radius ε centred at ξ, as in Fig.(A.1) below. This follows the idea suggested by Brebbia [24] for Laplace's equation. The new added portion Ω_ε will now enable Eq.(3.34)

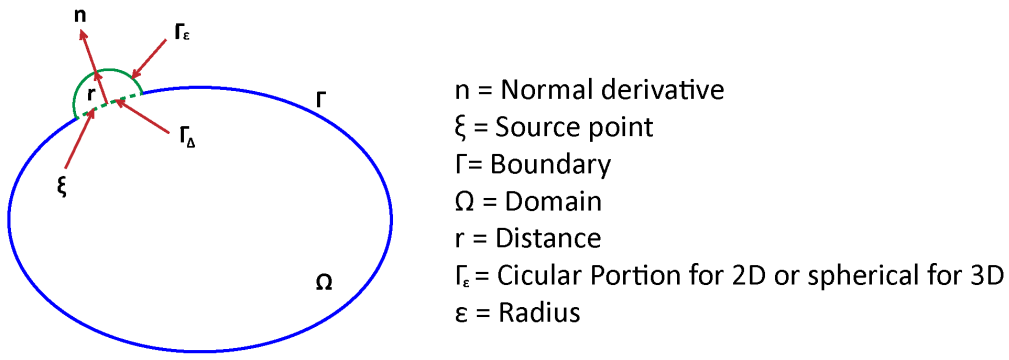

Figure A.1: The Augmented Domiain for the Limiting Process.

to be correctly applied, once the point ξ is an internal point of the augmented domain $\Omega+\Omega_\varepsilon$, which now has a boundary given by $\Gamma-\Gamma_\Delta+\Gamma_\varepsilon$. The equation would then be suitably written as

$$\int_{\Omega+\Omega_\varepsilon} \mathscr{L}^*\left[\Phi^*\right]\,\phi\,d\Omega = -\int_{(\Gamma-\Gamma_\Delta)+\Gamma_\varepsilon} \phi\,\Phi^*\,v_n\,d\Gamma + \int_{(\Gamma-\Gamma_\Delta)+\Gamma_\varepsilon} \Phi^*\,\frac{\partial\phi}{\partial n}\,d\Gamma$$

$$-\int_{(\Gamma-\Gamma_\Delta)+\Gamma_\varepsilon} \phi \, \frac{\partial \Phi^*}{\partial n} \, d\Gamma \tag{A.1}$$

We must notice that the radius of the little circle is ε and also that the outward normal has the same direction of this radius.

Applying the limit when ε tends to zero to Eq.(A.1), one has that:

$$\lim_{\varepsilon\to 0} \int_{\Omega+\Omega_\varepsilon} \mathscr{L}^* \left[\Phi^*\right] \phi \, d\Omega = -\lim_{\varepsilon\to 0} \int_{(\Gamma-\Gamma_\Delta)+\Gamma_\varepsilon} \phi \, \Phi^* \, v_n \, d\Gamma$$

$$+\lim_{\varepsilon\to 0} D \int_{(\Gamma-\Gamma_\Delta)+\Gamma_\varepsilon} \Phi^* \, \frac{\partial \phi}{\partial n} \, d\Gamma - \lim_{\varepsilon\to 0} D \int_{(\Gamma-\Gamma_\Delta)+\Gamma_\varepsilon} \phi \, \frac{\partial \Phi^*}{\partial n} \, d\Gamma. \tag{A.2}$$

Disregarding the kernel inside the boundary integrals, one can always write that

$$\int_{(\Gamma-\Gamma_\Delta)+\Gamma_\varepsilon} = \int_{\Gamma-\Gamma_\Delta} + \int_{\Gamma_\varepsilon} \; ; \tag{A.3}$$

and therefore

$$\lim_{\varepsilon\to 0} \int_{(\Gamma-\Gamma_\Delta)+\Gamma_\varepsilon} = \lim_{\varepsilon\to 0} \int_{\Gamma-\Gamma_\Delta} + \lim_{\varepsilon\to 0} \int_{\Gamma_\varepsilon} \; ; \tag{A.4}$$

Consequently

$$\lim_{\varepsilon\to 0} \int_{(\Gamma-\Gamma_\Delta)+\Gamma_\varepsilon} = \int_{\Gamma} + \lim_{\varepsilon\to 0} \int_{\Gamma_\varepsilon} \; . \tag{A.5}$$

That being so, Eq.(A.2) will produce

$$\lim_{\varepsilon\to 0} \int_{\Omega+\Omega_\varepsilon} \mathscr{L}^* \left[\Phi^*\right] \phi \, d\Omega = -\int_{\Gamma} \phi \, \Phi^* \, v_n \, d\Gamma + D \int_{\Gamma} \Phi^* \, \frac{\partial \phi}{\partial n} d\Gamma - D \int_{\Gamma} \phi \, \frac{\partial \Phi^*}{\partial n} d\Gamma$$

$$-\lim_{\varepsilon\to 0} \int_{\Gamma_\varepsilon} \phi \, \Phi^* v_n d\Gamma + D \lim_{\varepsilon\to 0} \int_{\Gamma_\varepsilon} \Phi^* \frac{\partial \phi}{\partial n} \, d\Gamma - D \lim_{\varepsilon\to 0} \int_{\Gamma_\varepsilon} \phi \, \frac{\partial \Phi^*}{\partial n} \, d\Gamma \tag{A.6}$$

Now, if one defines the integrals I_1, I_2 and I_3 as

$$I_1 = \lim_{\varepsilon\to 0}\int_{\Gamma_\varepsilon} \phi\,\Phi^*\,v_n\,d\Gamma, \quad I_2 = \lim_{\varepsilon\to 0}\int_{\Gamma_\varepsilon} \Phi^*\,\frac{\partial\phi}{\partial n}\,d\Gamma, \quad I_3 = \lim_{\varepsilon\to 0}\int_{\Gamma_\varepsilon} \phi\,\frac{\partial\Phi^*}{\partial n}\,d\Gamma. \tag{A.7}$$

Eq.(A.6) can be written as

$$\lim_{\varepsilon\to 0}\int_{\Omega+\Omega_\varepsilon} \mathscr{L}^*\left[\Phi^*\right]\,\phi\,d\Omega = -\int_\Gamma \phi\,\Phi^*\,v_n\,d\Gamma$$

$$+D\int_\Gamma \Phi^*\frac{\partial\phi}{\partial n}\,d\Gamma - D\int_\Gamma \phi\,\frac{\partial\Phi^*}{\partial n}\,d\Gamma - I_1 + DI_2 - DI_3. \tag{A.8}$$

A.1 The Integrals on Γ_ε as $\varepsilon \to 0$.

One integration will be very useful in the following, i.e.

$$\lim_{\varepsilon\to 0}\int_{\Gamma_\varepsilon} \Phi^*\,d\Gamma. \tag{A.9}$$

According to Fig. A.1, one sees that the boundary Γ_ε can be represented by a semicircle, when the boundary is smooth. Having this in mind, the integration over the circle sector can then be written in polar coordinates in the form:

$$\lim_{\varepsilon\to 0}\int_0^\beta \Phi^*\,\varepsilon\,d\theta \quad \text{for} \quad r=\varepsilon \quad \text{and} \quad d\Gamma = \varepsilon\,d\theta; \tag{A.10}$$

where $\beta = \pi$, for the particular case of the semicircular section just mentioned. Recalling that the fundamental solution of the convection-diffusion-reaction equation was derived in Chapter 3, Eq.(3.73).

$$\Phi^*(\xi,x) = \frac{1}{2\pi D}e^{\frac{-v.\mathbf{r}}{2D}}\,K_0\left(|\mu|\,|\mathbf{r}|\right) \tag{A.11}$$

then for this case one has

$$\lim_{\varepsilon\to 0}\int_{\Gamma_\varepsilon}\Phi^*\,d\Gamma=\lim_{\varepsilon\to 0}\frac{1}{2\pi D}\int_0^\beta \mathrm{e}^{\frac{-v.\varepsilon}{2D}}\,K_0\left(|\mu||\varepsilon|\right)\varepsilon\,d\theta. \tag{A.12}$$

From [150] one knows that as the argument of the Bessel function K_0 approaches zero, it behaves as a logarithm function of the argument. Then, as the exponential term tends to 1 as $\varepsilon\to 0$, it is correct to write that for any β:

$$\lim_{\varepsilon\to 0}\int_{\Gamma_\varepsilon}\Phi^*\,d\Gamma=\lim_{\varepsilon\to 0}\frac{1}{2\pi D}\int_0^\beta \ln\left(|\mu||\varepsilon|\right)\varepsilon\,d\theta=0. \tag{A.13}$$

A.1.1 Evaluation of Integral I_1

Writing integral I_1 in a more explicit form, one has

$$I_1=\lim_{\varepsilon\to 0}\int_{\Gamma_\varepsilon} v_n\phi\,\Phi^*\left(\xi,x\right)d\Gamma\left(x\right). \tag{A.14}$$

Let us add and subtract to the value of $\phi\left(x\right)$ under the integration sign a constant $\phi\left(x\right)$. Then

$$I_1=\lim_{\varepsilon\to 0}\int_{\Gamma_\varepsilon} v_n\left[\phi\left(x\right)-\phi\left(\xi\right)+\phi\left(\xi\right)\right]\Phi^*\left(\xi,x\right)d\Gamma\left(x\right). \tag{A.15}$$

As ξ is a fixed point, it is not difficult to visualize that $\phi\left(\xi\right)$ is a constant for the integration and also, with the help of the Fig. A.1, that as $\varepsilon\to 0$ one has that $\phi\left(x\right)\to\phi\left(\xi\right)$ and consequently

$$\left[\phi\left(x\right)-\phi\left(\xi\right)\right]\to 0; \tag{A.16}$$

This integral can be split in to as follows:

$$I_1=\lim_{\varepsilon\to 0}\int_{\Gamma_\varepsilon} v_n\left[\phi\left(x\right)-\phi\left(\xi\right)\right]\Phi^*\left(\xi,x\right)d\Gamma\left(x\right)+v_n\,\phi\left(\xi\right)\lim_{\varepsilon\to 0}\int_{\Gamma_\varepsilon}\Phi^*\left(\xi,x\right)d\Gamma\left(x\right). \tag{A.17}$$

The second integral vanishes as it was proved in Eq.(A.13) and as a corollary, the first as well, once the function Φ^* inside it is multiplied by $\left[\phi\left(x\right)-\phi\left(\xi\right)\right]$, which tends to zero as $\varepsilon\to 0$

and, of course, $x \to \xi$. One can conclude that $I_1 = 0$. The statement that $[\phi(x) - \phi(\xi)] \to 0$ as $x \to \xi$ imposes a continuity requirement on the function $\phi(x)$.

A.1.2 Evaluation of Integral I_2

Writing integral I_2 in a more explicit form, one has

$$I_2 = \lim_{\varepsilon \to 0} \int_{\Gamma_\varepsilon} \Phi^*(\xi, x) \frac{\partial \phi}{\partial n}(x)\, d\Gamma. \tag{A.18}$$

Applying the same scheme as to integral I_1, let us add and subtract a constant to the integrand. In this section the constant will be $\frac{\partial \phi}{\partial n}(\xi)$, then

$$I_2 = \lim_{\varepsilon \to 0} \int_{\Gamma_\varepsilon} \left[\frac{\partial \phi}{\partial n}(x) - \frac{\partial \phi}{\partial n}(\xi) + \frac{\partial \phi}{\partial n}(\xi) \right] \Phi^*(\xi, x)\, d\Gamma(x)$$

$$= \lim_{\varepsilon \to 0} \int_{\Gamma_\varepsilon} \left[\frac{\partial \phi}{\partial n}(x) - \frac{\partial \phi}{\partial n}(\xi) \right] \Phi^*(\xi, x)\, \varepsilon\, d\theta + \frac{\partial \phi}{\partial n}(\xi) \lim_{\varepsilon \to 0} \int_{\Gamma_\varepsilon} \Phi^*(\xi, x)\, \varepsilon\, d\theta. \tag{A.19}$$

The second integral vanishes as a consequence of Eq.(A.13). If we assume piecewise continuity of the derivative with respect to the normal in the neighborhood of ξ one can see that even if a jump of finite magnitude M occurs, i.e.

$$\left[\frac{\partial \phi}{\partial n}(x) - \frac{\partial \phi}{\partial n}(\xi) \right] \to M \quad \text{as} \quad x \to \xi, \tag{A.20}$$

the first integral still vanishes, producing $I_2 = 0$.

A.1.3 Evaluation of Integral I_3

Proceeding as we have done for the integral I_1, i.e. adding and subtracting $\phi(\xi)$, after some rearrangement one has

$$I_3 = \lim_{\varepsilon \to 0} \int_{\Gamma_\varepsilon} [\phi(x) - \phi(\xi)] \frac{\partial \Phi^*}{\partial n}\, d\Gamma + \phi(\xi) \lim_{\varepsilon \to 0} \int_{\Gamma_\varepsilon} \frac{\partial \Phi^*}{\partial n}\, d\Gamma. \tag{A.21}$$

The limit in the second term of this equation produces

$$\lim_{\varepsilon\to 0}\int_{\Gamma_\varepsilon}\frac{\partial\Phi^*}{\partial n}\,d\Gamma=\lim_{\varepsilon\to 0}\int_0^\beta\frac{\partial\Phi^*}{\partial n}\varepsilon\,d\theta. \tag{A.22}$$

Replacing in this equation the value of the normal derivative of the fundamental solution it becomes

$$\lim_{\varepsilon\to 0}\int_{\Gamma_\varepsilon}\frac{\partial\Phi^*}{\partial n}\,d\Gamma$$

$$=\lim_{\varepsilon\to 0}\frac{1}{2\pi D}\int_0^\beta e^{\frac{-v.\varepsilon}{2D}}\left[-|\mu|\,K_1\left(|\mu||\varepsilon|\right)\frac{\partial\varepsilon}{\partial n}-\frac{v_n}{2D}K_0\left(|\mu||\varepsilon|\right)\right]\varepsilon\,d\theta. \tag{A.23}$$

A closer look at the second term in the brackets involving K_0 shows that it is a multiple of the Eq.(A.12), and also proved to vanish for $\varepsilon\to 0$ in Eq.(A.13); then Eq.(A.23) becomes

$$\lim_{\varepsilon\to 0}\int_{\Gamma_\varepsilon}\frac{\partial\Phi^*}{\partial n}\,d\Gamma=\lim_{\varepsilon\to 0}\frac{1}{2\pi D}\int_0^\beta e^{\frac{-v.\varepsilon}{2D}}\left[-|\mu|\,K_1\left(|\mu||\varepsilon|\right)\frac{\partial\varepsilon}{\partial n}\right]\varepsilon\,d\theta. \tag{A.24}$$

In the neighborhood of zero K_z behaves like $1/z$, the exponential tends to 1 and $\frac{\partial\varepsilon}{\partial n}$ equals 1 everywhere in the semicircular sector. This leads us to write

$$\lim_{\varepsilon\to 0}\int_{\Gamma_\varepsilon}\frac{\partial\Phi^*}{\partial n}\,d\Gamma=-\frac{1}{2\pi D}\int_0^\beta|\mu|\frac{1}{|\mu||\varepsilon|}\varepsilon\,d\theta=-\frac{1}{2\pi D}\int_0^\beta d\theta. \tag{A.25}$$

Then finally

$$\lim_{\varepsilon\to 0}\int_{\Gamma_\varepsilon}\frac{\partial\Phi^*}{\partial n}\,d\Gamma=-\frac{\beta}{2\pi D}. \tag{A.26}$$

This value is evidently a constant for the point ξ; then the first integral in Eq.(A.21) vanishes for, as it was already discussed $[\phi(x)-\phi(\xi)]\to 0$ as $x\to\xi$, and consequently I_3 results in

$$I_3=-\phi(\xi)\frac{\beta}{2\pi D}. \tag{A.27}$$

A.1.4 Summing Up The Limits

Replacing the results obtained in the three sections into Eq.(A.8) it becomes

$$\lim_{\varepsilon\to 0}\int_{\Omega}\mathscr{L}^{*}\left[\Phi^{*}\right]\phi\, d\Omega = -\int_{\Gamma}\phi\,\Phi^{*}\,v_{n}\,d\Gamma$$

$$+D\int_{\Gamma}\Phi^{*}\frac{\partial\phi}{\partial n}\,d\Gamma - D\int_{\Gamma}\phi\,\frac{\partial\Phi^{*}}{\partial n}\,d\Gamma + \frac{\phi\left(\xi\right)\beta}{2\pi} \tag{A.28}$$

As it known from Eq.(3.32) that

$$\int_{\Omega}\mathscr{L}^{*}\left[\Phi^{*}\right]\phi\, d\Omega = \phi\left(\xi\right) \tag{A.29}$$

then

$$\phi\left(\xi\right) - \frac{\phi\left(\xi\right)\beta}{2\pi} = -\int_{\Gamma}\phi\,\Phi^{*}\,v_{n}\,d\Gamma + D\int_{\Gamma}\Phi^{*}\frac{\partial\phi}{\partial n}\,d\Gamma - D\int_{\Gamma}\phi\,\frac{\partial\Phi^{*}}{\partial n}\,d\Gamma, \tag{A.30}$$

that can be recast as

$$\frac{(2\pi-\beta)}{2\pi}\,\phi\left(\xi\right) + \int_{\Gamma}\phi\,\Phi^{*}\,v_{n}\,d\Gamma - D\int_{\Gamma}\Phi^{*}\frac{\partial\phi}{\partial n}\,d\Gamma + D\int_{\Gamma}\phi\,\frac{\partial\Phi^{*}}{\partial n}\,d\Gamma = 0. \tag{A.31}$$

where one can see that the coefficient of the term in $\phi\left(\xi\right)$ is a constant which depends on the angle of the boundary at ξ. We will call it $C\left(\xi\right)$.

Then

$$C\left(\xi\right) = \frac{(2\pi-\beta)}{2\pi} \tag{A.32}$$

and Eq.(3.34) will be written as

$$C\left(\xi\right)\phi\left(\xi\right) + \int_{\Gamma}\phi\,\Phi^{*}\,v_{n}\,d\Gamma - D\int_{\Gamma}\Phi^{*}\frac{\partial\phi}{\partial n}\,d\Gamma + D\int_{\Gamma}\phi\,\frac{\partial\Phi^{*}}{\partial n}d\Gamma = 0. \tag{A.33}$$

A special remark has to be made about the angle β, that is the angle drawn over the surface of the boundary at the point ξ. It must be emphasized that as the circular sector was added to the domain, therefore, external to it, the angle β is also the external angle of the boundary at ξ. If the surface is smooth, a complete semicircular sector can be drawn; then the angle $\beta \to \pi$; and $C(\xi) = \frac{1}{2}$.